ACCSCIENCE PUBLISHING

INNOSC Theranostics and Pharmacological Sciences

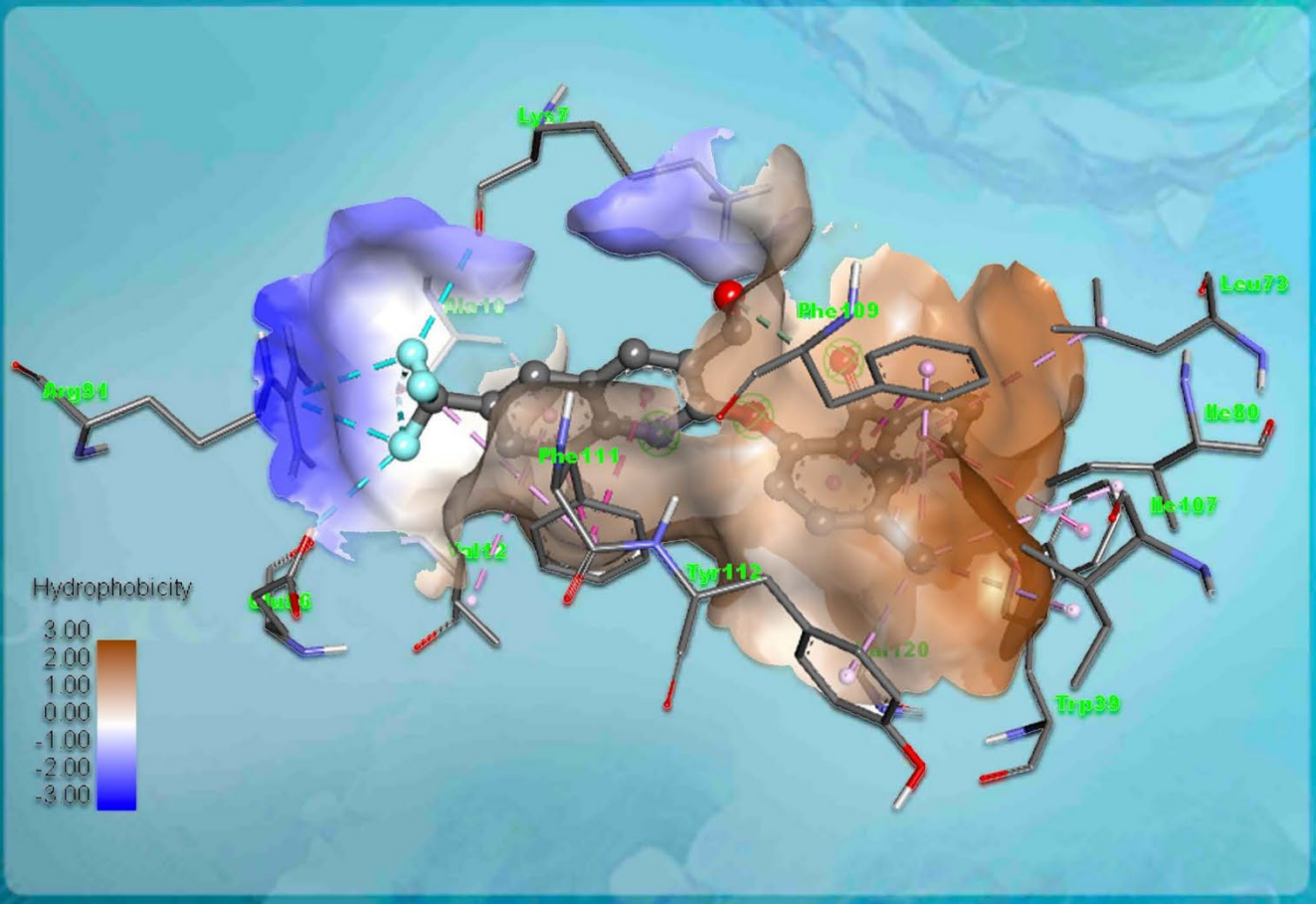

Plasmodium falciparum histoaspartic protease inhibitor: Toxicity investigation and docking study of 2-(2-benzoyl-4-methylphenoxy) quinoline-3-carbaldehyde derivatives

Volume 7 · Issue 1
January 2024
ISSN: 2705-0823 (Online)
ISSN: 2705-0734 (Print)

ACCSCIENCE PUBLISHING

INNOSC Theranostics and Pharmacological Sciences

Print ISSN: 2705-0734

Online ISSN: 2705-0823

INNOSC Theragnostics and Pharmacological Sciences (ITPS) is covering research across disciplines in all aspects of basic, experimental and clinical theragnostics (therapeutic and diagnosis) and pharmacological sciences. The impact of theragnostics has displayed a great advancement to be utilized efficiently in the fields of therapeutics, medical diagnosis and the associated aspects. Pharmacology is a branch of medicine concerned with the uses, effects and modes of action of drugs. This medical science with the impact of understanding the biochemical and therapeutic process gives us the handle to solve the crucial illness or chronic condition in life.

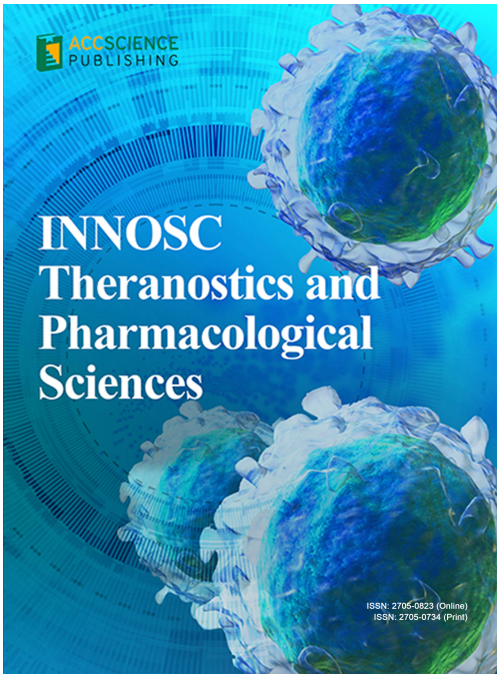

About the Publisher

AccScience Publishing is a publishing company based in Singapore. We publish a range of high-quality, open-access, peer-reviewed journals and books from a broad spectrum of disciplines.

Contact Us

Managing Editor
itps.office@accscience.sg

AccScience Publishing
8 Burn Road, #15-03 Trivex, Singapore 369977.

Volume 7 • Issue 1 • January 2024
ISSN 2705-0734 (print) ISSN 2705-0823 (online)

INNOSC Theranostics and Pharmacological Sciences

ACCSCIENCE PUBLISHING

Access Science Without Barriers

INNOSC THERANOSTICS AND PHARMACOLOGICAL SCIENCES

ISSN: 2705-0734 (print)

ISSN: 2705-0823 (online)

Editorial and Production Credits

Publisher: AccScience Publishing
Managing Editor: Zoe Zhang
Production Editor: Sharmila Velapasamy
Article Layout and Typeset: Sinjore Technologies (India)
Cover Design: ProPub (China)

For all advertising queries, contact itps.office@accscience.sg.

Supplementary file

Supplementary files of articles can be obtained at https://accscience.com/journal/ITPS/7/1.

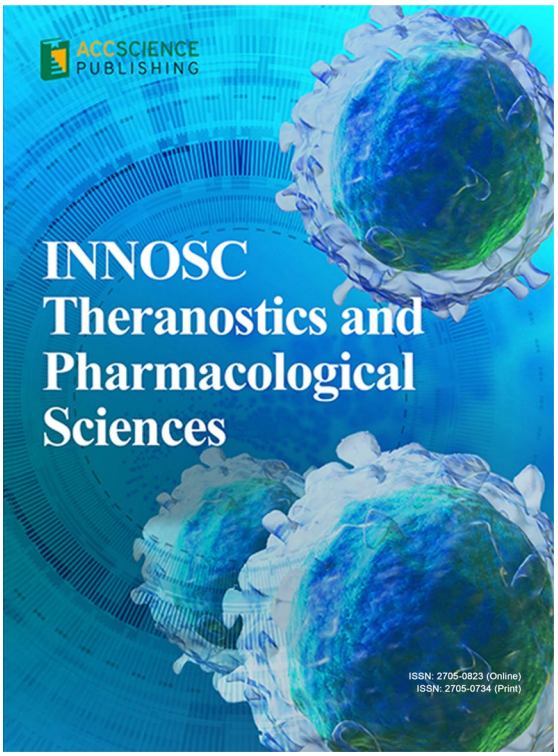

INNOSC Theranostics and Pharmacological Sciences

Editorial Board

ACCSCIENCE PUBLISHING

Volume 7 | Issue 1 | January 2024 |

INNOSC Theranostics and Pharmacological Sciences

https://accscience.com/journal/ITPS

CONTENTS

ACCSCIENCE PUBLISHING

INNOSC Theranostics and Pharmacological Sciences

REVIEW ARTICLE

Pharmacogenetic and liquid biopsy: The new tools of precision medicine in cancer

Verónica Alejandra Alonso, and Alberto Lazarowski*

INFIBIOC - Clinical Biochemistry Department, School of Pharmacy and Biochemistry, University of Buenos Aires, Buenos Aires, Argentina

Abstract

The main difficulty in the treatment of cancer lies in the already known mechanism of resistance to conventional chemotherapy. It is mainly due to the expression of the multidrug transport systems known as ABC transporters, both in neoplastic cells and in excretory organs that reduce the chemotherapeutic concentration. The cancer cell proliferation by activation of growth factor receptors induces their intrinsic tyrosine kinase activity, and their intracellular signaling pathways involved in such activation. Tumor proliferation can respond to the direct action of growth factors on their respective receptors, or due to somatic mutations in different steps of their signaling pathway, in an independent manner of growth factor stimulus. Pharmacogenetics studies have been performed to identify these drivers' mutations and their detection enables targeted inhibitory therapies against their abnormal proteins. The design of new molecules capable of inhibiting these signals has opened a new line of treatment for each type of tumor, thereby enabling tumor growth control and giving rise to the precision medicine approach. It is possible that mutations of sensitive and resistant to these targeted therapies coexist in the same tumor, from the start of therapy or as a consequence of the first-line treatment. The mutations in circulating DNA in body fluids, which are detected and quantified by droplet digital polymerase chain reaction-assisted liquid biopsy, are the ideal biomarkers for the evaluation of pharmacological response, which is crucial for facilitating the change of therapeutic strategy involving second- or third-generation drugs. The quantification of these mutations can be used to assess minimal residual disease in the therapeutic follow-up of each case.

Keywords: Liquid biopsy; Droplet digital polymerase chain reaction; Pharmacogenetics; Somatic mutations; Sensitive mutations; Resistant mutations; Minimal residual disease

***Corresponding author:**
Alberto Lazarowski
(alazarowski@gmail.com)

Citation: Alonso VA, Lazarowski A, 2024, Pharmacogenetic and liquid biopsy: The new tools of precision medicine in cancer. *INNOSC Theranostics and Pharmacological Sciences*, 7(1): 1227.
https://doi.org/10.36922/itps.1227

Received: July 3, 2023

Accepted: August 11, 2023

Published Online: September 11, 2023

1. Multidrug resistance (MDR) in cancer

Drug resistance in cancer is a common occurrence that refers to therapeutic failure characterized by tumor relapse with absolute refractory pharmacological behavior to classic chemotherapeutics, after the effectiveness of the chemotherapeutics reduces over time. One of the most characterized mechanisms of this type of response is driven by a family of genes that encode the MDR proteins or ATP-binding cassette (ABC)-transporters (ABC-t).

These membrane proteins are capable of expelling a wide spectrum of drugs out of cells, even though the drugs have highly diverse molecular structures and are directed

against different therapeutic targets. There are specific resistance mechanisms for each type of drug, which presupposes the possibility that such resistance can be avoided simply by changing the drug to be administered. However, this first drug can often induce the expression of this powerful ABC-t system, and consequently, the cancer cell will later reject any other therapeutic agent, and even combinations of several drugs administered simultaneously. Interestingly, these patients will be "non-responders" not only to the recommended doses, but even to high doses, constituting the classic cases that we call "drug-resistant." Unfortunately, these high doses will be ineffective for tumor treatment, and engender toxic effects on other tissues, forcing the suspension of the medication. The discovery of this powerful multidrug drug resistance system is due to the pioneering work of Ropert Juliano and Victor Ling in the late 1970s[1] (Figure 1).

2. First pharmacogenetics-based detection of driver's mutations of tumor growth

In recent decades, the development of new molecular methodologies has allowed the detection and characterization of the genetic profile of most tumors with high precision and specificity, as well as in a personalized way for each affected individual. In such a way, this information makes it possible to identify the presence of somatic mutations that drive the proliferation of tumor cells, and many of the mutations are pharmacologically actionable. This new theranostic reality is a gigantic breakthrough to overcome the multidrug-resistance mechanism described in the above. In this way, the

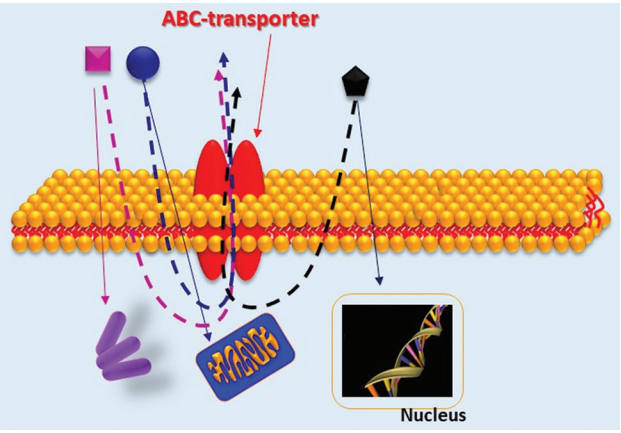

Figure 1. ATP-binding cassette transporters related to multidrug-resistance phenotype, such as P-glycoprotein (P-gp), breast cancer resistance protein, and multidrug resistance-associated proteins (MRPs), form an active ATP- and Ca^{2+}-dependent drug pumping system, which is capable of expelling a broad spectrum of substances (including drugs with different structures and directed to different targets) from the interior to the exterior of the cells, preventing the access of the drugs to their therapeutic targets.

administration of drugs directed exclusively against the mutated proteins, responsible for tumor proliferation, has meant an extraordinary advance in the therapy of neoplasia.

The pioneer in this new field of pharmacology was the advent of imatinib, an inhibitor of the tyrosine kinase (ITK) activity of the BCR-ABL fusion protein in chronic myeloid leukemia (CML), which contributes to an overall survival of 93%[2]. However, as a consequence of the pharmacological pressure exerted, new neoplastic clones with genetic variants resistant to said initial therapy may emerge. This concept is applicable to all the molecules introduced into the therapeutic arsenal of targeted drugs. Consequently, the molecular identification of these resistant-mutations, could allow alternative therapeutic strategies directed towards these new genetic variants.

In this regard, despite the very high percentages of remission achieved with this therapy in CML, it did not take long for a minority number of non-responders to arise, due to different mechanisms. Among them are the presence of ABC-t and the increase in the expression of BCR-ABL by leukemic cells, which necessitate administration of staggering doses culminating with only suboptimal therapeutic responses[3], and the appearance of cell clones with mutations in the BCR-ABL protein, which prevent the imatinib from taking effect and keep the activated tyrosine kinase intact[4].

Perhaps, the best example of how important this new modality of mutation detection and specific drug therapy is clearly described in CML. The appearance of different imatinib-resistant mutations in the *BCR-ABL* gene (L248V, F317L, G250E, H396R, M244V, T277A, F311I, M318T, Q252H, F359A, F359I, or Y326H) can be inhibited with second- and third-generation of ITKs drugs, such as dasatinib, nilotinib, and bosutinib[5]. Furthermore, the T315I mutation that confers resistance to imatinib and the second- and third-generation ITKs is sensitive to another ITK called ponatinib, allowing for the drug resistance in this leukemia to be overcome, and prolonging survival of the patients[6]. In addition, polymorphisms in the *MDR-1*/*ABCB1* gene, such as C3435T, may favor the overexpression of the transporter[7], which is associated with the poor prognosis with imatinib in CML[8].

All these mechanisms are not mutually exclusive and can simultaneously contribute to therapeutic failure with ITKs. More recently, the possible concomitance of mutations in the *JAK2* gene has been suggested, capable of activating the BCR-ABL clone, even under the pharmacological pressure of the corresponding ITK, and which requires the co-administration of a second ITK specific for JAK2[9,10].

3. Pharmacogenetics in cancer

The use of the molecular genetic methods that allows early detection of clones harboring driver mutations has achieved immediate and widespread in all aspects of clinical oncology, allowing the identification of a large number of mutations with pharmacological interest in most solid tumors. This also promotes the development of a wide spectrum of new therapeutic molecules directed at each of these genetic variants. Thus, this methodology allows early detection of tumor and enables informed decision-making in the selection of specific therapies that can control tumor growth, recurrence and metastatic progression. These stratagems of selective therapies only act on somatically mutated targets expressed in neoplastic cells, with no effect on normal cells. These developments ushered in the new era of the so-called personalized therapies, and more recently "precision medicine" in cancer. The new anti-cancer medications known as "targeted therapies" have emerged and aroused great interest in recent years. In this group of agents, there is a wide range of inhibitors of different tyrosine kinases or serine/threonine kinases, which are purportedly responsible for motorizing tumor growth, either by their stimulated (dependent) activation by extracellular growth factors, or by the presence of somatic mutations that activate said kinases in an independent manner on their corresponding growth factor. Several kinase inhibitors (KI) emerged as molecules with a high capacity to penetrate the active site of the kinase, preventing ATP access to that site, and thus inhibiting its tyrosine kinase activity with concentration values at the picomolar level[11-13].

The non-small cell lung cancer (NSCLC) affects almost 17% of Western patients that have an activating epidermal growth factor receptor (*EGFR*) gene mutation, with Del19 and L858R being the most common ones. These mutations are sensitive to ITK erlotinib (Tarceva; 60% response rate) or gefitinib (Iressa). However, a new clone carrying the drug-resistant *EGFR* T790M mutation emerges as a consequence of the pharmacological pressure exerted by first-line ITK treatment. Although there are drugs that specifically inhibit the second mutation, clear evidence has already emerged that various mechanisms of resistance activated by other or downstream signaling pathways, including RAS, RAF, and MAPK pathway[14].

Because the mutation of EGFR and KRAS are mutually exclusive, detection of *KRAS* mutations in patients with non-mutated *EGFR* could provide insights into other therapeutic options. In this regard, recently, the U.S. Food and Drug Administration (FDA) has approved sotorasib (AMG 510, Amgen), the covalent inhibitor on the more common *KRAS* mutant (G12C), for the treatment of NSCLC, and it is the first KRAS inhibitor to reach the market and enter clinical use[15].

The example provided by the first experience with imatinib and BCR-ABL allowed the development and rapid clinical use of new inhibitors of these mutated kinases to block different intracellular signals of proliferation, immortality, and metastasis present in different types of tumors, such as breast cancer, NSCLC, colon carcinoma, and melanoma. Many of these tumors proliferate at the expense of the stimulation produced by growth factors. However, the same tumors can also proliferate without the need for growth factor stimulation due to the presence of activating mutations of the proteins of the signaling cascades responsible for tumor growth (Figure 2).

The presence of sensitive mutations, which favor the insertion of ITKs in the active ATP binding site in the ATPase pocket of the enzyme, is a therapeutic opportunity that has significantly changed the prognosis and evolution of different types of tumors. Furthermore, analysis of circulating tumor DNA profiling has also enabled tracking of clonal variations in patients with colorectal carcinoma, assisting the monitoring of tumor progression and therapeutic resistance against EGFR blockade in real time[18].

On the other hand, the presence of mutations in the same gene but that modify its protein conformation, preventing the action of the corresponding ITKs mentioned above, makes it necessary to look for new second-line ITKs specific for this type of mutation, such is the case of sensitive and resistant mutations present in the *EGFR* in NSCLC. In these patients with NSCLC, a large number of different sensitive mutations but a smaller number of resistant mutations have been described[19,20].

To date, several EGFR tyrosine kinase inhibitors (TKIs) such as afatinib, erlotinib, gefitinib, and osimertinib have already been approved for first-line treatment of patients with advanced NSCLC harboring tumor growth driver mutations in *EGFR* gene. However, the correct indication of these drugs requires the identification of the corresponding sensitive and/or resistant mutations in this gene[21]. The most common sensitive mutations are deletions in exons 18, 19, and 21 (5%, 45%, and 45% of cases, respectively). Meanwhile, among the resistant mutations (5% of cases), the most frequent corresponds to the T790M mutation in exon 20, which can be treated with a specific ITK as second-line therapy. However, whether a significant number of mutations detected in *EGFR* gene are pharmacologically actionable remains to be explored[22].

The presence of these mutations necessitates personalized therapy with the corresponding ITK, but the

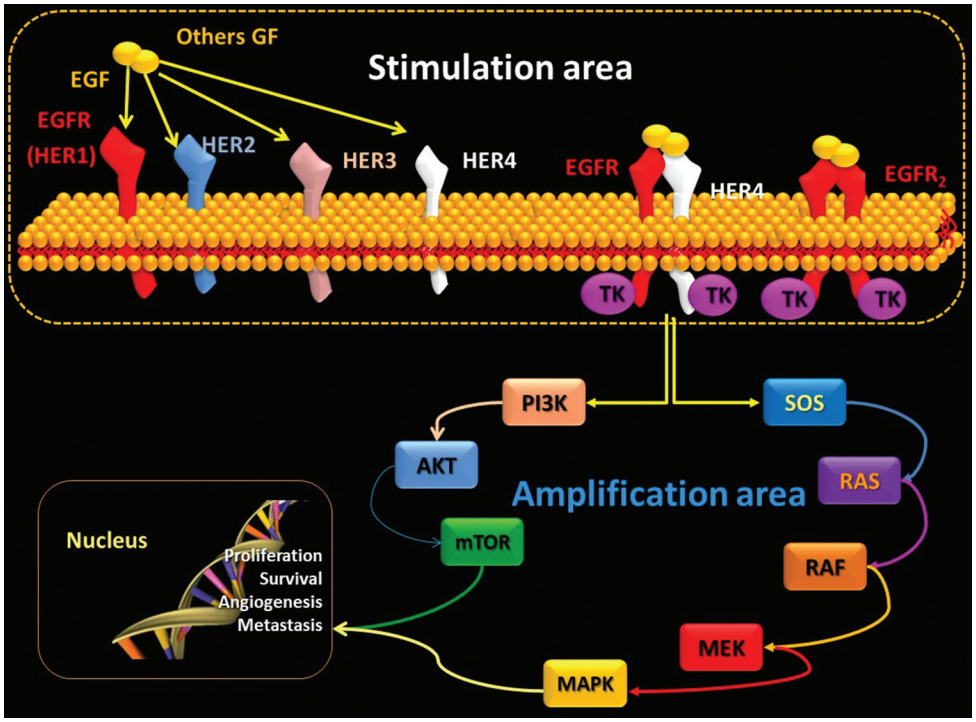

Figure 2. Schematic representation indicating how a growth factor stimulates its corresponding receptor, which contains an intrinsic tyrosine kinase (phosphorylated) in its intracytoplasmic domain and triggers a specific signal cascade, sequentially activating different proteins, until reaching the executing phase of the effect on the nucleus, activating cell proliferation[16,17]. Mutations found in the tyrosine kinases of growth factor receptors as well as on signaling pathway intermediaries are the entry points for therapy since they are sensitive to the action of first-line specific inhibitors. The presence of resistant mutations in the same tyrosine kinases forces the use of second- or third-generation drugs directed against said mutations. The identification and quantification of both types of somatic mutations, which are sensitive and resistant to first-line ITKs, are essential for identifying patients amenable to the treatment and assisting with the monitoring of tumor evolution.

presence of both types of sensitive and resistant mutations is an indication of the heterogeneity of the tumor population that may warrant joint treatment with both types of ITKs simultaneously. If this is the case, we are in the presence of two pharmaco genetically distinct populations, which occupy different percentages of the tumor mass. This duality can exist from the very moment of molecular diagnosis, or arise as a consequence of the pharmacological pressure exerted by treatment with first-line ITKs that will lead to gradual apoptosis in the cell clone carrying the sensitive mutation, giving place or biological space to the growth of the cell clone carrying the resistant mutation.

In the event that both the *EGFR* gene and its entire specific signaling cascade do not contain any somatic mutations that drive tumor growth, the therapeutic opportunity will lie in the use of monoclonal antibodies that inhibit and/or block growth factor binding with its specific receptor. Although it has not been possible to obtain positive results with this therapy in the case of NSCLC, it is usually effective in colon cancer[23,24].

Typically, in colon cancer, the *EGFR* gene does not have mutations of any kind, but mutated and activated tyrosine kinases are found downstream of the signaling pathway arising from EGFR. Thus, the mere presence of any of these mutations in the *KRAS* or *NRAS* genes prevents therapy with the aforementioned anti-EGFR monoclonal antibodies. This prompts the search for pharmacologically actionable mutations on other G proteins that are downstream of the KRAS/NRAS signaling, such as BRAF, MEK, and mTOR[25-27]. The therapy combining an anti-EGFR monoclonal antibody and an ITK directed at the tyrosine kinase mutations of the G-proteins has shown encouraging responses in colon cancer, even in the presence of *KRAS* mutations[28]. However, these strategies have failed to show any benefit in NSCLC with the same mutation background because the mutations in *KRAS*, *NRAS,* or *BRAF* (exclusive of each other) may drive the tumor growth, and they are genetic markers of drug resistance, which requires treatment with conventional chemotherapies[19,20]. It is also possible that we find EGFR gene mutations, whose biological and/or pharmacological action is unknown[22].

A particular situation arises in the case of the V600E mutation of the BRAF gene, where it was found that this

same mutation is good news for patients with melanoma, since it can be actionable with specific ITKs with very good results, but it becomes a biomarker of poor prognosis in colon cancer, where said ITKs have no effect[29]. Moreover, V600E is present in all hairy cell leukemia cases, serving as a marker of minimal residual disease of said hematological neoplasia[30]. The pharmacogenetic characterization of a tumor, from the very moment a biopsy sample is obtained and prior to the start of any treatment, makes it possible to obtain the so-called genetic fingerprint and identify its possible therapeutic targets. Given the large number of molecular variants described, high-throughput methodologies such as next-generation sequencing are the most appropriate tools for obtaining said fingerprint of each tumor, even from within each cell subclone of the same tumor[31,32]. In the aforementioned genetic footprint, we can, in turn, establish a biomarker map that provides us with different levels of information, such as tumor identity, aggressiveness, prognosis, drug sensitivity and resistance, and monitor its therapeutic evolution due to decay (sensitivity) of the initial clone, or its relapse due to the appearance of a clone with new escape mutations (resistance) to the pharmacological pressure exerted.

In turn, we must remember what was initially mentioned about the ABC-t. ITKs are substrates of ABC-t. A series of preclinical and clinical studies have shown that ABC-t can influence the bioavailability of several TKIs, modifying their pharmacokinetics and also playing a role in the development of resistance to this type of therapy, but that in turn, the ITKs can also inhibit ABC-t[33,34].

ABC-t gene polymorphisms can induce significant differences of therapeutic responses in the same pathology with the same TK mutations treated with the same ITK.

4. Liquid biopsy (LB), the ideal biomarker

Since the early report by Vietsch *et al.*, circulating tumor DNA and micro-RNA (later named as "LB") have been used as cancer diagnostic tools[35]. Today, there are more than 12,000 reports on LB on PubMed database.

The process searching for the ideal biomarker provides us with extensive information regarding the pathology of cancer. For this, the ideal biomarker must provide diagnostic, prognostic, and therapeutic information. The genesis and stability of the biomarker must reflect the kinetics of cancer evolution, and it should be quantitatively representative of tumor size or mass. In addition, its sampling must be accessible and repeatable without involving invasive, risky procedures on the patients. Importantly, the ideal biomarker must be highly sensitive and highly specific, surpassing the qualities seen in the classical clinical biochemical methods (Figure 3).

A great difficulty in the therapeutic follow-up of solid tumors is the limitation in repeatedly acquiring tissue biopsies from the same patient during the course of tumor evolution, especially if the site of tumor reappearance is clinically critical and there is no adequate access to it, or surgery acted on the tumor would leave serious sequelae or even put the patient in life-threatening situation.

A new biomarker concept known as "LB" can partially solve this dilemma. LB is a reflection of the genetic information possessed by all types of cells (normal and pathological) or generated by all tissues, and that is poured into the bloodstream and fluid in our body. Like all biological materials, it will have its elimination kinetics since it will be continuously degraded and replaced in the circulation as a result of the balance between production and elimination. The quantity, quality, and identity of this biological material provide an idea of its origin and clonality, and are proportional to the mass of the tissue that produces it. It can come from normal senescent cells, or from necrotic cells destroyed by the immune-macrophage system, and be detected as free circulating genetic material (microRNA, DNA, RNA)[36]. Genetic material may be presented in an encapsulated form within microvesicles, known as exosomes, actively secreted by both normal and tumor cells, which travel laden with adhesion molecules, enzymes, structural proteins, and specific genetic material [37] (Figure 4).

In addition, the circulating tumor cells (CTC) are part of the concept of liquid biopsy. CTC undoubtedly contain 100% of the genetic information of each tumor, but their presence is relatively rare in the circulation and it is extremely difficult to detect them. Together, all the circulating genetic material can be isolated, amplified, and properly deciphered, providing much of the information corresponding to the cells present in the tumor of origin.

LB provides very valuable information regarding the presence of somatic mutations that are pharmacologically actionable and mutations that are resistant to current available therapeutics. These genetic information can be used as a biomarker of minimal residual disease, and as a theranostics tool to evaluate therapeutic behavior, such as optimal, suboptimal, or null response. In addition, LB allows for early detection of tumor or its relapse of tumor harboring genetic variants resistant to the first treatment, even before the onset of clinical symptoms and/or its detection by imaging methods. This early detection reduces the risk of tumor evolution, improving the patient' life quality, and increase the event-free survival time. However, the main limitation of LB is that it cannot identify the site where the tumor is growing, or whether it is a primary or metastatic tumor.

Blood or other bodily fluids can be used in the early detection of information about a tumor that perhaps cannot yet be detected by imaging procedures. The high sensitivity of molecular detection methodologies allows LB to become the ideal tool for monitoring therapeutic responses. Since the circulating genetic material can be found as free form in plasma, cerebrospinal fluid, urine, pleural fluid, and ascites, or as RNA adhered to (protected by) the platelet membranes. Circulating genetic material may also be quantifiable. Thus, the "molecular charge" or number of copies of given genes detected by multiplex droplet digital polymerase chain reaction (ddPCR) procedure is proportional to the tumor mass that is producing it[38]. In this way, it is possible to verify the drop in the number of copies of sensitive mutations, but at the same time, detect resistant mutations after a period of treatment with first-line ITKs. Clearly, this simultaneous information gives us an idea of the degree of efficacy of the first treatment, and documents the presence of a tumor relapse at the expense of a change in the pharmacogenetic identity of the emerging clone of said tumor. These "mutational changes" produced in the original clone, largely to be expected after the pharmacological pressure is exerted, provide new therapeutic targets that can be acted upon with other second- or third-generation drugs in some cases. Thus, targeted therapy could be started long before the cancer is clinically evident or detected by imaging. In general, when the images appear, it is because there is an important tumor mass and often consistent with stages of dissemination.

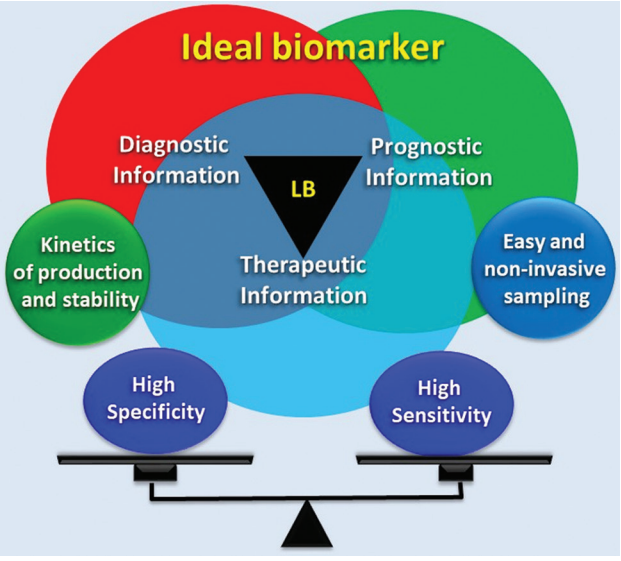

Figure 3. Liquid biopsy, implemented with droplet digital polymerase chain reaction, manifests the characteristics of an ideal biomarker. With high specificity and sensitivity, it can detect mutations of clonal lineage as well as sensitivity and resistance to treatment. The biomarker should be quantifiable, giving an idea of the magnitude of the tumor size, as well as serving as an indicator of minimal residual disease.

This property even makes it possible to verify the presence of metastasis in the central nervous system in cases of patients duly treated with first-line ITKs, where the original tumor is inactive, and is no longer releasing genetic material into the plasma, but as a consequence of the pharmacological pressure, sensitive mutations are still present in circulating DNA in the cerebrospinal fluid. Under this circumstance, the originally "sensitive" tumor managed to generate systemic metastases in different organs that can be abrogated by specific therapy, except those in the central nervous system since the access of the drugs is limited by the blood-brain barrier due to the high expression of the ABC-t of MDR. All positive results in the detection of one or several of these somatic mutations can identify and characterize a tumor constitute quantifiable markers, which can be used to detect minimal residual disease. Other important information is the presence of hypermethylated DNA fragments in CpG islands of promoter regions of tumor suppressor genes, such as *SEPT9* (colon cancer) or *SHOX2* (lung cancer). This type of epigenetic silencing, which inhibits tumor apoptosis, serves as an excellent marker of tumor lineage (Figure 5).

5. ddPCR applied to LB

At present, the latest ddPCR amplification techniques increases the sensitivity of detection, obtaining positive results even when the copy load of each of the mutations sought is extremely low. Under this circumstance, the tumor mass will be $<10^4$ cells, and the imaging studies will

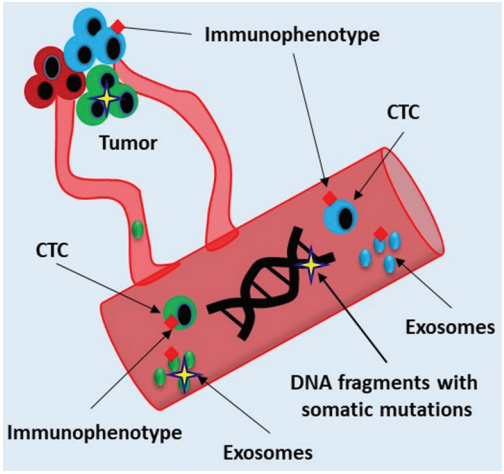

Figure 4. Every tumor usually presents a heterogeneous cell mass, and its genetic information will be present in the circulation. Circulating tumor cells, exosomes and different DNA fragments can be detected, quantified and identified according to the specific information they carry (i.e., immuophenotype and somatic mutations). The same information can be detected in virtually all bodily fluids. Furthermore, larger DNA fragments without specific genetic information are derived from cell turnover in normal tissues.

remain negative since they require around 10^9 cells to be clinically detectable, and the patient probably does not show clinical signs or symptoms of this incipient relapse. In this way, a positive LB result achieves a significant diagnostic anticipation of the presence of a primary tumor, and allows both monitoring of therapeutic efficacy and early detection of the emergence of resistant variants[39-41] (Figure 6). Today, LB is being applied to the detection of most tumors, and the use of gene panels provides extensive information on the genetic fingerprint of each tumor, with high levels of sensitivity and specificity.

In our experience, we have been able to show how a LB sample from a patient with NSCLC, which was positive for the L858R susceptibility mutation, became negative in the 1:125 dilution of the sample measured by real time PCR, but remained positive when the sample was processed by ddPCR in upto the 1:1250 dilution (Figure 7).

This difference in sensitivity allows very early detection of the presence of sensitive and/or resistant mutations, which have great value in anticipating the diagnosis of relapses and allows for informed decision-making regarding the early installation of therapies according to the detected mutations.

The combination of the use of LB and ddPCR results in a strategy of great diagnostic and prognostic value in the therapeutic monitoring of cancer with target drugs, and allows for the identification and quantification of biomarkers of minimal residual disease.

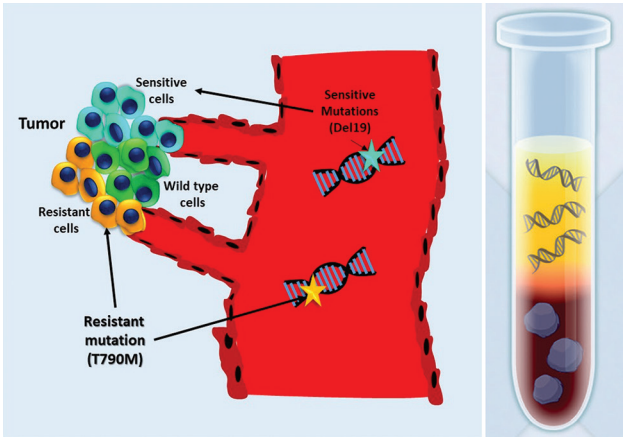

Figure 5. Non-small cell lung cancer. The tumor mass can be heterogeneous, containing a proportion of non-mutated cells (wild type), and another presenting a sensitive mutation, such as the deletion of exon 19 of the *EGFR* gene. Pharmacological pressure following first-line inhibitor of the tyrosine kinase treatment favors the appearance of clones harboring resistant mutations to this treatment, such as the T790M mutation. While the sensitive clone is disappearing, the resistant clone grows until a therapy with second- or third-generation TKIs specific for this tumor variant is started.

6. Strengths and limitations of LB

Due to the reproducibility, high sensitivity and high specificity of the method, LB constitutes a tool of great diagnostic and therapeutic indication value in cancer. Its main advantage is that it can be applied as many times as necessary, and that it can be quantifiable, serving as a parameter for monitoring the therapeutic evolution of a tumor, and for detecting its mutational changes that require modifications in the treatment strategy. In this way, it plays a role in the monitoring of minimal residual disease.

Furthermore, the advantage of using a highly sensitive molecular amplification methodology such as ddPCR significantly increases its sensitivity to detect the presence of tumors in advance compared to conventional techniques. Since it is a molecular biology procedure, the high specificity of the method lies in the design of the

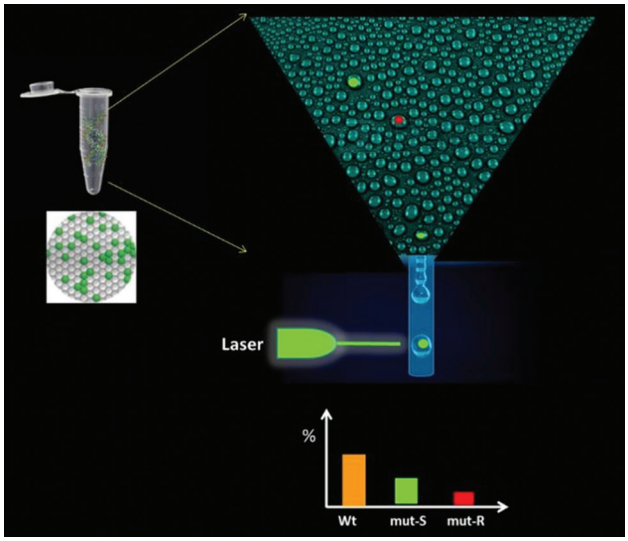

Figure 6. The working principle of droplet digital polymerase chain reaction (PCR) is based on the segmentation of samples using water-in-oil emulsion of the PCR mix to generates 20,000 microdroplets that contain all the components, e.g., genetic materials. After the corresponding cycles, microdroplets are read individually by a laser flow cytometry system, which can quantify mutation burden and sensitivity.

Sample dilution	Real time PCR	ddPCR
Not diluted	Positive	Positive
1:15	Positive	Positive
1:25	Positive	Positive
1:125	Negative	Positive
1:625	Negative	Positive
1:1250	Negative	Positive
1:3125	Negative	Negative

Figure 7. Comparative results of classical quantitative polymerase chain reaction (PCR) and droplet digital PCR.

primers to be used. Collectively, both diagnostic qualities strengthen the utility of liquid biopsy.

These advantages of LB and ddPCR indicate that their combination would provide the best tools in the precision medicine of cancer. However, the main limitation is that the LB cannot define the site of nesting and tumor growth.

7. Concluding remarks

Early detection of pharmacologically actionable somatic mutations by LB-ddPCR makes it possible to establish the corresponding therapy, regardless of the location of the tumor. This strategy allows for the detection of clonal changes that warrant therapeutic modifications, which is instrumental for controlling tumor growth without side effects, and improving the life quality and survival of cancer patients. Hence, LB is an ideal theranostic approach for cancer.

Acknowledgments

None.

Funding

None.

Conflict of interest

The authors have no conflict of interest.

Author contributions

Conceptualization: Verónica Alejandra Alonso
Writing – original draft: Alberto Lazarowski
Writing – review & editing: Alberto Lazarowski

Ethics approval and consent to participate

Not applicable.

Consent for publication

Not applicable.

Availability of data

Not applicable.

References

1. Juliano RL, Ling VA, 1976, Surface glycoprotein modulating drug permeability in Chinese hamster ovary cell mutants. *Biochim Biophys Acta*, 455: 152–162.

   https://doi.org/10.1016/0005-2736(76)90160-7

2. Sacha T, 2014, Imatinib in chronic myeloid leukemia: An overview. *Mediterr J Hematol Infect Dis*, 6: e2014007.

   https://doi.org/10.4084/mjhid.2014.007

3. Bianchini M, De Brasi C, Gargallo P, *et al*., 2009, Specific assessment of BCR-ABL transcript overexpression and imatinib resistance in chronic myeloid leukemia patients. *Eur J Haematol*, 82: 292–300.

   https://doi.org/10.1111/j.1600-0609.2008.01199.x

4. Pagnano KB, Bendit I, Boquimpani C, *et al*., 2015, BCR-ABL mutations in chronic myeloid leukemia treated with tyrosine kinase inhibitors and impact on survival. *Cancer Invest*, 33: 451–458.

   https://doi.org/10.3109/07357907.2015.1065499

5. Awidi A, Ababneh N, Magablah A, *et al*., 2012, ABL kinase domain mutations in patients with chronic myeloid leukemia in Jordan. *Genet Test Mol Biomarkers*, 16: 1317–1321.

   https://doi.org/10.1089/gtmb.2012.0147

6. Haddad FG, Issa GC, Jabbour E, *et al*., 2022, Ponatinib for the treatment of adult patients with resistant or intolerant Chronic-phase Chronic Myeloid Leukemia. *Expert Opin Pharmacother*, 23: 751–758.

   https://doi.org/10.1080/14656566.2022.2064742

7. Hoffmeyer S, Burk O, von Richter O, *et al*., 2000, Functional polymorphisms of the human multidrug-resistance gene: Multiple sequence variations and correlation of one allele with P-glycoprotein expression and activity *in vivo*. *Proc Natl Acad Sci U S A*, 97: 3473–3478.

   https://doi.org/10.1073/pnas.97.7.3473

8. Lardo M, Castro M, Moiraghi B, *et al*., 2015, MDR1/ABCB1 gene polymorphisms in patients with chronic myeloid leukemia. *Blood Res*, 50: 154–159.

   https://doi.org/10.5045/br.2015.50.3.154

9. Pieri L, Spolverini A, Scappini B, *et al*., 2011, Concomitant occurrence of BCR-ABL and JAK2V617F mutation. *Blood*, 118: 3445–3446.

   https://doi.org/10.1182/blood-2011-07-365007

10. Zhou A, Knoche EM, Engle EK, *et al*., 2015, Concomitant JAK2 V617F-positive polycythemia vera and BCR-ABL-positive chronic myelogenous leukemia treated with ruxolitinib and dasatinib. *Blood Cancer J*, 5: e351.

    https://doi.org/10.1038/bcj.2015.77

11. Fry DW, Kraker AJ, McMichael A, *et al*., 1994, A specific inhibitor of the epidermal growth factor receptor tyrosine kinase. *Science*, 265: 1093–1095.

    https://doi.org/10.1126/science.8066447

12. Ward WH, Cook PN, Slater AM, *et al*., 1994, Epidermal growth factor receptor tyrosine kinase. Investigation of catalytic mechanism, structure-based searching and discovery of a potent inhibitor. *Biochem Pharmacol*, 48: 659–666.

    https://doi.org/10.1016/0006-2952(94)90042-6

13. Osherov N, Levitzki A, 1994, Epidermal-growth-factor-dependent activation of the src-family kinases. *Eur J Biochem*, 225: 1047–1053.

https://doi.org/10.1111/j.1432-1033.1994.1047b.x

14. Laface C, Maselli FM, Santoro AN, *et al*., 2023, The resistance to EGFR-TKIs in non-small cell lung cancer: From molecular mechanisms to clinical application of new therapeutic strategies. *Pharmaceutics*, 15: 1604.

https://doi.org/10.3390/pharmaceutics15061604

15. Zhang SS, Nagasaka M, 2021, Spotlight on sotorasib (AMG 510) for KRAS G12C positive non-small cell lung cancer. *Lung Cancer* (*Auckl*), 12: 115–122.

https://doi.org/10.2147/lctt.s334623

16. Wee P, Wang Z, 2017, Epidermal growth factor receptor cell proliferation signaling pathways. *Cancers* (*Basel*), 9: 52.

https://doi.org/10.3390/cancers9050052

17. Miyamoto Y, Suyama K, Baba H, 2017, Recent advances in targeting the EGFR signaling pathway for the treatment of metastatic colorectal cancer. *Int J Mol Sci*, 18: 752.

https://doi.org/10.3390/ijms18040752

18. Ulz P, Belic J, Graf R, *et al*., 2016, Whole-genome plasma sequencing reveals focal amplifications as a driving force in metastatic prostate cancer. *Nat Commun*, 7: 12008.

https://doi.org/10.1038/ncomms12008

19. Yamaoka T, Ohba M, Ohmori T, 2017, Molecular-targeted therapies for epidermal growth factor receptor and its resistance mechanisms. *Int J Mol Sci*, 18: 2420.

https://doi.org/10.3390/ijms18112420

20. Sigismund S, Avanzato D, Lanzetti L, 2018, Emerging functions of the EGFR in cancer. *Mol Oncol*, 12: 3–20.

https://doi.org/10.1002/1878-0261.12155

21. An L, Wang Y, Wu G, *et al*., 2023, Defining the sensitivity landscape of EGFR variants to tyrosine kinase inhibitors. *Transl Res*, 255: 14–25.

https://doi.org/10.1016/j.trsl.2022.11.002

22. Hasenahuer MA, Parisi G, Gautier M, *et al*., 2015, Twenty-one novel EGFR kinase domain variants in patients with nonsmall cell lung cancer. *Ann Hum Genet*, 79: 385–393.

https://doi.org/10.1111/ahg.12127

23. Chen D, Li L, Zhang X, *et al*., 2018, FOLFOX plus anti-epidermal growth factor receptor (EGFR) monoclonal antibody (mAb) is an effective first-line treatment for patients with RAS-wild left-sided metastatic colorectal cancer: A meta-analysis. *Medicine* (*Baltimore*), 97: e0097.

https://doi.org/10.1097/MD.0000000000010097

24. Matsuhashi N, Takahashi T, Matsui S, *et al*., 2018, A novel therapeutic strategy of personalized medicine based on anti-epidermal growth factor receptor monoclonal antibodies in patients with metastatic colorectal cancer. *Int J Oncol*, 52: 1391–1400.

https://doi.org/10.3892/ijo.2018.4322

25. Gazdar AF, Minna JD, 2005, Inhibition of EGFR signaling: All mutations are not created equal. *PLoS Med*, 2: e377.

https://doi.org/10.1371/journal.pmed.0020377

26. Shigematsu H, Gazdar AF, 2006, Somatic mutations of epidermal growth factor receptor signaling pathway in lung cancers. *Int J Cancer*, 118: 257–262.

https://doi.org/10.1002/ijc.21496

27. Sanders HR, Albitar M, 2010, Somatic mutations of signaling genes in non-small-cell lung cancer. *Cancer Genet Cytogenet*, 203: 7–15.

https://doi.org/10.1016/j.cancergencyto.2010.07.134

28. Mésange P, Bouygues A, Ferrand N, *et al*., 2018, Combinations of bevacizumab and erlotinib show activity in colorectal cancer independent of RAS status. *Clin Cancer Res*, 24: 2548–2558.

https://doi.org/10.1158/1078-0432.ccr-17-3187

29. Dankner M, Rose AA, Rajkumar S, *et al*., 2018, Classifying BRAF alterations in cancer: New rational therapeutic strategies for actionable mutations. *Oncogene*, 37: 3183–3199.

https://doi.org/10.1038/s41388-018-0171-x

30. Maitre E, Bertrand P, Maingonnat C, *et al*., 2018, New generation sequencing of targeted genes in the classical and the variant form of hairy cell leukemia highlights mutations in epigenetic regulation genes. *Oncotarget*, 9: 28866–28876.

https://doi.org/10.18632/oncotarget.25601

31. Kamps R, Brandão RD, van den Bosch BJ, *et al*., 2017, Next-generation sequencing in oncology: Genetic diagnosis, risk prediction and cancer classification. *Int J Mol Sci*, 18: 308.

https://doi.org/10.3390/ijms18020308

32. Lehmann-Che J, Poirot B, Boyer JC, *et al*., 2017, Cancer genomics guide clinical practice in personalized medicine. *Therapie*, 72: 439–451.

https://doi.org/10.1016/j.therap.2016.09.015

33. Galetti M, Petronini PG, Fumarola C, *et al*., 2015, Effect of ABCG2/BCRP expression on efflux and uptake of gefitinib in NSCLC cell lines. *PLoS One*, 10: e0141795.

https://doi.org/10.1371/journal.pone.0141795

34. Shukla S, Patel A, Ambudkar SV, 2016, Mechanistic and pharmacological insights into modulation of ABC drug transporters by tyrosine kinase inhibitors. In: George AM, editor. ABC Transporters-40 Years On. Switzerland: Springer International Publishing, p227.

35. Vietsch EE, van Eijck CH, Wellstein A, 2015, Circulating

DNA and micro-RNA in patients with pancreatic cancer. *Pancreat Disord Ther*, 5: 156.

https://doi.org/10.4172/2165-7092.1000156

36. Azad AA, Volik SV, Wyatt AW, *et al*., 2015, Androgen receptor gene aberrations in circulating cell-free DNA: Biomarkers of therapeutic resistance in castration-resistant prostate cancer. *Clin Cancer Res*, 21: 2315–2324.

https://doi.org/10.1158/1078-0432.CCR-14-2666

37. Heitzer E, Perakis S, Geigl JB, *et al*., 2017, The potential of liquid biopsies for the early detection of cancer. *NPJ Precis Oncol*, 1: 36.

https://doi.org/10.1038/s41698-017-0039-5

38. De Kock R, van den Borne B, Youssef-El Soud M, *et al*., 2021, Therapy monitoring of EGFR-positive non-small-cell lung cancer patients using ddPCR multiplex assays. *J Mol Diagn*, 23: 495–505.

https://doi.org/10.1016/j.jmoldx.2021.01.003

39. Rolfo C, Castiglia M, Hong D, *et al*., 2014, Liquid biopsies in lung cancer: The new ambrosia of researchers. *Biochim Biophys Acta*, 1846: 539–546.

https://doi.org/10.1016/j.bbcan.2014.10.001

40. Diaz LA Jr., Bardelli A, 2014, Liquid biopsies: Genotyping circulating tumor DNA. *J Clin Oncol*, 32: 579–586.

https://doi.org/10.1200/jco.2012.45.2011

41. Montagut C, Argilés G, Ciardiello F, *et al*., 2018, Efficacy of Sym004 in patients with metastatic colorectal cancer with acquired resistance to anti-EGFR therapy and molecularly selected by circulating tumor DNA analyses: A phase 2 randomized clinical trial. *JAMA Oncol*, 4: e175245.

https://doi.org/10.1001/jamaoncol.2017.5245

ACCSCIENCE PUBLISHING

INNOSC Theranostics and Pharmacological Sciences

REVIEW ARTICLE

Guidelines for treating spinal cord injury without radiological abnormalities in children

Ruba Altahla[1], Jamal Alshorman[2], and Xu Tao[1]*

[1]Department of Rehabilitation, Tongji Hospital, Tongji Medical College, Huazhong University of Science and Technology, Wuhan, China

[2]Department of Orthopedics, Union Hospital, Tongji Medical College, Huazhong University of Science and Technology, Wuhan, China

Abstract

Spinal cord injury without radiological abnormality (SCIWORA) is a rare condition that predominantly affects children. The enigmatic nature of SCIWORA poses significant challenges in terms of diagnosis, treatment, and achieving full recovery. Various factors, such as different injury mechanisms, delayed symptom onset, normal magnetic resonance imaging findings in certain cases, and complex management decisions, contribute to the challenges of dealing with SCIWORA. Attaining a significant outcome and complete recovery through a single-treatment approach is difficult. Therefore, a multifaceted treatment strategy is proposed to yield more favorable results. This paper comprehensively addresses the assessment and management, examination and diagnosis procedures, treatment methods, rehabilitation techniques, and potential complications associated with SCIWORA in children. The paper provides therapeutic guidance for physicians and medical staff, with the aim of enhancing survival rates and improving recovery outcomes. Moreover, it offers suggestions for restoring neurological functions in pediatric patients suffering from SCIWORA.

Keywords: Spinal cord injury without radiological abnormality; Pediatrics; Magnetic resonance imaging; Surgery; Therapeutic treatment; Rehabilitation

***Corresponding author:**
Xu Tao
(i202122089@hust.edu.cn)

Citation: Altahla R, Alshorman J and Tao X, 2024, Guidelines for treating spinal cord injury without radiological abnormalities in children. *INNOSC Theranostics and Pharmacological Sciences*, 7(1): 1386. https://doi.org/10.36922/itps.1386

Received: July 27, 2023

Accepted: September 6, 2023

Published Online: October 13, 2023

1. Introduction

The original description of spinal cord injury without radiological abnormality (SCIWORA) was first published in 1982[1]. SCIWORA is a rare disease that primarily affects children but also occurs in adults, with a higher prevalence in children due to anatomical differences and the mechanism of injury (MOI). In children outside of China, 75% of spinal cord injuries (SCIs) are attributed to violent trauma, such as sports-related injuries, child abuse, motor vehicle accidents, falls, and diving accidents. Conversely, in China, 50% of cases result from nonviolent trauma during dance training, particularly related to backbend movements[2]. The underlying mechanism of SCIWORA in children is complicated and differs from that in adults[3]. The biomechanics of the pediatric spine plays an important role in this condition. Compared to adults, the higher elasticity of the children's spine increases the risk of developing SCIWORA. Factors such as flexion, hyperextension, longitudinal distraction, and ischemia can contribute to SCIWORA in

children. When children engage in repetitive backbend movements, dynamic compression of the spinal vessel, and longitudinal traction of the spine during sustained or repeated hyperextension play critical roles in the onset of SCIWORA. Magnetic resonance imaging (MRI) serves as the gold standard for diagnosis and prognosis evaluation, although it may initially show a normal appearance. In addition, the symptoms of SCIWORA can exhibit delayed onset, and there is a possibility of recurrence[4,5]. Education and awareness are imperative for accurate diagnosis, treatment, prevention, and mitigation of further neurological function deterioration. Timely management of SCIWORA is essential to prevent secondary injury. At the same time, treatment decisions and management should be tailored on a case-by-case basis[6]. This article aims to provide essential insights into SCIWORA in children, assisting practitioners in achieving precise diagnoses and significant prognoses.

2. MOI

The pediatric spine exhibits significant differences from the adult spine, rendering the spinal cord susceptible to injury due to factors such as flexion, hyperextension, longitudinal distraction, and ischemia. The MOI underlying SCIWORA remains unclear, as some patients initially present with normal MRI findings. SCIWORA can be categorized based on the cause of injury:

i. SCIWORA caused by violent trauma (motor vehicle accidents and sports-related incidents), which has been reported by many researchers
ii. SCIWORA caused by minor trauma.
iii. Many children engage in backbend movement (repetitive hyperextension of the spine) during dance training (Figure 1). This practice is common Chinese dance training and bears similarities to movements commonly performed during surfing. Some children suffer non-traumatic SCIWORA, necessitating differential diagnosis to rule out conditions such as arteriovenous malformation, multiple sclerosis, acute transverse myelitis, acute disseminated encephalomyelitis, infarction, intramedullary neoplasms, and myelin oligodendrocyte glycoprotein antibody-associated disease[2,7-9]. External forces acting on the pediatric spinal column often do not result in fractures but instead cause elongation, gliding, and vertebral slippage. Longitudinal traction of the spine leads to violent distraction of the spinal cord, causing nerve fiber rupture[10]. Simultaneously, sustained or repeated hyperextension of the spine during dance training can lead to dynamic compression of the spinal vessel, resulting in vascular injury, venous hypertension, and venous congestion, ultimately leading to spinal cord ischemic injury. At present, the MOI following sustained or repeated hyperextension of the spine is believed to be caused by spinal cord ischemic injury, which exhibits similarities to a surfer's myelopathy.

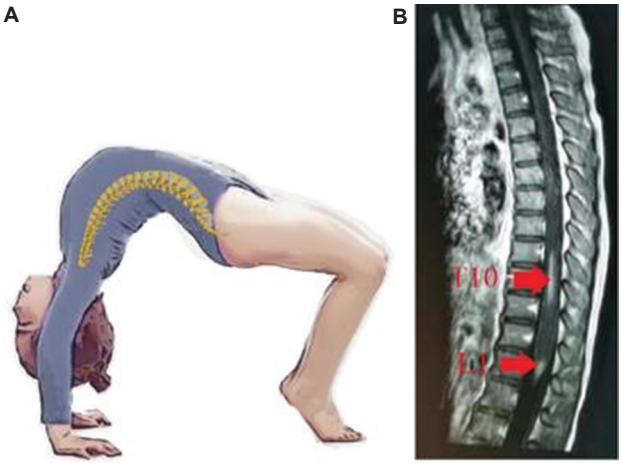

Figure 1. Backbend movement. (A) Children's hyperextension and spine shape; (B) spinal cord injury at T9 – T10, involving transient slippage of the apical vertebral body and facet joints, lateral compression injury of the spinal cord by the anterior and posterior ligaments, excessive longitudinal traction injury concentrated at the junction of the cauda equina and conus (similar to the different mechanics of the tendon-muscle body), and interfacial stretch injury.

3. Assessment and management

Managing SCIWORA in children, especially those aged ≤8 years old, poses several challenges[11]. SCIWORA encompasses traumatic myelopathy, a condition not associated with visible vertebral fractures or ligamentous abnormalities on ordinary radiographs and computed tomography (CT) scans, with some cases even presenting normal MRI findings[4,5,12]. These distinct case profiles exhibit significant variations in their presentation, medical management, and final neurologic outcome[13]. In the early period following onset, SCIWORA patients should undergo a neurological examination to assess sensorimotor functions and determine the appropriate treatment method. The American Spinal Injury Association Impairment Scale (ASIA) is recommended for evaluating their quality of daily life. ASIA is widely used as a quantitative diagnostic classification tool for neurological assessment post-SCI[14,15]. Early identification and evaluation of neurological deficits facilitate a deeper understanding and early intervention of each case[16]. Neurological deficits tend to worsen progressively and should be subject to repeated evaluations. The neurological dysfunctions typically reach their nadir after 8 – 24 h. Therefore, a case-by-case evaluation is essential before initiating SCIWORA management[17]. The evaluation of these cases goes beyond the ABCs of resuscitation[18].

4. Imaging examination

Accurate imaging is vital for diagnosing SCIWORA in children. This section explores imaging techniques and their role in diagnosis and management.

i. X-ray imaging: The essential steps involve performing anterior-posterior, lateral view, and open-mouth X-rays. While X-ray imaging shows the alignment of the spinal column, it may not be sufficient for detecting many pathological changes in cases of SCIWORA.

ii. CT scans serve as the gold standard for evaluating and screening spine fractures, offering superior sensitivity and specificity in detecting bone abnormalities[19]. They offer enhanced and accurate details for identifying fracture types and bony abnormalities[20]. The use of multi-detector CT not only improves precision but also accelerates imaging compared to older CT technologies, making it an effective method for detecting vertebral fractures[21]. In addition, axial and 3D views in the CT scans are valuable tools for illustrating spinal canal shape, assessing facet joint stability, and distinguishing small, hidden lesions that may not be apparent on X-ray images[22,23].

iii. MRI becomes a routine examination when X-ray and CT results are normal, and it is the preferred method for determining the integrity, location, severity, and involvement of structures such as the intervertebral disk, ligaments, cauda equina, and nerve roots[24,25]. The T2-MRI signal allows for differentiation between edema, contusion, or ischemia (high signal) and hemorrhage (low signal), making the T2-MRI image the most valuable diagnostic tool for SCIWORA diagnosis[26,27]. Moreover, it is essential not to restrict MRI to a single vertebral level[28]. MRI stands as the best choice for assessing the severity of SCIWORA, and it is important to perform MRI examinations at every follow-up visit[29]. In addition, performing follow-up MRIs can reveal dynamic pathological changes in the spinal cord. Examining the entire spine can be particularly helpful in identifying soft-tissue injuries and micropathological abnormalities. Early MRI scans offer some advantages, especially in cases of severe injury, that may reveal pathological changes[30]. The extent of edema on MRI is not consistent with neurological injury level. In certain cases, features of spinal cord abnormalities may only become apparent on MRI after 1 – 2 days[31]. The timing of MRI scans has proven to be critical; serial scans can detect active intramedullary and extramedullary lesions and signal variations, or previously undetected anomalies. MRI is capable of revealing transaction, contusive hemorrhage, traumatic edema, and concussion[32]. Many cases of SCIWORA showed no abnormalities on MRI, leading to their classification as "real SCIWORA"[9,13,28]. The "real SCIWORA" syndrome is a condition that necessitates a complete spinal MRI to rule out structural and potentially dangerous causes of neurologic dysfunction[33]. Furthermore, various quantitative MRI techniques, including diffusion tensor imaging (DTI), can indicate micropathological changes in white matter (WM) by observing the diffusion direction and distribution of water molecules. More precisely, DTI provides an evaluation of injury severity, location, and classification[34-38]. However, to confirm a SCIWORA diagnosis, it is essential to conduct multiple MRI examinations or incorporate other imaging techniques, such as MRA.

5. Diagnosis

The diagnosis of SCIWORA should be based on an evaluation of the patient's symptoms and, subsequently, an assessment of the stability of the bony structures, with the exclusion of fractures, dislocations, soft-tissue injuries, and micropathological changes as revealed by MRI scans. It is imperative to differentiate SCIWORA from other potential conditions such as arteriovenous malformation, multiple sclerosis, acute transverse myelitis, acute disseminated encephalomyelitis, infarction, and intramedullary neoplasms during the diagnostic process. The severity of SCIs is currently categorized based on the ASIA grading system and MRI findings[39-41]. The ASIA grades are as follows:

i. Grade A: Complete loss of motor and sensory function below the injury site.

ii. Grade B: Sensory incomplete injury, where neither sensory nor motor function is maintained below the injury level or on either side of the body, and no motor function is preserved for more than three levels below the injury site.

iii. Grade C: Motor incomplete injury, characterized by preserved motor function below the injury level, with more than half of key muscle functions graded at <3 at a single level below the injury.

iv. Grade D: Motor incomplete injury, which is similar to grade C but involves a higher degree of preserved key muscle function, with muscle grades exceeding three.

v. Grade E: A return to normal function, where all sensory and motor function segments are classified as normal in a patient who previously exhibited deficits.

However, it is important to note that there are limitations in applying the ASIA classification system to young children, and accurately assessing the severity and ASIA grade of SCI in pediatric patients is difficult. Therefore, repeated assessments of neurological function are important. Moreover, a 72-h examination provides a more accurate prediction of outcomes in patients with

motor complete injuries (Grades A and B)[42]. The MRI features help to classify the severity of the injury, as they can reveal various conditions, including normal appearance, edema, hemorrhage, soft-tissue injury, or contusion[9]. Moreover, repetitive MRI examinations can reveal distinct pathological changes, even in cases where the initial MRI appears normal, which is attributed to the strength of the external forces. Notably, during the acute stage, diagnosing spinal shock can be challenging. Therefore, the utilization of DTI and diffusion tensor tractography (DTT) may provide a more accurate diagnosis[43].

6. Treatment

SCIWORA patients with complete neurological deficits often experience poor recovery in their neurological function. It is essential to consider the developmental changes that children undergo and to provide appropriate care as they mature. It is essential to consider the developmental changes that children undergo and to provide appropriate care as they mature. Treatment for SCIWORA varies according to the patient's MRI findings and ASIA grade[44]. Whether surgical or non-surgical, the primary objective remains the prevention of secondary injuries and the achievement of a favorable prognosis[45]. Surgery becomes necessary if the spine is unstable or if symptoms deteriorate during conservative treatment. The treatment approach for SCIWORA should be individualized, taking into account the unique circumstances of each case[46]. Treatment options for SCIWORA include immobilization, surgical decompression, pharmaceutical therapy, early rehabilitation, preventive measures, and post-treatment care[39,47-52].

6.1. Pre-hospital aid

Appropriate and accurate pre-hospital medical attention is critical in managing SCIWORA, as it significantly contributes to lowering mortality and improving overall patient prognosis. Achieving early diagnosis and developing more effective treatment strategies for SCIWORA necessitate the close collaboration of a multidisciplinary team of healthcare professionals[53]. Multiple medical teams, including emergency medical technicians, paramedics, orthopedic specialists, emergency physicians, neurosurgeons, general surgeons, intensive care unit personnel, radiologists, neurologists, and anesthesiologists, must work in concert to address the complex nature of SCIWORA cases[54]. Given the lack of precise scientific data supporting standardized treatment protocols, therapeutic decisions should be tailored to individual patient needs and should involve a multidisciplinary team of experts[55]. The implementation of transfer and pre-hospital care guidelines for SCIWORA is essential and should be universally adopted across all health-care facilities[56,57].

After a spinal cord injury, paramedic staff should promptly assess the patient's condition and immobilize the patient to prevent further movement of the head and the entire spine, thus reducing the risk of secondary injury[9,18,58-60]. Health-care teams must be cautious when obtaining the medical history of SCIWORA patients. Moreover, it is crucial to show care and attention during intra-hospital transfers within a single institution to minimize the risk of adverse events during the transfer procedure[61,62]. Effective communication between emergency services and the treatment facility is essential. Absolute cooperation between multiple disciplines not only safeguards the patient from further SCI but also expedites diagnosis and facilitates better treatment decisions[63-65].

6.2. Conservative treatment

Once the diagnosis of SCIWORA and the assessment of injury severity have been established, it is essential to monitor the patient's vital signs to ensure stability. Conservative treatment, characterized by the avoidance of surgery and reliance on non-operative treatments, is always the first choice, and surgical intervention is considered the last option. However, in emergency situations, surgical intervention may become necessary. Moreover, if symptoms worsen during conservative treatment and the patient's stability is compromised, alternative treatment options must be considered. Notably, some patients respond well to conservative treatment, achieving significant improvements[9,66,67]. Conversely, there are cases where conservative treatment does not yield any improvement[18,27,68].

6.3. Pharmaceutical therapy

Methylprednisolone (MP) therapy has shown potential for improvement and favorable clinical outcomes in some cases[13,32,69-71]. However, recent studies have reported poor prognoses associated with MP treatment[25,58,72-75]. Since 2013, the American Association of Neurosurgeons and the Congress of Neurological Surgeons guidelines no longer recommend the use of MP. In 2017, AOSpine recommended MP as a treatment option for patients within 8 h of acute SCI. Notably, in pediatric patients with acute SCI, high-dose MP administered within the first 8 h failed to show any advantages but showed an increase in incidences of pneumonia and other complications such as osteoporosis and femur head necrosis, especially in intensive care unit cases[76,77]. However, certain forms of SCIWORA (e.g., surfer's myelopathy and acute hyperextension SCI) result from ischemic insults to the spinal cord, and there is no place for the use of steroids or other drugs such as Ganglioside (GM), in the treatment of these patients.

Furthermore, there is a lack of evidence supporting the use of drugs in the treatment of SCIWORA in children.

6.3.1. Considerations for determining drug dosage

The determination of drug dosage should take into account the following criteria:

i. Age of the children
ii. If the child's age, weight, and vital signs are stable, ensure open communication with the child's family regarding the potential risks associated with the use of these drugs
iii. For intravenous (IV) drug therapy, consider factors such as infusion rate, body weight, dosage, initial IV dose, and maintenance infusion rate before administering MP
iv. To minimize the risk of complications, discontinue MP as soon as previous neurological issues have been resolved
v. Ideally, pharmaceutical therapy should commence within the first 8 h after the injury, but it can be considered up to 24 h post-injury[76,78]
vi. Contraindications for MP use include patients at risk of pneumonia, diabetes patients, those with gastrointestinal abnormalities, a time gap of more than 24 h since injury, complete SCI, open injuries associated with SCI, and cases where operative treatment is indicated.

6.4. Immobilization

Immobilization serves as the first step in the treatment of SCIWORA, with removal following injury stabilization[74]. Immediate immobilization at the accident scene should be maintained until a comprehensive assessment of the child can be conducted. The practice is essential for preventing further damage and risky activities[79,80]. External immobilization is recommended for a duration of up to 12 weeks. Moreover, early discontinuation is suggested for asymptomatic patients with confirmed spinal stability[81]. Early immobilization is associated with a favorable prognosis. However, cervical spine immobilization is complicated due to its intrinsic elastic characteristics. Furthermore, the inherent limitations of the cervical collar (allowing some degree of rotation leading to incomplete stability) and potential risks associated with the use of the halo vest (infection, pin loosening, and psychological effects) are all crucial points to consider[41]. The benefit of rigid immobilization is unproven in the case of strictly normal MRI[82].

6.4.1. Points to consider in immobilization following points

i. Initiate early immobilization, perform extrication, provide initial resuscitation, and arrange for evacuation to a trauma facility capable of diagnosing and treating the patient
ii. Maintain immobilization until the patient becomes asymptomatic
iii. Discontinue cervical immobilization if an MRI conducted within 48 h of injury reveals no pathological changes
iv. In cases associated with atlanto-occipital ligamentous injuries, consider recommending halo vest immobilization or occipitocervical stabilization and fusion.

6.5. Surgery

Non-operative treatment is always the first choice for SCIWORA, especially in cases of stable spine injuries. Surgical intervention becomes an option if conservative therapy fails or if the injury is unstable. However, in cases of progressive neurologic deterioration with or without spinal cord compartment syndrome or spinal cord intramedullary hypertension during conservative treatment, as well as in instances involving cord compression due to a hematoma, extruded disk, bony fragment, or unreduced dislocation, immediate surgical intervention is required to achieve a favorable recovery. Surgical intervention, when indicated in SCIWORA cases, has been shown to be safe and associated with significant positive outcomes, especially when performed promptly after the onset[47,49,75]. When the thoracolumbar injury classification and severity score (TLICS) is <3, conservative treatment is generally suitable. However, when the score reaches 4 points, the decision may lean toward operative or non-operative treatment. Moreover, the TLICS system provides guidance for surgical treatment decisions in patients with a TLICS score of 5 or higher[83,84].

6.5.1. Novel surgical approaches

Non-fusion laminectomy, followed by immobilization, has shown promise in significantly improving outcomes in children while reducing complications related to the growth scales[85]. However, it can have adverse effects on children's growth, potentially leading to spine misalignment and internal fixator loosening. Laminectomy is a procedure that can alleviate pressure on the spinal cord. However, minimizing muscle dissection and reducing the number of vertebrae involved in the laminectomy can enhance post-operative stability. In an effort to mitigate the complications associated with other treatment methods and achieve significant results, cerebrospinal fluid lumbar drainage has been considered as a potential treatment choice. It is essential to exercise caution when using this approach, and further clinical studies are required to establish its effectiveness[86].

6.6. Treatment decision

The treatment decision for SCIWORA in children is complex as it depends on various key factors, including:

i. Age of the child
ii. Severity of the injury
iii. Time of symptoms onset
iv. ASIA grade at the time of admission
v. Symptoms deterioration
vi. Patient stability and associated injuries
vii. Presence of deformity or other spine-affecting diseases
viii. MOI
ix. Number of affected segments
x. Presence of intradural, extradural, or both
xi. Appearance of edema, hematoma, or both.

6.7. Rehabilitation procedure

Rehabilitation techniques are designed to avoid secondary effects, promote neurological recovery, and improve motor function. Once injury stabilization has been achieved, the focus of rehabilitation shifts to preventing secondary complications. In SCI patients, it is crucial to consider the physical, neurological, emotional, and psychological changes that arise during childhood and early adolescence. This holistic approach, often referred to as the "medical home," is the most important and critical factor in the management of SCI[87]. The ultimate goals of recovery are as follows: (i) Strengthening everyday independent life practices; (ii) facilitating adaptation to a new way of life through recreational activities and household events; and (iii) supporting reintegration into the children's environment[88]. Home-based interventions during rehabilitation therapy have proven effective in promoting the development of motor functions[89,90]. Following a SCI, extensive practice, including over-ground practice, results in significant recovery[91]. In pediatric rehabilitation, numerous tools are available, but some present disadvantages, particularly in young children. Achieving optimal recovery can be challenging, as it often requires a significant amount of space for assessment. In addition, item-based tasks can be time-consuming, and certain trials may not be appropriate, especially for young children[92]. Initiating early rehabilitation training following the selected treatment method can help reduce the incidence of pressure sores, deep vein thrombosis (DVT), and other complications. This approach can also lead to a better prognosis and improved outcomes[93]. Spasticity following SCI is a motor disorder characterized by increased muscle tone with exaggerated tendon jerks. Some medications, such as tizanidine, can cause hypotension and bradycardia, while *Clostridium botulinum* works as a neuromuscular blocker. If the patient does not exhibit any changes, it is important to consider the secondary complications of SCI, such as DVT, fractures, gastric ulcers, heterotopic ossification, or syringomyelia. To prevent these complications, it is advisable to use the lowest spasticity medication that is effective, ensure the patient stays warm, and be mindful of cold weather conditions[15,94].

6.8. Complications of SCI in children

Complications resulting from SCI in younger children differ from those in adolescents and adults, necessitating early prevention and intervention. Among younger children with SCI, 96% developed scoliosis, 57% had hip dysplasia, and 7% exhibited a latex allergy. In cases where injuries were at or above the T6 level, 34% experienced autonomic dysreflexia, 41% developed pressure ulcers, and 61% suffered from spasticity, particularly in the absence of bowel or bladder control. Notably, 82% were on intermittent catheterization, and 69% were on a bowel program. Additional complications include hyperhidrosis, kidney stones, ambulation, wheelchair dependence, lifelong growth and developmental issues, and various secondary complications, such as decreased bone density, increased risk of fracture, muscle atrophy, and cardiovascular impairments, all of which may arise from SCI[29]. Complications such as pulmonary compromise, pneumonia, urinary tract infection, gastrointestinal bleeding secondary to stress ulcers, DVT, decubitus ulcers, and even the risk of death pose significant challenges in the treatment of children with thoracic and lumbar spinal cord lesions[95]. Preventing DVT is helpful in reducing patient mortality and the risk of pulmonary embolisms. Moreover, the early elevation of the patient's head of the bed is essential to prevent various respiratory-related complications. These complications should be viewed as risks of SCI, emphasizing the need for early prevention and intervention throughout the rehabilitation process.

6.9. Traditional Chinese medicine (TCM)

TCM is an important supplementary treatment in potentially repairing injured spinal cords. Early implementation of TCM therapy has demonstrated effectiveness in improving motor function in SCI patients[96]. Six active natural compounds found in herbs commonly used in TCM exhibit anti-inflammatory and antioxidant properties. These compounds have been shown to significantly reduce bleeding, edema, and necrotic tissue in the damaged area[97]. Consequently, TCM can serve as an auxiliary therapy to promote functional recovery following SCI[98].

6.10. Post-treatment suggestions

Delays in symptom presentation and the potential for recurrence pose significant risks in SCIWORA cases, and nursing management should be vigilant in this regard[99]. To

mitigate the risk of disease recurrence, patients are advised to avoid physical activities during the first 6 months post-treatment[81,100]. In cases of asymptomatic craniocervical arterial dissection, the use of aspirin, clopidogrel, or other antithrombotic agent for 3 to 6 months is recommended as first-line therapy. Furthermore, if symptoms progress, consideration may be given to anticoagulation therapy (using low-molecular-weight heparin or warfarin). It is important to note that these medical therapies carry an increased risk of hemorrhage[39]. In addition, conducting post-operative CT and MRI on the 2nd day following treatment can help assess treatment complications, monitor the patient's progress, and evaluate the stability of the injury[101].

7. Prognosis

Differences in the MOI present significant challenges in the diagnosis, treatment, and prognosis of SCIWORA. SCIWORA can be devastating. According to the previous reports, early improvement within the first 24 – 72 h of presentation has been observed in some patients. Children who experience minor trauma, have incomplete injuries, or remain stable throughout treatment can achieve full recovery. In contrast, the prognosis for patients with complete injuries, instability, or worsening symptoms depends on factors such as the treatment method, treatment time, and the severity of injury. Moreover, the presence of spinal cord disruption or major hemorrhage on MRI in cases of severe neurologic deficit is associated with a poor prognosis. Conversely, mild SCIWORA (spinal cord concussion) usually results in full recovery, and a normal MRI appearance is indicative of a favorable prognosis[81]. The use of DTI and DTT to categorize SCI can help in determining the severity, prognosis, and optimizing diagnosis by detecting microscopic pathological changes in the WM[34,43,93]. The prognosis in cases of SCIWORA depends on the child's age, injury location, neurological examination findings, detected MRI abnormalities, and classification based on DTI-DTT.

8. Prevention

Given the rarity and complexity of SCIWORA cases, where multiple treatment attempts often fail to control the condition, it becomes imperative to address the underlying causes. Public awareness, especially among individuals and their families, is crucial, particularly for children under the age of 8 who may exhibit warning signs. Those engaged in activities involving prolonged and repeated spinal hyperextension, such as dance instructors, should take measures to minimize this risk. Parents should avoid actions that could potentially harm their child's spine, such as shaking the baby or rough handling. It is essential for everyone to be well-informed about how to respond in case a child experiences SCIWORA symptoms. In addition, health-care professionals should be vigilant, as some SCIWORA cases may present with normal initial MRI scans.

9. Conclusion

SCIWORA is frequently diagnosed in children aged ≤8 years old, and the unique characteristics of the pediatric spinal cord play a critical role in this condition. Various MOIs can result in SCI or ischemia. The objective of this guideline is to provide a comprehensive framework and treatment approach for addressing SCIWORA in children. Moving forward, effective treatments should be developed through multidisciplinary collaboration and supported by robust evidence-based medicines. As new treatment measures continue to evolve to improve the quality of life for children with SCIWORA, this guideline will undergo further revisions and improvements.

Acknowledgments

We would like to thank the medical team of the Orthopedics Department, especially Dr. Jamal Alshorman and the Union Hospital Orthopedics team, who contributed to the ideas and for editing and revision of this manuscript.

Funding

This research was funded by the National Natural Science Foundation of China (grant number: 82072556).

Conflict of interest

All the authors declare no conflicts of interest.

Author contributions

Conceptualization: Ruba Altahla, Xu Tao
Writing – original draft: Ruba Altahla, Jamal Alshorman
Writing – review & editing: Jamal Alshorman

Ethics approval and consent to participate

Not applicable.

Consent for publication

Not applicable.

Availability of data

Not applicable.

References

1. Pang D, 2004, Spinal cord injury without radiographic abnormality in children, 2 decades later. *Neurosurgery*, 55: 1325–1342; discussion 1342–1343.

https://doi.org/10.1227/01.neu.0000143030.85589.e6

2. Tong AN, Zhang JW, Zhou HJ, *et al*., 2020, Ischemic damage may play an important role in spinal cord injury during dancing. *Spinal Cord*, 58: 1310–1316.

https://doi.org/10.1038/s41393-020-0503-x

3. Scatchard R, Rosa JA, Bowen P, *et al*., 2018, A case report: Paediatric surfer's myelopathy. *Eur J Paediatr Neurol*, 22: 199–202.

https://doi.org/10.1016/j.ejpn.2017.09.011

4. Ayaz SB, Gill ZA, Khan AA, *et al*., 2014, Spinal cord injury without radiographic abnormalities (SCIWORA) in a preschool child: A case report. *J Postgrad Med Inst*, 28: 228–230.

5. Liang QC, Yang B, Song YH, *et al*., 2019, Real spinal cord injury without radiologic abnormality in pediatric patient with tight filum terminale following minor trauma: A case report. *BMC Pediatr*, 19: 513.

https://doi.org/10.1186/s12887-019-1894-8

6. Alshorman JA, Wang Y, Zhu F, *et al*., 2020, Clinical diagnosis and treatment of spinal cord injury without evidence of abnormality in children: A review. *Int Surg J*, 7: 3847–3855.

https://doi.org/10.18203/2349-2902.isj20204437

7. Albuja AC, Qaiser S, Lightner DD, *et al*., 2017, Surfer's myelopathy without surfing: A report of two pediatric patients. *Spinal Cord Ser Cases*, 3: 17008.

https://doi.org/10.1038/scsandc.2017.8

8. AbdelRazek MA, Mowla A, Farooq S, *et al*., 2016, Fibrocartilaginous embolism: A comprehensive review of an under-studied cause of spinal cord infarction and proposed diagnostic criteria. *J Spinal Cord Med*, 39: 146–154.

https://doi.org/10.1080/10790268.2015.1116726

9. Sidram V, Tripathy P, Ghorai SP, *et al*., 2009, Spinal cord injury without radiographic abnormality (SCIWORA) in children: A Kolkata experience. *Indian J Neurotrauma*, 6: 133–136.

https://doi.org/10.1016/S0973-0508(09)80007-5

10. Wang Y, Zhu F, Zeng L, *et al*., 2021, Surfer myelopathy in children: A case series study. *World Neurosurg*, 148: e227–e241.

https://doi.org/10.1016/j.wneu.2020.12.135

11. Martin BW, Dykes E, Lecky FE, 2004, Patterns and risks in spinal trauma. *Arch Dis Child*, 89: 860–865.

https://doi.org/10.1136/adc.2003.029223

12. Trigylidas T, Yuh SJ, Vassilyadi M, *et al*., 2010, Spinal cord injuries without radiographic abnormality at two pediatric trauma centers in Ontario. *Pediatr Neurosurg*, 46: 283–289.

https://doi.org/10.1159/000320134

13. Mahajan P, Jaffe DM, Olsen CS, *et al*., 2013, Spinal cord injury without radiologic abnormality in children imaged with magnetic resonance imaging. *J Trauma Acute Care Surg*, 75: 843–847.

https://doi.org/10.1097/ta.0b013e3182a74abd

14. Feng YP, Sun TS, Chen L, *et al*., 2017, Clinical therapeutic guideline for neurorestoration in spinal cord injury (Chinese version 2016). *J Neurorestoratol*, 5: 73–83.

https://doi.org/10.2147/jn.s119581

15. Huang H, Young W, Skaper S, *et al*., 2020, Clinical neurorestorative therapeutic guidelines for spinal cord injury (IANR/CANR version 2019). *J Orthop Translat*, 20: 14–24.

https://doi.org/10.1016/j.jot.2019.10.006

16. Farrell CA, Hannon M, Lee LK, 2017, Pediatric spinal cord injury without radiographic abnormality in the era of advanced imaging. *Curr Opin Pediatr*, 29: 286–290.

https://doi.org/10.1097/MOP.0000000000000481

17. Bosch PP, Vogt MT, Ward WT, 2002, Pediatric spinal cord injury without radiographic abnormality (SCIWORA): The absence of occult instability and lack of indication for bracing. *Spine* (*Phila Pa 1976*), 27: 2788–2800.

https://doi.org/10.1097/00007632-200212150-00009

18. Koestner AJ, Hoak SJ, 2001, Spinal cord injury without radiographic abnormality (SCIWORA) in children. *J Trauma Nurs*, 8: 101–108.

https://doi.org/10.1097/00043860-200108040-00002

19. Eckert MJ, Martin MJ, 2017, Trauma: Spinal cord injury. *Surg Clin North Am*, 97: 1031–1045.

https://doi.org/10.1016/j.suc.2017.06.008

20. Sharif S, Ali MY, 2020, Outcome prediction in spinal cord injury: Myth or reality. *World Neurosurg*, 140: 574–590.

https://doi.org/10.1016/j.wneu.2020.05.043

21. Fatehi D, Dayani MA, Rostamzadeh A, 2018, Role of CT scan in theranostic and management of traumatic spinal cord injury. *Saudi J Biol Sci*, 25: 739–746.

https://doi.org/10.1016/j.sjbs.2016.08.004

22. Ryken TC, Hadley MN, Walters BC, *et al*., 2013, Radiographic assessment. *Neurosurgery*, 72: 54–72.

https://doi.org/10.1227/neu.0b013e318276edee

23. Acheson MB, Livingston RR, Richardson ML, *et al*., 1987, High-resolution CT scanning in the evaluation of cervical spine fractures: Comparison with plain film examinations. *AJR Am J Roentgenol*, 148: 1179–1185.

https://doi.org/10.2214/ajr.148.6.1179

24. Zhang R, Zhou Z, Wu W, *et al*., 2018, An improved fuzzy connectedness method for automatic three-dimensional

liver vessel segmentation in CT images. *J Healthc Eng*, 2018: 2376317.

https://doi.org/10.1155/2018/2376317

25. Feldman KW, Avellino AM, Sugar NF, *et al*., 2008, Cervical spinal cord injury in abused children. *Pediatr Emerg Care*, 24: 222–227.

https://doi.org/10.1097/pec.0b013e31816b7aa4

26. Sesmat H, Hayoun T, Bonnet J, *et al*., 2018, Spinal cord injury without radiographic abnormality (SCIWORA): About 3 cases and review of the literature. *Biomed J Sci Tech Res*, 8: 6208–6211.

27. Matsumura A, Meguro K, Tsurushima H, *et al*., 1990, Magnetic resonance imaging of spinal cord injury without radiologic abnormality. *Surg Neurol*, 33: 281–283.

https://doi.org/10.1016/0090-3019(90)90049-u

28. Dreizin D, Kim W, Kim JS, *et al*., 2015, Will the real SCIWORA please stand up? Exploring clinicoradiologic mismatch in closed spinal cord injuries. *AJR Am J Roentgenol*, 205: 853–860.

https://doi.org/10.2214/AJR.14.13374

29. Schottler J, Vogel LC, Sturm P, 2012, Spinal cord injuries in young children: A review of children injured at 5 years of age and younger. *Dev Med Child Neurol*, 54: 1138–1143.

https://doi.org/10.1111/j.1469-8749.2012.04411.x

30. Reid S, Sell E, 2015, Case 2: Acute paralysis in a 10-year-old girl. *Paediatr Child Health*, 20: 289–290.

https://doi.org/10.1093/pch/20.6.289a

31. Pawar NH, Loke E, Aw DC, 2017, Spinal cord infarction mimicking acute transverse myelitis. *Cureus*, 9: e1911.

https://doi.org/10.7759/cureus.1911

32. Liao CC, Lui TN, Chen LR, *et al*., 2005, Spinal cord injury without radiological abnormality in preschool-aged children: Correlation of magnetic resonance imaging findings with neurological outcomes. *J Neurosurg*, 103: 17–23.

https://doi.org/10.3171/ped.2005.103.1.0017

33. Freigang V, Butz K, Seebauer CT, *et al*., 2021, Management and mid-term outcome after "real SCIWORA" in children and adolescents. *Global Spine J*, 12: 1208–1213.

https://doi.org/10.1177/2192568220979131

34. Zhu F, Liu Y, Zeng L, *et al*., 2021, Evaluating the severity and prognosis of acute traumatic cervical spinal cord injury: A novel classification using diffusion tensor imaging and diffusion tensor tractography. *Spine* (*Phila Pa 1976*), 46: 687–694.

https://doi.org/10.1097/brs.0000000000003923

35. Mulcahey MJ, Samdani AF, Gaughan JP, *et al*., 2013, Diagnostic accuracy of diffusion tensor imaging for pediatric cervical spinal cord injury. *Spinal Cord*, 51: 532–537.

https://doi.org/10.1038/sc.2013.36

36. Huien C, Jingsong S, Houhong C, *et al*., 2016, The application value of DTI imaging technology in spinal cord concussion injury. *Chin J CT MRI*, 14: 84. (Article in Chinese).

https://doi.org/10.3969/j.issn.1672-5131.2016.10.010

37. Alizadeh M, Fisher J, Saksena S, *et al*., 2018, Reduced field of view diffusion tensor imaging and fiber tractography of the pediatric cervical and thoracic spinal cord injury. *J Neurotrauma*, 35: 452–460.

https://doi.org/10.1089/neu.2017.5174

38. Zaninovich OA, Avila MJ, Kay M, *et al*., 2019, The role of diffusion tensor imaging in the diagnosis, prognosis, and assessment of recovery and treatment of spinal cord injury: A systematic review. *Neurosurg Focus*, 46: E7.

https://doi.org/10.3171/2019.1.focus18591

39. Copley PC, Tilliridou V, Kirby A, *et al*., 2019, Management of cervical spine trauma in children. *Eur J Trauma Emerg Surg*, 45: 777–789.

https://doi.org/10.1007/s00068-018-0992-x

40. Hadley MN, Walters BC, Aarabi B, *et al*., 2013, Clinical assessment following acute cervical spinal cord injury. *Neurosurgery*, 72: 40–53.

https://doi.org/10.1227/NEU.0b013e318276edda

41. Konovalov N, Peev N, Zileli M, *et al*., 2020, Pediatric cervical spine injuries and SCIWORA: WFNS spine committee recommendations. *Neurospine*, 17: 797–808.

https://doi.org/10.14245/ns.2040404.202

42. Fawcett JW, Curt A, Steeves JD, *et al*., 2007, Guidelines for the conduct of clinical trials for spinal cord injury as developed by the ICCP panel: Spontaneous recovery after spinal cord injury and statistical power needed for therapeutic clinical trials. *Spinal Cord*, 45: 190–205.

https://doi.org/10.1038/sj.sc.3102007

43. Zhu F, Zeng L, Gui S, *et al*., 2021, The role of diffusion tensor imaging and diffusion tensor tractography in the assessment of acute traumatic thoracolumbar spinal cord injury. *World Neurosurg*, 150: e23–e30.

https://doi.org/10.1016/j.wneu.2021.01.146

44. Atesok K, Tanaka N, O'Brien A, *et al*., 2018, Posttraumatic spinal cord injury without radiographic abnormality. *Adv Orthop*, 2018: 7060654.

https://doi.org/10.1155/2018/7060654

45. Stein DM, Sheth KN, 2015, Management of acute spinal cord injury. *Continuum* (*Minneap Minn*), 21: 159–187.

https://doi.org/10.1212/01.con.0000461091.09736.0c

46. Qi C, Xia H, Miao D, *et al*., 2020, The influence of timing of surgery in the outcome of spinal cord injury without radiographic abnormality (SCIWORA). *J Orthop Surg Res*,

15: 223.

https://doi.org/10.1186/s13018-020-01743-1

47. Grollmus J, Hoff J, 1975, Spontaneous spinal epidural haemorrhage: Good results after early treatment. *J Neurol Neurosurg Psychiatry*, 38: 89–90.

https://doi.org/10.1136/jnnp.38.1.89

48. Green E, Zishan US, Robertson N, *et al*., 2018, Non-traumatic myelopathy associated with prolonged hyperextension during swimming: An unusual variation of Surfer's myelopathy. *Spinal Cord Ser Cases*, 4: 22.

https://doi.org/10.1038/s41394-018-0055-x

49. Fehlings MG, Tetreault LA, Wilson JR, *et al*., 2017, A clinical practice guideline for the management of patients with acute spinal cord injury and central cord syndrome: Recommendations on the timing (≤24 hours versus >24 hours) of decompressive surgery. *Global Spine J*, 7: 195S–202S.

https://doi.org/10.1177/2192568217706367

50. Kandziora F, Pingel A, 2017, Expert's comment concerning grand rounds case entitled: "Increased intrathecal pressure after traumatic spinal cord injury: An illustrative case presentation and a review of the literature" by Grassner L, Winkler PA, Strowitzki M, *et al*.(Eur Spine J (2016). doi: 10.1007/s00586-016-4769-9) Surgical treatment of SICS (spinal intradural compartment syndrome)? *Eur Spine* J 26: 26–27.

https://doi.org/10.1007/s00586-016-4804-x

51. Yılmaz T, Kaptanoğlu E, 2015, Current and future medical therapeutic strategies for the functional repair of spinal cord injury. *World J Orthop*, 6: 42–55.

https://doi.org/10.5312/wjo.v6.i1.42

52. Tykocki T, Poniatowski Ł, Czyż M, *et al*., 2017, Intraspinal pressure monitoring and extensive duroplasty in the acute phase of traumatic spinal cord injury: A systematic review. *World Neurosurg*, 105: 145–152.

https://doi.org/10.1016/j.wneu.2017.05.138

53. Alizo G, Sciarretta JD, Gibson S, *et al*., 2018, Multidisciplinary team approach to traumatic spinal cord injuries: A single institution's quality improvement project. *Eur J Trauma Emerg Surg*, 44: 245–250.

https://doi.org/10.1007/s00068-017-0776-8

54. Durojaiye AB, Levin S, Toerper M, *et al*., 2019, Evaluation of multidisciplinary collaboration in pediatric trauma care using EHR data. *J Am Med Inform Assoc*, 26: 506–515.

https://doi.org/10.1093/jamia/ocy184

55. Ellis MJ, McDonald PJ, Cordingley D, *et al*., 2016, Retirement-from-sport considerations following pediatric sports-related concussion: Case illustrations and institutional approach. *Neurosurg Focus*, 40: E8.

https://doi.org/10.3171/2016.1.focus15600

56. Knight PH, Maheshwari N, Hussain J, *et al*., 2015, Complications during intrahospital transport of critically ill patients: Focus on risk identification and prevention. *Int J Crit Illn Inj Sci*, 5: 256–264.

https://doi.org/10.4103/2229-5151.170840

57. Pal R, Agarwal A, Galwankar S, *et al*., 2014, The 2014 academic college of emergency experts in India's INDO-US joint working group (JWG) white paper on "developing trauma sciences and injury care in India". *Int J Crit Illn Inj Sci*, 4: 114–130.

https://doi.org/10.4103/2229-5151.134151

58. Kim SH, Yoon SH, Cho KH, *et al*., 2008, Spinal cord injury without radiological abnormality in an infant with delayed presentation of symptoms after a minor injury. *Spine* (*Phila Pa 1976*), 33: E792–E794.

https://doi.org/10.1097/BRS.0b013e3181878719

59. Panagopoulos D, 2018, A case of SCIWORA with uncommon combination of neurological and imaging findings. *EC Paediatrics*, 7: 498–506.

60. Pang D, Pollack IF, 1989, Spinal cord injury without radiographic abnormality in children--the SCIWORA syndrome. *J Trauma*, 29: 654–664.

https://doi.org/10.1097/00005373-198905000-00021

61. Tolentino JC, Schadt J, Bird B, *et al*., 2018, Adverse events during intrahospital transfers: Focus on patient safety. In: Vignettes in Patient Safety-Volume 3. United Kingdom: IntechOpen.

https://doi.org/10.5772/intechopen.76777

62. Salt O, Akpınar M, Sayhan MB, *et al*., 2020, Intrahospital critical patient transport from the emergency department. *Arch Med Sci*, 16: 337–344.

https://doi.org/10.5114/aoms.2018.79598

63. Jiang B, 2015, The challenges faced in the field of trauma care in China. *Zhonghua Wai Ke Za Zhi* [*Chin J Surg*], 53: 401–404.

64. Wang T, Yin X, Zhang P, *et al*., 2015, Road traffic injury and rescue system in China. *Lancet*, 385: 1622.

https://doi.org/10.1016/S0140-6736(15)60794-2

65. China Trauma Rescue and Treatment Association, 2017, Consensus on the establishment of urban trauma rescue system in China. *Zhonghua Wai Ke Za Zhi*, 55: 830–833.

https://doi.org/10.3760/cma.j.issn.0529-5815.2017.11.002

66. Silman E, Langdorf MI, Rudkin S, *et al*., 2008, Images in emergency medicine: Pediatric spinal cord injury without radiographic abnormality. *West J Emerg Med*, 9: 124.

67. Nagasawa H, Ishikawa K, Takahashi R, *et al*., 2017, A case of real spinal cord injury without radiologic abnormality in

a pediatric patient with spinal cord concussion. *Spinal Cord Ser Cases*, 3: 17051.

https://doi.org/10.1038/scsandc.2017.51

68. Kriss VM, Kriss TC, 1996, SCIWORA (spinal cord injury without radiographic abnormality) in infants and children. *Clin Pediatr* (*Phila*), 35: 119–124.

https://doi.org/10.1177/000992289603500302

69. Beck A, Gebhard F, Kinzl L, *et al*., 2000, Spinal cord injury without radiographic abnormalities in children and adolescents: Case report of a severe cervical spine lesion and review of literature. *Knee Surg Sports Traumatol Arthrosc*, 8: 186–189.

https://doi.org/10.1007/s001670050212

70. Bansal KR, Chandanwale AS, 2016, Spinal cord injury without radiological abnormality in an 8 months old female child: A case report. *J Orthop Case Rep*, 6: 8–10.

https://doi.org/10.13107/jocr.2250-0685.363

71. Ergun A, Oder W, 2003, Pediatric care report of spinal cord injury without radiographic abnormality (SCIWORA): Case report and literature review. *Spinal Cord*, 41: 249–253.

https://doi.org/10.1038/sj.sc.3101442

72. Hon EK, Chan J, Ng BK, *et al*., 2006, Spinal cord injury without radiographic abnormality (SCIWORA): A mere 50-cm fall that matters. *Injury Extra*, 37: 364–370.

https://doi.org/10.1016/j.injury.2006.03.021

73. Klakeel M, Thompson J, Srinivasan R, *et al*., 2015, Anterior spinal cord syndrome of unknown etiology. *Proc* (*Bayl Univ Med Cent*), 28: 85–87.

https://doi.org/10.1080/08998280.2015.11929201

74. Kalra V, Gulati S, Kamate M, *et al*., 2006, SCIWORA-spinal cord injury without radiological abnormality. *Indian J Pediatr*, 73: 829–831.

https://doi.org/10.1007/BF02790395

75. Kim C, Vassilyadi M, Forbes JK, *et al*., 2016, Traumatic spinal injuries in children at a single level 1 pediatric trauma centre: Report of a 23-year experience. *Can J Surg*, 59: 205–212.

https://doi.org/10.1503/cjs.014515

76. Sultan I, Lamba N, Liew A, *et al*., 2020, The safety and efficacy of steroid treatment for acute spinal cord injury: A systematic review and meta-analysis. *Heliyon*, 6: e03414.

https://doi.org/10.1016/j.heliyon.2020.e03414

77. Caruso MC, Daugherty MC, Moody SM, *et al*., 2017, Lessons learned from administration of high-dose methylprednisolone sodium succinate for acute pediatric spinal cord injuries. *J Neurosurg Pediatr*, 20: 567–574.

https://doi.org/10.3171/2017.7.PEDS1756

78. Fehlings MG, Wilson JR, Tetreault LA, *et al*., 2017, A clinical practice guideline for the management of patients with acute spinal cord injury: Recommendations on the use of methylprednisolone sodium succinate. *Global Spine J*, 7: 203S–211S.

https://doi.org/10.1177/2192568217703085

79. Mortazavi M, Gore PA, Chang S, *et al*., 2011, Pediatric cervical spine injuries: A comprehensive review. *Childs Nerv Syst*, 27: 705–717.

https://doi.org/10.1007/s00381-010-1342-4

80. Theodore N, Hadley MN, Aarabi B, *et al*., 2013, Prehospital cervical spinal immobilization after trauma. *Neurosurgery*, 72: 22–34.

https://doi.org/10.1227/neu.0b013e318276edb1

81. Rozzelle CJ, Aarabi B, Dhall SS, *et al*., 2013, Spinal cord injury without radiographic abnormality (SCIWORA). *Neurosurgery*, 72: 227–33.

https://doi.org/10.1227/NEU.0b013e3182770ebc

82. Brauge D, Plas B, Vinchon M, *et al*., 2020, Multicenter study of 37 pediatric patients with SCIWORA or other spinal cord injury without associated bone lesion. *Orthop Traumatol Surg Res*, 106: 167–171.

https://doi.org/10.1016/j.otsr.2019.10.006

83. Tatka J, Elbayer J, Vojdani S, *et al*., 2016, Pediatric spinal cord injury. *J Spine*, S7: 7.

https://doi.org/10.4172/2165-7939.S7-007

84. Sellin JN, Steele WJ 3rd, Simpson L, *et al*., 2016, Multicenter retrospective evaluation of the validity of the Thoracolumbar Injury Classification and Severity Score system in children. *J Neurosurg Pediatr*, 18: 164–170.

https://doi.org/10.3171/2016.1.peds15663

85. Santipas B, Wejjakul W, Luksanapruksa P, *et al*., 2020, Nonfusion muscle-sparing technique to treat long-segment thoracolumbar extradural arachnoid cyst in a child: A case report and review of the literature. *World Neurosurg*, 142: 222–226.

https://doi.org/10.1016/j.wneu.2020.06.185

86. Li G, Zhang Y, Zhao J, *et al*., 2016, Some cool considerations of external lumbar drainage during its widespread application in neurosurgical practice: A long way to go. *Chin Neurosurg J*, 2: 117–124.

https://doi.org/10.1186/s41016-016-0033-8

87. Zebracki K, Melicosta M, Unser C, *et al*., 2020, A primary care provider's guide to pediatric spinal cord injuries. *Top Spinal Cord Inj Rehabil*, 26: 91–99.

https://doi.org/10.46292/sci2602-91

88. Fehlings MG, Tetreault LA, Wilson JR, *et al*., 2017, A clinical practice guideline for the management of acute spinal cord

injury: Introduction, rationale, and scope. *Global Spine J*, 7: 84S–94S.

https://doi.org/10.1177/2192568217703387

89. Yalçınkaya EY, Saygı EK, Taşkıran ÖO, *et al*., 2021, Consensus recommendations for botulinum toxin injections in the spasticity management of children with cerebral palsy during COVID-19 outbreak. *Turk J Med Sci*, 51: 385–392.

https://doi.org/10.3906/sag-2009-5

90. Corti C, Urgesi C, Poggi G, *et al*., 2020, Home-based cognitive training in pediatric patients with acquired brain injury: Preliminary results on efficacy of a randomized clinical trial. *Sci Rep*, 10: 1391.

https://doi.org/10.1038/s41598-020-57952-5

91. Gandhi P, Chan K, Verrier MC, *et al*., 2017, Training to improve walking after pediatric spinal cord injury: A systematic review of parameters and walking outcomes. *J Neurotrauma*, 34: 1713–1725.

https://doi.org/10.1089/neu.2016.4501

92. Baharudin NS, Harun D, Kadar M, 2020, An assessment of the movement and function of children with specific learning disabilities: A review of five standardised assessment tools. *Malays J Med Sci*, 27: 21–36.

https://doi.org/10.21315/mjms2020.27.2.3

93. Xiaodong G, Yaping F, Tiansheng S, *et al*., 2021, Clinical guidelines for neurorestorative therapies in spinal cord injury (2021 China version). *J Neurorestoratol*, 9: 31–49.

https://doi.org/10.26599/jnr.2021.9040003

94. Chinese Association of Orthopedic Surgeons; Editorial Committee of the 'Evidence-based Guideline for the Management of Acute Subaxial Cervical Spine Injury' of Chinese Association of Orthopedic Surgeons, 2018, Evidence-based guideline for the management of acute subaxial cervical spine injury. *Zhonghua Wai Ke Za Zhi* 56: 5–9. (Articles in Chinese).

https://doi.org/10.3760/cma.j.issn.0529-5815.2018.01.003

95. Slotkin JR, Lu Y, Wood KB, 2007, Thoracolumbar spinal trauma in children. *Neurosurg Clin N Am*, 18: 621–630.

https://doi.org/10.1016/j.nec.2007.07.003

96. Wang Y, Zhang L, Pan G, *et al*., 2016, Traditional Chinese Medicine comprehensive therapy for the improvement of motor function in spinal cord injury patients. *J Tradit Chin Med*, 36: 618–624.

https://doi.org/10.1016/s0254-6272(16)30081-4

97. Zhang Q, Yang H, An J, *et al*., 2016, Therapeutic effects of traditional Chinese medicine on spinal cord injury: A promising supplementary treatment in future. *Evid Based Complement Alternat Med*, 2016: 8958721.

https://doi.org/10.1155/2016/8958721

98. Lu Y, Yang J, Wang X, *et al*., 2020, Research progress in use of traditional Chinese medicine for treatment of spinal cord injury. *Biomed Pharmacother*, 127: 110136.

https://doi.org/10.1016/j.biopha.2020.110136

99. Marinier M, Rodts MF, Connolly M, 1997, Spinal cord injury without radiographic abnormality (SCIWORA). *Orthop Nurs*, 16: 57–63; quiz 64–65.

https://doi.org/10.1097/00006416-199709000-00015

100. Martin-Rojas T, Sastre-Oliva T, Esclarín-Ruz A, *et al*., 2020, Effects of growth hormone treatment and rehabilitation in incomplete chronic traumatic spinal cord injury: Insight from proteome analysis. *J Pers Med*, 10: 183.

https://doi.org/10.3390/jpm10040183

101. Fiaschi P, Severino M, Ravegnani GM, *et al*., 2016, Idiopathic cervical hematomyelia in an infant: Spinal cord injury without radiographic abnormality caused by a trivial trauma? Case report and review of the literature. *World Neurosurg*, 90: 38–44.

https://doi.org/10.1016/j.wneu.2016.01.094

ACCSCIENCE PUBLISHING

INNOSC Theranostics and Pharmacological Sciences

REVIEW ARTICLE

Antiplatelet, anticoagulation, and elective aneurysm treatments in neurological patients

Anjali Patel[1], Daisy Valle[1], Drashti Patel[1], Marco Foreman[1], Akash Nijhawan[2], Devon Foster[2], Alexander Nguyen[3], and Brandon Lucke-Wold[4]*

[1]University of Florida College of Medicine, Gainesville, FL, USA

[2]Florida International University Herbert Wertheim College of Medicine, Miami, FL, USA

[3]Creighton University School of Medicine, Omaha, Nebraska, USA

[4]Department of Neurosurgery, University of Florida, Gainesville, FL, USA

Abstract

Developing more specialized care for neurological disorders, such as aneurysms, arteriovenous malformations, and strokes, can revolutionize patient healthcare and outcomes. With the advent of surgical techniques such as flow diversion, non-stent- and stent-assisted coiling, and catheter embolization for elective aneurysm treatment in neurological patients, the adverse effects and morbidities associated with aneurysms can be reduced. This paper aims to highlight three specific strengths and weaknesses of the newly emerged techniques. Flow diversion devices involve placing a stent in the parent artery, whereas Woven EndoBridge embolization involves manipulation of the wall of the artery without the administration of dual-antiplatelet therapy. In addition to aneurysm treatment, the administration of antiplatelets and anticoagulants is helpful in disrupting the coagulation cascade. As stated in the new and enhanced guidelines released by the American Heart Association, the administration of dual anticoagulants is beneficial to the patients if they have low ischemic severity. Understanding the various benefits and complications associated with each treatment can allow clinicians to gain insight into the potential trajectory of treatment for different patients.

Keywords: Aneurysm; Stent-assisted embolization; Antiplatelet therapy; Woven Endobridge embolization; Catheter embolization

***Corresponding author:**
Brandon Lucke-Wold (Brandon.Lucke-Wold@neurosurgery.ufl.edu)

Citation: Patel A, Valle D, Patel D, *et al.* 2024, Antiplatelet, anticoagulation, and elective aneurysm treatments in neurological patients. *INNOSC Theranostics and Pharmacological Sciences,* 7(1): 1202. https://doi.org/10.36922/itps.1202

Received: June 29, 2023

Accepted: August 23, 2023

Published Online: October 18, 2023

1. Introduction

In the realm of neurosurgical care, emerging approaches have opened up new frontiers and revolutionized the management of challenging neurovascular manifestations by offering patients minimally invasive treatments that come with exceptionally promising outcomes[1-3]. The field of neurovascular diseases encompasses a wide range of neurological disorders, such as intracranial aneurysms, acute ischemic strokes, cerebral arteriovenous malformations, and vascular growths, which require specialized expertise and thorough, comprehensive care. For instance, cerebral aneurysms — abnormal bulges that develop in the blood vessels of the brain — and arteriovenous malformations — tangled networks of abnormal blood vessels in the brain or spine — are both vascular conditions that

can disrupt the normal flow of blood in the brain[4]. These vascular anomalies pose a considerable threat of rupture, which can consequently result in severe neurological implications, including the onset of subarachnoid hemorrhage[4-6]. These challenges have driven the rapid development of vascular devices and surgical techniques, such as flow diversion, non-stent- and stent-assisted coiling (SAC), and catheter embolization[3,7], promoting the rapid evolution of the neurovascular surgery field.

Neurovascular disorders pose serious risks to heightened morbidity and mortality rates among the affected patients if such conditions are left uncontrolled, and thus, the management of these disorders has become an emerging area of concern in the field of neurology and neurosurgery, which has a bearing on the patients' quality of life[6]. In essence, the regulation of neurovascular diseases is a critical aspect of healthcare that emphasizes the minimization of thromboembolic events while ensuring adequate blood supply to the brain[8-10]. This, in particular, is a crucial area of research and clinical practice, as neurovascular conditions can have severe consequences for patients, such as cognitive impairments and, under serious circumstances, even death. To address these clinical issues, health-care professionals must employ a range of strategies that include not only surgical procedures but also pharmacological interventions. By implementing these approaches, health-care providers can help improve patient outcomes and reduce the burden of neurovascular manifestations on individuals and society as a whole.

The administration of antiplatelet and anticoagulant agents is a widely accepted approach to achieving therapeutic goals in patients with neurovascular disorders (Figure 1). Primarily, these agents are utilized to prevent the formation of blood clots, which could potentially lead to the development of severe complications, such as stroke, myocardial infarction, and pulmonary embolism[11]. Antiplatelet agents are widely utilized to prevent thrombus formation by inhibiting platelet aggregation[12]. Of interest, aspirin and clopidogrel are two commonly used drugs — efficacious in diminishing the risk for thrombosis[12,13]. Similarly, anticoagulant agents act by impeding the coagulation cascade, thereby inhibiting the formation of blood clots[14]. Warfarin and heparin are two commonly used anticoagulants that clinical studies have shown to be effective in preventing the formation of thrombi in vascular disease[15-17]. As such, the administration of antithrombotic agents is of paramount significance in patients with neurovascular disease, as they are at an increased risk of thromboembolic events[17,18]. However, the administration of the pharmacological agents mentioned above necessitates meticulous management, and their impact on bleeding and thromboembolic events must be closely monitored. The administration of antiplatelet and anticoagulant therapy is a crucial aspect of medical care that necessitates a personalized approach, contingent on the patient's symptoms and presentations, as well as the nature of the intervention being executed.

As of recently, the American Heart Association and the American Stroke Association have jointly released a revised set of management guidelines for the administration of antiplatelet and anticoagulant therapy in patients subjected to neurovascular procedures[19,20]. These guidelines cover a range of topics, including the selection of appropriate pharmaceutical interventions, the timing of therapy initiation and discontinuation, and the management of bleeding complications[19,20]. Ultimately, the purpose of this document serves to establish a uniform methodology for health-care practitioners to administer these treatments, with the aim of improving patient outcomes and minimizing the likelihood of unfavorable incidents[21]. Through dedicated adherence to these guidelines, health-care professionals can ensure that patients undergoing neurovascular interventions will receive optimal care and achieve the best possible outcomes. The efficacy and safety of these pharmaceutical agents have been rigorously scrutinized in several studies, which also further highlighted the significant role of these agents in the reduction of adverse outcomes in high-risk patient[22-24]. Therefore, the use of antiplatelet and anticoagulant agents remains a cornerstone of modern medical practice, but most importantly, in the world of neurovascular diseases.

2. Utility and efficacy of flow diversion

Flow-diverter devices (FDDs) are an emerging method for treating cerebral aneurysms. As seen in Figure 2, this method is performed by placing a stent in the parent artery where the aneurysm neck is located to disrupt intra-aneurysmal flow, favoring intra-aneurysmal thrombosis[25]. Using this device, the growth of endothelial cells over the neck of the aneurysm progressively excludes the aneurysm sac from circulation[26].

Specifically, the utilization of FDD promotes flow disruption and formation of a stable blood clot within the aneurysm, ultimately contributing to aneurysm occlusion. The endothelization process begins as soon as the FDD is deployed, and adhesion of undifferentiated cells occurs indiscriminately along the implanted stent[27,28]. Within 1 day of implantation, inflammatory cells cluster across the aneurysm neck. Compared to coil embolized aneurysms, the presence of tumor necrosis factor-alpha and monocyte chemoattractant protein-1 in FDD-treated aneurysms suggests that invading inflammatory biological units like macrophages may support healing following implantation

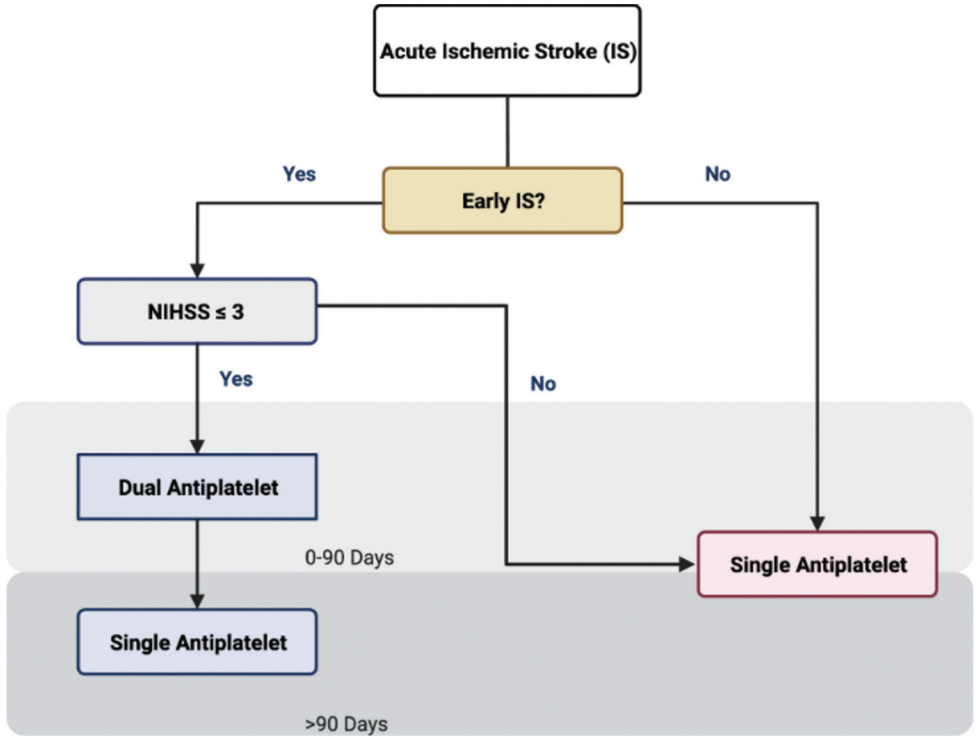

Figure 1. Acute ischemic stroke guidelines. Simplified, schematic representation of the 2021 revised American Heart Association/American Stroke Association recommendations for antiplatelet therapy in patients with acute ischemic stroke, a prevalent neurovascular disorder. NIHSS indicates National Institutes of Health Stroke Scale, an assessment of the severity of ischemic activity.

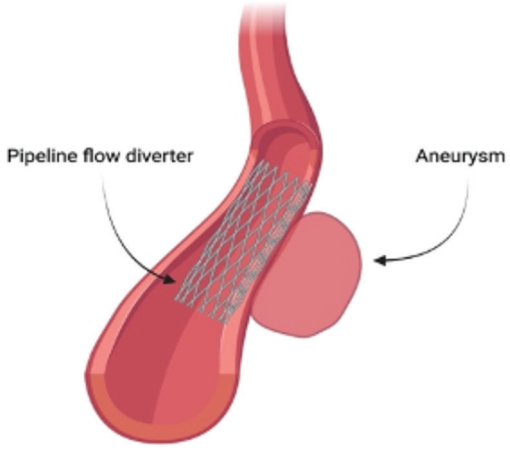

Figure 2. Flow diversion device following implantation.

of FDDs[29]. In addition, it has been shown that utilization of FDD in the treatment of aneurysms upregulates expression of apelin, cyclin B1, intercellular adhesion molecule 2, and CXCL8, key genes involved in endothelial function, mitogenic activity, cell cycle progression, and angiogenesis[30]. Thus, it is believed that due to enhanced gene expression, FDD intrinsically facilitates upregulated endothelization[26].

In addition, adhesion of differentiated smooth muscle cells results in the formation of a histologically visible initial neointima layer ~7 days after FDD implantation. At the ~8-week mark, $CD31^+$ endothelial cells appear over the neointimal layer of the smooth muscle antigen-positive cells[27].

Most current studies regarding intracranial aneurysm treatment utilized FDDs, pipeline embolization device, and silk embolization device[31,32]. In treatment of cerebral aneurysms, flow diversion has been shown to have a high success rate of 93 – 95% and a low complication rate of 2.3 – 5.6%[33]. Finally, a recent study has shown 83.5% and 85.2% occlusion rates for 1-year and 3-year follow-ups, and confirmed that FDDs are effective and safe in short-term and long-term follow-ups[34].

3. Flow diversion devices compared to traditional embolization techniques

Traditional methods for treating intracranial aneurysms include coil embolization (CE), stenting, and Woven EndoBridge (WEB) embolization (Figure 3).

CE involves the insertion of a microcatheter into the femoral artery before it moves to the site of the aneurysm for navigation. On reaching the aneurysm site, small

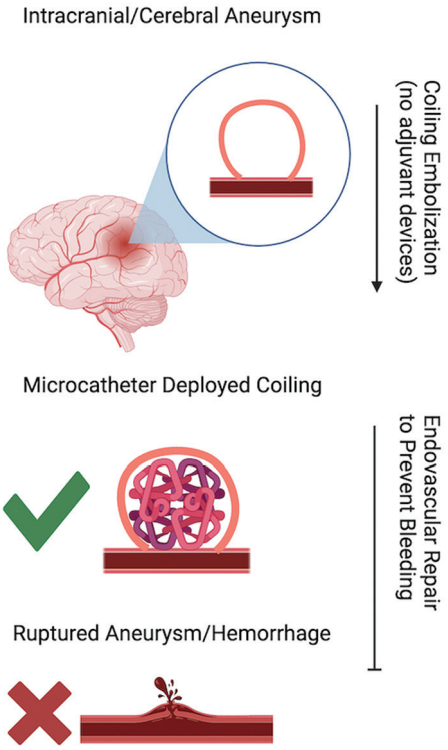

Figure 3. Impact of administering a microcatheter-deployed coiling to patients suffering from intracranial or intracerebral aneurysms.

helical platinum coils are deployed to fill the aneurysm and prevent further expansion[35]. Compared to FDD, CE devices have shown relatively low rates of complete occlusion but unfortunately are correlated with high rates of recurrence, especially when used to treat large intracranial aneurysms[36]. Stent-assisted CE has been shown to achieve more optimal outcomes compared to traditional CE but still faces high recurrence rates of 20 – 57% in treated patients[37,38].

On the other hand, WEB embolization is a device used to disrupt flow along the neck of the aneurysm[39]. This device functions as an intrasaccular flow diverter by placing a metabolic mesh along the wall of the aneurysm and the neck[39]. It is designed as a stand-alone therapy for the management of saccular aneurysms, unruptured or ruptured[39]. Other flow-disruption devices require the use of dual antiplatelet therapy (DAPT), while data suggest that the WEB device may be placed without the need for DAPT due to the high degree of neck coverage[39].

4. Protocol for antiplatelets and anticoagulant therapy

Although neurointerventional surgery offers benefits to patients with neurovascular diseases and stroke, the complications are difficult to avoid and ultimately diminish the efficacy of the intervention[40]. One possible complication that carries significant risk is the development of a thromboembolism[40]. Thromboembolisms are more inclined to attach to devices such as catheters due to repeated damage to the vascular walls[40]. Therefore, anticoagulation agents, such as heparin, and antiplatelet agents are commonly employed to decrease risk of thromboembolism. The use of antiplatelet agents before and during the procedure is deemed safe and efficacious in reducing the risk of a thromboembolism for unruptured aneurysms[40]. Antiplatelet agents, such as aspirin and clopidogrel, show evidence of reducing thromboembolism risk in coronary angiography and coronary endovascular interventions[41]. Aspirin works by irreversibly inhibiting the enzyme, cyclooxygenase-1 (COX1), preventing the conversion of arachidonic acid to thromboxane A2[42]. Conventionally, aspirin and clopidogrel are used in combination during aneurysm coiling and have shown to reduce thromboembolic events[43]. Heparin is an anticoagulant that is not traditionally used in diagnostic angiographic procedures but may be used in coiling procedures for patients with uninterpreted aneurysms[44]. Heparin use has shown to be efficacious in selected cases where there is cerebral ischemia or coil migration into the lumen of the parent vessel, but the use of heparin in ruptured aneurysms is not indicated[44]. Current guidelines recommend the use of DAPT for 3 – 6 months, but a meta-analysis published in 2021 found that single antiplatelet therapy involving aspirin reduced bleeding without raising the risk for stroke or death[45].

Abciximab is a Fab monoclonal antibody which blocks the IIb/IIIa receptor to inhibit platelet blockade[40]. Its effects occur within 10 min of administration and may persist for up to 48 h[46]. Abciximab inhibits platelets throughout the duration of intravenous infusion[47]. One study found that abciximab engendered a better response to clots in aneurysm coiling procedures, which were complicated by the formation of a thrombus[48]. Therefore, abciximab proves to be efficacious for intra-procedural thrombus formation. In addition, the risk of hemorrhagic complications is reduced in both unruptured and ruptured aneurysms[40].

5. Coiling

Endovascular coiling or embolization and open microsurgical clipping are considered the main standard non-conservative preventive treatment options in patients afflicted by unruptured cerebral aneurysms in addition to arteriovenous malformations[49]. In general, surgical clipping is commonly performed in younger patients, especially those admitted due emergency[50]. During the non-SAC process, a wired catheter is passed through the

femoral artery and is then threaded up to the affected artery with the aid of fluoroscopic guidance[51,52]. A microcatheter is then inserted through the original catheter, delivering soft platinum metal coils into the aneurysm space[53]. These initially straight-configured metal coils vary in sizes and, after detachment from the microcatheter by means of electrical induction, conform to various predetermined circular shapes[51]. Multiple coils may be deployed to sufficiently fill the aneurysm compartment[54,55]. Short-term success is indicated by coil-induced thrombus of the post-operative space shown on immediate angiography, resulting in an adequate seal from arterial blood flow[56].

Coiling without stent assistance is distinct in that a stent is not placed in the arterial space either before or after coil deployment into the aneurysm[57,58]. Intravascular tent assistance has been generally indicated based on aneurysm neck size. More specifically, stent use for cases of wide-necked aneurysms has been shown to provide structural scaffolding support for coiling integrity and density within the aneurysm sac[59]. However, ongoing studies have been aimed at establishing comparisons between coiling alone and coiling with stent assistance based on criteria including overall efficacy and safety in addition to solely anatomic parameters such as aneurysm diameter[60]. Both Hong *et al.* and Phan *et al.* conducted separate meta-analyses comparing the two aforementioned procedures with data analysis suggesting that SAC results in significantly higher progressive thrombosis rates and lower recurrent rates than coiling alone[61,62]. Conversely, immediate occlusion rates and complications including hematoma, dissection, perforation, stroke, and mortality were statistically similar between the two pooled groups[61,62]. As expected, mean aneurysm size was calculated to be slightly over 1 mm in the SAC cohort. Although both studies were based on retrospective cohort analysis, the evidence leads way to current and future randomized controlled trials to determine if standard intracranial aneurysm treatment should shift toward SAC, particularly if this option does not pose any significantly increased concern for complication. Endovascular coiling alone carries an approximately 25% recanalization rate, but technological advancements to coil properties have been made in an effort to reduce this trend[63]. Variation of coils in terms of shape, size, malleability, material, and detachment sites allows providers to employ more effective thrombotic structures for each intracranial aneurysm case. Moreover, adjunctive devices and techniques to coiling alone have been developed and extensively studied studied[64].

As previously mentioned, endovascular coiling of cerebral aneurysms presents as a relatively conservative treatment option, particularly in cases of unruptured aneurysm. Similarly, coiling alone entails similar rates of complication when compared to adjunctive coiling such as SAC. Thromboembolic events are one of the most significant, yet frequent (up to 8.2% rate), complications that can potentially arise from CE therapy[44,65]. Given the significant risk for neurologic impairment and/or death associated with thromboembolism, antiplatelet and anticoagulant therapy is a major point of concern in the therapeutic landscape of cerebral aneurysms. Moreover, ischemic event incidence in patients undergoing aneurysm intervention can range from 10% to 40% when detected with diffusion-weighted imaging techniques (DWI)[66,67]. Thrombus formation can stem from a number of different intraoperative interactions between devices and pre-existing aneurysm structure[40]. Mechanisms include vessel injury, coil migration, existing thrombus dislodgement, and incomplete aneurysm obliteration with subsequent thrombosis[68]. Intraoperative heparin loading is frequently utilized during aneurysm coiling as a preventive measure against the aforementioned thromboembolic complications[69].

With regards to endovascular coiling pre-operative standard of care in patients with unruptured aneurysms, antiplatelet therapy includes one dose of aspirin 81 or 325 mg either 1 day out from surgery or preoperatively on the same day. Of note, coiling alone does not necessarily indicate the administration of a second antiplatelet medication such as clopidogrel[36]. However, an aspirin 100 mg/clopidogrel 75 mg regimen may be recommended in some cases, more so when a stent is required[40]. Complicated aneurysm configuration requiring multiple catheters and challenging coiling may also indicate a pre-operative dual antiplatelet regimen. Interestingly, Hwang *et al.* observed no significant reduction in thromboembolism cases where only simple coiling from a single microcatheter was needed[43]. The evidence suggests antiplatelet therapy may or may not be critical to thromboembolic complication prophylaxis depending on the extent of coiling involvement. In addition to this finding, antiplatelet therapy was found to have no significant effect on hemorrhagic complications in cases of unruptured aneurysms[43]. Combining these two findings, it appears that dual, and even single, antiplatelet therapy may only have a beneficial effect on certain coiling procedures but administering either aspirin or an aspirin/clopidogrel combo as a pre-operative prophylactic measure renders no apparent harm. Although other studies have found slight nonsignificant trends in hemorrhagic complications after antiplatelet therapy, there is more evidence to suggest that the potentially significant reductions in thromboembolism outweigh the risks[70]. Given the possibility for hemorrhagic complications, a monotherapy dose of aspirin 81 mg or 325 mg shortly before coiling is generally a conservative measure, whereas DAPT is reserved for more complicated cases not consistently characteristic of endovascular

coiling alone. As aspirin only partially inhibits GPIIb/IIIa, it provides a low barrier effect on the risk of a thromboembolic event[71]. Postoperatively, coiling alone does not generally indicate prolonged antiplatelet or anticoagulant therapy, both mono and dual therapy, particularly after the point of discharge[72]. The addition of a stent may require an antiplatelet/anticoagulation therapy regimen postoperatively. Aside from prior medical histories such as atrial fibrillation that necessitates chronic medication; antiplatelet/anticoagulation therapy in cases of simple coiling is usually confined within the duration of a hospital course. Given resistance to antiplatelet agents may be a possibility, prolonged therapy that is not indicated for would not be a practical option[73]. The advantages and disadvantages of endovascular coiling for cerebral aneurysms are listed in Table 1.

In the case of ruptured aneurysm and subarachnoid hemorrhage, antiplatelet/anticoagulant therapy standards are distinct from the cases previously discussed, as subarachnoid hemorrhage was observed to be independently linked to thromboembolic complications associated with endovascular coiling[65]. In these cases, anticoagulant therapy can be initiated in the form of subcutaneous heparin approximately 12 h after CE. Supplemental aspirin administration may be flexible but has to be administered at the discretion of the neurointerventional provider[72]. More care must be taken to assess the appropriate antiplatelet therapy when dealing with CE of ruptured aneurysms. Patients with ruptured intracranial aneurysm are considered at significant risk for thromboembolism. Edwards *et al.* found that periprocedural monotherapy in the form of aspirin can significantly reduce periprocedural thromboembolic events without significantly increasing hemorrhage risk even in ruptured aneurysm and subarachnoid hemorrhage cases[74]. Of note, treatment cohorts received intraoperative aspirin at 650 mg near the end of the procedure. This group continued on aspirin 325 mg once daily for 2 weeks. In comparison, the control group received no aspirin or any other antiplatelet/anticoagulant agents[74]. Despite trends in randomized controlled trials, multiple factors, in addition to whether or not an aneurysm has ruptured, must be considered to provide the ideal antiplatelet/anticoagulant therapy mode for each patient undergoing endovascular coiling. Parameters include medical history, extent of procedure, recovery, follow-up status, and magnetic resonance angiography assessment. In less frequent cases suffering from intraoperative clotting despite having received antiplatelet therapy, glycoprotein IIb/IIIa inhibitors such as abciximab may prove effective in producing fast-onset platelet inhibition[40]. However, the safety and efficacy of these drugs must be further studied to determine accurate timing, dosing, and administration route for successful treatment in patients.

Table 1. Advantages and disadvantages of endovascular coiling for cerebral aneurysm

Advantages	Disadvantages
Coiling alone	
Minimally invasive	Ruptured aneurysms cannot be treated with coiling alone; stent/balloon may be required
Quicker recovery	Requires blood thinners to prevent coagulation of coil
SAC	
Lower rates of aneurysm recurrence	Increased mortality rate
Can be used for wide-necked aneurysms	Difficulty visualizing aneurysms using fluorescence
WEB embolization	
Adaptable to wide-necked and bifurcation aneurysms	Not indicated for aneurysms that are not wide-necked
Reduced intraoperative time and long-term antiplatelet therapy; increased safety	Prevalence of recanalization postoperatively

Abbreviations: SAC: Stent-assisted coiling; WEB: Woven EndoBridge.

6. SAC

Although coiling has been used successfully for aneurysm repair, it can prove to be a difficult process. Aneurysms can occur in numerous locations with a wide variety of shapes, dimensions, and rupture capacities[75]. Stabilizing the aneurysm is one way to minimize the risks of coiling without reducing its advantageous effects. This stabilization can be engineered by utilizing a stent. In SAC, a stent can be placed within an aneurysm to bolster its shape, allowing for secure coil deposition[76]. The endovascular technique used in SAC is minimally invasive, accompanied by a high success rate, and a reduced risk of complications in comparison to other options available for treating aneurysms. Hence, it has the potential to significantly improve outcomes in cerebral aneurysm coiling.

SAC was originally used to treat wide-necked aneurysms[58,59]. Not only did it provide structural support to bolster the coils in the wide aneurysm sac, but it also prevented the coils from protruding into the parent artery[77]. Coil migration affects 14% of patients undergoing aneurysm coiling, and its effects are relatively understudied and can range from life-threatening infarcts to no significant thromboembolic impact[78]. Using a mesh design for a stent helps maintain unobstructed blood flow while preventing the movement of coils out of the aneurysm sac. Further, the development of more flexible intravascular stents over

time has expanded the utility of SAC to improve outcomes for aneurysms in smaller vessels[79-81]. Hence, recent studies have explored utilizing SAC in patients with intracranial aneurysms.

The major complications of coiling aneurysms arise due to a lack of regulatory control over the migration and deposition of the coil. The wide variety of stents that can be used provides an additional level of modulation to have the optimal effect for each distinct aneurysm in every patient. Aneurysms with different proportions may require a different stent material or density to achieve the desired outcome. One study by Masuda *et al.* classified aneurysms by size and identified mesh wire densities that allowed for the greatest change in flow velocity through the aneurysm[82]. Aneurysm size can be classified into the following categories: small, medium, large, and giant[83]. Masuda *et al.* determined that a 46.2% mesh density led to the greatest change in blood flow for every aneurysm. This mesh density, however, had different effects on aneurysms of different sizes. Aneurysms smaller than 4.0 mm showed an 80% reduction in blood flow, whereas giant aneurysms greater than 25.0 mm showed a blood flow reduction of only 50%[81]. Hence, the mesh density can be changed to achieve the appropriate blood flow reduction in aneurysms with different dimensions. Another study by Piotin *et al.* found that stents with a higher packing density were associated with a lower rate of angiographic recurrence[60]. Hence, mesh density can be adjusted to create an optimal stent that allows for improved outcomes in coiling for aneurysms.

SAC, however, is not without risks. Accessing aneurysms surgically always carries a risk of morbidity due to procedure-related complications and the potential aneurysm rupture[84]. Possible complications of SAC include the piercing of vessels, thromboembolic events, and hemorrhaging[85]. An additional issue that can arise if the stent becomes occluded is in-stent stenosis, which contributes to blood flow reduction within the parent artery to the extent of pathological level[86]. These complications, however, typically have a prevalence of < 7%, and most of these risks can be attributed to aneurysm size, older patient age, sensitive aneurysm location, or issues from a previously coiled aneurysm[84].

In recent years, numerous studies analyzed the safety and efficacy of SAC with regard to complication rates. For instance, one retrospective study by Aguilar-Salinas *et al.* evaluated data from 124 patients with unruptured wide-necked intracranial aneurysms[85]. Only 3.3% of these patients experienced complications from the procedure, such as vessel occlusion or aneurysm rupture. These patients also had a low risk of severe in-stent stenosis and recanalization, which affect 1% and 6.6% of patients, respectively. The Glasgow Outcome Scale was used to analyze the extent of impaired consciousness in these cases. About 80.7% of patients had a score of 5 or above at a 30-day follow-up, which later increased to 83.9%[85]. With this data, the study concluded that SAC is an effective and safe way to treat wide-necked intracranial aneurysms, with lower risks of complications and higher rates of success. Another study by Chalouhi *et al.* analyzed 461 elective SAC procedures[84]. They found favorable outcomes in 99% of these patients. About 87% of patients were available for follow-up at 26 months, who had recanalization and retreatment rates of 12% and 6.4%, respectively[84]. Overall, both studies concluded that SAC is a safe and efficacious procedure with minimal complications that can significantly improve the prognosis of patients with aneurysms.

Numerous research studies have evaluated the prevalence of adverse effects following SAC compared to non-SAC procedures. The results of these studies are summarized in Table 2. Most studies noted no significant differences in adverse effects between SAC and non-SAC. Piotin *et al.*, however, reviewed 1049 cases of aneurysm coiling and found that SAC was associated with more adverse effects than non-SAC[60]. Patients undergoing SAC faced 4.6% of procedural complications and 7.4% of permanent neurological procedure-related complications compared to 1.2% and 3.8% of patients, respectively, with non-SAC[60]. One limitation of the study that must be taken into consideration is that around 40 – 50% of patients in both groups were lost to long-term follow-up; therefore, the conduction of more comprehensive studies is needed in the future to draw more definitive conclusions. In addition, different stent types were used in this study, including balloon-expandable models and self-expandable stents, but no significant difference was noted in their outcomes. Despite potential differences in conclusions regarding adverse outcomes, data from all of these studies show that SAC improved long-term outcomes for patients when compared to non-SAC. Multiple studies found lower rates of recurrence, reduced recanalization rates, and improvements in clinically acceptable levels of occlusion in patients who had undergone SAC. These large-scale studies imply that SAC has significant utility in the treatment of intracranial aneurysms. Despite the differences observed between SAC and non-SAC procedures, more studies are needed to validate these findings and analyze their impacts on patient's quality of life.

As safety and efficacy of SAC are continuously evaluated, the appropriateness of use for SAC changes over time. For instance, SAC is now regarded as a useful

Table 2. An assessment of outcomes in patients treated with SAC compared to those treated with non-SAC

Study	Aneurysm type	Patients enrolled	Outcome
Zhang *et al.*, 2019[87]	Ruptured intracranial aneurysms	1049 patients; SAC (*n*=499), non-SAC (*n*=409)	The SAC group had a lower recurrence rate and incomplete occlusion rate than the non-SAC group. There was no significant difference in mortality at discharge; there was no favorable clinical outcome at discharge or follow-up.
Yi *et al.*, 2022[88]	Ruptured intracranial aneurysms	375 patients; SAC (*n*=101), non-SAC (*n*=274)	The SAC group had higher rates of complete occlusion, lower rates of recanalization, and lower need for treatment. There was no significant difference in periprocedural complications.
Piotin *et al.*, 2012[60]	Intracranial aneurysms	1325 patients; SAC (*n*=216), non-SAC (*n*=1109)	The SAC group had a lower rate of angiographic recurrence, as well as higher rates of procedural complications and permanent neurological procedure-related complications.
Liu *et al.*, 2017[89]	Ruptured intracranial aneurysms	279 patients; SAC (*n*=113), non-SAC (*n*=166)	The SAC group had better initial aneurysm occlusion status, implying better durability and safety. There was no significant difference in adverse outcomes, including permanent neurological deficits.
Zhang *et al.*, 2022[90]	Ruptured tiny intracranial aneurysms	245 patients; SAC (*n*=93), non-SAC (*n*=152)	The SAC group had a higher complete occlusion rate, a lower recurrence rate, and a higher rate of hemorrhagic complications. There was no significant difference in mortality or other adverse effects.
Goertz *et al.*, 2021[91]	Ruptured intracranial aneurysms	284 patients; SAC (*n*=64), non-SAC (*n*=220)	The SAC group had higher rates of complete occlusion and lower recanalization rates at 6-month follow-up. There were no significant differences in mortality or adverse effects.
Muller *et al.*, 2017[92]	Wide-necked aneurysms	355 patients; SAC (*n*=33), non-SAC (*n*=322)	The SAC group had higher rates of complete and clinically acceptable levels of occlusion.

Abbreviation: SAC: Stent-assisted coiling.

therapy for smaller berry aneurysms due to the improved long-term outcomes associated with SAC and the availability of stents that are effective in treating different sizes of aneurysms[60,61]. Considering that it was initially only used for wide-necked aneurysms, its implications are now countless. The adverse effects and long-term outcomes of SAC in comparison to non-SAC should be further researched, along with the impact of different sizes and densities of the stents that can be used in SAC. With future studies focusing on such topics, we believe that SAC can significantly contribute to harm reduction and better prognosis for patients with intracranial aneurysms.

7. WEB embolization

A trial known as the *International Subarachnoid Aneurysm Trial* has truly revolutionized our understanding of endovascular coiling in the treatment for ruptured aneurysms[93]. Since that trial, endovascular coiling has become one of the more prominent choices in the treatment of ruptured aneurysms[93]. While promising, endovascular coiling treating wide-necked bifurcating aneurysms (WNBA) remains a challenge due to the balance between preserving major vessels while properly occluding the aneurysm[94-97]. As the prevailing option for treating WNBAs, SAC has shown a ten-time higher risk in adverse events, which is largely caused by the requirement of DAPT post-procedure[94-99]. In addition, SAC poses durability concerns, exemplified by the frequent need for support from stents or flow diverters, and has limitations in safely achieving proper coil packing density[99,100].

The idea of the WEB was initially conceptualized in Aliso Viejo, California, USA in 2011 and is now FDA-approved. The WEB is a unique device that has a barrel-shape with a platinum core and nitinol mesh that employs intrasaccular flow disruption. The low porosity of the device causes disrupted flow at the aneurysm neck causing thrombosis and eventually occlusion[93,97]. The device allows for a seal of the aneurysm neck eliminating structural effects of the parent artery[101]. This, in combination with the WEB's lack of a metallic mesh, allows patients to avoid DAPT[93,99]. In addition, if the positioning of the deployed WEB is suboptimal, recapturing and resheathing can be performed to allow for better placement[102]. Further, devices employed in WEB have demonstrated an improved safety profile[102,103].

A prominent complication of WEB is the possibility of thromboembolic events[104]. Tau *et al.* conducted a meta-analysis by researching patients treated with unruptured aneurysms with WEB and found that 70% of periprocedural complications were thromboembolic[105]. It is theorized that this occurs for many reasons including lack of pre-treatment antiplatelet therapy, the thrombogenic state of the device, and the prothrombotic state of subarachnoid hemorrhage[93,106].

Typically, the WEB embolization procedure is performed by a neurointerventionalist and involves radial access.

Sizing of the WEB is selected according to measurements of the aneurysm on 2D digital subtraction angiography (DSA). The WEB should be oversized to properly fill the aneurysm sac while allowing it to completely cover its neck. Afterward, the device is delivered through a microcatheter[101,102].

A review published in 2021 by Crinnion *et al.*[93] summarized 11 articles encompassing 405 aneurysms in 398 patients diagnosed with ruptured aneurysms or subarachnoid hemorrhages that were treated with WEB embolization. Aneurysm characteristics included a range of 45%–92% anterior circulation and 7 – 56% with severe SAH. They found that the rate of success varied between 95.8% and 100%, and the number of aneurysms requiring additional techniques for occlusion was from 0% to 15%. Adequate occlusion was achieved in 71 – 96% of patients[107-114].

The safety profile of WEB embolization demonstrated that thromboembolic event rates range from 0% to 25% and overall, a thromboembolic event rate of 9.8% in all 398 patients. The authors cite two prominent studies, the CLARITY trial and the ARETA study which characterized thromboembolic event rates in CE. The CLARITY trial demonstrated a thromboembolic event rate of 20.8% for wide-necked aneurysms and the ARETA study showed a thromboembolic event rate of 10.4% in 753 aneurysms; both of the studies used coiling for treatment. Based on this, the TE rates of coiling and WEB embolization approaches are similar[93,115,116]. Other important safety endpoints included a 4% of morbidity, 1.8% of mortality, and rebleeding in 1.2% of patients. The authors concluded that WEB has proven to be safe and efficient in treating ruptured aneurysms when comparing it to other endovascular therapies[93].

In a retrospective review by Kabbasch *et al.* in 2019, around 66 patients that underwent WEB embolization were compared to 66 patients that underwent SAC. In the WEB group, 65 patients were treated with only WEB embolization, and the remaining one was treated with a combination of both WEB embolization and additional coiling. In the SAC group, both single stent and double stents were used in 80.3% and 19.7% of patients, respectively. Out of all of the patients, those that achieved complete occlusion immediately were 59.1% of WEB embolization patients and 92.4% of SAC patients. Halfway through their studies, complete occlusion was achieved in 83.3% of WEB embolization patients and 84.8% of SAC patients. Favorable outcomes were found in 86.4% of WEB embolization patients and 86.4% of SAC patients. The average treatment time was significantly longer for SAC when compared to WEB embolization. Complications occurred in 12.1% of the WEB embolization patients and 21.2% of SAC patients; however, these results were not statistically significant. Of note, 18.2% of SAC patients and 12.1% of WEB embolization patients developed thromboembolic complications. The authors conclude that WEB embolization is a viable alternative for the treatment of wide-neck bifurcation aneurysms, given that it limits long-term DAPT[101].

Another review performed in 2022 by Monteiro *et al.* analyzed nine articles with 377 acutely ruptured aneurysms treated with WEB embolization. Of the samples, 85.9% were anterior circulation aneurysms and 82.7% of them were wide-necked. Adequate occlusion occurred in 84.8% of cases and 4.5% of the patients required retreatment at follow-up. During catheterization, there were seven cases of perforation in the dome of the aneurysm. In all circumstances, once the WEB was deployed, the bleeding halted. The rate of post-procedural complications was 1% and was all thromboembolic[99].

A study performed by Stanca *et al.* characterized the long-term effects of WEB device. They included 35 ruptured WNBAs in 21 patients treated with WEB. They examined patients at the 3-year mark using DSA. After 3 years of follow-up, three death cases were recorded, which were not related to aneurysms. They also found complete occlusion in 61.1% of patients, 0% rebleeding rate, and 0% morbidity (no neurological signs). Although there was incomplete occlusion in 11.1% of patients, in this case, the neck showed no growth or minimal size increase (<2 mm); therefore, treatment was not required. The authors conclude that there is high stability 2 and 3 years after the procedure[117].

Overall, the WEB device demonstrates feasibility, a high rate of occlusions, and a low rate of complications. The clear advantages of this device include a reduction in long-term DAPT and fewer perioperative complications. The risk for thromboembolic events remains a challenge with using the WEB device, but compared with traditional coiling methods, the rates of these events are much lower. The WEB device should be considered a viable option in the treatment of WNBA.

8. Conclusion

For decades, numerous studies have contributed to diversifying treatment options of aneurysms. This review presents a detailed amount of information concerning the modern techniques of aneurysm treatment, including pharmaceuticals, SAC, coiling, and WEB embolization. Different techniques demonstrate varying levels of feasibility, safety, and patient satisfaction. The ability of WEB to disrupt intrasaccular flow is circumstantial evidence that it could be used to manage thrombotic

events. In comparison, the SAC method is rather complex due to a lack of regulatory control over the migration and deposition of the coil. In conclusion, this review provides details regarding various aneurysm treatments, and we believe a thorough understanding of these treatment methods could facilitate more personalized and monitored care.

Acknowledgments

None.

Funding

None.

Conflict of interest

The authors declare no conflicts of interest.

Author contributions

Conceptualization: Brandon Lucke-Wold
Writing – original draft: Anjali Patel, Daisy Valle, Drashti Patel, Marco Foreman, Devon Foster, and Alexander Nguyen
Writing – review and editing: Anjali Patel

Ethics approval and consent to participate

Not applicable.

Consent for publication

Not applicable.

Availability of data

Not applicable.

References

1. Spiotta AM, Chaudry MI, Hui FK, *et al.*, 2015, Evolution of thrombectomy approaches and devices for acute stroke: A technical review. *J Neurointerv Surg*, 7: 2–7.

   https://doi.org/10.1136/neurintsurg-2013-011022

2. Spiotta AM, Hussain MS, Sivapatham T, *et al.*, 2011, The versatile distal access catheter: The Cleveland Clinic experience. *Neurosurgery*, 68: 1677–1686.

   https://doi.org/10.1227/NEU.0b013e31820edfd8

3. Turk A, Manzoor MU, Nyberg EM, *et al*, 2013, Initial experience with distal guide catheter placement in the treatment of cerebrovascular disease: Clinical safety and efficacy. *J Neurointerv Surg*, 5: 247–252.

   https://doi.org/10.1136/neurintsurg-2011-010256

4. Nguyen TN, 2023, Management of unruptured intracranial aneurysms and brain arteriovenous malformations. *Continuum* (*Minneap Minn)*, 29: 584–604.

   https://doi.org/10.1212/CON.0000000000001247

5. Hackenberg KAM, Etminan N, 2021, Neurovascular disease, diagnosis, and therapy: Brain aneurysms. *Handb Clin Neurol*, 176: 121–134.

   https://doi.org/10.1016/B978-0-444-64034-5.00001-8

6. Gross BA, Du R, 2013, Natural history of cerebral arteriovenous malformations: A meta-analysis. *J Neurosurg*, 118: 437–443.

   https://doi.org/10.3171/2012.10.JNS121280

7. Pierot L, Wakhloo AK, 2013, Endovascular treatment of intracranial aneurysms: Current status. *Stroke*, 44: 2046–2054.

   https://doi.org/10.1161/Strokeaha.113.000733

8. Astrup J, Siesjö BK, Symon L, 1981, Thresholds in cerebral ischemia-the ischemic penumbra. *Stroke*, 12: 723–725.

   https://doi.org/10.1161/01.str.12.6.723

9. Shuaib A, Butcher K, Mohammad AA, *et al.*, 2011, Collateral blood vessels in acute ischaemic stroke: A potential therapeutic target. *Lancet Neurol*, 10: 909–921.

   https://doi.org/10.1016/S1474-4422(11)70195-8

10. Jackman K, Iadecola C, 2015, Neurovascular regulation in the ischemic brain. *Antioxid Redox Signal*, 22: 149–160.

    https://doi.org/10.1089/ars.2013.5669

11. Weber R, Brenck J, Diener HC, 2012, Antiplatelet therapy in cerebrovascular disorders. *Handb Exp Pharmacol*, 210: 519–546.

    https://doi.org/10.1007/978-3-642-29423-5_21

12. Kamarova M, Baig S, Patel H, *et al.*, 2022, Antiplatelet use in ischemic stroke. *Ann Pharmacother*, 56: 1159–1173.

    https://doi.org/10.1177/10600280211073009

13. Powers WJ, Rabinstein AA, Ackerson T, *et al.*, 2019, Guidelines for the early management of patients with acute ischemic stroke: 2019 Update to the 2018 guidelines for the early management of acute ischemic stroke: A guideline for healthcare professionals from the American heart association/American stroke association. *Stroke*, 50: e344–e418.

    https://doi.org/10.1161/STR.0000000000000211

14. Alquwaizani M, Buckley L, Adams C, *et al.*, 2013, Anticoagulants: A review of the pharmacology, dosing, and complications. *Curr Emerg Hosp Med Rep*, 1: 83–97.

    https://doi.org/10.1007/s40138-013-0014-6

15. Ross JA, Miller MM, Rojas Hernandez CMR, 2017, Comparative effectiveness and safety of direct oral anticoagulants (DOACs) versus conventional anticoagulation for the treatment of cancer-related venous

thromboembolism: A retrospective analysis. *Thromb Res*, 150: 86–89.

https://doi.org/10.1016/j.thromres.2016.12.016

16. Giustozzi M, Franco L, Vedovati MC, *et al*., 2019, Safety of direct oral anticoagulants versus traditional anticoagulants in venous thromboembolism. *J Thromb Thrombolysis*, 48: 439–453.

https://doi.org/10.1007/s11239-019-01878-x

17. Paciaroni M, Agnelli G, Micheli S, *et al*., 2007, Efficacy and safety of anticoagulant treatment in acute cardioembolic stroke: A meta-analysis of randomized controlled trials. *Stroke*, 38: 423–430.

https://doi.org/10.1161/01.STR.0000254600.92975.1f

18. Lip GYH, Kamath S, Hart RG, 2002, ABC of antithrombotic therapy: Antithrombotic therapy for cerebrovascular disorders. *BMJ*, 325: 1161–1163.

https://doi.org/10.1136/bmj.325.7373.1161

19. Kleindorfer DO, Towfighi A, Chaturvedi S, *et al*., 2021, 2021 guideline for the prevention of stroke in patients with stroke and transient ischemic attack: A guideline from the American heart association/American stroke association. *Stroke*, 52: e364–e467.

https://doi.org/10.1161/STR.0000000000000375

20. 2021, Correction to: 2021 Guideline for the prevention of stroke in patients with stroke and transient ischemic attack: A guideline from the American heart association/American stroke association. *Stroke*, 52: e483–e484.

https://doi.org/10.1161/STR.0000000000000383

21. Ford B, Peela S, Roberts C, 2022, Secondary prevention of ischemic stroke: Updated guidelines from AHA/ASA. *Am Fam Physician*, 105: 99–102.

22. Liu L, Wong KS, Leng X, *et al*., 2015, Dual antiplatelet therapy in stroke and ICAS: Subgroup analysis of chance. *Neurology*, 85: 1154–1162.

https://doi.org/10.1212/WNL.0000000000001972

23. Sindet-Pedersen C, Pallisgaard JL, Olesen JB, *et al*., 2015, Safety and efficacy of direct oral anticoagulants compared to warfarin for extended treatment of venous thromboembolism -a systematic review and meta-analysis. *Thromb Res*, 136: 732–738.

https://doi.org/10.1016/j.thromres.2015.07.022

24. Ma X, Li D, Liu S, *et al*., 2023, Efficacy and safety of ticagrelor versus aspirin and clopidogrel for stroke prevention in patients with vascular disease: A systematic review and meta-analysis. *Eur Neurol*, 86: 229–241.

https://doi.org/10.1159/000530504

25. Briganti F, Leone G, Marseglia M, *et al*., 2015, Endovascular treatment of cerebral aneurysms using flow-diverter devices: A systematic review. *Neuroradiol J*, 28: 365–375.

https://doi.org/10.1177/1971400915602803

26. Ravindran K, Casabella AM, Cebral J, *et al*., 2020, Mechanism of action and biology of flow diverters in the treatment of intracranial aneurysms. *Neurosurgery*, 86: S13–S19.

https://doi.org/10.1093/neuros/nyz324

27. Kadirvel R, Ding YH, Dai D, *et al*., 2014, Cellular mechanisms of aneurysm occlusion after treatment with a flow diverter. *Radiology*, 270: 394–399.

https://doi.org/10.1148/radiol.13130796

28. Matsuda Y, Chung J, Lopes DK, 2018, Analysis of neointima development in flow diverters using optical coherence tomography imaging. *J Neurointerv Surg*, 10: 162–167.

https://doi.org/10.1136/neurintsurg-2016-012969

29. Puffer C, Dai D, Ding YH, *et al*., 2015, Gene expression comparison of flow diversion and coiling in an experimental aneurysm model. *J Neurointerv Surg*, 7: 926–930.

https://doi.org/10.1136/neurintsurg-2014-011452

30. Huang MT, Mason JC, Birdsey GM, *et al*., 2005, Endothelial intercellular adhesion molecule (ICAM)-2 regulates angiogenesis. *Blood*, 106: 1636–1643.

https://doi.org/10.1182/blood-2004-12-4716

31. Arrese I, Sarabia R, Pintado R, *et al*., 2013, Flow-diverter devices for intracranial aneurysms: Systematic review and meta-analysis. *Neurosurgery*, 73: 193–200.

https://doi.org/10.1227/01.neu.0000430297.17961.f1

32. Brinjikji W, Murad MH, Lanzino G, *et al*., 2013, Endovascular treatment of intracranial aneurysms with flow diverters: A meta-analysis. *Stroke*, 44: 442–447.

https://doi.org/10.1161/STROKEAHA.112.678151

33. Binh NT, Luu VD, Thong PM, *et al*., 2020, Flow diverter stent for treatment of cerebral aneurysms: A report of 130 patients with 134 aneurysms. *Heliyon*, 6: e03356.

https://doi.org/10.1016/j.heliyon.2020.e03356

34. Shehata MA, Ibrahim MK, Ghozy S, *et al*., 2022, Long-term outcomes of flow diversion for unruptured intracranial aneurysms: A systematic review and meta-analysis. *J Neurointerv Surg*, 15: 898–902.

https://doi.org/10.1136/jnis-2022-019240

35. Medical Advisory Secretariat, 2006, Coil embolization for intracranial aneurysms: An evidence-based analysis. *Ont Health Technol Assess Ser*, 6: 1–114.

36. Raymond J, Guilbert F, Weill A, *et al*., 2003, Long-term angiographic recurrences after selective endovascular treatment of aneurysms with detachable coils. *Stroke*, 34: 1398–1403.

https://doi.org/10.1161/01.STR.0000073841.88563.E9

37. Chalouhi N, Tjoumakaris S, Gonzalez LF, *et al*., 2014, Coiling of large and giant aneurysms: Complications and long-term results of 334 cases. *AJNR Am J Neuroradiol*, 35: 546–552.

https://doi.org/10.3174/ajnr.A3696

38. Consoli A, Vignoli C, Renieri L, *et al*., 2016, Assisted coiling of saccular wide-necked unruptured intracranial aneurysms: Stent versus balloon. *J Neurointerv Surg*, 8: 52–57.

https://doi.org/10.1136/neurintsurg-2014-011466

39. Ding YH, Lewis, DA, Kadirvel R, *et al*., 2011, The woven EndoBridge: A new aneurysm occlusion device. *AJNR Am J Neuroradiol*, 32: 607–611.

https://doi.org/10.3174/ajnr.A2399

40. Rahme RJ, Zammar SG, El Ahmadieh TY, *et al*., 2014, The role of antiplatelet therapy in aneurysm coiling. *Neurol Res*, 36: 383–388.

https://doi.org/10.1179/1743132814Y.0000000317

41. Willard JE, Lange RA, Hillis LD, 1992, The use of aspirin in ischemic heart disease. *New Engl J Med*, 327: 175–181.

https://doi.org/10.1056/NEJM199207163270308

42. Fiehler J, Ries T, 2009, Prevention and treatment of thromboembolism during endovascular aneurysm therapy. *Klin Neuroradiol*, 19: 73–81.

https://doi.org/10.1007/s00062-009-8029-9

43. Hwang G, Jung C, Park SQ, *et al*., 2010, Thromboembolic complications of elective coil embolization of unruptured aneurysms: The effect of oral antiplatelet preparation on periprocedural thromboembolic complication. *Neurosurgery*, 67: 743–748.

https://doi.org/10.1227/01.NEU.0000374770.09140.FB

44. Qureshi AI, Luft AR, Sharma M, *et al*., 2000, Prevention and treatment of thromboembolic and ischemic complications associated with endovascular procedures: Part II--Clinical aspects and recommendations. *Neurosurgery*, 46: 1360–1375.

https://doi.org/10.1097/00006123-200006000-00014

45. Kuno T, Yokoyama Y, Briasoulis A, *et al*., 2021, Duration of antiplatelet therapy following transcatheter aortic valve replacement: Systematic review and network meta-analysis. *J Am Heart Assoc*, 10: e019490.

https://doi.org/10.1161/JAHA.120.019490

46. Motovska Z, Widimsky P, Petr R, *et al*., 2009, Factors influencing clopidogrel efficacy in patients with stable coronary artery disease undergoing elective percutaneous coronary intervention: Statin's advantage and the smoking "paradox". *J Cardiovasc Pharmacol*, 53: 368–372.

https://doi.org/10.1097/FJC.0b013e31819d616b

47. Prabhakaran S, Wells KR, Lee VH, *et al*., 2008, Prevalence and risk factors for aspirin and clopidogrel resistance in cerebrovascular stenting. *AJNR Am J Neuroradiol*, 29: 281–285.

https://doi.org/10.3174/ajnr.A0818

48. Ryu DS, Hong CK, Sim YS, *et al*., 2010, Anti-platelet drug resistance in the prediction of thromboembolic complications after neurointervention. *J Korean Neurosurg Soc*, 48: 319–324.

https://doi.org/10.3340/jkns.2010.48.4.319

49. Gerlach R, Beck J, Setzer M, *et al*., 2007, Treatment related morbidity of unruptured intracranial aneurysms: Results of a prospective single centre series with an interdisciplinary approach over a 6 year period (1999–2005). *J Neurol Neurosurg Psychiatry*, 78: 864–871.

https://doi.org/10.1136/jnnp.2006.106823

50. Barker FG 2nd, Amin-Hanjani S, Butler WE, *et al*., 2004, Age-dependent differences in short-term outcome after surgical or endovascular treatment of unruptured intracranial aneurysms in the United States, 1996-2000. *Neurosurgery*, 54: 18–28.

https://doi.org/10.1227/01.neu.0000097195.48840.c4

51. Currie S, Mankad K, Goddard A, 2011, Endovascular treatment of intracranial aneurysms: Review of current practice. *Postgrad Med J*, 87: 41–50.

https://doi.org/10.1136/pgmj.2010.105387

52. Chun YI, Roh HG, Choe WJ, *et al*., 2013, Tiny aneurysms treated with single coil: Morphological comparison between bare platinum coil and matrix coil. *Clin Neurol Neurosurg*, 115: 529–534.

https://doi.org/10.1016/j.clineuro.2012.05.023

53. Khan SNH, Nichols C, Depowell JJ, *et al*., 2012, Comparison of coil types in aneurysm recurrence. *Clin Neurol Neurosurg*, 114: 12–16.

https://doi.org/10.1016/j.clineuro.2011.07.017

54. Patel P, Sarayi SMMJ, Chen D, *et al*., 2021, Fast virtual coiling algorithm for intracranial aneurysms using pre-shape path planning. *Comput Biol Med*, 134: 104496.

https://doi.org/10.1016/j.compbiomed.2021.104496

55. Hu J, Albadawi H, Chong BW, *et al*., 2019, Advances in biomaterials and technologies for vascular embolization. *Adv Mater*, 31: e1901071.

https://doi.org/10.1002/adma.201901071

56. Babiker MH, Gonzalez LF, Albuquerque F, *et al*., 2013, An *in vitro* study of pulsatile fluid dynamics in intracranial aneurysm models treated with embolic coils and flow diverters. *IEEE Trans Biomed Eng*, 60: 1150–1159.

https://doi.org/10.1109/TBME.2012.2228002

57. Benitez RP, Silva MT, Klem J, *et al*., 2004, Endovascular occlusion of wide-necked aneurysms with a new intracranial

microstent (Neuroform) and detachable coils. *Neurosurgery*, 54: 1359–1367.

https://doi.org/10.1227/01.neu.0000124484.87635.cd

58. Biondi A, Janardhan V, Katz JM, *et al*., 2007, Neuroform stent-assisted coil embolization of wide-neck intracranial aneurysms: Strategies in stent deployment and midterm follow-up. *Neurosurgery*, 61: 460–469.

https://doi.org/10.1227/01.NEU.0000290890.62201.A9

59. Higashida RT, Smith W, Gress D, *et al*., 1997, Intravascular stent and endovascular coil placement for a ruptured fusiform aneurysm of the basilar artery. Case report and review of the literature. *J Neurosurg*, 87: 944–949.

https://doi.org/10.3171/jns.1997.87.6.0944

60. Piotin M, Blanc R, Spelle L, *et al*., 2010, Stent-assisted coiling of intracranial aneurysms: Clinical and angiographic results in 216 consecutive aneurysms. *Stroke*, 41: 110–115.

https://doi.org/10.1161/STROKEAHA.109.558114

61. Hong Y, Wang YJ, Deng Z, *et al*., 2014, Stent-assisted coiling versus coiling in treatment of intracranial aneurysm: A systematic review and meta-analysis. *PLoS One*, 9: e82311.

https://doi.org/10.1371/journal.pone.0082311

62. Phan K, Huo YR, Jia F, *et al*., 2016, Meta-analysis of stent-assisted coiling versus coiling-only for the treatment of intracranial aneurysms. *J Clin Neurosci*, 31: 15–22.

https://doi.org/10.1016/j.jocn.2016.01.035

63. Ben-Israel D, Belanger BL, Adibi A, *et al*., 2021, Innovation in unruptured intracranial aneurysm coiling: At which price or efficacy are new technologies cost-effective? *PLoS One*, 16: e0255870.

https://doi.org/10.1371/journal.pone.0255870

64. Campos JK, Lien BV, Wang AS, *et al*., 2020, Advances in endovascular aneurysm management: Coiling and adjunctive devices. *Stroke Vasc Neurol*, 5: 14–21.

https://doi.org/10.1136/svn-2019-000303

65. Kocur D, Paździora P, Przybyłko N, *et al*., 2020, Thromboembolism during coiling of intracranial aneurysms: Predictors and clinical outcome. *Wideochir Inne Tech Maloinwazyjne*, 15: 319–328.

https://doi.org/10.5114/wiitm.2019.89118

66. Willinsky RA, Taylor SM, TerBrugge K, *et al*., 2003, Neurologic complications of cerebral angiography: Prospective analysis of 2,899 procedures and review of the literature. *Radiology*, 227: 522–528.

https://doi.org/10.1148/radiol.2272012071

67. Waugh JR, Sacharias N, 1992, Arteriographic complications in the DSA era. *Radiology*, 182: 243–246.

https://doi.org/10.1148/radiology.182.1.1727290

68. Laing AB, Gooi HC, Gelber RH, 1974, Letter: An acute attack of quartan malaria in a leprosy patient being treated with diaminodiphenylsulphone. *Trans R Soc Trop Med Hyg*, 68: 165–166.

https://doi.org/10.1016/0035-9203(74)90191-6

69. Choi J, Koo Y, Whang K, *et al*., 2021, Safety of heparin loading during endovascular embolization in patients with aneurysmal subarachnoid hemorrhage. *Clin Neurol Neurosurg*, 201: 106453.

https://doi.org/10.1016/j.clineuro.2020.106453

70. Ries T, Buhk JH, Kucinski T, *et al*., 2006, Intravenous administration of acetylsalicylic acid during endovascular treatment of cerebral aneurysms reduces the rate of thromboembolic events. *Stroke*, 37: 1816–1821.

https://doi.org/10.1161/01.STR.0000226933.44962.a6

71. Watala C, Golanski J, Rozalski M, *et al*., 2003, Is platelet aggregation a more important contributor than platelet adhesion to the overall platelet-related primary haemostasis measured by PFA-100? *Thromb Res*, 109: 299–306.

https://doi.org/10.1016/s0049-3848(03)00238-x

72. Eskey CJ, Meyers PM, Nguyen TN, *et al*., 2018, Indications for the performance of intracranial endovascular neurointerventional procedures: A scientific statement from the American heart association. *Circulation*, 137: e661–e689.

https://doi.org/10.1161/CIR.0000000000000567

73. Kang HS, Kwon BJ, Kim JE, *et al*., 2010, Preinterventional clopidogrel response variability for coil embolization of intracranial aneurysms: Clinical implications. *AJNR Am J Neuroradiol*, 31: 1206–1210.

https://doi.org/10.3174/ajnr.A2051

74. Edwards NJ, Jones WH, Sanzgiri A, *et al*., 2017, Antiplatelet therapy for the prevention of peri-coiling thromboembolism in high-risk patients with ruptured intracranial aneurysms. *J Neurosurg*, 127: 1326–1332.

https://doi.org/10.3171/2016.9.JNS161340

75. Raghavan ML, Ma B, Harbaugh RE, 2005, Quantified aneurysm shape and rupture risk. *J Neurosurg*, 102: 355–362.

https://doi.org/10.3171/jns.2005.102.2.0355

76. Horowitz MB, Levy EI, Koebbe CJ, *et al*., 2001, Transluminal stent-assisted coil embolization of a vertebral confluence aneurysm: Technique report. *Surg Neurol*, 55: 291–296.

https://doi.org/10.1016/s0090-3019(01)00421-9

77. Luo CB, Chang FC, Teng MM, *et al*., 2008, Stent management of coil herniation in embolization of internal carotid aneurysms. *AJNR Am J Neuroradiol*, 29: 1951–1955.

https://doi.org/10.3174/ajnr.A1268

78. Ishihara H, Ishihara S, Niimi J, *et al*., 2015, Risk factors for coil protrusion into the parent artery and associated

thrombo-embolic events following unruptured cerebral aneurysm embolization. *Interv Neuroradiol*, 21: 178–183.

https://doi.org/10.1177/1591019915582375

79. Sekhon LH, Morgan MK, Sorby W, *et al*., 1998, Combined endovascular stent implantation and endosaccular coil placement for the treatment of a wide-necked vertebral artery aneurysm: Technical case report. *Neurosurgery*, 43: 380–383.

https://doi.org/10.1097/00006123-199808000-00127

80. Lylyk P, Cohen JE, Ceratto R, *et al*., 2001, Combined endovascular treatment of dissecting vertebral artery aneurysms by using stents and coils. *J Neurosurg*, 94: 427–432.

https://doi.org/10.3171/jns.2001.94.3.0427

81. Mericle RA, Lanzino G, Wakhloo AK, *et al*., 1998, Stenting and secondary coiling of intracranial internal carotid artery aneurysm: Technical case report. *Neurosurgery*, 43: 1229–1234.

https://doi.org/10.1097/00006123-199811000-00130

82. Masuda S, Fujimura S, Takao H, *et al*., 2022, Effects of different stent wire mesh densities on hemodynamics in aneurysms of different sizes. *PLoS One*, 17: e0269675.

https://doi.org/10.1371/journal.pone.0269675

83. Merritt WC, Berns HF, Ducruet AF, *et al*., 2021, Definitions of intracranial aneurysm size and morphology: A call for standardization. *Surg Neurol Int*, 12: 506.

https://doi.org/10.25259/SNI_576_2021

84. Chalouhi N, Jabbour P, Singhal S, *et al*., 2013, Stent-assisted coiling of intracranial aneurysms: Predictors of complications, recanalization, and outcome in 508 cases. *Stroke*, 44: 1348–1353.

https://doi.org/10.1161/strokeaha.111.000641

85. Aguilar-Salinas P, Brasiliense LB, Santos R, *et al*., 2019, Safety and efficacy of stent-assisted coiling in the treatment of unruptured wide-necked intracranial aneurysms: A single-center experience. *Cureus*, 11: e4847.

https://doi.org/10.7759/cureus.4847

86. Buccheri D, Piraino D, Andolina G, *et al*., 2016, Understanding and managing in-stent restenosis: A review of clinical data, from pathogenesis to treatment. *J Thorac Dis*, 8: E1150–E1162.

https://doi.org/10.21037/jtd.2016.10.93

87. Zhang X, Zuo Q, Tang H, *et al*., 2019, Stent assisted coiling versus non-stent assisted coiling for the management of ruptured intracranial aneurysms: A meta-analysis and systematic review. *J Neurointerv Surg*, 11: 489–496.

https://doi.org/10.1136/neurintsurg-2018-014388

88. Yi HJ, Shin DS, Kim BT, *et al*., 2023, Comparison of neuroform atlas stent-assisted coiling and coiling alone in ruptured intracranial aneurysms: A propensity score matching analysis. *Neurosurgery*, 92: 607–614.

https://doi.org/10.1227/neu.0000000000002254

89. Liu Y, Wang F, Wang M, *et al*., 2017, Comparison of stent-assisted coil placement and coiling-only for the treatment of ruptured intracranial aneurysms. *Med Sci Monit*, 23: 5697–5704.

https://doi.org/10.12659/msm.905107

90. Zhang G, Wu Y, Wei Y, *et al*., 2022, Stent-assisted coiling vs. Coiling alone of ruptured tiny intracranial aneurysms: A contemporary cohort study in a high-volume center. *Front Neurol*, 13: 1076026.

https://doi.org/10.3389/fneur.2022.1076026

91. Goertz L, Liebig T, Pennig L, *et al*., 2021, Propensity score-adjusted analysis on stent-assisted coiling versus coiling alone for ruptured intracranial aneurysms. *Sci Rep*, 11: 21742.

https://doi.org/10.1038/s41598-021-01156-y

92. Müller M, Brockmann C, Afat S, *et al*., 2017, Temporary stent-assisted coil embolization as a treatment option for wide-neck aneurysms. *AJNR Am J Neuroradiol*, 38: 1372–1376.

https://doi.org/10.3174/ajnr.A5204

93. Crinnion W, Bhogal P, Makalanda HLD, *et al*., 2021, The Woven Endobridge as a treatment for acutely ruptured aneurysms: A review of the literature. *Interv Neuroradiol*, 27: 602–608.

https://doi.org/10.1177/1591019921991397

94. Molyneux AJ, Kerr RSC, Yu LM, *et al*., 2005, International subarachnoid aneurysm trial (ISAT) of neurosurgical clipping versus endovascular coiling in 2143 patients with ruptured intracranial aneurysms: A randomised comparison of effects on survival, dependency, seizures, rebleeding, subgroups, and aneurysm occlusion. *Lancet*, 366: 809–817.

https://doi.org/10.1016/S0140-6736(05)67214-5

95. Fernandez Zubillaga A, Guglielmi G, Viñuela F, *et al*., 1994, Endovascular occlusion of intracranial aneurysms with electrically detachable coils: Correlation of aneurysm neck size and treatment results. *AJNR Am J Neuroradiol*, 15: 815–820.

96. Debrun GM, Aletich VA, Kehrli P, *et al*., 1998, Selection of cerebral aneurysms for treatment using Guglielmi detachable coils: The preliminary university of Illinois at Chicago experience. *Neurosurgery*, 43: 1281–1295.

https://doi.org/10.1097/00006123-199812000-00011

97. Goyal N, Hoit D, DiNitto J, *et al*., 2020, How to WEB: A practical review of methodology for the use of the Woven EndoBridge. *J Neurointerv Surg*, 12: 512–520.

https://doi.org/10.1136/neurintsurg-2019-015506

98. Kozakiewicz J, Wrzolkowa T, 1976, Vascular changes of chronic lupus erythematosus. Electron microscopic studies.

Arch Dermatol Res (*1975*), 256: 327–331.

https://doi.org/10.1007/BF00572499

99. Monteiro A, Lazar AL, Waqas M, *et al*., 2022, Treatment of ruptured intracranial aneurysms with the Woven EndoBridge device: A systematic review. *J Neurointerv Surg*, 14: 366–370.

https://doi.org/10.1136/neurintsurg-2021-017613

100. Mascitelli JR, Lawton MT, Hendricks BK, *et al*., 2019, Analysis of wide-neck aneurysms in the barrow ruptured aneurysm trial. *Neurosurgery*, 85: 622–631.

https://doi.org/10.1093/neuros/nyy439

101. Kabbasch C, Goertz L, Siebert E, *et al*., 2019, WEB embolization versus stent-assisted coiling: Comparison of complication rates and angiographic outcomes. *J Neurointerv Surg*, 11: 812–816.

https://doi.org/10.1136/neurintsurg-2018-014555

102. Lee JE, Srinivasan VM, Kan P, 2022, Woven EndoBridge embolization in the retreatment of basilar apex aneurysm. *Neurosurg Focus Video*, 7: V8.

https://doi.org/10.3171/2022.7.FOCVID21152

103. Pierot L, Moret J, Barreau X, *et al*., 2018, Safety and efficacy of aneurysm treatment with WEB in the cumulative population of three prospective, multicenter series. *J Neurointerv Surg*, 10: 553–559.

https://doi.org/10.1136/neurintsurg-2017-013448

104. Arthur AS, Molyneux A, Coon AL, *et al*., 2019, The safety and effectiveness of the Woven EndoBridge (WEB) system for the treatment of wide-necked bifurcation aneurysms: Final 12-month results of the pivotal WEB intrasaccular therapy (WEB-IT) study. *J Neurointerv Surg*, 11: 924–930.

https://doi.org/10.1136/neurintsurg-2019-014815

105. Tau N, Sadeh-Gonik U, Aulagner G, *et al*., 2018, The Woven EndoBridge (WEB) for endovascular therapy of intracranial aneurysms: Update of a systematic review with meta-analysis. *Clin Neurol Neurosurg*, 166: 110–115.

https://doi.org/10.1016/j.clineuro.2018.01.025

106. Itoyama Y, Fujioka S, Takaki S, *et al*., 1994, Significance of elevated thrombin-antithrombin III complex and plasmin-alpha 2-plasmin inhibitor complex in the acute stage of nontraumatic subarachnoid hemorrhage. *Neurosurgery*, 35: 1055–1060.

https://doi.org/10.1227/00006123-199412000-00006

107. Liebig T, Kabbasch C, Strasilla C, *et al*., 2015, Intrasaccular flow disruption in acutely ruptured aneurysms: A multicenter retrospective review of the use of the WEB. *AJNR Am J Neuroradiol*, 36: 1721–1727.

https://doi.org/10.3174/ajnr.A4347

108. Van Rooij SB, Van Rooij WJ, Peluso JP, *et al*., 2017, WEB treatment of ruptured intracranial aneurysms: A single-center cohort of 100 patients. *AJNR Am J Neuroradiol*, 38: 2282–2287.

https://doi.org/10.3174/ajnr.A5371

109. Da Ros V, Bozzi A, Comelli C, *et al*., 2019, Ruptured intracranial aneurysms treated with woven endobridge intrasaccular flow disruptor: A multicenter experience. *World Neurosurg*, 122: e498–e505.

https://doi.org/10.1016/j.wneu.2018.10.088

110. Raj R, Rautio R, Pekkola J, *et al*., 2019, Treatment of ruptured intracranial aneurysms using the Woven EndoBridge device: A two-center experience. *World Neurosurg*, 123: e709–e716.

https://doi.org/10.1016/j.wneu.2018.12.010

111. Al Saiegh F, Hasan D, Mouchtouris N, *et al*., 2020, Treatment of acutely ruptured cerebral aneurysms with the Woven EndoBridge device: Experience post-FDA approval. *Neurosurgery*, 87: E16–E22.

https://doi.org/10.1093/neuros/nyaa092

112. Behme D, Berlis A, Weber W, 2015, Woven EndoBridge intrasaccular flow disrupter for the treatment of ruptured and unruptured wide-neck cerebral aneurysms: Report of 55 cases. *AJNR Am J Neuroradiol*, 36: 1501–1506.

https://doi.org/10.3174/ajnr.A4323

113. Clajus C, Strasilla C, Fiebig T, *et al*., 2017, Initial and mid-term results from 108 consecutive patients with cerebral aneurysms treated with the WEB device. *J Neurointerv Surg*, 9: 411–417.

https://doi.org/10.1136/neurintsurg-2016-012276

114. Popielski J, Berlis A, Weber W, *et al*., 2018, Two-center experience in the endovascular treatment of ruptured and unruptured intracranial aneurysms using the WEB device: A retrospective analysis. *AJNR Am J Neuroradiol*, 39: 111–117.

https://doi.org/10.3174/ajnr.A5413

115. Cognard C, Pierot L, Anxionnat R, *et al*., 2011, Results of embolization used as the first treatment choice in a consecutive nonselected population of ruptured aneurysms: Clinical results of the clarity GDC study. *Neurosurgery*, 69: 837–841.

https://doi.org/10.1227/NEU.0b013e3182257b30

116. Pierot L, Barbe C, Nguyen HA, *et al*., 2020, Intraoperative complications of endovascular treatment of intracranial aneurysms with coiling or balloon-assisted coiling in a prospective multicenter cohort of 1088 participants: Analysis of recanalization after endovascular treatment of intracranial aneurysm (ARETA) study. *Radiology*, 295: 381–389.

https://doi.org/10.1148/radiol.2020191842

117. Stanca C, Carriero S, Negroni D, *et al*., 2022, Woven EndoBridge in wide-neck bifurcation aneurysms: Digital subtraction angiography at 3-year follow-up. *J Clin Med*, 11: 2879.

https://doi.org/10.3390/jcm11102879

ACCSCIENCE PUBLISHING

INNOSC Theranostics and Pharmacological Sciences

REVIEW ARTICLE

Cytotoxicity of bioactive compounds derived from cyanobacteria

Hanaa Ali Hussein*, Fatin L. Khaphi, and Zahra Kadhum Saeed

Department of Basic Sciences, College of Dentistry, University of Basrah, Basrah, Iraq

Abstract

Cyanobacteria are rich in bioactive compounds that exhibit diverse biological activities, including antiproliferative, cytotoxic, and antineoplastic properties. Many of these compounds are currently being studied in clinical trials. In this paper, newly discovered bioactive compounds from various cyanobacteria species that have demonstrated anticancer effects against multiple cancer cell lines, such as apratoxin, symplostatin 1, bartolosides, caylobolide, bisebromoamides, carmaphycins, and anaenamides, are reviewed. At present, there are no clear guidelines on approving cyanobacteria-derived bioactive compounds for use in treating diseases. While it is not uncommon that the intake of these compounds is accompanied by side effects, investigations on these compounds should focus on increasing the safety and efficacy of the compounds, or at least tread a fine line between drug safety and effectiveness for cancer patients. This review overviews the efficacy and cytotoxicity of cyanobacteria-derived bioactive compounds, providing researchers insights into how to maximize the benefits of these compounds through research.

Keywords: Bioactive compounds; Cyanobacteria; Cytotoxicity

***Corresponding author:**
Hanaa Ali Hussein
(hanaa.hussein@uobasrah.edu.iq)

Citation: Hussein HA, Khaphi FL, Saeed ZK, 2024, Cytotoxicity of bioactive compounds derived from cyanobacteria. *INNOSC Theranostics and Pharmacological Sciences*, 7(1): 1388.
https://doi.org/10.36922/itps.1388

Received: July 27, 2023

Accepted: September 5, 2023

Published Online: October 26, 2023

1. Introduction

Cancer is the leading cause of death worldwide, resulting in approximately 10 million deaths in 2020.In addition, there were 19.3 million new cases reported[1]. There are over 200 types of cancer that can spread throughout the body, leading to metastasis and potentially fatal consequences[2]. Many chemotherapy drugs used to fight cancer can harm both cancerous and healthy cells. Natural compounds derived from natural sources, such as marine organisms, plants, and microorganisms, have become popular therapeutic candidates for treating cancer because they can effectively target cancer cells with little to no harmful effects on healthy cells[3,4]. Cyanobacteria, also known as blue-green microalgae, contain a variety of bioactive compounds with low to high molecular weight, such as hapalindole A, oscillapeptin A, minutissamide A, lyngbic acid, caylobolide B, anabaenopeptin E, lobocyclamides, lyngbyacyclamides A and B, homodolostatin, malyngamides, glicomacrolides, swinholides, macrolactones, and viridamides. Approximately 40% of these compounds can be utilized as anticancer and antimicrobial agents[5,6], and most of these compounds are currently under clinical investigations[7]. Cyanobacteria-derived bioactive compounds have shown promising anticancer activity against cancer cells. This can be attributed to various mechanisms, such as inducing cell cycle arrest in the G1 phase, inhibiting serine proteases such as

elastase and trypsin, causing DNA fragmentation and oxidative stress, disrupting microfilaments, modulating Bcl-2 protein, and even modifying cell membrane dynamics (Figure 1)[8,9]. In this review, the potential cytotoxicity of compounds derived from cyanobacteria is discussed.

2. Cyanobacteria

Cyanobacteria is a Gram-negative prokaryote rich in the pigment c-phycocyanin and is capable of oxygenic photosynthesis[10]. Cyanobacteria can be found in different environments, such as oceans, freshwater, bare rock, and soil, and can survive in extreme high-temperature conditions, such as geothermal and hot spring water[11]. Cyanobacteria exist as individual cells (Spirulina), filaments (Oscillatoria), or colonies (Nostoc) enclosed by a mucilaginous sheath. Cyanobacteria are typically microscopic but become visible when they form colonies[12]. The classification of cyanobacteria was proposed in 1985, and it was initially classified into four orders: Nostocales, stigonematales, chroococcales, and oscillatoriales. At present, there are five orders of cyanobacteria, namely, pleurocapsales, chroococcales, stigonematales, nostocales, and oscillatoriales (Table 1)[13].

Cyanobacteria are known to contain a variety of bioactive compounds, such as peptides, polyketides, terpenes, alkaloids, fatty acids, and ultraviolet-absorbing compounds. The biosynthesis pathways of these compounds are illustrated in Figure 2. These bioactive compounds are produced through both non-ribosomal (non-ribosomal peptide synthetases) and ribosomal pathways. Polyketide metabolites, for instance, contain cis- and trans-acyltransferases, with the trans-face having non-repetitive acyltransferases and the cis-face having repetitive acyltransferases[14]. There are several traditional extraction methods used to extract bioactive compounds from different marine sources (such as cyanobacteria). The traditional methods include Soxhlet extraction (extract organic compounds such as phenols, pesticides, and polycyclic aromatic hydrocarbons), hydrodistillation, hot continuous extraction, percolation, maceration, infusion, and decoction. In contrast, modern extraction methods include supercritical fluid extraction, microwave-assisted extraction, pressurized liquid extraction, and enzyme-assisted extraction[15].

3. Anticancer compounds from cyanobacteria

Cyanobacteria contain a variety of anticancer drugs, which are reviewed in the following sub-sections.

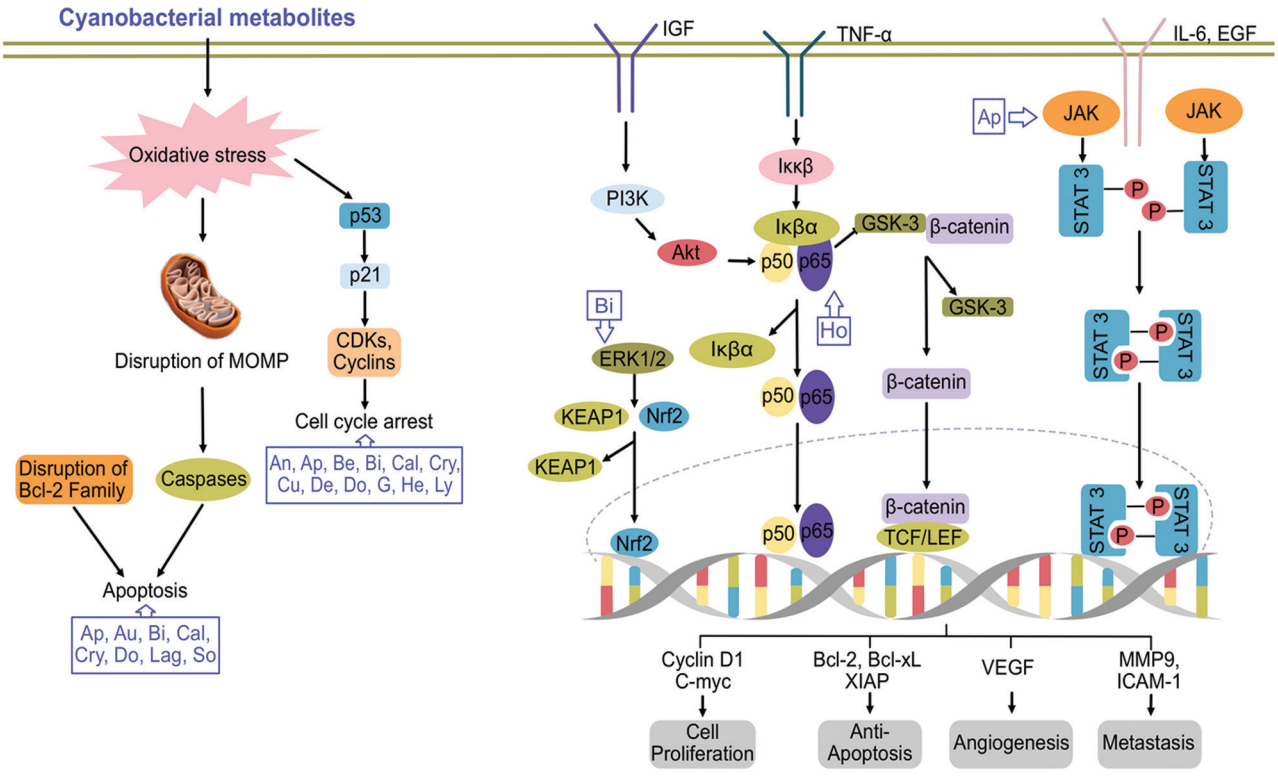

Figure 1. Potential anticancer mechanisms of bioactive compounds derived from cyanobacteria. Adapted from Qamar *et al.*[9], distributed under Creative Commons Attribution (CC BY) license.

Table 1. Classification of cyanobacteria[13]

No.	Order	Species	Environment	Morphology
1	Nostocales	*Anabaena* sp.	Freshwater	Filamentous
		Nostoc sp.		Terrestrial
2	Chroococcales	*Microcystis* sp.	Freshwater	Unicellular
		Synechococcus sp.	Marine water	
		Synechocystis sp.	Freshwater	
3	Pleurocapsales	*Hyella caespitosa*	Marine water	Unicellular
4	Stigonematales	*Fischerella muscicola*	Freshwater	Filamentous
5	Oscillatoriales	*Oscillatoria* sp.	Freshwater	Filamentous
		Lyngbya majuscula	Tropical marine water	

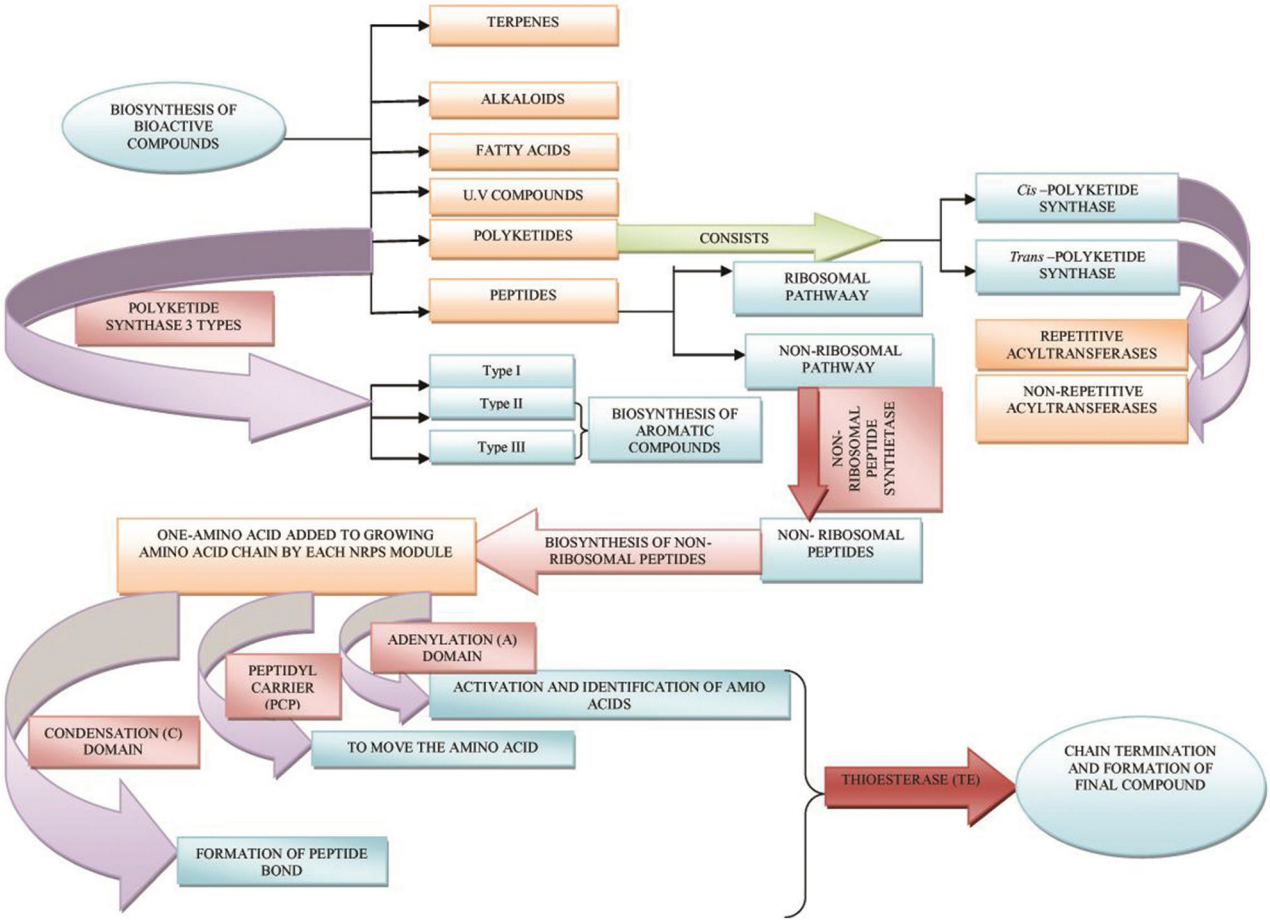

Figure 2. Biosynthesis pathway of the cyanobacteria bioactive compounds. Adapted from Pattnaik and Singh, 2020[14], distributed under a Creative Commons Attribution (CC BY) license.

3.1. Cyclic depsipeptides

3.1.1. Apratoxin

Apratoxin A is a new potent cytotoxic compound derived from marine cyanobacteria *Lyngbya majuscula*. Apratoxin A is a cyclic depsipeptide made up of R (â-unsaturated modified cysteine residues), proline, 3-dihydroxyliety fatty acid, 7-dihydroxy-2,5,8,-tetramethylnonenoic acid, and 3-methylated amino acids (O-methyltyrosine, N-methyl isoleucine, and N-methyl-alanine)[16] (Figure 3). Apratoxin A exhibited significant cytotoxicity against KB (0.52 nM) and colon LoVo (0.36 nM) cancer cells. *In vivo*

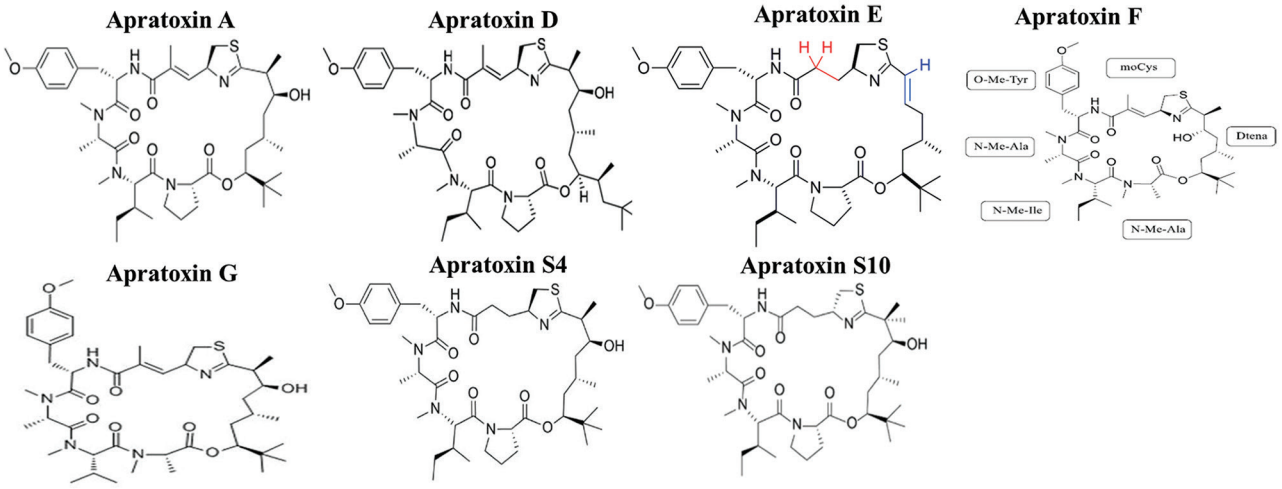

Figure 3. Chemical structure of apratoxin and its analogs.

testing demonstrated that apratoxin A induced moderate tumor inhibition on day 9, with a T/C ratio of 51%, and a weight loss of 21%. However, by day 23, complete recovery was observed, indicating a lengthy recovery period of 14 days[17]. Apratoxins have been found to exhibit strong anticancer activity through the down-regulation of receptor tyrosine kinases and their ligands, including interleukin-6 and vascular endothelial growth factor A (VEGF-A). This is achieved through the blocking of a specific stage of secretory pathways, namely, cotranslation on the Sec61 channel[18].

Apratoxin D (Figure 3) is a cyclodepsipeptide extracted from *Lyngbya sordida* and *L. majuscula*. Its structure is similar to apratoxin A but contains a polyketide carbon chain of 3,7-dihydroxy-2,5,8,10,10-pentamethylundecanoic acid. Apratoxin D has been found to have potent anticancer effects against H-460 cells, a human lung cancer cell line, with a half maximal inhibitory concentration (IC_{50}) of 2.6 nM[19,20]. Apratoxin E, isolated from *Lyngbya bouillonii*, is a polypeptide domain that is similar to apratoxin A. Apratoxin E is known for its potent cytotoxic effects on various cancer cell lines, such as cervical cancer cells (HeLa), human osteosarcoma cells (U-2 OS), and human colorectal adenocarcinoma cells (HT29). Its IC_{50} values for HeLa, U-2 OS, and HT29 cells are 72, 59, and 21 nM, respectively[21,22].

Apratoxins F and G are also derived from *L. bouillonii*. The polyketide moiety in apratoxins G and F is similar to that in apratoxin A (Figure 3). However, apratoxins F and G possess an N-methyl alanine unit in place of a proline unit in apratoxins A to E. Apratoxins G and F exhibited high cytotoxicity to H-460 cells with IC_{50} of 14 and 2 nM, respectively[19,21]. Apratoxin H and apratoxin A sulfoxide are derived from *Moorea producens*. Apratoxin H has pipecolic acid instead of the proline residue found in apratoxin A. Meanwhile, apratoxin A sulfoxide differs from apratoxin A in terms of the degree of oxidation. Both apratoxin H and apratoxin A sulfoxide exhibited cytotoxicity against H460 cells, with IC_{50} values of 3.4 and 89.9 nM, respectively[23]. Apratoxin S4 and S10 (Figure 3) are novel Sec61 inhibitor that blocks the translocation of secretory proteins into the endoplasmic reticulum. Apratoxin S4 and S10 are cytotoxic to pancreatic cells and suppress the overall secretion from pancreatic cancer cells by inhibiting cytokines from stromal cells or reducing the level of factors secreted by other cells[18,24]. This difference in the anticancer activity of apratoxin and its analogs might be due to the differences in their structure and stability.

3.1.2. Cocosamides

Cocosamides A and B, obtained from *L. majuscula*, are cyclic depsipeptides consisting of six amino/hydroxy units, including proline, NMe-Phe (two units), 2,2-dimethyl-3-hydroxy-7-octenoic acid (Dhoea), or a β-amino acid of 2,2-dimethyl-3-hydroxy-7-octynoic acid (Dhoya), glycine, and valine (Figure 4). These compounds exhibit moderate cytotoxicity against MCF-7 cancer cells (IC_{50} between 30 and 39 mM,) and HT-29 cells (IC_{50} between 24 and 11 mM)[19,25].

3.1.3. Aurilides

Aurilides are a type of cyclic depsipeptides. They contain a α-hydroxy-acid residue, a pentapeptide, and a polyketide fragment with three or four stereogenic centers (Figure 4). These compounds are isolated from *L. majuscula*. Two specific types, aurilides B and C, have demonstrated high levels of cytotoxicity against NCI-H460 (50% lethal

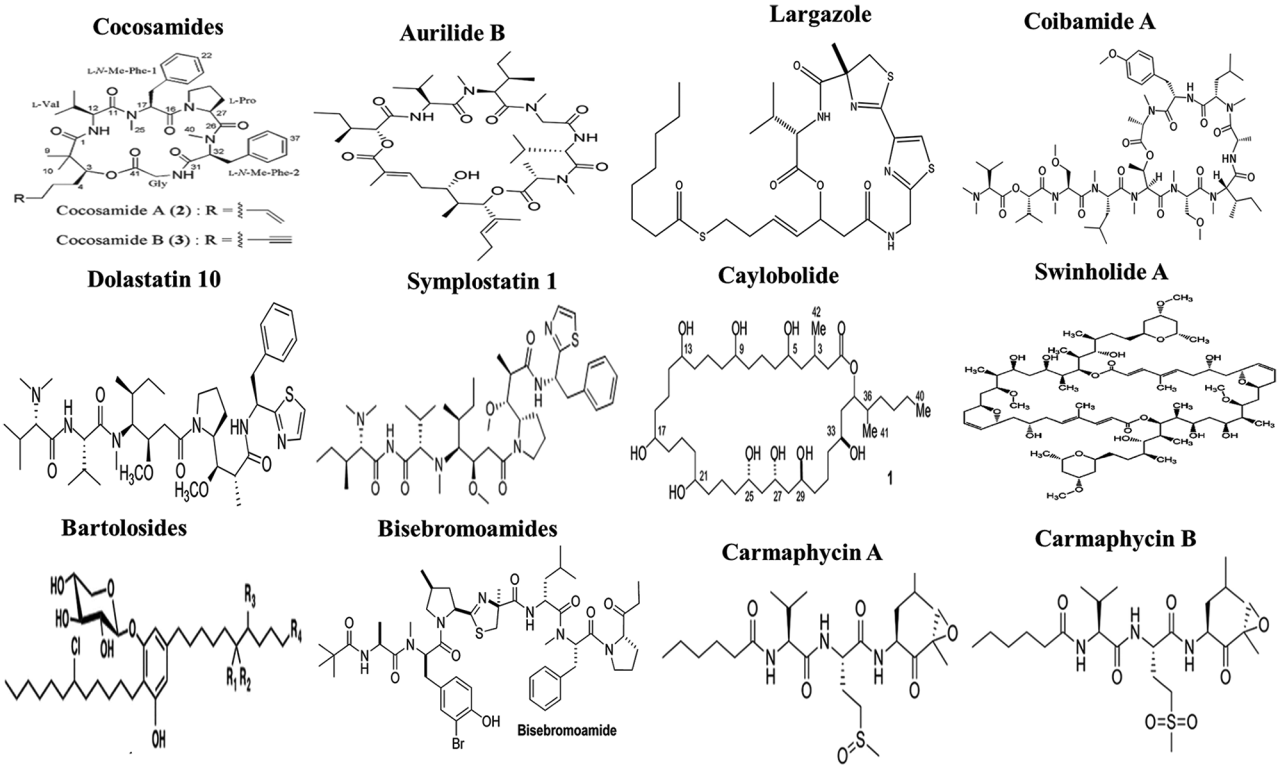

Figure 4. Chemical structure of cocosamides, aurilide B, largazole, coibamide A, dolastatin 10, symplostatin 1, caylobolide, swinholide A, bartolosides, bisebromoamides, carmaphycin A, and carmaphycin B.

concentration [LC_{50}] of 40 and 130 nM) and Neuro-2a mouse neuroblastoma cells (LC_{50} of 10 and 50 nM), respectively[9,26,27].

3.1.4. Largazole

Isolated from *Symploca* spp., Largazole (Figure 4) is a potent histone deacetylase inhibitor. These compounds showed anticancer activity against various cancer cell lines such as HCT-116 (GI_{50} = 80 nM), MDA-MB-231 (GI_{50} = 7.7 nM), HT-29 (GI_{50} = 12 nM), U-2 OS (GI_{50} = 55 nM), SK-OV-3 ($IC5_0$ = 250 nM), IMR-32 (GI_{50} = 16 nM), A549 (GI_{50} = 320 nM), HeLa (IC_{50} = 170 nM), Eca-109 (IC_{50} = 100 nM), Bel 7402 (IC_{50} = 170 nM), U937 (IC_{50} = 20 nM), 797 (IC_{50} = 24 nM), 10326 (IC_{50} = 25 nM), PC3 (IC_{50} ≤ 500 nM), LNCap (IC_{50} ≤ 500 nM), panel of melanoma cell lines (IC_{50} = 45-315 nM), NCI-H1975 (IC_{50} = 83 nM), NCI-H460 (IC_{50} = 120 nM), GLC-82 (IC_{50} = 190 nM), L78 (IC_{50} = 570 nM), SPC-A1 (IC_{50} = 140 nM), 95D (IC_{50} = 420nM), NCI-H466 (IC_{50} = 520 nM), SW620 (IC_{50} = 26.5 nM), MiaPaCa (IC_{50} = 206.4 nM), SH-SY5Y (IC_{50} = 102 nM), SF-268 (IC_{50} = 62 nM), and SF-295 (IC_{50} = 68 nM). This compound suppresses cancer probably by virtue of its ability to modulate cell cycle and antagonize AKT, KRAS, and HIF[19,28].

3.1.5. Coibamide A

Coibamide, a cyclic depsipeptides cyanotoxin derived from *Leptolyngbya* sp., has been found to have a significant impact on various types of cancer cells. In a dose-dependent manner, coibamide increases the percentage of NCI-H460 cells and mouse Neuro-2a cells in the sub-G1 population. In addition, it has been demonstrated to arrest the cell cycle of NCI-H460, Neuro-2a cells (LC_{50} = 23 nM), MDA-MB-231, melanoma LOX IMVI, NCI-60 (GI_{50} between 0.4 and 7.6 nM), astrocytoma SNB75, and leukemia HL-60 in the G1 phase.

The anticancer effect of coibamide A (Figure 4) is distinctly mediated through the activation of caspase 3 (in SF-295 cells) to induce apoptosis or the activation of autophagy via an mTOR-independent mechanism (in U87-MG cells). It also prevents autophagosome-lysosome binding in MDA-MB-231 cells through protein glycosylation modification-lysosome membrane (LAMP1 and LAMP2). Moreover, it reduces VEGFR2 expression and inhibits VEGF-A secretion in MDA-MB-231 and U87-MG cells. Coibamide A also decreases the expression of human epidermal growth factor receptor receptor in non-small cell lung and breast cancer cells. The effectiveness of coibamide

in fighting cancer makes it a promising candidate for further study and development[29-34].

3.2. Cyclic peptides and depsipeptides

3.2.1. Dolastatins

Dolastatins represent a group of cyclic and linear peptides, depsipeptides, and macrolides, containing oxazole heterocycles and thiazole. These peptides are derived from *Symploca sp*. Dolastatin 10 and 15 (Figure 4) can depolymerize microtubules and are also capable of inducing apoptosis by arresting the cell cycle in the G2/M phase of various cancer cell lines, including A549, KB, DU-145, and LoVo cells. Their IC_{50} values are 0.97, 0.052, 0.5, and 0.076 nM, respectively[9].

3.2.2. Symplostatin 1

Symplostatin 1 (Figure 4), a dolastatin 10 analog derived from marine cyanobacteria *Symploca hydnoides*, is shown to possess potent cytotoxic effects against MDA-MB-435 (breast cancer) and ovarian cancer cell lines (IC50 of 0.15 and 0.09 nM, respectively). An *in vivo* study revealed that symplostatin 1 can effectively suppress the growth of murine mammary 16/C and murine colon 38 cell lines, which took a longer time for the cells to recover from toxicity[35].

3.3. Macrolides

3.3.1. Caylobolide

Caylobolides (Figure 4) are macrolides (macrolactones) isolated from the *Phormidium sp.* and *L. majuscula*. Caylobolide A exhibited cytotoxic properties against HCT-116 cells (human colon tumor) with an IC_{50} of 9.9 μM[36], while caylobolide B showed anticancer activity against HeLa and HT-29 cells, with IC_{50} values of 12.2 and 4.5 μM, respectively[37].

3.3.2. Swinholide

Swinholide is a type of macrolide containing a unique, larger lactone ring structure known as a dimeric 44-membered ring (Figure 4). Swinholide A is derived from *Phormidium sp.* and has been found to possess anti-cancer properties against fibrosarcoma cells (HT-1080) and H-460, with IC_{50} values of 0.017 μg/mL and between 170 and 910 nM, respectively[28,38].

3.4. Glycolipids

3.4.1. Bartolosides

Bartoloside (Figure 4) is a newly discovered type of chlorinated aromatic glycolipid. It is composed of mono- and/or di-glycosylated dialkylresorcinols (DARs) with halogenated alkyl moieties. The marine cyanobacteria, *Synechocystis salina,* and *Nodosilinea sp.*, are the principal sources of this compound[28]. According to Afonso *et al.*,[39] Bartoloside A has been found to have anticancer effect on human osteosarcoma (MG-63), colon carcinoma (RKO), and human breast cancer (T-47D) cells, with IC_{50} values of 22, 40, and 23 μM, respectively.

3.5. Linear peptides

3.5.1. Bisebromoamides

Bisebromoamides are linear peptides (Figure 4) derived from *Lyngbya sp.* They are known to impair actin dynamics and have demonstrated anticancer properties against various cancer cell lines, including HeLa S3, JFCR39 (a panel of 39 human cancers)[40], NRK, 769-P, 786-O kidney cancer cells[41], and HCT-116 (with EC_{50} ranging between 45 and 483 nM)[42]. The compound showed an IC_{50} of 40 nM against HeLa S3 cells and a GI_{50} of 40 nM against JFCR39 cells[40].

3.5.2. Carmaphycins

Extracted from *Symploca* sp., carmaphycins A and B (Figure 4) are new forms of marine-based epoxyketone 20S proteasome inhibitors. These substances have demonstrated strong anticancer effect against NCI-H460, HCT-116, and the NCI-60 cell lines, with a GI_{50} range of 1 – 50 nM[43].

3.6. Depsipeptides

3.6.1. Anaenamides

Anaenamides A and B are new geometric isomers and linear depsipeptides derived from *Hormoscilla sp.* These compounds contain two α-hydroxy acid residues, an alkylated-salicylic fragment, and an abnormal α-chlorinated-α,β-unsaturated (E/Z) ester. Anaenamides A and B (Figure 4) were found to have mild anticancer properties against the HCT-116 cell line, with IC_{50} values of 4.5 and 8.7 μM, respectively[44]. Different from anaenamides A and B, anaenamides C and D possesses a primary amide instead of a methyl ester. However, anaenamides C and D have been demonstrated to display anticancer effect against HCT-116 cells at an IC_{50} of 100 μM but no cytotoxic activity against human embryonic kidney cells (HEK293)[44,45].

3.7. Linear lipopeptides

3.7.1. Almiramides

Almiramides are linear lipopeptides that are highly N-methylated. They are derived from *Oscillatoria nigroviridis* and *L. majuscula*. Almiramides B and D (Figure 5) have been found to display strong cytotoxic effects against MDA-MB-231, with an IC_{50} of 13 μM[46].

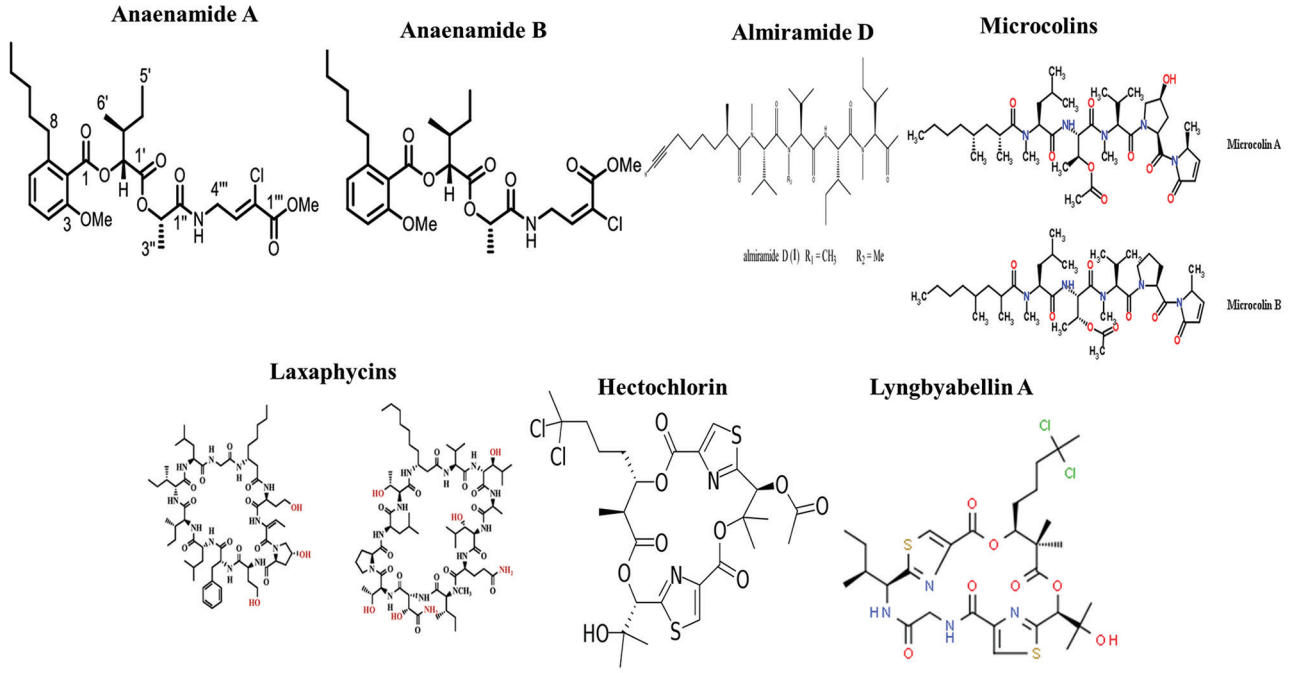

Figure 5. Chemical structure of anaenamide A, anaenamide B, almiramide D, microcolins, laxaphycins, hectochlorin, and lyngbyabellin A.

They also showed similar effects on HeLa cells, with an IC_{50} of 17 µM, and on other cells such as A549, HT-29, and PC3, with IC_{50} ranging from 18 to 107 µM[46].

3.7.2. Microcolins

Microcolins (Figure 5) are new linear lipopeptides, which are isolated from *L. polychroa* and *M. producens*. These lipopeptides have demonstrated powerful cytotoxicity against NCI-H460, with IC_{50} ranging between 6 nM to 1 µM[47]. In addition, microcolins A and B, along with deacetylmicrocolin B, have shown cytotoxicity against IMR-32 and HT-29, with IC_{50} between 0.28 and 14 nM[47,48].

3.7.3. Wenchangamides

Wenchangamide A is a lipopeptide recently discovered from the filamentous *Neolyngbya* sp. This compound has been found to have anticancer properties against HCT-116, with an IC_{50} of 38 µM[49]. It works by either arresting the cell cycle at the G2/M phase or inducing apoptosis. Importantly, wenchangamide A does not have any toxic effects on normal human dermal fibroblasts (NHDF), indicating that it specifically targets cancer cells[49].

3.8. Cyclic lipopeptides

3.8.1. Hectochlorins

Hectochlorins (Figure 5) are cyclic lipopeptides isolated from *M. producens*. Hectochlorins demonstrated potent cytotoxic activity against various types of cancer cells, including NCI-H 187, B lymphocyte CA46, and human mouth epithelial KB cells, with IC_{50} values of 1.2, 0.02, and 0.86 µM, respectively[50]. It has also been found to display high cytotoxicity to melanoma, colon, and kidney cancer cell lines, with a GI_{50} of 5.1 µM[51]. The previous studies also reported that hectochlorins are cytotoxic against NCI-H187 and KB cell lines, with IC_{50} values of 0.32 and 0.31 µM, respectively[50-52].

3.8.2. Laxaphycins

Laxaphycins (Figure 5) are cyclic-lipopeptides that are isolated from marine cyanobacterium *Hormothamnion enteromorphoides*. Laxaphycin B4 demonstrated cytotoxic effects against HCT116 cells with an IC_{50} of 1.7 µM[53]. Laxaphycin A2, on the other hand, showed low cytotoxicity with an IC_{50} of 2 µM[53,54].

3.9. Peptolides

3.9.1. Lyngbyabellins

Lyngbyabellins represent a group of cyclic depsipeptides and lipopeptides containing dichlorinated polyketide-derived moiety. Lyngbyabellins are isolated from *L. bouillonii* and *L. majuscula*. One of these compounds, lyngbyabellin A (Figure 5), showed moderate anticancer activity against KB and LoVo cell lines, with IC_{50} values of 0.03 µg/mL and 0.5 µg/mL, respectively[28]. However, *in vivo* studies have revealed that lyngbyabellin A is toxic to mice at concentrations between 0.01 and 5.0 µg/mL[55,56]. On

the other hand, lyngbyabellin B is more toxic to mice than lyngbyabellin A. In addition, lyngbyabellin E to I exhibited cytotoxicity against NCI-H460 and Neuro-2a cells, with LC_{50} values ranging from 0.2 to 4.8 μM[55]. Lyngbyabellin N has been shown to possess potent cytotoxicity against the HCT116 cell line, with an IC_{50} of 40.9 ± 3.3 nM[57]. However, lyngbyabellins K, L, M, and 7-epi-lyngbyabellin L did not show any toxic activity compared to other compounds[55-57].

3.9.2. Majusculamides

Majusculamide C and D (Figure 6) and desmethoxymajusculamide C are cyclopeptolides derived from the marine cyanobacterium *L. majuscula*. Majusculamide C demonstrated potent cytotoxicity against ovarian carcinoma (OVCAR-3), kidney cancer (A498), glioblastoma SF-295, NCI-H460, and colorectal cancer (KM20L2) cell lines with IC_{50} values of 0.51, 0.058, 0.013, 0.0032, and 0.0013 μg/mL, respectively[58]. Desmethoxymajusculamide C has been shown to display strong cytotoxicity against HCT-116, with an IC_{50} value of 20 nM[9]. Moreover, majusculamide D is cytotoxic to PANC-1, U251N, HepG2, NCI-H125, and P388, with IC_{50} values of 0.32, 36.8, 1396, 147, and 3.3 nM, respectively[58].

3.9.3. Patellamides

Patellamides (Figure 6) are cyclic octa-peptides containing thiazoles and oxazolines. These compounds are obtained from *Prochloron didemni*. Patellamides A, B, and C have been found to exhibit anticancer activity against the L1210 cell line, with IC_{50} values ranging from 2 to 3.9 μg/mL[59].

In addition, patellamide A has demonstrated cytotoxicity against acute CEM leukemia cells, with an IC_{50} of 0.028 μg/mL[28,59].

3.10. Polyketides

3.10.1. Aplysiatoxins

The aplysiatoxins (Figure 6) are polyketide metabolites derived from various types of cyanobacteria, such as *Oscillatoria sp.*, *L. majuscula*, *Lyngbya sp.*, *Schizothrix calcicola*, *Oscillatoria nigroviridis*, *Trichodesmium erythraeum*, and *M. producens*. Among these aplysiatoxins, some are new analogs such as neo-aplysiatoxin A, neo-debromoaplysiatoxin A, dolastatin 3, lyngbic acid, malyngamide M, hermitamide A, (−)-loliolide, and (+)-epiloliolide. These compounds have been found to be cytotoxic against mouse leukemia cells, with IC_{50} values ranging from 4.6 to 10 μg/mL[28,60].

3.10.2. Caldorazole

Extracted from *Caldora sp.*, caldorazole (Figure 6) has two thiazole rings and an O-methylenolpyruvamide moiety. This compound has been found to be effective against a few different cancer cell lines, such as CaSki and HT-1080 (with IC_{50} of 0.068 and 0.074 μM, respectively)[61]. It has also been shown to be cytotoxic against three types of HeLa cell lines (HeLa, HeLa S3Mer−, and HeLa S3), with IC_{50} values ranging from 0.023 to 0.048 μM[61]. The cytotoxicity of caldorazole might be executed through the inhibition of the activity of complex I in mitochondria; therefore, caldorazole is a promising selective targeting agent for cancer cells when glucose is restricted[61].

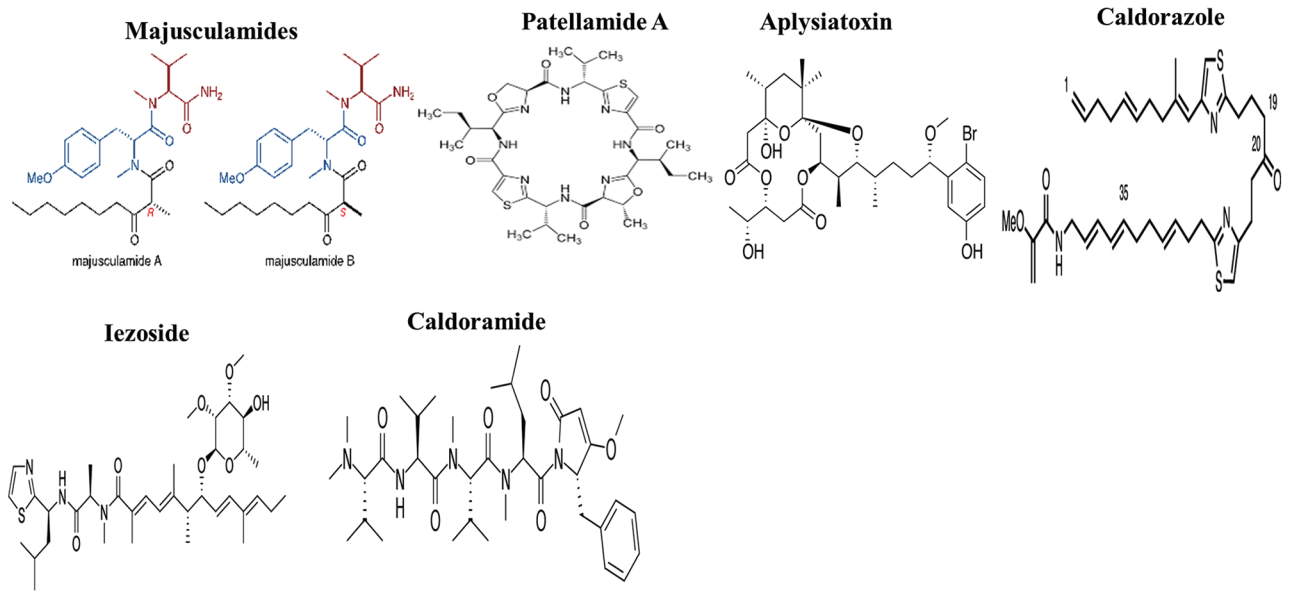

Figure 6. Chemical structure of majusculamides, patellamide A, aplysiatoxin, caldorazole, iezoside, and caldoramide.

3.11. Metabolites from other chemical families

3.11.1. Iezoside

A new compound called iezoside (Figure 6) is isolated from marine cyanobacterium *Leptochromothrix valpauliae*. It is a polyketide peptide with a unique structure that includes a 2,3-O-dimethyl-α-l-rhamnose branch, a conjugated diene group, and an α,β,γ,δ-unsaturated-amide group. Iezoside has been found to exhibit potent anticancer properties against HeLa cells with an IC_{50} value of 6.7 nM, causing a delay in the cell cycle, inducing morphological changes (spindle-like), and activating the apoptosis-induction pathways[62].

3.11.2. Caldoramide

Caldoramide (Figure 6) is a pentapeptide compound derived from the marine cyanobacterium *Caldora penicillata*. This compound exhibits potent cytotoxic activity against HCT116, HT-29, and MCF-7, with IC_{50} values of 43.8 ± 3.7, 77.5 ± 1.3, and 33.9 ± 1.3, respectively. However, its cytotoxicity is lower than that of belamide A and dolastatin 10[63].

Based on reviews in the literature, several compounds have been isolated from different cyanobacteria strains which may be due to the ability of cyanobacteria to produce these metabolites as a chemical defense technique against predators and compete for space and nutrients or to produce these metabolites when growing in extreme environment and/or cultivation under different cultivation condition or stress condition (such as high or low pH, temperature, and salinity).

Some metabolites have been found to exhibit cytotoxicity against different cancer cell lines, with varying cellular responses depending on the type of cancer cell. The mechanisms underpinning their cytotoxic effects include cell cycle arrest, caspase activation, impairment of the actin cytoskeleton, histone deacetylase inhibition, inhibition of the trimeric Sec61 translocon, depolymerization of microtubules, 20S proteasome inhibition, mitochondrial fragmentation, and prevention of multidrug resistance. Several other compounds are not reviewed in this paper due to a lack of information concerning their cytotoxicity or their selectivity toward normal cells rather than cancer cells. Therefore, modifying the structure of these compounds is necessary to create analogs that exhibit high cytotoxicity and are more selective against cancer cells than the original metabolite.

4. Conclusions

Cyanobacteria are known to contain various bioactive compounds, including apratoxin, symplostatin 1, bartolosides, caylobolide, bisebromoamides, carmaphycins, anaenamides, cocosamides, aurilides, wenchangamides, coibamide A, largazole, almiramides, dolastatins, microcolins, hectochlorins, lyngbyabellins, patellamides, majusculamides, aplysiatoxins, caldorazole, laxaphycins, iezoside, and caldoramide. These compounds can be found in various cyanobacteria species and have been shown to possess anticancer properties against a range of cancer cell lines, such as human colon carcinoma, osteosarcoma, breast cancer, lung cancer, cervical cancer, and fibrosarcoma cells. However, further research is needed to determine the safety and effectiveness of these compounds in animal models and clinical applications. It is of utmost importance to find the right balance between drug safety and effectiveness for these compounds in the treatment of cancer. Although the general rule of thumb is to discontinue any further investigations on the slightly effective compounds that elicit severe side effects, there are still no clear guidelines on whether effective compounds that can cause significant side effects should be approved for further studies. This uncertainty poses a challenge for drug developers in selecting the appropriate drugs that have the highest potential to maximize the overall patient outcome in cancer treatment.

Acknowledgments

None.

Funding

None.

Conflict of interest

The authors declare that they have no competing interests.

Author contributions

Conceptualization: Hanaa Ali Hussein, Fatin L. Khaphi
Writing – original draft: Hanaa Ali Hussein
Writing – review & editing: All authors

Ethics approval and consent to participate

Not applicable.

Consent for publication

Not applicable.

Availability of data

Not applicable.

References

1. IARC, 2021, Global Cancer Observatory. France: International Agency for Research on Cancer.

2. Hussein HA, Abdullah MA, 2020, Anticancer compounds derived from marine diatoms. *Mar Drugs*, 18: 356.

https://doi.org/10.3390/md18070356

3. Hussein HA, Khaphi FL, 2023, The apoptotic activity of curcumin against oral cancer cells without affecting normal cells in comparison to paclitaxel activity. *Appl Biochem Biotechnol*, 195: 5019–5033.

https://doi.org/10.1007/s12010-023-04454-5

4. Salem O, El Assi R, Saleh M, 2020, Bioactive constituents of three algal species extracts and their anticancer activity against human cancer cell lines. *Egypt J Phycol*, 21: 1–18.

5. Kar J, Ramrao DP, Zomuansangi R, *et al*., 2022, Revisiting the role of cyanobacteria-derived metabolites as antimicrobial agent: A 21st century perspective. *Front Microbiol*, 13: 103441.

https://doi.org/10.3389/fmicb.2022.1034471

6. Nainangu P, Antonyraj APM, Subramanian K, *et al*., 2020, *In vitro* screening of antimicrobial, antioxidant, cytotoxic activities, and characterization of bioactive substances from freshwater *Cyanobacteria Oscillatoria* sp. SSCM01 and *Phormidium* sp. SSCM02. *Biocatal Agric Biotechnol*, 29: 101772.

7. Khalifa SAM, Shedid ES, Saied EM, *et al*., 2021, *Cyanobacteria*--from the oceans to the potential biotechnological and biomedical applications. *Mar Drugs*, 19: 241.

https://doi.org/10.3390/md19050241

8. Costa M, Garcia M, Costa-Rodrigues J, *et al*., 2014, Exploring bioactive properties of marine cyanobacteria isolated from the Portuguese coast: High potential as a source of anticancer compounds. *Mar Drugs*, 12: 98–114.

https://doi.org/10.3390/md12010098

9. Qamar H, Hussain K, Soni A, *et al*., 2021, *Cyanobacteria* as natural therapeutics and pharmaceutical potential: Role in antitumor activity and as nanovectors. *Molecules*, 26: 247.

https://doi.org/10.3390/molecules26010247

10. Mehta A, Soni VK, Shukla D, *et al*., 2020, *Cyanobacteria*: A potential source of anticancer drugs. In: Advances in Cyanobacterial Biology. United States: Academic Press, p369–384.

https://doi.org/10.1016/B978-0-12-819311-2.00024-3

11. Jones MR, Pinto E, Torres MA, *et al*., 2021, CyanoMetDB, a comprehensive public database of secondary metabolites from *Cyanobacteria*. *Water Res*, 196: 117017.

https://doi.org/10.1016/j.watres.2021.117017

12. Zahra Z, Choo DH, Lee H, *et al*., 2020, *Cyanobacteria*: Review of current potentials and applications. *Environments*, 7: 13.

13. Pooja S, Niveshika, 2022, Insight into the potential cyanobacterial metabolites and their screening strategies. *Biosci Biotechnol Res Asia*, 19: 255–279.

14. Pattnaik S, Singh L, 2020, *Cyanobacteria* bioactive compound, their production and extraction with pharmaceutical applications - a review. *Int J Curr Microbiol Appl Sci*, 9: 3394–3405.

15. Sosa-Hernández JE, Escobedo-Avellaneda Z, Iqbal HMN, *et al*., 2018, State-of-the-art extraction methodologies for bioactive compounds from algal biome to meet bio-economy challenges and opportunities. *Molecules*, 23: 2953.

https://doi.org/10.3390/molecules23112953

16. Kumar R, Tewari AK, 2018, Medicinal properties of marine plants. In: Synthesis of Medicinal Agents from Plants. Netherlands: Elsevier Ltd., p257–282.

https://doi.org/10.1016/B978-0-08-102071-5.00011-8

17. Luesch H, Yoshida WY, Moore RE, *et al*., 2001, Total structure determination of apratoxin A, a potent novel cytotoxin from the marine cyanobacterium *Lyngbya majuscula*. *J Am Chem Soc*, 123: 5418–5423.

https://doi.org/10.1021/ja010453j

18. Cai W, Chen QY, Dang LH, *et al*., 2017, Apratoxin S10, a dual inhibitor of angiogenesis and cancer cell growth to treat highly vascularized tumors. *ACS Med Chem Lett*, 8: 1007–1012.

https://doi.org/10.1021/acsmedchemlett.7b00192

19. Tan LT, 2012, Marine *Cyanobacteria*: A treasure trove of bioactive secondary metabolites for drug discovery. In: Studies in Natural Products Chemistry. Vol. 36. Netherlands: Elsevier, p67–110.

20. Gutiérrez M, Suyama TL, Engene N, *et al*., 2008, Apratoxin D, a potent cytotoxic cyclodepsipeptide from papua new Guinea collections of the marine *Cyanobacteria Lyngbya majuscula* and *Lyngbya sordida*. *J Nat Prod*, 71: 1099–1103.

https://doi.org/10.1021/np800121a

21. Tarsis EM, Rastelli EJ, Wengryniuk SE, *et al*., 2015, The apratoxin marine natural products: Isolation, structure determination, and asymmetric total synthesis. *Tetrahedron*, 71: 5029–5044.

22. Matthew S, Schupp PJ, Luesch H, 2008, Apratoxin E, a cytotoxic peptolide from a guamanian collection of the marine cyanobacterium *Lyngbya bouillonii*. *J Nat Prod*, 71: 1113–1116.

https://doi.org/10.1021/np700717s

23. Thornburg CC, Cowley ES, Sikorska J, *et al*., 2013, Apratoxin H and Apratoxin A sulfoxide from the red sea cyanobacterium *Moorea producens*. *J Nat Prod*, 76: 1781–1788.

https://doi.org/10.1021/np4004992

24. Cai1 W, Ratnayake R, Gerber MH, *et al*., 2019, Development of apratoxin S10 (Apra S10) as an anti-pancreatic cancer

agent and its preliminary evaluation in an orthotopic patient-derived xenograft (PDX) model. *Invest New Drugs*, 37: 364–374.

https://doi.org/10.1007/s10637-018-0647-0

25. Gunasekera SP, Owle CS, Montaser R, *et al*., 2011, Malyngamide 3 and cocosamides A and B from the marine cyanobacterium *Lyngbya majuscula* from Cocos Lagoon, guam. *J Nat Prod*, 74: 871–876.

https://doi.org/10.1021/np1008015

26. Michon S, Cavelier F, Salom-Roig XJ, 2021, Synthesis and biological activities of cyclodepsipeptides of aurilide family from marine origin. *Mar Drugs*, 19: 55.

https://doi.org/10.3390/md19020055

27. Han B, Gross H, Goeger DE, *et al*., 2006, Aurilides B and C, cancer cell toxins from a Papua new Guinea collection of the marine cyanobacterium *Lyngbya majuscula*. *J Nat Prod*, 69: 572–575.

https://doi.org/10.1021/np0503911

28. Robles-Bañuelos B, Durán-Riveroll LM, Rangel-López E, *et al*., 2022, Marine *Cyanobacteria* as sources of lead anticancer compounds: A review of families of metabolites with cytotoxic, antiproliferative, and antineoplastic effects. *Molecules*, 27: 4814.

https://doi.org/10.3390/molecules27154814

29. Yao G, Wang W, Ao L, *et al*., 2018, Improved total synthesis and biological evaluation of coibamide A analogues. *J Med Chem*, 61: 8808–8916.

https://doi.org/10.1021/acs.jmedchem.8b01141

30. Medina RA, Goeger DE, Hills P, *et al*., 2008, Coibamide A, a potent antiproliferative cyclic depsipeptide from the panamanian marine cyanobacterium *Leptolyngbya* sp. *J Am Chem Soc*, 130: 6324–6325.

https://doi.org/10.1021/ja801383f

31. Kazemi S, Kawaguchi S, Badr CE, *et al*., 2021, Targeting of HER/ErbB family proteins using broad spectrum Sec61 inhibitors coibamide A and apratoxin A. *Biochem Pharmacol*, 183: 114317.

https://doi.org/10.1016/j.bcp.2020.114317

32. Shi W, Lu D, Wu C, *et al*., 2021, Coibamide A kills cancer cells through inhibiting autophagy. *Biochem Biophys Res Commun*, 547: 52–58.

https://doi.org/10.1016/j.bbrc.2021.01.112

33. Tranter D, Paatero AO, Kawaguchi S, *et al*., 2020, Coibamide A targets Sec61 to prevent biogenesis of secretory and membrane proteins. *ACS Chem Biol*, 15: 2125–2136.

https://doi.org/10.1021/acschembio.0c00325

34. Serrill JD, Wan X, Hau AM, *et al*., 2016, Coibamide A, a natural lariat depsipeptide, inhibits VEGFA/VEGFR2 expression and suppresses tumor growth in glioblastoma xenografts. *Invest New Drugs*, 34: 24–40.

https://doi.org/10.1007/s10637-015-0303-x

35. Mooberry SL, Leal RM, Tinley TL, *et al*., 2003, The molecular pharmacology of symplostatin 1: A new antimitotic dolastatin 10 analog. *Int J Cancer*, 104: 512–521.

https://doi.org/10.1002/ijc.10982

36. MacMillan JB, Molinski TF, 2002, Caylobolide A, a unique 36-membered macrolactone from a bahamian *Lyngbya majuscula*. *Org Lett*, 4: 1535–1538.

https://doi.org/10.1021/ol025759p

37. Salvador LA, Paul VJ, Luesch H, 2010, Caylobolide B, a macrolactone from symplostatin 1-producing marine *Cyanobacteria Phormidium* spp. from Florida. *J Nat Prod*, 73: 1606–1609.

https://doi.org/10.1021/np100467d

38. Tao Y, Li P, Zhang D, *et al*., 2018, Samholides, swinholide-related metabolites from a marine Cyanobacterium cf. *Phormidium* sp. *J Org Chem*, 83: 3034–3046.

https://doi.org/10.1021/acs.joc.8b00028

39. Afonso TB, Costa MS, Rezende De Castro R, *et al*., 2016, Bartolosides E-K from a marine coccoid cyanobacterium. *J Nat Prod*, 79: 2504–2513.

https://doi.org/10.1021/acs.jnatprod.6b00351

40. Sasaki H, Teruya T, Fukazawa H, *et al*., 2011, Revised structure and structure-activity relationship of bisebromoamide and structure of norbisebromoamide from the marine cyanobacterium *Lyngbya* sp. *Tetrahedron*, 67: 990–994.

41. Suzuki K, Mizuno R, Suenaga K, *et al*., 2013, Bisebromoamide, an extract from *Lyngbya* species, induces apoptosis through ERK and mTOR inhibitions in renal cancer cells. *Cancer Med*, 2: 32–39.

https://doi.org/10.1002/cam4.53

42. Johnston HJ, Boys SK, Makda A, *et al*., 2016, Naturally inspired peptide leads: Alanine scanning reveals an actin-targeting thiazole analogue of bisebromoamide. *Chembiochem*, 17: 1621–1627.

https://doi.org/10.1002/cbic.201600257

43. Pereira AR, Kale AJ, Fenley AT, *et al*., 2012, The carmaphycins, new proteasome inhibitors exhibiting an α,β-epoxyketone warhead from a marine cyanobacterium. *Chembiochem*, 13: 810–817.

https://doi.org/10.1002/cbic.201200007

44. Brumley DA, Gunasekera SP, Chen QY, *et al*., 2020, Discovery, total synthesis and SAR of anaenamides A and B: Anticancer cyanobacterial depsipeptides with a chlorinated pharmacophore. *Org Lett*, 22: 4235–4239.

https://doi.org/10.1021/acs.orglett.0c01281

45. Trauner D, Shemet A, 2020, Discovery and total synthesis of anaenamides A and B. *Synfacts*, 16: 0982.

46. Quintana J, Bayona LM, Castellanos L, *et al*., 2014, Almiramide D, cytotoxic peptide from the marine cyanobacterium *Oscillatoria* nigroviridis. *Bioorg Med Chem*, 22: 6789–6795.

https://doi.org/10.1016/j.bmc.2014.10.039

47. Yu HB, Glukhov E, Li Y, *et al*., 2019, Cytotoxic microcolin lipopeptides from the marine cyanobacterium *Moorea producens*. *J Nat Prod*, 82: 2608–2619.

https://doi.org/10.1021/acs.jnatprod.9b00549

48. Meickle T, Matthew S, Ross C, *et al*., 2009, Bioassay-guided isolation and identification of desacetylmicrocolin B from *Lyngbya* cf. polychroa. *Planta Med*, 75: 1427–1430.

https://doi.org/10.1055/s-0029-1185675

49. Ding L, Bar-Shalom R, Aharonovich D, *et al*., 2021, Metabolomic characterization of a cf. *Neolyngbya* cyanobacterium from the South China sea reveals wenchangamide a, a lipopeptide with *in vitro* apoptotic potential in colon cancer cells. *Mar Drugs*, 19: 397.

https://doi.org/10.3390/md19070397

50. Suntornchashwej S, Chaichit N, Isobe M, *et al*., 2005, Hectochlorin and morpholine derivatives from the Thai sea hare, *Bursatella leachii*. *J Nat Prod*, 68: 951–955.

https://doi.org/10.1021/np0500124

51. Marquez BL, Watts KS, Yokochi A, *et al*., 2002, Structure and absolute stereochemistry of hectochlorin, a potent stimulator of actin assembly. *J Nat Prod*, 65: 866–871.

https://doi.org/10.1021/np0106283

52. Amin N, Kannaujiya VK, 2021, Metabolic pathways for production of anticancer compounds in *Cyanobacteria*. In: Evolutionary Diversity as a Source for Anticancer Molecules. United States: Academic Press, p127–154.

53. Cai W, Matthew S, Chen QY, *et al*., 2018, Discovery of new A- and B-type laxaphycins with synergistic anticancer activity. *Bioorg Med Chem*, 26: 2310–2319.

https://doi.org/10.1016/j.bmc.2018.03.022

54. Perera RMTD, Herath KHINM, Sanjeewa KKA, *et al*., 2023, Recent reports on bioactive compounds from marine *Cyanobacteria* in relation to human health applications R. *Life* (*Basel*), 13: 1411.

https://doi.org/10.3390/life1306141

55. Kwan JC, Taori K, Paul VJ, *et al*., 2009, Lyngbyastatins 8-10, elastase inhibitors with cyclic depsipeptide scaffolds isolated from the marine cyanobacterium *Lyngbya semiplena*. *Mar Drugs*, 7: 528–538.

https://doi.org/10.3390/md7040528

56. Matthew S, Ross C, Rocca JR, *et al*., 2007, Lyngbyastatin 4, a dolastatin 13 analogue with elastase and chymotrypsin inhibitory activity from the marine cyanobacterium *Lyngbya confervoides*. *J Nat Prod*, 70: 124–127.

https://doi.org/10.1021/np060471k

57. Choi H, Mevers E, Byrum T, *et al*., 2012, Lyngbyabellins K-N from two Palmyra atoll collections of the marine cyanobacterium *Moorea bouillonii*. *European J Org Chem*, 2012: 5141–5150.

https://doi.org/10.1002/ejoc.201200691

58. Mondal A, Bose S, Banerjee S, *et al*., 2020, Marine *Cyanobacteria* and microalgae metabolites--a rich source of potential anticancer drugs. *Mar Drugs*, 18: 476.

https://doi.org/10.3390/md18090476

59. Baur P, Kühl M, Comba P, *et al*., 2022, Possible functional roles of patellamides in the ascidian-prochloron symbiosis. *Mar Drugs*, 20: 119.

https://doi.org/10.3390/md20020119

60. Kawaguchi M, Satake M, Zhang BT, *et al*., 2020, Neo-aplysiatoxin A isolated from Okinawan cyanobacterium *Moorea producens*. *Molecules*, 25: 457.

https://doi.org/10.3390/molecules25030457

61. Ohno O, Iwasaki A, Same K, *et al*., 2022, Isolation of caldorazole, a thiazole-containing polyketide with selective cytotoxicity under glucose-restricted conditions. *Org Lett*, 24: 4547–4551.

https://doi.org/10.1021/acs.orglett.2c01566

62. Kurisawa N, Iwasaki A, Teranuma K, *et al*., 2022, Structural determination, total synthesis, and biological activity of iezoside, a highly potent Ca2+-ATPase inhibitor from the marine cyanobacterium *Leptochromothrix valpauliae*. *J Am Chem Soc*, 144: 11019–11032.

https://doi.org/10.1021/jacs.2c04459

63. Wunder A, Rothemund M, Schobert R, 2018, Synthesis and anticancer activity of the proposed structure of caldoramide, an N-peptidyltetramate from the cyanobacterium *Caldora penicillata*. *Tetrahedron*, 74: 5138–5142.

ACCSCIENCE PUBLISHING

INNOSC Theranostics and Pharmacological Sciences

REVIEW ARTICLE

Management and maintenance of oral health: Personalized primary prevention strategies and protocols in patients at risk of developing medication-related osteonecrosis of the jaw

Giovanna Mosaico[1]* and Cinzia Casu[2]

[1]Independent Researcher, Carovigno, Brindisi, Italy

[2]Department of Surgical Science, Oral Biotechology Laboratory, University of Cagliari, Italy

Abstract

Skeletal complications arising from osteoporosis or bone metastases are associated with considerable pain, increased mortality, and diminished quality of life. Agents that prevent bone resorption, such as bisphosphonates, denosumab, and antiangiogenic agents, prove effective in reducing fracture risk and find extensive use in patients with osteoporosis or bone cancer metastases. Medication-related osteonecrosis of the jaw (MRONJ) is a potentially serious adverse event associated with high cumulative doses of antiresorptive drugs. Other risk factors for osteonecrosis of the jaw include glucocorticoid use, maxillary or mandibular bone surgery, poor oral hygiene, chronic inflammation, diabetes mellitus, inappropriate dentures, and other MRONJ-related medications. Preventive strategies encompass completing necessary oral surgery before initiating antiresorptive drug therapy, administering antibiotics before and/or after the procedure, rinsing the mouth with chlorhexidine, ensuring adequate wound healing post-tooth extraction, and maintaining good oral hygiene. The primary goal of treatment is to improve the patient's quality of life by managing pain and infection, preventing the development of new lesions, and decelerating disease progression. Dentists and dental hygienists, operating within a multi-professional team, play a key role in the primary prevention of MRONJ. However, a standardized multidisciplinary approach, fostering sustained dialog between specialists involved in the management of patients at risk for MRONJ, remains essential. This review describes the preventive and individualized oral hygiene management in patients at risk for this condition.

Keywords: Preventive protocols; Patients at risk of MRONJ; Antiresorptive drugs; Oral hygiene; Healthy lifestyles

***Corresponding author:**
Giovanna Mosaico
(gimosaico@tiscali.it)

Citation: Mosaico G, Casu C. 2024, Management and maintenance of oral health: Personalized primary prevention strategies and protocols in patients at risk of developing medication-related osteonecrosis of the jaw. *INNOSC Theranostics and Pharmacological Sciences*, 7(1): 1419. https://doi.org/10.36922/itps.1419

Received: July 31, 2023

Accepted: November 9, 2023

Published Online: January 11, 2024

1. Introduction

Medication-related osteonecrosis of the jaw (MRONJ) is an adverse event associated with antiresorptive drug therapy, often administered in combination with anti-angiogenics. It is a potentially serious and debilitating complication defined by the American Association of Oral and Maxillofacial Surgeons as the presence of an area of exposed bone in the maxillofacial region persisting for more than 8 weeks in the absence of prior radiotherapy treatment[1,2]. The diagnosis of MRONJ relies on the patient's history and clinical and

radiological features demonstrating progressive bone destruction (both exposed and unexposed)[3-5]. Common signs and symptoms of MRONJ include exposed necrotic bone, sinus tract or fistula, recurring abscesses, gingival swelling, bad breath, loosening of teeth, jaw fracture, sinus pain, and numbness or dysesthesia of the lower lip. Diagnosis of MRONJ is considered when exposed bone in the maxillofacial region does not heal within 8 weeks in a patient treated with an antiresorptive agent[1-7]. While MRONJ is reported as a rare adverse event in patients with osteoporosis, its incidence is higher in cancer patients with bone metastases or malignant hypercalcemia (up to 1 – 10% of patients)[8,9]. However, even in patients with osteoporosis, there is an increased risk of MRONJ following oral surgical therapies. For this reason, an evaluation of the route of administration of antiresorptive drugs, the duration of treatment, and the drug withdrawal period are essential to prevent post-operative MRONJ in this patient category[10]. The pathophysiology of MRONJ remains incompletely understood, with oral microbiota and dental infections considered central to its development[11-14]. Since the initial reporting of MRONJ more than 20 years ago, attention has been directed toward the association between tooth extraction and adverse events in patients already receiving ONJ-related medications[15,16]. Recently, dentoperiodontal and peri-implant infections have been highlighted as key local risk factors for MRONJ, often serving as the primary rationale for surgical procedures involving tooth extraction or implant removal[17-22]. The link between periodontal disease and the development of MRONJ has been extensively demonstrated, with the spread of bacteria through periodontal pockets identified as a primary mechanism for infection propagation through the alveolar bone. Notably, the promotion of MRONJ development is likely influenced not only by the presence of *Porphyromonas gingivalis* and other periodontogenic bacteria in the periodontal pockets but also by IgG products[3,18,23-26].

1.1. Monitoring and evaluation of the patient candidate for therapy with antiresorptive drugs

Primary prevention aims to eliminate oral and dental risk factors by focusing on restoring and/or maintaining good oral health, thereby reducing the risk of pathological conditions or other adverse events[26-30].

The preventive protocols and recommendations include several key practices, including completing necessary oral surgery before initiating antiresorptive drug therapy, administering antibiotics 2 – 4 days before and 7 – 10 days after the surgery procedures, using antimicrobial mouthwash, ensuring adequate wound closure after tooth extraction, and maintaining good oral hygiene[31,32]. Therefore, the International Task Force on Osteonecrosis of the Jaw recommends that during invasive oral surgery, patients should have their anti-resorptive therapy withheld until soft-tissue healing occurs[33]. Another equally important recommendation includes initiating MRONJ prevention before, during, and after the end of antiresorptive therapy[6,10,26,27,33-36] (Table 1). For low-risk patients, the same recommendations apply to preventive dental visits, maintaining optimal oral health aligned with general population standards. However, for cancer patients, the dental checks will be more stringent.

2. Systematic review methods

We conducted a literature review to compile practical guidelines for health-care professionals regarding the management and maintenance of oral health in patients at risk of MRONJ. The search for scientific articles was conducted on medical databases such as PubMed, Cochrane, and Google Scholar on October 23, 2023. The keywords used were "Prevention and MRONJ," "Oral hygiene and MRONJ," and "Microbiota and MRONJ". In addition, a manual search was conducted to improve the article pool. The search strategy is summarized in Table 2.

After preliminary screening and removal of duplicates, the abstracts and titles of articles were assessed to determine eligibility for further evaluation. The selected

Table 1. Prevention of osteonecrosis of the jaw related to antiresorptive drugs

Prevention before, during, and after treatment	• First visit with complete radiographic examinations • Complete oral-dental examination, evaluation of the mucous membranes and tongue • Careful examination of the condition of the back of the tongue • Dental formula • Compilation/updating of the periodontal record • Evaluation of the quantity and consistency of saliva • Mapping of oral lesions • Photographic documentation • Oral checks (4 – 6 months) • Instruct the patients to maintain optimal oral health and to recognize possible signs and symptoms of MRONJ

Table 2. Article search strategy

Search strategy	Parameters
Keywords	• Prevention and MRONJ • Microbiota and MRONJ • Oral hygiene and MRONJ
Publication years	• 2003 – 2023
Electronic database	• PubMed • Cochrane • Google Scholar

Abbreviation: MRONJ: Medication-related osteonecrosis of the jaw.

articles were ultimately included for qualitative analysis. The inclusion criteria encompassed articles in any language reporting clinical trials, expert reviews, literature reviews, meta-analyses, and systematic reviews. The exclusion criteria were scientific articles not reporting on primary prevention and oral hygiene in patients with MRONJ, as well as case reports.

3. Results

A total of 1,735 articles were retrieved from manual and electronic databases. Out of these, 1,323 articles were reviewed, and eight were considered to meet the inclusion criteria for qualitative review (Figure 1).

3.1. Synthesis of results

In efforts to prevent MRONJ, there is a significant focus on optimizing oral health, given its demonstrated effectiveness in reducing the associated risk. The included articles concur that primary prevention plays a fundamental role in maintaining healthy oral microbiota and mitigating the risk of MRONJ (Table 3).

4. Discussion

The included studies affirm and emphasize the need for multidisciplinary dialog among specialists involved in both primary and secondary prevention of MRONJ. While systemic risk factors, such as oncological disease and comorbidities associated with hyperthyroidism, diabetes, hypovitaminosis D, rheumatoid arthritis, hypocalcemia, osteomyelitis, chronic renal failure, and anemia, pose challenges in terms of modification, they remain open to improvement. In contrast, local risk factors are modifiable and offer a wide field of intervention through primary prevention and secondary. The control of local inflammatory factors, especially those associated with dento-periodontal and peri-implant conditions, is considered one of the main risk factors contributing to the development of ONJ. The ONJ International Task Force highlights the importance of managing periodontal disease before the commencement of antiresorptive therapy[6,9,26,27,32,37-52]. Preventive protocols and comprehensive oral and extraoral clinical examination must be conducted indiscriminately in patients with dentition, as well as in edentulous patients, especially for those utilizing removable dentures. This is crucial since removable dentures are identified as risk factors linked to ONJ and have the potential to induce microtrauma to the oral mucosa, creating an environment conducive to predominantly fungal bacteriology. Mechanical cleansing of the mucous membranes is beneficial not only for disorganizing the bacterial biofilm but also for stimulating blood circulation and improving resistance to trauma[53]. Therefore, even in these patients, the initial pre-treatment visit should include a complete clinical and radiographic examination, along with precise mapping of the oral mucosa through accurate photographic documentation. For individuals utilizing prosthetic devices, meticulous

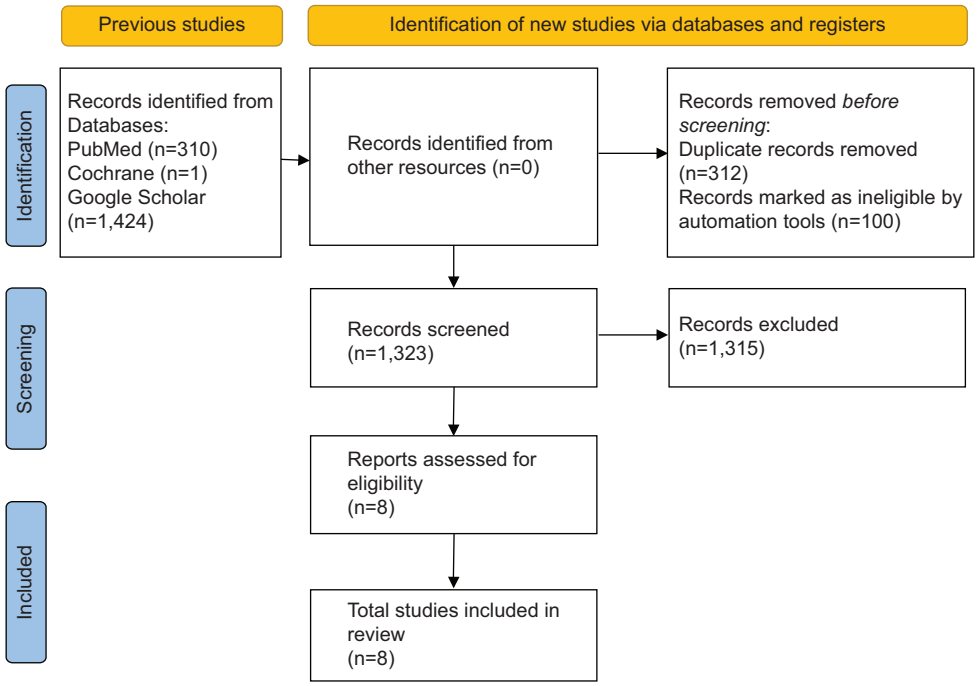

Figure 1. PRISMA flowchart assessment of the included studies.

Table 3. Information of articles included in this review

Studies	Key outcomes/findings
AlRowis *et al.*[41]	Careful dental preparation and instructions on oral hygiene significantly reduce the risk of ONJ.
Nicolatou-Galitis *et al.*[27]	Oral clinicians play a critical role in the prevention of MRONJ as part of a multidisciplinary team.
Drudge-Coates *et al.*[38]	Health-care professionals can play a key role alongside prescribers and oral clinicians in assessing the risk of MRONJ, thereby contributing to the prevention and management of the care pathway for these patients.
Fassio *et al.*[9]	The majority of patients with MRONJ can be managed conservatively through optimal oral hygiene, regular professional dental care, and elimination of active dental and periodontal disease.
Khan *et al.*[32]	The development of ONJ can be mitigated by optimizing oral hygiene, and periodontal disease must be managed before starting doses of antiresorptive drugs.
Migliario *et al.*[42]	Primary prevention, carried out by dental hygienists, and secondary prevention, through professional oral hygiene and periodic monitoring of the oral health status of patients at risk, are of fundamental importance to prevent the onset of lesions.
Campisi *et al.*[6]	The diagnosis and prevention of MRONJ play a significant role not only in the quality of life of patients but also in the decision-making process of the majority of doctors involved in the prevention of ONJ (primary and secondary).
Di Fede *et al.*[26]	The application of primary and secondary prevention protocols by doctors and oral hygienists, in synergy with prescribers and adequate patient awareness, is key to implementing strategies aimed at a common objective – the reduction of MRONJ outbreaks.

Abbreviations: MRONJ: Medication-related osteonecrosis of the jaw; ONJ: Osteonecrosis of the jaw.

Figure 2. A brochure outlining oral hygiene clinical protocols for patients undergoing antiresorptive drug treatment. The content of the brochure is modified from references Giovanna Mosaico *et al.*[30], Drudge-Coates *et al.*[38], Migliario *et al.*[42], and National Cancer Institute[44].

finishing and polishing, especially in the lower jaw, are imperative, as the edges of these prosthetic artifacts must be rounded and beveled[54,55].

At each follow-up visit, it is essential to reinforce the motivation for maintaining oral health and controlling diabetes and MRONJ-related risk factors (Table 3)[56]. To encourage patient compliance and raise patients' awareness of the importance of home oral hygiene, an oral hygiene manual may be provided during the first visit with oral health professionals. Furthermore, this same informational brochure could be disseminated in advance by the rheumatologist, orthopedist, and oncologist, aiming to promptly activate the MRONJ preventive

protocols. This approach is consistently directed toward the patients' health and underscores the importance of a multidisciplinary manner (Figure 2). Maintaining healthy lifestyles in MRONJ patients includes several key elements:

- Blood sugar control;
- Elimination of risk factors such as smoking and alcohol consumption;
- Adherence to proper nutrition rich in vitamins and avoiding excessively sour, spicy, crunchy and hot food;
- Vigilance toward possible injuries or pains in the oral cavity;
- Control of bacterial biofilm through oral hygiene practice, including brushing of teeth, gums, and tongue, conducted twice a day.

4.1. Professional oral hygiene in cancer patients at risk of MRONJ

Professional oral hygiene is increasingly indicated in the recent literature for cancer patients at risk of MRONJ. However, a clear and unequivocal operating protocol for oral professionals caring for these patients is currently lacking[43].

Minimally invasive non-surgical periodontal therapy must be carefully planned to ensure regular removal of plaque and tartar, together with periodic clinical screening of the oral and periodontal health status of patients undergoing treatment. For the management of acute gum disease, chlorhexidine rinses at concentrations between 0.12% and 0.2% are recommended, administered 2 to 4 times a day, depending on the severity. Nonsurgical periodontal therapy can be performed when there are no significant oral lesions that limit mouth opening and when the neutrophil count is >2,000/ml and the platelet count is >40,000/ml. The professional oral hygiene program includes the compilation and updating of the periodontal record, including recording the probing depth, clinical level of attachment, recessions, mobility, and furcation involvement. Furthermore, the evaluation of periodontal health includes the evaluation of the quality of oral hygiene, including plaque and bleeding indices. Professional oral hygiene procedures encompass deplaquing and tartar removal utilizing low-frequency mechanical instruments. Moreover, the program emphasizes the strengthening and education of home oral hygiene practices, covering both the oral cavity and dentures, to mitigate the risk of periodontal infections[42,44]. Therefore, it is essential to plan a follow-up period of 3 – 4 months for cancer patients undergoing treatment and 6 months for patients at low risk of MRONJ. This planning should not overlook the significant role of the patient in maintaining effective oral hygiene at home, including self-screening[45,46].

If MRONJ is suspected, it is imperative to refer the patient promptly to an oral and maxillofacial surgeon or a specialized cancer center. In the meantime, the dentist may consider prescribing a mouthwash containing 0.12% chlorhexidine and/or a course of amoxicillin with clavulanic acid to treat any related infections[47-50].

4.2. Limitations

MRONJ remains a condition marked by uncertain and controversial aspects among the most recently studied oral diseases. Numerous questions persist, particularly concerning the diagnosis, the optimal frequency of checks, and the formulation of effective professional and home oral hygiene protocols. The objective of this review is to shed light on the management of primary prevention and provide guidance to oral health professionals for patients at risk. The limited number of studies available for analysis is a notable constraint, indicative of the scarcity of studies conducted on this specific topic. Future studies will be essential to validate the preliminary findings and establish a more comprehensive understanding of MRONJ.

5. Conclusion

The number of patients, both with cancer and without, undergoing treatment with MRONJ-related drugs and, therefore, the potential occurrence of adverse events appears to be steadily increasing. Recent confirmation highlights that effective prevention of MRONJ necessitates the application of appropriate protocols for primary prevention in both pre-treatment and treatment phases for patients receiving antiresorptive drugs. The Consensus Conference emphasizes the importance of adherence to these principles by key figures such as physicians, drug prescribers, dentists, and oral hygienists. To improve the efficacy of therapeutic strategies and enhance the quality of life for patients, a standardized multidisciplinary approach is recommended. Central to the prevention strategy is periodontal therapy, personalized oral hygiene education, and motivation for adopting healthy lifestyles. Periodontal screening remains indispensable for clinicians, facilitating the establishment of a correct multidisciplinary approach to managing MRONJ. The examination of the posterior aspect of the tongue emerges as a valid indicator of the patient's microbiota status, offering the possibility of conducting minimally invasive bacteriological tests to monitor bacterial load.

Acknowledgments

None.

Funding

None.

Conflict of interest

The authors declare that they have no competing interests.

Author contributions

Conceptualization: Giovanna Mosaico
Formal analysis: Giovanna Mosaico
Investigation: Giovanna Mosaico
Methodology: Cinzia Casu
Writing – original draft: Giovanna Mosaico
Writing – review & editing: Cinzia Casu

Ethics approval and consent to participate

Not applicable.

Consent for publication

Not applicable.

Availability of data

The document has been uploaded or deposited to a Qeios preprint server ID: BGMWYJ, https://doi.org/10.32388/BGMWYJ.

Further disclosure

Part or the entire set of results was presented at an ONJ (MRONJ) UPDATE 2021 conference on MAY 8 and 9, 2021, organized by the Piedmont-Valle D'aosta oncology network in Italy.

References

1. Ruggiero SL, Dodson TB, Aghaloo T, *et al.*, 2022, American association of oral and maxillofacial surgeons' position paper on medication-related osteonecrosis of the jaws-2022 update. *J Oral Maxillofac Surg*. 80: 920–943.

   https://doi.org/10.1016/j.joms.2022.02.008

2. Ruggiero SL, Dodson TB, Fantasia J, *et al.*, 2014, American association of oral and maxillofacial surgeons. American association of oral and maxillofacial surgeons position paper on medication-related osteonecrosis of the jaw--2014 update. *J Oral Maxillofac Surg*, 72:1938–1956.

   https://doi.org/10.1016/j.joms.2014.04.031. Erratum in: 2015, *J Oral Maxillofac Surg*, 73: 1440. Erratum in: 2015, *J Oral Maxillofac Surg*, 73: 1879.

3. Otto S, Pautke C, Van den Wyngaert T, *et al.*, 2018, Medication-related osteonecrosis of the jaw: Prevention, diagnosis and management in patients with cancer and bone metastases. *Cancer Treat Rev*, 69: 177–187.

   https://doi.org/10.1016/j.ctrv.2018.06.007

4. Yarom N, Shapiro CL, Peterson DE, *et al.*, 2019, Medication-related osteonecrosis of the jaw: MASCC/ISOO/ASCO Clinical practice guideline. *J Clin Oncol*, 37: 2270–2290.

   https://doi.org/10.1200/JCO.19.01186

5. Bonachea R, Katz J. 2022, Medication-related osteonecrosis of the jaw: A multifaceted diagnostic challenge. Mini review. *Am J Dent*, 35: 109–112.

6. Campisi G, Mauceri R, Bertoldo F, *et al.*, 2020, Medication-related osteonecrosis of jaws (MRONJ) prevention and diagnosis: Italian consensus update 2020. *Int J Environ Res Public Health*, 17: 5998.

   https://doi.org/10.3390/ijerph17165998

7. Kün-Darbois JD and Fauvel F, 2021, Medication-related osteonecrosis and osteoradionecrosis of the jaws: Update and current management. *Morphologie*, 105: 170–187.

   https://doi.org/10.1016/j.morpho.2020.11.008

8. Hamadeh IS, Ngwa BA, Gong Y. 2015, Drug induced osteonecrosis of the jaw. *Cancer Treat Rev*, 41: 455–464.

   https://doi.org/10.1016/j.ctrv.2015.04.007

9. Fassio A, Bertoldo F, Idolazzi L, *et al.*, 2017, Drug-induced osteonecrosis of the jaw: The state of the art. *Reumatismo*, 69: 9–15.

   https://doi.org/10.4081/reumatismo.2017.983

10. Seki K, Kaneko T, Kamimoto A, 2022, Medication-related osteonecrosis of the jaw after tooth extraction in patients receiving pharmaceutical treatment for osteoporosis: A retrospective cohort study. *J Dent Sci*, 17: 1619–1625.

    https://doi.org/10.1016/j.jds.2022.03.014

11. Yahara H, Hiraki A, Maruoka Y, *et al.*, Shotgun metagenome sequencing identification of a set of genes encoded by *Actinomyces* associated with medication-related osteonecrosis of the jaw. *PLoS One*, 15: e0241676.

    https://doi.org/10.1371/journal.pone.0241676

12. Williams DW, Vuong HE, Kim S, *et al.*, 2020, Indigenous microbiota protects against inflammation-induced osteonecrosis. *J Dent Res*, 99: 676–684.

    https://doi.org/10.1177/0022034520908594

13. McGowan K, McGowan T, Ivanovski S, 2018, Risk factors for medication-related osteonecrosis of the jaws: A systematic review. *Oral Dis*, 24: 527–536.

14. Sobczak-Jaskow H, Kochańska B, Drogoszewska B, 2023, A study of oral health parameters and the properties and composition of saliva in oncological patients with and without medication-related osteonecrosis of the jaw who take bisphosphonates. *Medicina* (*Kaunas*), 59: 1073.

    https://doi.org/10.3390/medicina59061073

15. Migliorati CA, 2003, Bisphosphanates and oral cavity

avascular bone necrosis. *J Clin Oncol*, 21: 4253–4254.

https://doi.org/10.1200/JCO.2003.99.132

16. Marx RE, 2003, Pamidronate (Aredia) and zoledronate (Zometa) induced avascular necrosis of the jaws: A growing epidemic. *J Oral Maxillofac Surg*, 61: 1115–1117.

https://doi.org/10.1016/s0278-2391(03)00720-1

17. Kwoen MJ, Park JH, Kim KS, *et al.*, 2023, Association between periodontal disease, tooth extraction, and medication-related osteonecrosis of the jaw in women receiving bisphosphonates: A national cohort-based study. *J Periodontol*, 94: 98–107.

https://doi.org/10.1002/JPER.21-0611

18. Wick A, Bankosegger P, Otto S, *et al.*, 2022, Risk factors associated with onset of medication-related osteonecrosis of the jaw in patients treated with denosumab. *Clin Oral Investig*, 26: 2839–2852.

https://doi.org/10.1007/s00784-021-04261-4

19. Troeltzsch M, Cagna D, Stähler P, *et al.*, 2016, Clinical features of peri-implant medication-related osteonecrosis of the jaw: Is there an association to peri-implantitis? *J Craniomaxillofac Surg*, 44: 1945–1951.

https://doi.org/10.1016/j.jcms.2016.09.018

20. Landi L, Leali PT, Barbato L, *et al.*, 2023, Anti-resorptive therapy in the osteometabolic patient affected by periodontitis. A joint position paper of the Italian society of orthopaedics and traumatology (SIOT) and the Italian society of periodontology and implantology (SIdP). *J Orthop Traumatol*, 24: 36.

https://doi.org/10.1186/s10195-023-00713-7

21. Wazzan T, Kashtwari D, Almaden WF, *et al.*, 2018, Radiographic bone loss and the risk of medication-related osteonecrosis of the jaw (MRONJ) in multiple myeloma patients-a retrospective case control study. *Spec Care Dentist*, 38: 356–361.

https://doi.org/10.1111/scd.12318

22. Mauceri R, Coniglio R, Abbinante A, *et al.*, 2022, The preventive care of medication-related osteonecrosis of the jaw (MRONJ): A position paper by Italian experts for dental hygienists. *Support Care Cancer*, 30: 6429–6440.

https://doi.org/10.1007/s00520-022-06940-8

23. Elsayed R, El-Awady A, Cutler C, *et al.*, 2021, Matrix-bound zolzoledronate enhances the biofilm colonization of hydroxyapatite: Effects on osteonecrosis. *Antibiotics* (*Basel*), 10: 1380.

https://doi.org/10.3390/antibiotics10111380

24. Hellstein JW, Adler RA, Edwards B, *et al.*, 2011, Managing the care of patients receiving antiresorptive therapy for prevention and treatment of osteoporosis: Executive summary of recommendations from the American dental association council on scientific affairs. *J Am Dent Assoc*, 142: 1243–1251.

https://doi.org/10.14219/jada.archive.2011.0108

25. Beth-Tasdogan NH, Mayer B, Hussein H, *et al.*, 2017, Interventions for managing medication-related osteonecrosis of the jaw. *Cochrane Database Syst Rev*, 10: CD012432.

https://doi.org/10.1002/14651858.CD012432.pub2. Update in: 2022, *Cochrane Database Syst Rev*, 7: CD012432.

26. Di Fede O, Panzarella V, Mauceri R, *et al.*, 2018, The dental management of patients at risk of medication-related osteonec1rosis of the jaw: New paradigm of primary prevention. *Biomed Res Int*, 2018: 2684924.

https://doi.org/10.1155/2018/2684924

27. Nicolatou-Galitis O, Schiødt M, Mendes RA, *et al.*, 2019, Medication-related osteonecrosis of the jaw: Definition and best practice for prevention, diagnosis, and treatment. *Oral Surg Oral Med Oral Pathol Oral Radiol*, 127: 117–135.

https://doi.org/10.1016/j.oooo.2018.09.008

28. Al Abdullateef A, Alhareky MS, 2020, Awareness among patient at risk of developing medication related osteonecrosis of the jaw (MRONJ)-a primary prevention strategy. *Saudi Pharm J*, 28: 771–778.

https://doi.org/10.1016/j.jsps.2020.05.004

29. Steel BJ, 2019, Management of medication-related osteonecrosis of the jaw (MRONJ) risk in patients due to commence anti-resorptive/anti-angiogenic drugs-how should pre-drug-treatment dental preventive care be organised? *Community Dent Health*, 36: 244–254.

https://doi.org/10.1922/CDH_4582Steel11

30. Mosaico, G, Casu C, 2021, A primary prevention strategy: Oral hygiene and correct lifestyles among patients at risk of developing drug-related osteonecrosis of the Jaw. *Qeios*, preprint.

https://doi.org/10.32388/bgmwyj

31. Ramaglia L, Guida A, Iorio-Siciliano V, *et al.*, 2018, Stage-specific therapeutic strategies of medication-related osteonecrosis of the jaws: A systematic review and meta-analysis of the drug suspension protocol. *Clin Oral Investig*, 22: 597–615.

https://doi.org/10.1007/s00784-017-2325-6

32. Khan AA, Morrison A, Kendler DL, *et al.*, 2017. Case-based review of osteonecrosis of the jaw (ONJ) and application of the international recommendations for management from the international task force on ONJ. *J Clin Densitom*, 20: 8–24.

https://doi.org/10.1016/j.jocd.2016.09.005

33. Kawahara M, Kuroshima S, Sawase T, 2021, Clinical considerations for medication-related osteonecrosis of the jaw: A comprehensive literature review. *Int J Implant Dent*, 7: 47.

https://doi.org/10.1186/s40729-021-00323-0

34. Poxleitner P, Engelhardt M, Schmelzeisen R, *et al.*, 2017, The prevention of medication-related osteonecrosis of the jaw. *Dtsch Arztebl Int*, 114: 63–69.

https://doi.org/10.3238/arztebl.2017.0063

35. Rosella D, Papi P, Giardino R, *et al.*, 2016, Medication-related osteonecrosis of the jaw: Clinical and practical guidelines. *J Int Soc Prev Community Dent*, 6: 97–104.

https://doi.org.10.4103/2231-0762.178742

36. Casu C, Mosaico G, Natoli V, *et al.*, 2021, Microbiota of the tongue and systemic connections: The examination of the tongue as an integrated approach in oral medicine. *Hygiene, 1*: 56–68.

https://doi.org/10.3390/hygiene1020006

37. Ohnishi, Y, Ito K, Kitamura R, *et al.*, 2017, Importance of professional oral hygiene in preventing medication-related osteonecrosis of the jaw. *Int J Oral Med Sci*, 15: 85–92.

38. Drudge-Coates L, Van den Wyngaert T, Schiødt M, *et al.*, 2020, Preventing, identifying, and managing medication-related osteonecrosis of the jaw: A practical guide for nurses and other allied healthcare professionals. *Support Care Cancer*, 28: 4019–4029.

https://doi.org/10.1007/s00520-020-05440-x

39. Pickett F, American Academy of Oral Medicine, 2006, Bisphosphonate-associated osteonecrosis of the jaw: A literature review and clinical practice guidelines. *Am Dent Hygienists Assoc*, 80: 10.

40. Rayman S, Almas K, Dincer E, 2009, Bisphosphonate-related jaw necrosis: A team approach management and prevention. *Int J Dent Hyg*, 7: 90–95.

41. AlRowis R, Aldawood A, AlOtaibi M, *et al.*, 2022, Medication-related osteonecrosis of the jaw (MRONJ): A review of pathophysiology, risk factors, preventive measures and treatment strategies. *Saudi Dent J*, 34: 202–210.

42. Mario M, Melle M, Bonda PL, 2010, Bisfosfonati e osteonecrosi dei mascellari: Protocolli clinici per igienisti dentali. *Prev Assist Dent*, 36: 42–48.

43. Yong CW, Robinson A, Hong C, 2022, Dental evaluation prior to cancer therapy. *Front Oral Health*, 3: 876941.

https://doi.org.10.3389/froh.2022.876941

44. National Cancer Institute. Available from: https://www. oral and dental management prior to cancer therapy and management following cancer therapy [Last accessed on 2023 May 20].

45. Abed HH, Al-Sahafi EN, 2018, The role of dental care providers in the management of patients prescribed bisphosphonates: Brief clinical guidance. *Gen Dent*, 66: 18–24.

46. D'Agostino S, Valentini G, Dolci M, 2023, Potential relationship between poor oral hygiene and MRONJ: An observational retrospective study. *Int J Environ Res Public Health*, 20: 5402.

https://doi.org/10.3390/ijerph20075402

47. Lorenzo-Pouso AI, Pérez-Sayáns M, Chamorro-Petronacci C, *et al.*, 2020, Association between periodontitis and medication-related osteonecrosis of the jaw: A systematic review and meta-analysis. *J Oral Pathol Med*, 49: 190–200.

https://doi.org/10.1111/jop.12963

48. Ruggiero S, Gralow J, Marx RE, *et al.*, 2006, Practical guidelines for the prevention, diagnosis, and treatment of osteonecrosis of the jaw in patients with cancer. *J Oncol Pract*, 2: 7–14.

https://doi.org/10.1200/JOP.2006.2.1.7

49. Kunchur R, Goss AN, 2008, The oral health status of patients on oral bisphosphonates for osteoporosis. *Aust Dent J*, 53: 354–357, quiz 366.

https://doi.org/10.1111/j.1834-7819.2008.00078.x

50. Migliorati CA, Brennan MT, Peterson DE, 2019, Medication-related osteonecrosis of the jaws. *J Natl Cancer Inst Monogr*, 53: lgz009.

https://doi.org/10.1093/jncimonographs/lgz009

51. He L, Sun X, Liu Z, *et al.*, 2020. Pathogenesis and multidisciplinary management of medication-related osteonecrosis of the jaw. *Int J Oral Sci*, 12: 30.

https://doi.org/10.1038/s41368-020-00093-2

52. Bedogni A, Mauceri R, Fusco V, *et al.*, 2023. Italian position paper (SIPMO-SICMF) on medication-related osteonecrosis of the jaw (MRONJ). *Qeios*, preprint.

https://doi.org/10.32388/PBUJ6Z

53. Ali IE, Sumita Y, 2022, Medication-related osteonecrosis of the jaw: Prosthodontic considerations. *Jpn Dent Sci Rev*, 58: 9–12.

54. Winter A, Schulz SM, Schmitter M, *et al.*, 2022, Oral-health-related quality of life in patients with medication-related osteonecrosis of the jaw: A prospective clinical study. *Int J Environ Res Public Health*, 19: 11709.

55. Ali IE, Murase M, Yonehara Y, *et al.*, 2022, Time and cost of maxillofacial prosthetic treatment: The need for assessment. *Jpn Dent Sci Rev*, 58: 67–68.

https://doi.org/10.1016/j.jdsr.2022.02.001

56. Kammerhofer G, Vegh D, Bányai D, *et al.*, 2023, Association between hyperglycemia and medication-related osteonecrosis of the jaw (MRONJ). *J Clin Med*, 12: 2976.

https://doi.org/10.3390/jcm12082976

ACCSCIENCE PUBLISHING

INNOSC Theranostics and Pharmacological Sciences

ORIGINAL RESEARCH ARTICLE

Plasmodium falciparum histoaspartic protease inhibitor: Toxicity investigation and docking study of 2-(2-benzoyl-4-methylphenoxy) quinoline-3-carbaldehyde derivatives

Oluwafemi S. Aina[1], Luqman A. Adams[1], Adebayo J. Bello[2], and Oluwole B. Familoni[1]*

[1]Drug Design Research Group, Department of Chemistry, University of Lagos, Lagos State, Nigeria

[2]Department of Chemistry and Biology, Redemeer's University, Osun State, Nigeria

Abstract

Aspartic proteases can hydrolyze peptide bonds, making them potential targets for drug development against malaria parasites. In particular, inhibiting the histoaspartic protease (HAP) can disrupt the growth phase of *Plasmodium falciparum* and its ability to degrade hemoglobin for protein synthesis. Compound 5, specifically designed as 2-(2-benzoyl-4-methylphenoxy)quinoline-3-carbaldehyde, served as the basis for designing 50 hypothetical compounds (A1-A50). These compounds were subjected to *in silico* screening to assess their toxicity profiles, pharmacokinetics, bioactivity scores, and theoretical binding affinities, as a part of the drug design protocol. Out of the 50 compounds, nine lead candidates showed no toxicity to human cells. In addition, ten standard reference antimalarial drugs were included in this study for comparison. The highest binding energies were observed for compound A5 (−11.2 kcal/mol) and A31 (−11.3 kcal/mol), surpassing the performance of mefloquine, the best reference drug, which ranked ninth with a binding energy of (−9.6 kcal/mol). Compound A31 did not exhibit the evidence of interaction with either Asp215 or His32, whereas compound A5 displayed π-π stacking interactions with His_{32}. Mefloquine also did not show any interaction with Asp215 or His32. Moreover, compound A5 demonstrated greater hydrophobic interactions at the active site with most binding residues, except for Lys_7 in the hydrophobic region. This characteristic suggests that compound A5 may have the ability to adopt a smaller surface area, exhibit increased biological activity, and have reduced interactions with water, which could facilitate slower clearance. Based on the assessment of various drug-likeness parameters, compound A5 (2-(2-benzoyl-4-methylphenoxy)-7-methylquinoline-3-carbaldehyde) is a potential lead candidate for the development of a new antimalarial drug.

Keywords: Malaria; Mefloquine; Binding energy; Drug leads; Oral bioactivity score; Pharmacokinetics; Docking

***Corresponding author:**
Oluwole B. Familoni
(familonio@unilag.edu.ng)

Citation: Aina OS, Adams LA, Bello AJ, *et al.*, 2024, *Plasmodium falciparum* histoaspartic protease inhibitor: Toxicity investigation and docking study of 2-(2-benzoyl-4-methylphenoxy) quinoline-3-carbaldehyde derivatives. *INNOSC Theranostics and Pharmacological Sciences*, 7(1): 0976. https://doi.org/10.36922/itps.0976

Received: May 23, 2023

Accepted: July 26, 2023

Published Online: September 13, 2023

1. Introduction

Malaria, a significant infectious disease characterized by acute febrile illness, continues to pose a global health concern. The World Health Organization estimates that the global

burden of malaria in the year 2020 ranged between 200 and 300 million cases, resulting in approximately 627,000 deaths[1]. Among the various species of *Plasmodium* that cause malaria, *Plasmodium falciparum* is the most formidable and widespread in Africa[2]. In the recent decades, drug-resistant strains of *P. falciparum* have emerged, leading to a worrisome situation where the effectiveness of currently available drugs has diminished. These persistent challenges have prompted the search for new drugs or the redesigning of existing chemical compounds, aiming to establish a sustainable global public health strategy.

An emerging approach to combat drug resistance in malaria involves exploring alternative biological components distinct from the traditional target sites. Plasmepsins, a type of aspartic proteinase present in malaria parasites, have emerged as promising targets for malaria treatment[3]. Histoaspartic protease (HAP) is one of the four plasmepsins found in the food vacuole of *P. falciparum*[4]. During the growth phase of the *Plasmodium* parasite, HAP is responsible for catalyzing the degradation of erythrocyte hemoglobin at specific peptide bonds, which serve as cleavage sites in the degradation pathway. This degradation process provides the parasite with essential amino acids for protein nutrient enrichment[5], whereas the other plasmepsins play different roles[6].

An effective strategy to inhibit the protease activity of the *Plasmodium* parasite is to target the active site of HAP, considering the presence of the aspartate residue (Asp215) and histidine residue (His32) in it. The high affinity of the aspartic protease inhibitor pepstatin-A for this active site makes it a potential candidate for blocking the functionality of HAP and thereby inhibiting the protease of the *Plasmodium* parasite[7]. By disabling HAP's ability to degrade hemoglobin, the propagation of the parasite within host cells could be reduced while preserving the hemoglobin of infected erythrocytes.

Quinoline is a major component of these drugs. As an important organic compound found in certain natural compounds such as alkaloids and pharmacologically active substances, quinoline has been reported to exhibit inhibitory effects on *Plasmodium* proteases both *in vitro* and *in vivo*[8].

Figure 1 illustrates the presence of quinoline moieties (highlighted in red) in some current standard antimalarial drugs, whereas Figure 2 shows the presence of phenolic groups (red ring) at position 2 of quinoline derivatives, which are also found in various pharmacologically active compounds with antibacterial, anthelmintic, anticancer, antifungal, antihypertensive, anti-inflammatory, analgesic, and antiviral properties[9-12].

The drug-targeted design of quinoline derivatives as inhibitors of HAP is currently lacking substantial information. Therefore, our study aimed to assess the relative binding affinity of hypothetical quinoline derivatives with HAP of *P. falciparum* using *in silico* methods. We chose HAP of *P. falciparum* specifically because it possesses a unique, divergent vacuolar plasmepsin, which is distinct from the plasmepsin of any known *Plasmodium* species[13,14].

To study the relative binding affinity of hypothetical quinoline derivatives with HAP of *P. falciparum*, we synthesized 2-(2-benzoyl-4-methylphenoxy)quinoline-3-carbaldehyde (5 in Scheme 1; Figures S1–S3) and

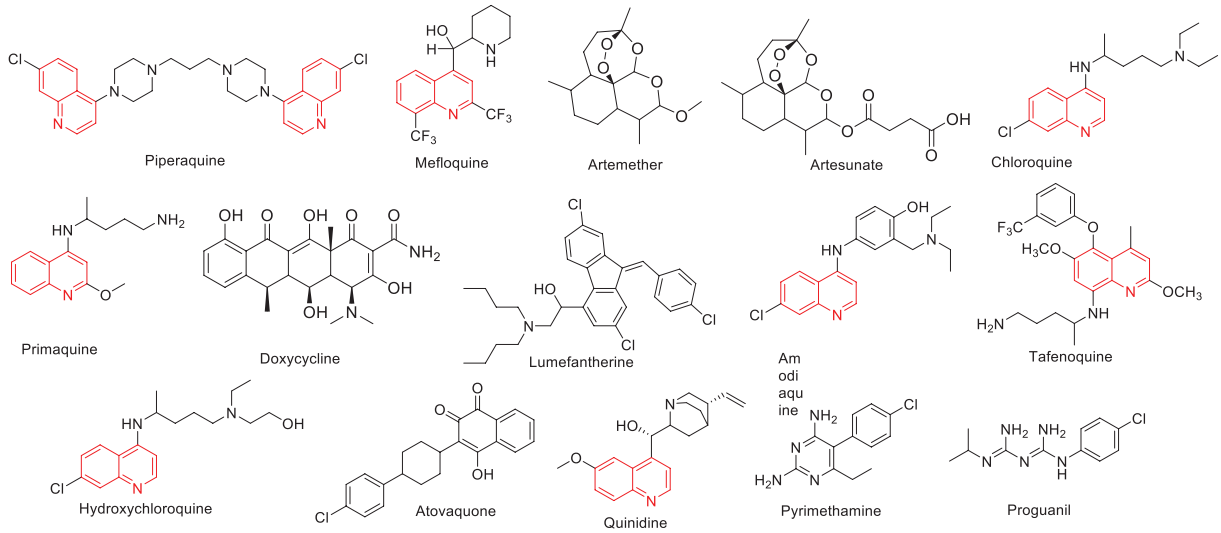

Figure 1. Common antimalarial drugs (mostly containing quinoline moieties).

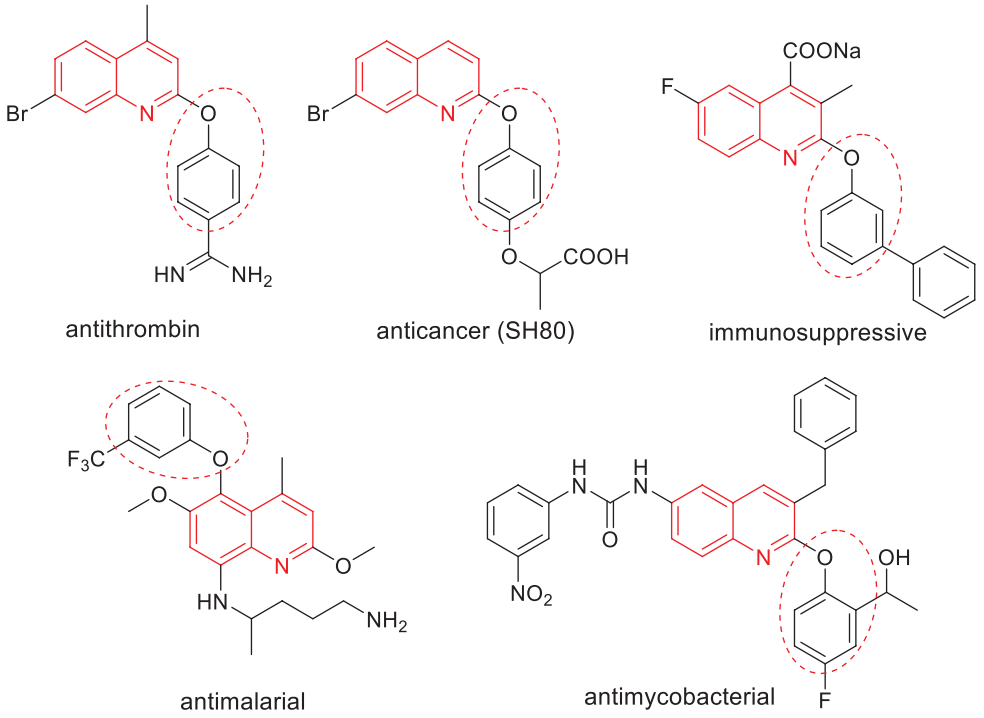

Figure 2. Properties of 2-phenoxyquinoline derivatives.

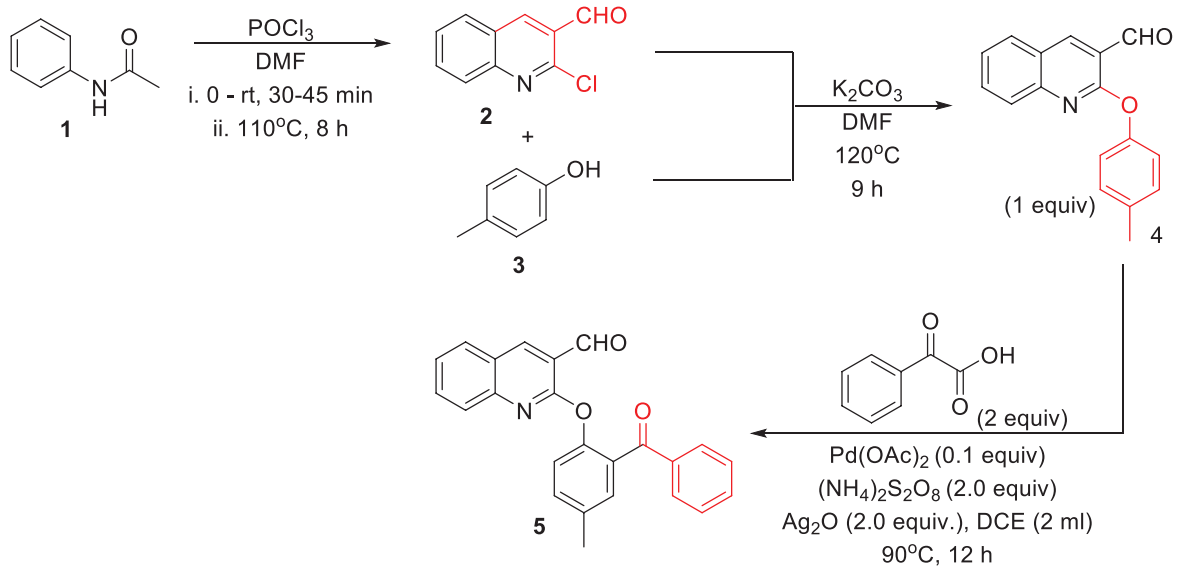

Scheme 1. Synthesis of 2-(2-benzoyl-4-methylphenoxy)quinoline-3-carbaldehyde (5).

evaluated its *in silico* toxicity, which was found to be mildly carcinogenic (Table 1). Subsequently, we designed 50 hypothetical derivative compounds (Figure 3) for *in silico* screening, aiming to identify lead candidates for antimalarial activity based on absorption, distribution, metabolism, excretion, and toxicity (ADMET) tests. Furthermore, we conducted investigations on their pharmacokinetics and bioactivity scores and performed molecular docking simulations into the binding pockets of HAP of *P. falciparum*. This drug-design protocol enabled us to gain insights into the binding interactions between the ligand compounds and the amino acid residues of the HAP enzyme's active sites, which represent a crucial aspect in the development of potential drug-like inhibitors.

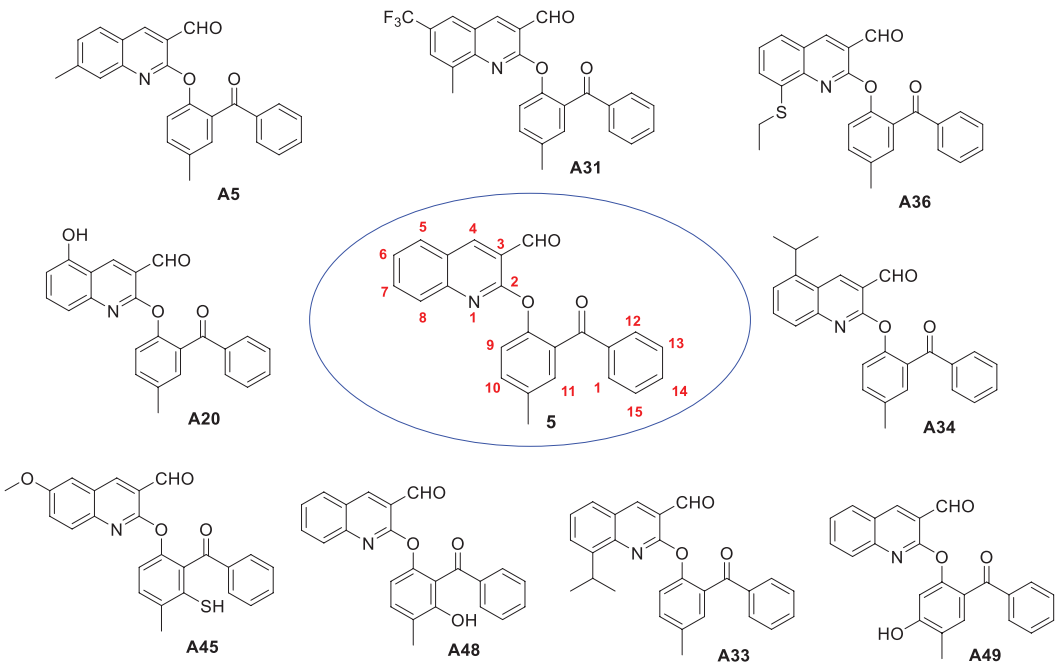

Figure 3. Nine non-toxic hypothetical derivatives of compound 5.

2. Methodology

2.1. Synthesis of 2-(2-benzoyl-4-methylphenoxy) quinoline-3-carbaldehyde (5)

The synthesis of 2-(2-benzoyl-4-methylphenoxy)quinoline-3-carbaldehyde (5) involves three steps, which are described as follows:

2.1.1. Synthesis of 2-chloroquinoline-3-carbaldehyde (2)

Phosphorous oxychloride ($POCl_3$; 28 ml) was added dropwise to dimethylformamide (DMF) in a round-bottom flask while maintaining it an ice bath at 0°C. During this process, an orange color change was observed. The resulting mixture was then combined with acetanilide (10 g, 1 equivalent) dissolved in 30 ml of DMF. The temperature of the reaction was raised from 0°C to 80°C and maintained for 9 h. Thin-layer chromatography was used to monitor the progress of the reaction. After completion, the reaction mixture was allowed to cool and then slowly poured into an ice bath while stirring for 30 min. The resulting precipitate was washed with distilled water (50 ml × 5) to remove any residual acid. The precipitate was then filtered and left to air-dry for 48 h.

2.1.2. 2-(p-tolyloxy)quinoline-3-carbaldehyde (4)

Next, a mixture of *p*-cresol (1.70 ml, 10.44 mmol) and K_2CO_3 (4.33 g, 31.32 mmol) in 15 ml of DMF was prepared, and to this mixture, the precipitate obtained in the previous step, i.e., 2-chloroquinoline-3-carbaldehyde (2) (2.00 g, 10.44 mmol), was added. The reaction mixture was stirred at 90°C for 9 h. Upon completion, water (15 ml × 3) was added to the reaction mixture, and the resulting solid was filtered and recrystallized from ethyl acetate (10 ml). This yielded a white solid, 2-phenoxyquinoline-3-carbaldehyde (4), which served as the precursor for the benzoylation reaction.

2.1.3. Synthesis of 2-(2-benzoyl-4-methylphenoxy) quinoline-3-carbaldehyde (5)

A mixture of ammonium thiosulfate, $(NH_4)_2S_2O_8$ (0.24 g, 2.0 equivalents), and Ag_2O (a co-oxidant; 1.0 equivalent) was added to 2-phenoxychloroquinoline-3-carbaldehyde (4) (0.10 g, 0.38 mmol, 1.0 equivalent) in an oven-dried reaction tube, and $Pd(OAc)_2$ (0.008 g, 0.04 mmol, 0.1 equivalent) was used as a catalyst. The reaction mixture was flushed with nitrogen to remove air, and then dichloroethane (2 ml) was added before sealing the reaction vessel. The mixture was stirred at 100°C for 12 h with thin-layer chromatography monitoring. After completion, ethyl acetate (20 ml × 3) was used to extract the product. The organic layer was washed with water (15 ml × 3), dried with anhydrous sodium sulfate, filtered, and concentrated under vacuum. The resulting residue was purified through column chromatography on silica gel (60–120 mesh) using a hexane: ethyl acetate (1:19) solvent system, yielding compound 5 (2-phenoxyquinoline-3-carbaldehyde) in a 60% yield. The product's characterization was carried out using

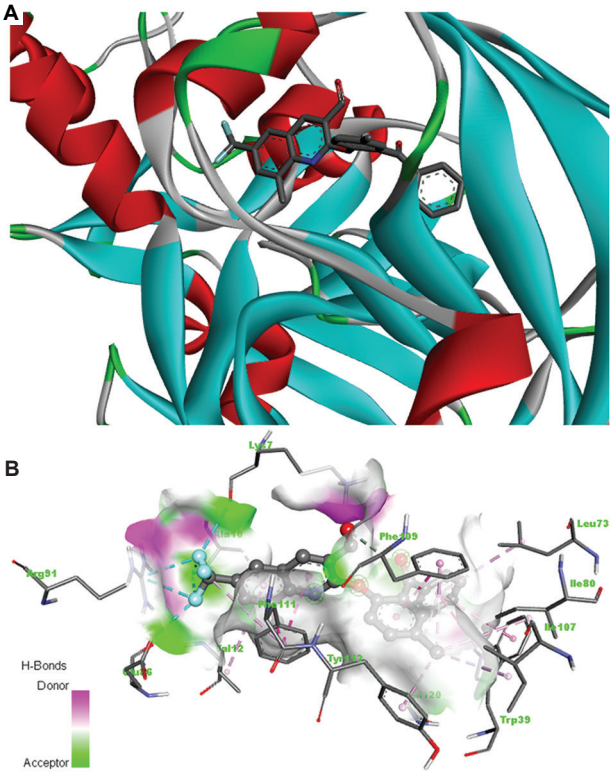

Figure 4A. (A and B) 3D interaction diagram and hydrogen bond donor and acceptor interaction of compound A31 with *Plasmodium falciparum* histoaspartic protease residues.

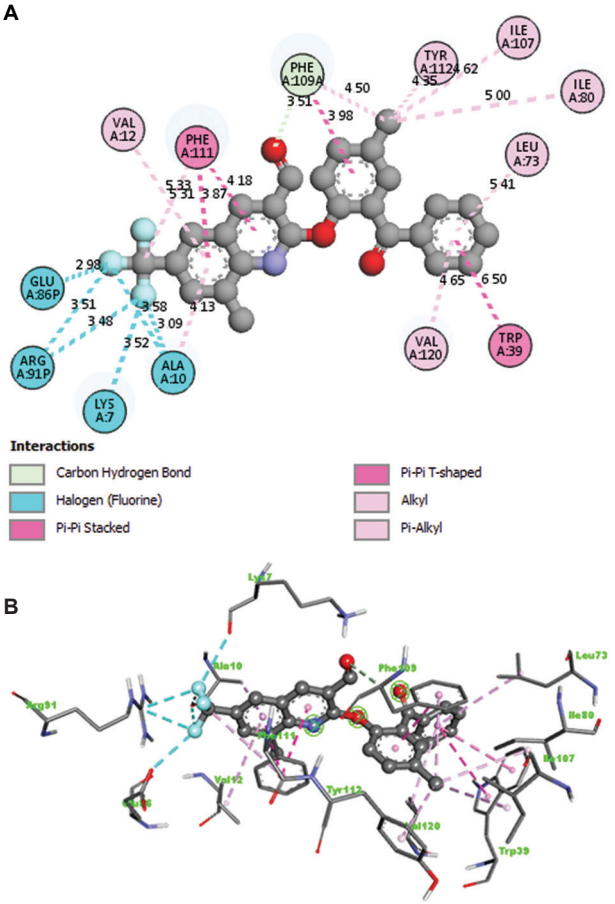

Figure 4B. (A and B) 2D diagram of the bond length and interacting residues of *Plasmodium falciparum* histoaspartic protease with compound A31.

Fourier transform-infrared spectroscopy (FT-IR), proton nuclear magnetic resonance (^{1}H-NMR), and high-resolution mass spectrometry (HRMS) techniques.

2.1.4. Structural elucidation of compound 5

A white solid was obtained after a reaction time of 12 h with a yield of 60 %; m.pt: 119 – 121°C; IR (neat) *v* max (cm^{-1}) 3057, 2922, 2856, 2739, 1754, 1690, 1612, 1590, 1494, 1461, 1343, 1257, 1199, 1097, 760; ^{1}H-NMR (400 MHz, $CDCl_3$) δ 9.75 (s, 1H), 8.32 (s, 1H), 7.97 (d, *J* = 8.3 Hz, 1H), 7.82 (d, *J* = 8.2 Hz, 1H), 7.80 (t, *J* = 8.2 Hz, 1H), 7.74 (t, *J* = 7.5 Hz, 1H), 7.61 (d, *J* = 8.2 Hz, 1H), 7.51 (d, 1H), 7.39 (t, 1H), 7.19 (s, 1H), 6.86 (d, 1H), 6.84 (d, 1H), 2.41 (s, 3H). HRMS (ESI): Calc. for $[(C_{24}H_{17}NO_3)]$ $(M+H)^+$ 368.1281, found 368.1283.

2.2. Toxicity prediction of compound 5

The synthesized compound 5 was subjected to toxicity testing by inputting its SMILES representation, which was drawn using ChemDraw 14.0 and saved as an.sdf file. The Protox II web server (https://tox-new.charite.de/protox_II/) was utilized for this purpose. The web server provided data on hepatoxicity, carcinogenicity, immunotoxicity, mutagenicity, and cytotoxicity, which were then extracted[13].

2.3. Preparation of hypothetical compounds (A1–A50) and antimalarial reference drugs

A set of 50 hypothetical compounds were generated and visually represented using ChemDraw 14.0. These structures were saved in the.sdf format, and their corresponding SMILES notations were uploaded into the Protox II web server[15], as depicted in Figure 4. In addition, ten antimalarial drugs, namely, artesunate, doxycycline, tafenoquine, amodiaquine, artemether, lumefantrine, primaquine, piperaquine, mefloquine, and chloroquine, were obtained from PubChem[16] for comparative purposes. The structures of these drugs were downloaded and saved in the. sdf format, and their corresponding SMILES representations were also uploaded into the Protox II web server[16] to conduct virtual screening. This screening aimed to investigate their toxicity profiles and assess their compliance with all drug-likeness rules as outlined by Lipinski *et al.*[17]

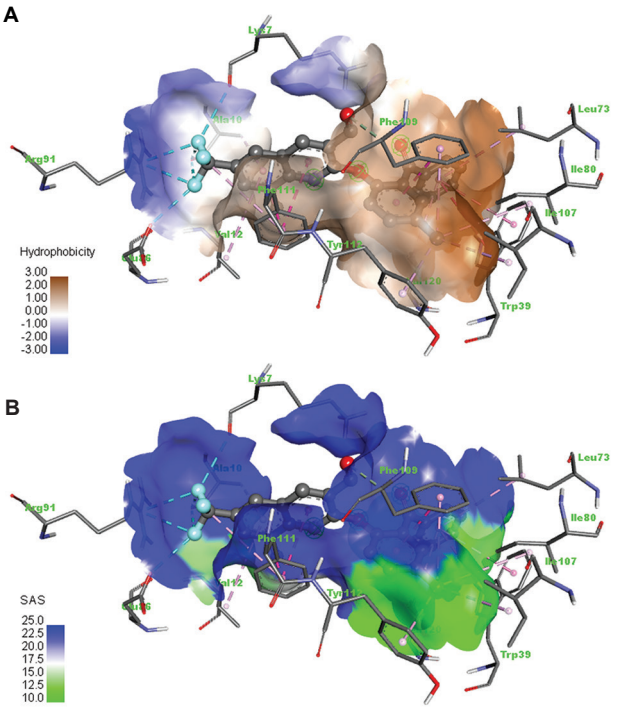

Figure 4C. (A and B) Hydrophobic/hydrophilic and solvent accessibility surface interaction of compound A31 with *Plasmodium falciparum* histoaspartic protease residues.

2.4. Selection of HAP protein receptor

The crystal structure of the HAP protein molecule, with a resolution of 2.10 Å, was acquired from the Protein Data Bank at rcsb.org[18]. The structure was obtained in the.pdb format and subsequently processed using BIOVIA Discovery Studio DS 2020 to eliminate any unwanted ligands and water molecules. In addition, polar hydrogen atoms were added to the structure as required.

2.5. *In silico* drug-likeness and ADME predictions

Compounds A1–A50 were subjected to drug-likeness analysis utilizing admetSAR2[19] to predict crucial adsorption, distribution, metabolism, and excretion (ADME) parameters for potential drug candidates[20]. The SMILES representations of these compounds were uploaded onto the web server, and the generated results were extracted and thoroughly analyzed.

2.6. Bioactivity score

To assess their suitability as drug candidates, compounds A1–A50 underwent drug-likeness analysis using admetSAR2[19]. This analysis aimed to predict vital parameters related to ADME for these compounds, with the goal of identifying potential candidates for further drug development[20]. The SMILES representations of the compounds were submitted to the web server, and the resulting data were carefully extracted and comprehensively examined.

2.7. Molecular docking study

To evaluate the inhibitory potential of synthesized compound 5, as well as the selected hypothetical compounds, docking simulations were performed against HAP using the PyRx 0.8 AutoDock Vina Wizard. The macromolecules were converted to Autodock format, and a flexible ligand to rigid protein approach was employed. All possible binding sites on the target protein were explored during the docking process. The docking calculations were performed within a cubic grid of dimensions 90 × 75 × 60 centered on the protein, encompassing the entire protein structure. This process lasted approximately 1 h. A grid spacing of 1.00 Å was utilized to generate the grid maps using the autogrid module of AutoDock Tools. Each ligand underwent nine independent runs to ensure accuracy.

Based on the identified potential binding sites, energetically favorable binding conformations were selected using AutodockVina[21]. The binding modes, along with their respective binding affinities and RSB (upper and lower) values, were obtained to guide the selection of the highest scoring binding conformation for each ligand. The binding mode with the best binding affinity was chosen. The ligand-protein complexes were analyzed using DS Visualizer. All software applications were executed on PC-based machines running the Microsoft Windows 10 operating system.

3. Results and discussion

3.1. Synthesis of 2-(2-benzoyl-4-methylphenoxy) quinoline-3-carbaldehyde (5) and preparation of hypothetical compounds (A1–A50) as ligands

Compound 5, which is 2-(2-benzoyl-4-methylphenoxy) quinoline-3-carbaldehyde, was synthesized through a series of steps starting from 2-phenoxyquinoline, derived from 2-chloroquinoline-3-carbaldehyde using the Vismeier-Haack formylation method (as discussed in Section 2.1 and depicted in Scheme 1). The characterization of compound 5 involved the use of FT-IR, HRMS, and ^{1}H-NMR spectroscopy (Figures S4–S9). In each step of the synthesis, newly added sections of the molecule were highlighted in red.

Initial docking studies revealed that compound 5 (2-(2-benzoyl-4-methylphenoxy)quinoline-3-carbaldehyde) displayed noteworthy bioactivity. However, it was also found to have a mild carcinogenic effect, as indicated in

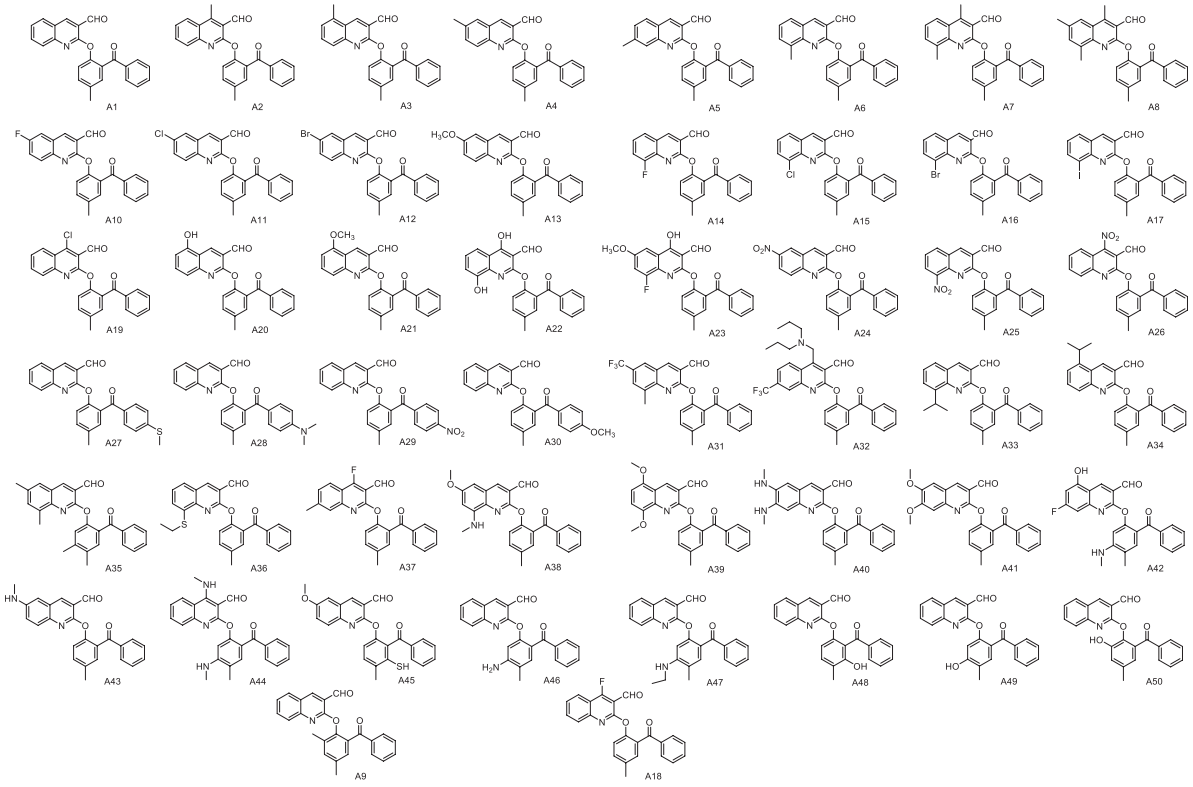

Figure 5. Hypothetical compounds A1–A50 obtained from structural modifications of compound 5.

Table 1. Toxicity prediction and probability values of lead compounds using Protox II webserver

Target	Compound 5	A5	A31	A36	A20
Hepatotoxicity	Inactive (0.56)	Inactive (0.97)	Inactive (0.50)	Inactive (0.52)	Inactive (0.54)
Carcinogenicity	Active (0.54)	Inactive (0.57)	Inactive (0.52)	Inactive (0.52)	Inactive (0.54)
Immunotoxicity	Inactive (0.83)	Inactive (0.99)	Inactive (0.82)	Inactive (0.71)	Inactive (0.67)
Mutagenicity	Inactive (0.55)	Inactive (0.85)	Inactive (0.56)	Inactive (0.56)	Inactive (0.60)
Cytotoxicity	Inactive (0.75)	Inactive (0.78)	Inactive (0.74)	Inactive (0.75)	Inactive (0.75)

Table 2. Toxicity prediction and probability values of lead compounds using Protox II webserver

Target	A33	A34	A45	A48	A49
Hepatotoxicity	Inactive (0.60)	Inactive (0.60)	Inactive (0.52)	Inactive (0.54)	Inactive (0.54)
Carcinogenicity	Inactive (0.56)	Inactive (0.56)	Inactive (0.51)	Inactive (0.41)	Inactive (0.54)
Immunotoxicity	Inactive (0.65)	Inactive (0.62)	Inactive (0.67)	Inactive (0.69)	Inactive (0.60)
Mutagenicity	Inactive (0.53)	Inactive (0.53)	Inactive (0.52)	Inactive (0.60)	Inactive (0.60)
Cytotoxicity	Inactive (0.71)	Inactive (0.71)	Inactive (0.76)	Inactive (0.75)	Inactive (0.75)

Table 1. Therefore, the rationale behind the research was to propose structural modifications by introducing various substituents at specific positions of the quinoline, tolyoxy, and benzoyl components of compound 5. These substituents included methyl, halogens, thiol, amino, methoxy, nitro, hydroxy, and isopropyl groups at positions 4, 5, 6, 7, and 8 of the quinoline moiety. For the tolyloxy scaffold, methyl, amino, thiol, and hydroxy groups were considered at the ortho and meta positions. Furthermore, for the *para* positions of the benzoyl scaffold, thiol, amino, nitro, and methoxy substituents were taken into account (Figure 5).

3.2. Toxicity results of compound (5), hypothetical compounds (A1–A50), and ten antimalarial reference drugs

A total of 50 hypothetical compounds (A1–A50) depicted in Figure 5, along with ten reference drugs (artesunate, doxycycline, tafenoquine, amodiaquine, arthemeter, lumefantrine, primaquine, piperaquine, mefloquine, and chloroquine), were subjected to virtual investigations to evaluate their toxicity profiles. The specific toxicity parameters examined included hepatoxicity, carcinogenicity, immunogenicity, mutagenicity, and cytotoxicity, as outlined in Table 1.

Notably, compound 5 and forty-one of the hypothetical derivatives exhibited failures in one or more of these tests, suggesting potential toxic and carcinogenic activities[22]. However, nine lead compounds (A5, A20, A31, A33, A34, A36, A45, A48, and A49) shown in Figure 3 demonstrated full compliance with the evaluated toxicity parameters (Tables 1 and 2).

Notably, the toxicity results for the reference drugs, as shown in Tables 3 and 4, revealed that only mefloquine demonstrated compliance with the evaluated parameters. In contrast, the other reference drugs exhibited one or more violations when compared to the nine lead compounds.

Table 3. Toxicity prediction of standard drugs against *P. falciparum* using Protox II webserver

Target	Mefloquine	Piperaquine	Artesunate	Doxycycline	Tafenoquine
Hepatotoxicity	Inactive (0.75)	Inactive (0.78)	Inactive (0.76)	Active (0.54)	Inactive (0.78)
Carcinogenicity	Active (0.76)	Inactive (0.71)	Inactive (0.65)	Inactive (0.77)	Inactive (0.63)
Immunotoxicity	Inactive (0.84)	Active (0.93)	Active (0.87)	Active (0.99)	Active (0.99)
Mutagenicity	Inactive (0.68)	Active (0.50)	Inactive (0.63)	Inactive (0.95)	Active (0.54)
Cytotoxicity	Inactive (0.74)	Inactive (0.82)	Inactive (0.87)	Inactive (0.90)	Inactive (0.63)

Table 4. Toxicity prediction of standard drugs against *P. falciparum* using Protox II webserver

Target	Amodiaquine	Artemether	Lumefantrine	Primaquine	Chloroquine
Hepatotoxicity	Inactive (0.61)	Inactive (0.77)	Inactive (0.70)	Inactive (0.84)	Inactive (0.90)
Carcinogenicity	Active (0.61)	Inactive (0.66)	Inactive (0.61)	Inactive (0.59)	Inactive (0.66)
Immunotoxicity	Active (0.99)	Active (0.92)	Active (0.99)	Active (0.99)	Active (0.69)
Mutagenicity	Inactive (0.75)	Inactive (0.60)	Inactive (0.60)	Active (0.79)	Active (0.94)
Cytotoxicity	Inactive (0.53)	Inactive (0.94)	Inactive (0.67)	Inactive (0.61)	Inactive (0.93)

Table 5. Physicochemical properties and drug-likeness of lead compounds using SwissADME webserver

Physico*	5	A5	A31	A36	A20	A33	A34	A45	A48	A49	Mefloq
MW	367.40	381.42	449.42	427.51	383.40	409.48	409.48	429.49	383.40	383.40	378.31
#rot_b	5	5	6	7	5	6	6	6	5	5	4
#HA	4	4	7	4	5	4	4	5	5	5	9
#HD	0	0	0	0	1	0	0	0	1	1	2
TPSA	56.26	56.26	56.26	81.56	76.49	56.26	56.26	104.29	76.49	76.49	45.15
natoms	28	29	33	31	29	31	31	31	29	29	26
nviol	1	1	1	1	1	1	1	1	1	1	2
log Kp	−4.83	−4.66	−4.45	−4.58	−5.18	−4.29	−4.29	−5.13	−4.79	−5.18	−6.04
Bioav	0.55	0.55	0.55	0.55	0.55	0.55	0.55	0.55	0.55	0.55	0.55
GI	High	High	Low	Low	High	High	High	Low	High	High	High
BBB	Yes	No	No	No	No	No	No	No	No	No	No
Pgp	No	No	Yes	Yes	No	Yes	Yes	No	No	No	Yes

Abbreviations: TPSA: Total polar surface area; natoms: Number of atoms in the molecule; MW: Molecular weight; #HA: Number of hydrogen bond acceptors; #HD: Number of hydrogen bond donors; nviol: Number of violations; #rot_b: Number of rotatable bonds; bioav: Bioavailability; GI: Gastrointestinal absorption; BBB: Blood–brain barrier; Pgp: Permeability glycoprotein substrate; Mefloq: Mefloquine.

Table 6. Drug violations and cytochrome inhibition ability of compound 5 and the leads using SwissADME webserver

Derivative	Lipinski	Ghose	Veber	Egan	Muegge	CYP2C19	CYP2D6
5	0	0	0	0	1	Yes	No
A5	0	1	0	0	1	Yes	No
A31	1	1	0	1	1	Yes	No
A36	0	1	0	1	1	Yes	No
A20	0	0	0	0	0	Yes	No
A33	0	1	0	1	1	Yes	No
A34	0	1	0	1	1	Yes	No
A45	0	1	0	0	1	Yes	No
A48	0	0	0	0	1	Yes	No
A49	0	0	0	0	0	Yes	No

Based on this finding, mefloquine was chosen for further virtual studies alongside the selected lead compounds.

3.3. *In silico* drug-likeness and ADME predictions

The results presented in Table 5 indicate that the lead compounds exhibit characteristics in compliance with the Rule of Five (RO5). These compounds have a suitable number of hydrogen bond donors (0–1 for nitrogen-hydrogen and oxygen-hydrogen bonds) and hydrogen bond acceptors (4–7 for nitrogen or oxygen atoms), which fall within the recommended ranges (<5 and <10, respectively). Their molecular weights range from 367.40 to 449.40 g/mol, aligning with the guideline of 150 to 500 g/mol. The observed topological polar surface area (TPSA) values range from 56.26 to 104 Å2, which also conform to the acceptable range of 20 to 130 Å2. In addition, the number of rotatable bonds in these compounds does not exceed 9.

According to a previous reported by Daina *et al.*[23], the negative log Kp values (−5.13 to −5.18) suggest that compounds A20, A45, and A49 are predicted to have lower permeability through human skin compared to the other compounds. On the contrary, compounds A31, A36, and A45 exhibit reduced gastrointestinal absorption rates. These characteristics can be attributed to specific structural features, such as the presence of a trifluoromethyl group at position 6 in compound A31, a thiol group at position 8 in compound A36, and a combination of a methoxy group at position 6 and a thiol group at position 3 in the methylphenoxyl ring. Notably, compound 5 displays permeability through the blood–brain barrier, unlike the other lead compounds. Furthermore, compounds A31, A33, A34, and A36 are identified as substrates for P-glycoprotein (P-gp) based on the studies conducted by Daina *et al.* Klopman *et al.*[23,24].

Out of the nine lead compounds, six, including compound 5, exhibited high gastrointestinal absorption rates, except for A31, A36, and A45. Moreover, unlike the other lead compounds, compound 5 has the ability to penetrate the blood–brain barrier, as indicated in Table 5. All nine lead compounds demonstrate good oral bioavailability, with a value of 0.55, with only one permissible violation according to Lipinski *et al.*[25] The inhibition of cytochrome P450 (CYP) isoenzymes is recognized as a major factor contributing to pharmacokinetics-related drug–drug interactions[26]. Such

Table 7. Binding energies of pure derivatives and reference drugs

Ligand	Binding affinity
A31_uff_E=300.34	−11.3
A5_uff_E=278.30	−11.2
A1/5_uff_E=277.56	−10.9
A20_uff_E=282.50	−10.8
A33_uff_E=300.83	−10.5
A49_uff_E=284.88	−10.5
A48_uff_E=343.12	−9.9
A36_uff_E=283.54	−9.8
A45_uff_E=414.27	−9.8
Mefloquine	−9.6
Piperaquine	−9
A34_uff_E=340.75	−8.7
Artesunate	−8.5
Doxycycline	−8.5
Tafenoquine	−8.5
Amodiaquine	−8.4
Artemether	−8.3
Lumefantrine	−7.3
Primaquine	−6.9
Chloroquine	−6

interactions can lead to toxic or adverse effects due to decreased drug clearance or the accumulation of drugs or their metabolites. Table 6 reveals that the lead compounds act as inhibitors of CYP2C19 while serving as substrates for CYP2D6. These cytochromes play crucial roles in the metabolism and elimination of approximately 25% of clinically utilized drugs, involving the addition or removal of specific functional groups through hydroxylation, demethylation, and dealkylation processes[27].

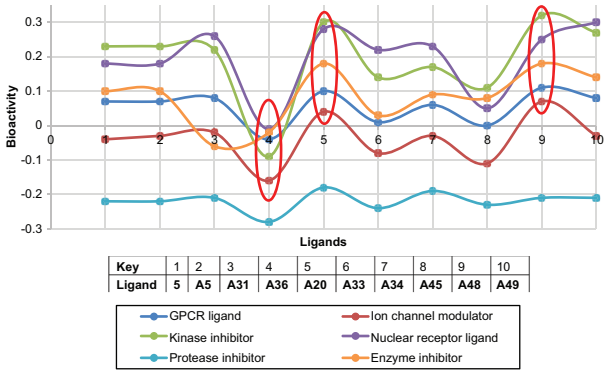

Figure 6. Bioactivity score of pure derivatives in compliance with the Pearson's correlation coefficient.

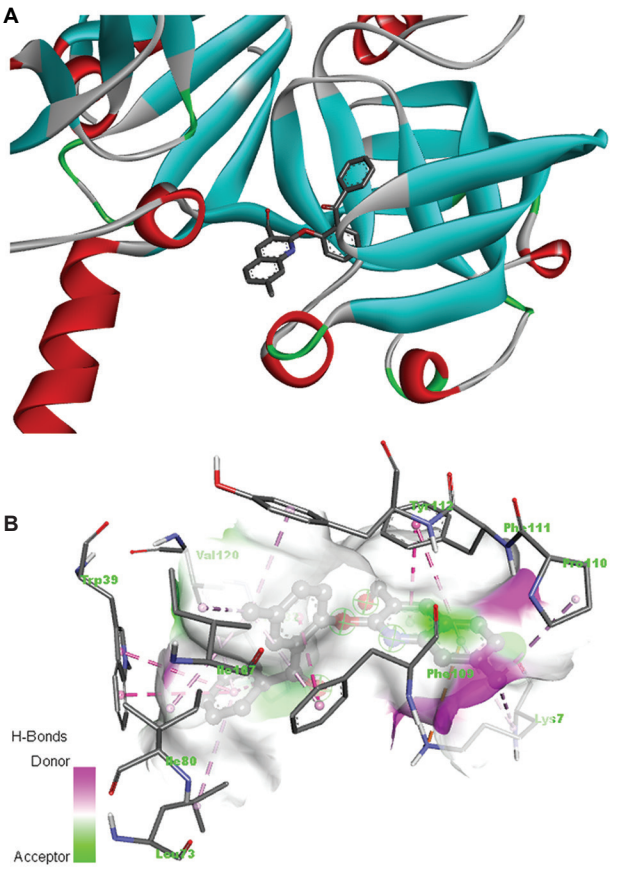

Figure 7A. (A and B) 3D interaction diagram and hydrogen bond donor and acceptor interaction of compound A5 with *Plasmodium falciparum* histoaspartic protease residues.

3.4. Bioactivity score

The potential candidacy of drug leads can be assessed by evaluating their bioactivity scores. In Figure 6, it can be observed that all the lead compounds generally exhibit high or moderate bioactivity across various parameters. Specifically, compounds A20 and A48 display high activity in five out of the six parameters, with bioactivity scores ranging from 0.00 to 0.33. Compounds A5 and A31 demonstrate high bioactivity as kinase inhibitors (with scores of 0.23 and 0.22, respectively), which suggests their potential in inhibiting cancer cells[28]. They also exhibit high bioactivity as nuclear receptor ligands (with scores of 0.18

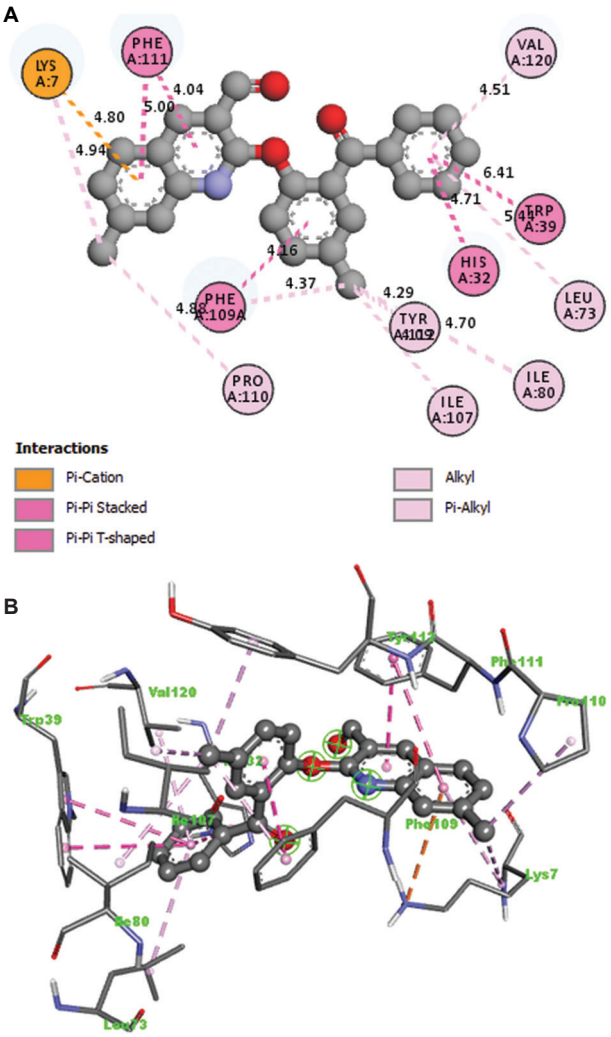

Figure 7B. (A and B) 2D diagram of the bond length and interacting residues of *Plasmodium falciparum* histoaspartic protease with compound A5.

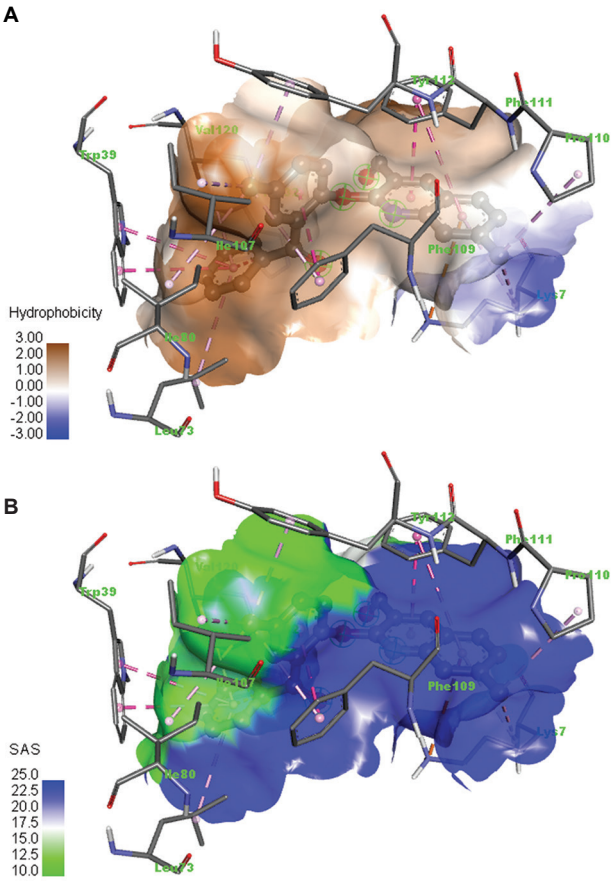

Figure 7C. (A and B) Hydrophobic/hydrophilic and solvent accessibility surface interaction of compound A5 with *Plasmodium falciparum* histoaspartic protease residues.

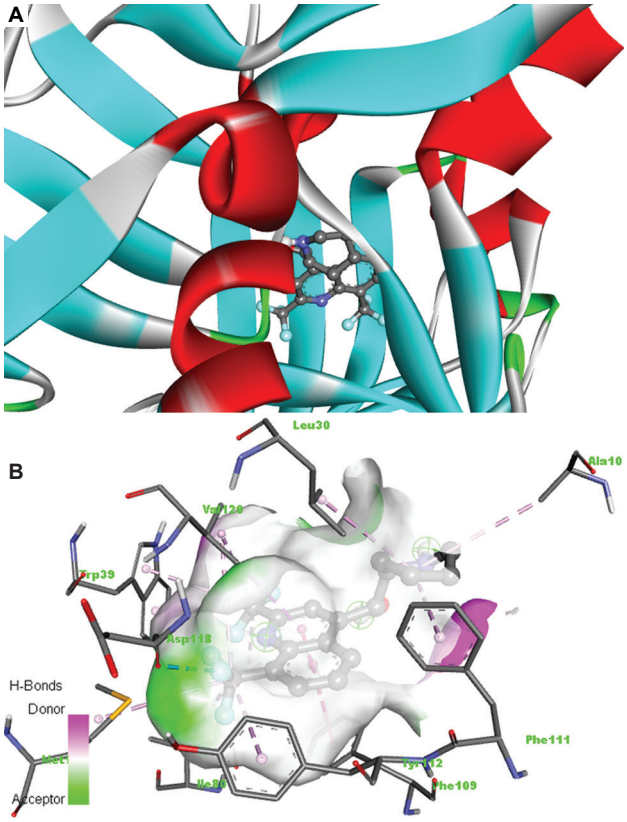

Figure 8A. (A and B) 3D interaction diagram and hydrogen bond donor and acceptor interaction of mefloquine with *Plasmodium falciparum* histoaspartic protease residues.

and 0.26, respectively), indicating their ability to interact with hydrophobic molecules such as fatty acids, cholesterol, and lipophilic hormones[29]. Furthermore, compounds A5 and A31 demonstrate bioactivity as glycoprotein receptors GPCR (with scores of 0.07 and 0.08, respectively), which regulate metabolic enzymes and promoter proteins, among other functions[30]. Compound A5 is also an enzyme inhibitor (with a score of 0.1), indicating its capability to bind to additional sites on the enzyme[31]. Among the lead compounds, A36 exhibits the lowest bioactivity score.

In terms of protease inhibition, all the lead compounds display moderate activity (with scores ranging from −0.18 to −0.28), suggesting their potential to impede the maturation of new HIV cells[32]. Only compounds A20 and A48 exhibit high activity as ion channel modulators, with scores of 0.04 and 0.07, respectively, surpassing the threshold of 0.00[33].

3.5. Molecular docking study

The findings from the docking simulations of ligands and reference drugs against HAP are summarized in Table 7. The binding energies for compound A31 (−11.3 kcal/mol) and compound A5 (−11.2 kcal/mol) are higher than that of compound 5 (−10.9 kcal/mol). Furthermore, the following six lead compounds exhibit binding energies ranging from −10.8 to −9.8 kcal/mol, all of which are higher than those of the ten reference drugs examined. Among the reference drugs, mefloquine performs the best with a binding energy of −9.6 kcal/mol, whereas chloroquine displays the lowest binding energy of −6.0 kcal/mol.

In Figures 4A, 7A, and 8A, the interaction between hydrogen acceptors and donors is depicted. In this representation, the donor group (indicated by a pink region, typically a hydrogen atom) from the ligand engages with the hydrogen bond acceptor site (depicted in green) on the surface of the enzyme. This electrostatic attraction between the partially positively charged hydrogen atom and the lone pair of electrons on the acceptor atom contributes to the stability of the molecular complexes formed, as illustrated in Figures 4, 7, and 8. Such interactions play a vital role in various biological and chemical processes, including protein-ligand binding, DNA base pairing, and solvation phenomena in the

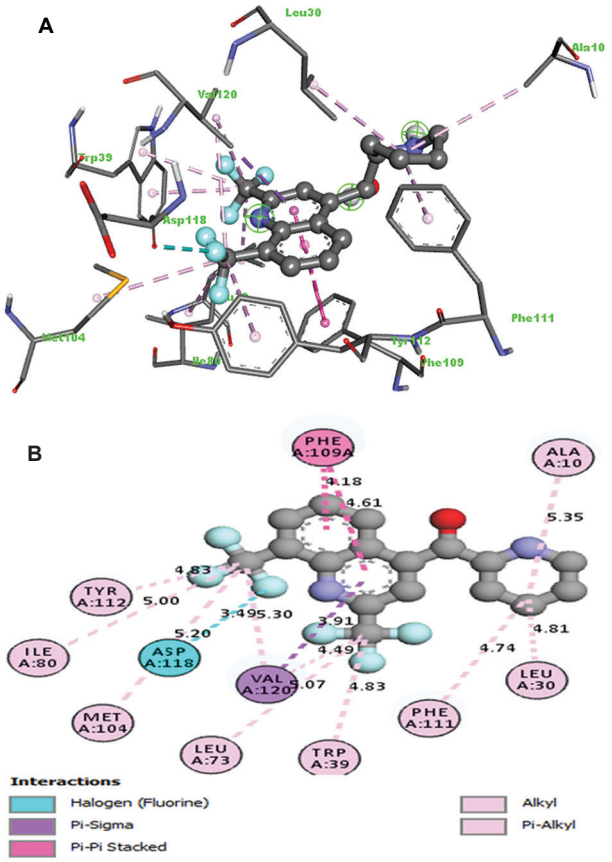

Figure 8B. (A and B) 2D diagram of the bond length and interacting residues of *Plasmodium falciparum* histoaspartic protease with mefloquine.

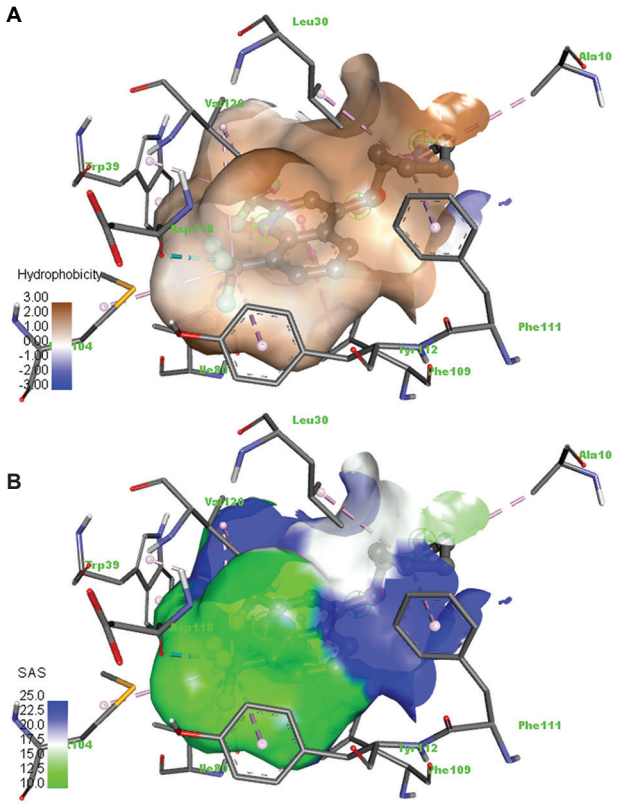

Figure 8C. (A and B) Hydrophobic/hydrophilic and solvent accessibility surface interaction of mefloquine with *Plasmodium falciparum* histoaspartic protease residues.

context of the *P. falciparum* HAP (PDB ID: 3QVC) and the lead compounds.

In the 2D view shown in Figure 4B, we observed hydrogen-binding interactions between the carbaldehyde oxygen atom of the quinoline core and Phe109, with a bond length of 3.51 Å. In addition, the strong fluorine bonds formed by the trifluoromethyl groups at position 7 with Glu86, Arg91, Lys7, and Ala10 (bond lengths ranging from 2.98 to 3.58 Å) likely contribute to the potent inhibitory interactions of 2-(2-benzoyl-4-methylphenoxy)-8-methyl-6-(trifluoromethyl) quinoline-3-carbaldehyde (A31) with *P. falciparum* (HAP). Other types of bonds observed in the interaction, as depicted in Figure 4B, include alkyl, π-π alkyl, π-π stacked, and π alkyl interactions at various bond lengths with residues of the protein.

Hydrophobic interactions (Figure 4C) are highly crucial for the folding of proteins, especially in keeping the protein stable and biologically active through decrease in surface area, thereby reducing the undesirable interactions with water[34]. Herein, compound A31 exhibits hydrophobic interactions with the *P. falciparum* HAP amino acid residues, especially the 2-benzoyl-4-methylphenoxy side of the molecule interacting with Leu_{73}, Ile_{80}, Tyr_{112}, Phe_{111}, $Trp_{39,}$ and Ile_{107}.

The interaction of the trifluoromethyl side of the quinoline molecule with Glu86, Arg91, Lys7, and Ala10 exhibits a distinct hydrophilic nature, attributed to the electronegative character of the fluorine atom. Solvent accessibility plays a significant role in protein folding and stability[35]. In Figure 4C, the solvent accessibility surface is represented by the blue region, indicating a large surface area. This suggests that compound A31 has a favorable interaction with the binding pocket of the HAP protein, potentially leading to enhanced binding and stability.

Similarly, the 3D structure of compound A5 is shown in Figure 7A with binding energy of −11.2 kcal/mol. The absence of hydrogen bond does not reduce its efficacy as HAP inhibitor due to other interactions such as π-cation (π electrons of the quinoline core and the amino hydrogen of the side chain of Lys_7), alkyl and π-alkyl (ligand and amino acid residues such as Val120, Leu73, Tyr410, Leu73, Ile80, Ile107, and Pro110), and π-π stacked and π-π T-shaped (compound A5 and Phe111, Phe109, His32, and Trp39) all contributed to its high binding energy (Figure 7B).

Figure 7C reveals that compound A5 exhibits notable hydrophobic interactions with all observed binding residues, except for Lys7. This observation suggests that compound A5 may possess favorable water–lipid interface transport properties, facilitating its movement across the cell membrane of the Pf HAP protein. In addition, the quinoline core of compound A5 demonstrates improved solvent accessibility, indicating a more open conformation. This conformation may promote easier interaction with the reactive sites of the target residues, as suggested by Gromiha and Ahmad[36].

The binding interactions between the best reference drug, mefloquine, and the residues of *P. falciparum* HAP (Figures 8A and 8B) indicate that the trifluoro groups attached to position 6 in compound A31 and position 8 in mefloquine play a role in their enhanced activity. However, unlike compound A31, mefloquine does not exhibit any hydrogen-bonding interactions, which could potentially contribute to its lower binding energy.

Similarly, the solvent accessibility surface interaction of compound A31 is greater than that of mefloquine, as indicated in Figure 8C, indicating a more favorable interaction within the binding pocket of the HAP protein.

4. Conclusion

In this study, we conducted toxicity profile tests to evaluate the synthesized compound 5 and fifty hypothetical compounds A1–A50 for their drug-likeness. The aim was to identify lead drug candidates that can overcome resistance to current standard reference antimalarial drugs. Among the hypothetical compounds, nine showed no toxicity to human cells.

Compounds A5 and A31 exhibited high bioactivity as kinase inhibitors, nuclear receptor ligands, and glycoprotein receptors GPCR. In addition, compound A5 acted as an enzyme inhibitor, capable of binding to other available sites on the HAP enzyme. It is hypothesized that the interaction of ligands at the active site of HAP, specifically the aspartate (Asp215) and histidine (His32) residues, can be treated as therapeutic targets, due to their importance for parasite growth and virulence, for developing effective inhibitors.

Interestingly, compound A31, with a binding energy of −11.3 kcal/mol, did not show any evidence of interaction with Asp215 or His32. However, compound A5, with a binding energy of −11.2 kcal/mol, exhibited π-π stacking interactions with His32. The best-performing reference drug, mefloquine, also did not show any interaction with Asp215 or His32.

Furthermore, compound A5 displayed significant hydrophobic interactions with all observed binding residues, except Lys7. This suggests that it has good water–lipid interface transport properties within the cell membrane of the Pf HAP protein. In addition, the quinoline core of compound A5 had better solvent accessibility, indicating a more open conformation that facilitates binding with reactive sites on the target residues. Based on our study findings, compound A5 shows promise as a potential candidate for developing drugs against antimalarial diseases.

Acknowledgments

None.

Funding

This work was funded, in part, by the University of Lagos Central Research Committee (CRC No. 2015/25) and Nigerian Government TetFund IBR (CRC/TETFUND/No. 2018/016).

Conflict of interest

The authors declare they have no competing interests.

Author contributions

Conceptualization: Luqman A. Adams, Oluwole B. Familoni
Formal analysis: Oluwafemi S. Aina, Luqman A. Adams
Investigation: Oluwafemi S. Aina, Adebayo J. Bello
Methodology: Oluwafemi S. Aina, Adebayo J. Bello
Writing – original draft: Oluwafemi S. Aina, Luqman A. Adams
Writing – review & editing: Luqman A. Adams, Oluwole B. Familoni

Ethics approval and consent to participate

Not applicable.

Consent for publication

Not applicable.

Availability of data

Not applicable.

Further disclosure

The paper has been uploaded to or deposited in a preprint server (Research Square): https://doi.org/10.21203/rs.3.rs-2748975/v1

References

1. World Health Organization, 2022, WHO Guidelines for Malaria. WHO/UCN/GMP/2022.01 Rev. 2. Geneva: World Health Organization.

2. Jensen AR, Adams Y, Hviid L, 2020, Cerebral *Plasmodium falciparum* malaria: The role of PfEMP1 in its pathogenesis and immunity, and PfEMP1-based vaccines to prevent it. *Immunol. Rev*., 293: 230–252.

https://doi.org/10.1111/imr.12807

3. Karthik L, Kumar G, Keswani T, *et al*., 2014, Protease inhibitors from marine actinobacteria as a potential source for antimalarial compound. *PLoS One*, 9: e90972.

4. Francis SE, Banerjee R, Goldberg DE, 1997, Biosynthesis and maturation of the malaria aspartic hemoglobinases plasmepsins I and II. *J Biol Chem*, 272: 14961–14968.

https://doi.org/10.1074/jbc.272.23.14961

5. Nasamu AS, Polino AJ, Istvan ES, 2020, Malaria parasite plasmepsins: More than just plain old degradative pepsins. *J Biol Chem*, 295: 8425–8441.

https://doi.org/10.1074/jbc.REV120.009309

6. Boddey JA, Hodder AN, Günther S, *et al*., 2010, An aspartyl protease directs malaria effector proteins to the host cell. *Nature*, 463: 627–631.

https://doi.org/10.1038/nature08728

7. Roy KK, 2017, Targeting the active sites of malarial proteases for antimalarial drug discovery: Approaches, progress and challenges. *Int J Antimicrob Agents*, 50: 287–302.

https://doi.org/10.1016/j.ijantimicag.2017.04.006

8. Zhou W, Wang H, Yang Y, *et al*., 2020, Chloroquine against malaria, cancers and viral diseases. *Drug Discov Today*, 25: 2012–2022.

https://doi.org/10.1016/j.drudis.2020.09.010

9. Hong SH, Ismail IA, Kang SM, *et al*., 2016, Cinnamaldehydes in cancer chemotherapy. *Phytother Res*, 30: 754–767.

https://doi.org/10.1002/ptr.5592

10. Nair A, Amalraj A, Jacob J, *et al*., 2019, Non-curcuminoids from turmeric and their potential in cancer therapy and anticancer drug delivery formulations. *Biomolecules*, 9: 13.

https://doi.org/10.3390/biom9010013

11. Ma HS, Wang EL, Xu WF, *et al*., 2018, Overexpression of DNA (cytosine-5)-methyltransferase 1 (DNMT1) and DNA (cytosine-5)-methyltransferase 3A (DNMT3A) is associated with aggressive behavior and hypermethylation of tumor suppressor genes in human pituitary adenomas. *Med Sci Monit*, 24: 4841–4850.

https://doi.org/10.12659/MSM.910608

12. Schneidman-Duhovny D, Inbar Y, Nussinov R, *et al*., 2005, Geometry-based flexible and symmetric protein docking. *Proteins*, 60: 224–231.

https://doi.org/10.1002/prot.20562

13. Banerjee R, Liu J, Beatty W, *et al*., 2002, Four plasmepsins are active in the *Plasmodium falciparum* food vacuole, including a protease with an active-site histidine. *Proc Natl Acad Sci*, 99: 990–995.

https://doi.org/10.1073/pnas.022630099

14. Bhaumik P, Gustchina A, Wlodawer A, 2012, Structural studies of vacuolar plasmepsins. *Biochim Biophys Acta*, 1824: 207–223.

https://doi.org/10.1016/j.bbapap.2011.04.008

15. Available from: https://tox-new.charite.de [Last accessed on 2023 May 31].

16. Available from: https://pubchem.ncbi.nlm.nih.gov [Last accessed on 2023 May 25].

17. Lipinski B, Herzog H, Kops ER, *et al*., 1997 Expectation maximization reconstruction of positron emission tomography images using anatomical magnetic resonance information. *IEEE Trans Med Imaging*, 16: 129–136.

https://doi.org/10.1109/42.563658

18. Available from: https://www.rcsb.org/ [Last accessed on 2023 Apr 20].

19. Available from: https://lmmd.ecust.edu.cn/admetsar2 [Last accessed on 2023 Mar 15].

20. Yang H, Sun L, Li W, *et al*., 2018, *In silico* prediction of chemical toxicity for drug design using machine learning methods and structural alerts. *Front Chem*, 6: 30.

https://doi.org/10.3389/fchem.2018.00030

21. Trott O, Olson AJ, 2010, AutoDock Vina: Improving the speed and accuracy of docking with a new scoring function, efficient optimization, and multithreading. *J Comput Chem*, 31: 455.

https://doi.org/10.1002/jcc.21334

22. Jacobs AC, Hatfield KP, 2013. History of chronic toxicity and animal carcinogenicity studies for pharmaceuticals. *Vet Pathol*, 50: 324-333.

https://doi.org/10.1177/0300985812450727

23. Daina A, Olivier M, Vincent Z, 2017, SwissADME: A free web tool to evaluate pharmacokinetics, drug-likeness and medicinal chemistry friendliness of small molecules. *Sci Rep*, 7: 42717.

https://doi.org/10.1038/srep42717

24. Klopman G, Stefan LR, Saiakhov RD, 2002, ADME evaluation: 2. A computer model for the prediction of intestinal absorption in humans. *Eur J Pharm Sci*, 17: 253–263.

https://doi.org/10.1016/s0928-0987(02)00219-1

25. Lipinski CA, Lombardo F, Dominy BW, *et al*., 2012, Experimental and computational approaches to estimate solubility and permeability in drug discovery and development settings. *Adv Drug Deliv Rev*, 64: 4–17.

https://doi.org/10.1016/j.addr.2012.09.019

26. Huang H, Rong H, Li X, *et al*., 2008, The crystal structure and identification of NQM1/YGR043C, a transaldolase from *Saccharomyces cerevisiae*. Proteins, 73: 1076–1081.

https://doi.org/10.1002/prot.22237

27. Wang B, Yang, LP, Zhang XZ, *et al*., 2009, New insights into the structural characteristics and functional relevance of the human cytochrome P450 2D6 enzyme. *Drug Metab Rev*, 41: 573–643.

https://doi.org/10.1080/03602530903118729

28. Kakinuma T, Hwang, ST, 2006, Chemokines, chemokine receptors, and cancer metastasis. *J. Leukoc Biol*, 79: 639–651.

https://doi.org/10.1189/jlb.1105633

29. McEwan IJ, 2009, Nuclear receptors: One big family. *Methods Mol Biol*, 505: 3–18.

https://doi.org/10.1007/978-1-60327-575-0_1

30. Schwab A, Fabian A, Hanley PJ, *et al*., 2012, Role of ion channels and transporters in cell migration. *Physiol Rev*, 92: 1865–1913.

https://doi.org/10.1152/physrev.00018.2011

31. Copeland RA, 2013, Evaluation of Enzyme Inhibitors in Drug Discovery: A Guide for Medicinal Chemists and Pharmacologists. United States: John Wiley & Sons.

32. Leung D, Abbenante G, Fairlie DP, 2000, Protease inhibitors: Current status and future prospects. *J Med Chem*, 43: 305–341.

https://doi.org/10.1021/jm990412m

33. Barker BS, Young GT, Soubrane CH, *et al*., 2017, Ion channels. In: Conn's Translational Neuroscience. 1st ed. London: Elsevier Academic Press, p11–43.

https://doi.org/10.1016/B978-0-12-802381-5.00002-6

34. Ma FH, Li C, Liu YL, 2020, Mimicking molecular chaperones to regulate protein folding. *Adv Mater*, 32: e1805945.

https://doi.org/10.1002/adma.201805945

35. Savojardo C, Manfredi M, Martelli PL, *et al*., 2021, Solvent accessibility of residues undergoing pathogenic variations in humans: From protein structures to protein sequences. *Front Mol Biosci*, 7: 626363.

https://doi.org/10.3389/fmolb.2020.626363

36. Gromiha MM, Ahmad S, 2005, Role of solvent accessibility in structure based drug design. *Curr Comput Aided Drug Des*, 1: 223–235.

ACCSCIENCE PUBLISHING

INNOSC Theranostics and Pharmacological Sciences

ORIGINAL RESEARCH ARTICLE

In silico evaluation of heat shock proteins reveals an interplay with polyamines as a survival strategy for the *Plasmodium falciparum*

Godlo Sesethu[1], Maxam Nombalentle[1], Mthembu Yamkela[1], Mpumza Anelisa[1], Stanley Makumire[2,3], Noxolo Mkwetshana[1], Krishna K. Govender [4], and Xolani H. Makhoba[5]*

[1]Department of Microbiology and Biochemistry, University of Fort Hare, Alice Campus, South Africa

[2]Structural Biology Research Unit, Department of Integrative Biomedical Sciences, Institute of Infectious Diseases and Molecular Medicine, University of Cape Town, Observatory 7925, South Africa

[3]Protein and Structural Biology Research Unit, Faculty of Biochemistry and Molecular Medicine, University of Oulu, Aapistie 7A, 90220 Oulu, Finland

[4]Department of Chemical Sciences, University of Johannesburg, P. O. Box 17011, Doornfontein Campus, 2028, Johannesburg, South Africa

[5]Department of Biochemistry, Microbiology and Biotechnology, University of Limpopo, Turfloop Campus, Sovenga, South Africa

Abstract

The current drugs available in the market are not effective due to growing numbers of resistance to the causative agent of malaria. There are various *Plasmodium* parasites, of which *Plasmodium falciparum* is the main cause of morbidity and mortality reported worldwide. Therefore, there is an urgent need to come up with an innovative and effective treatment for this disease. Polyamines play a major role in the parasite's well-being and growth, while heat shock proteins keep the proteomics of the parasite in good shape. In this study, an *in silico* analysis of the interaction between putrescine, spermidine, spermine, and heat shock proteins was carried out to establish the binding site for drug discovery. Computational tools such as Bioedit, PROCHECK, KNIME Hub, and Schrodinger were used. The results revealed interactions between polyamines and heat shock proteins with glutamine and aspartic acid being common amino acids where interaction occurs between the chaperones and polyamines. Molecular dynamics showed a strong interaction between PfHsp70-1 and putrescine, but the best interaction is observed for PfHsp70-1 and spermidine. Based on these results, a follow-up study will be conducted to establish the synthesis of drugs that will be used as targets for both polyamines and heat shock proteins to eradicate malaria.

Keywords: Malaria; *In silico*; Putrescine; Spermidine; Spermine; Heat shock proteins; Multi-drug development

***Corresponding author:**
Xolani H. Makhoba
(Xolani.Makhoba@ul.ac.za)

Citation: Sesethu G, Nombalentle M, Yamkela M, *et al.*, 2024, *In silico* evaluation of heat shock proteins reveals an interplay with polyamines as a survival strategy for the *Plasmodium falciparum*. *INNOSC Theranostics and Pharmacological Sciences,* 7(1): 1228.
https://doi.org/10.36922/itps.1228

Received: July 3, 2023

Accepted: August 15, 2023

Published Online: September 13, 2023

1. Introduction

Malaria is a mosquito-borne disease, it is one of the most predominant parasitic diseases that threaten human life. Malaria affects about half of the world's population. Most

deaths occur in Sub-Saharan Africa and high-risk areas such as South-east Asia, the Eastern Mediterranean, the Western Pacific, and the Americas[1]. In 2019, the World Health Organization (WHO) reported approximately 229 million cases and 409,000 malarial deaths. Sub-Saharan Africa accounted for 94% of these deaths[2]. This parasitic disease is transmitted to humans by female *Anopheles* mosquitoes. Of more than 430 *Anopheles* species known to exist, approximately 40 can transmit malaria. In humans, five *Plasmodium* species are causative agents of malaria infection: *Plasmodium falciparum*, *Plasmodium vivax*, *Plasmodium ovale*, *Plasmodium malariae,* and *Plasmodium knowlesi*.

P. falciparum is the most common malaria parasite as it accounts for over 99% of malaria cases in Africa, 71.9% in the West Pacific region, 69% in the Mediterranean, and 62.8% in South-east Asia[2]. The most vulnerable groups at risk of contracting malaria include pregnant women and children under the age of 5, with 67% of malaria death cases being children under the age of 5[1]. Malaria mostly affects developing tropical and subtropical countries. In these countries, outcomes of malaria include loss of education for children, and adults not being able to provide for their families due to physical and intellectual distress caused by cerebral damage. The disease results in financial burdens for both the government and individuals. The WHO reported that in Africa, direct costs of malaria sum up to approximately US$12 million annually, while households spend a quarter of their income on treating malaria at home.

The drug of choice for treating malaria is determined by several variables including age, the severity of the infection, baseline immunity, parasite sensitivity, and drug cost and availability. In the early 1900s, quinine and its derivatives were widely used to treat malaria[3]. Many of these anti-malarial drugs are no longer in use due to *P. falciparum* and *P. vivax* resistance against the drugs and undesirable side effects from compounds such as mepacrine[3,4]. However, some quinine derivatives such as mefloquine are still in use in combination with artesunate as binary combination drugs[3]. At present, classes of drugs used for malaria include artemisinin, antifolates, 4-aminoquinolines, 8-aminoquinolines aryl-amino alcohols, and antibiotics. Artemisinin is the most widely used antimalarial drug globally due to its efficacy against all forms of *P. falciparum* strains by inhibiting the parasite's phosphatidylinositol-3-kinase during the early ring stage[5] with artemisinin combination therapies being recommended to treat both complicated and uncomplicated *P. falciparum* malaria. However, gene modification in the *Plasmodium* parasite results in resistance of the parasite to antimalaria drugs as the genes that encode target regions mutate, and this raises a crucial need for new innovative, and effective antimalarial drugs[3,4]. Newly developed drugs should at least be able to terminate the parasite growth at any stage, in the erythrocytic stage, mosquito stage, and human liver stage[6] as a way of changing the usual sequence of drug targets.

Positively charged organic compounds with two or more amino groups found in cells of living organisms are referred to as polyamines[7], and they play an important part in cell division and differentiation of *P. falciparum*[7,8]. These include diamine, putrescine, and triamine spermidine as well as tetramine spermine, which are synthesized uniquely by the action of S-adenosylmethionine decarboxylase (AdometDC) and ornithine decarboxylase (ODC) functioning as a single enzyme and spermidine synthase. The absence of spermine synthase, in *P. falciparum,* makes spermidine synthase responsible for both spermidine and spermine synthesis[8].

The malaria parasite survives between the mosquito host and the human host. During transmission between these two hosts, the parasite moves from a poikilothermic mosquito to a warm-blooded human, causing severe heat shock to the parasite. Thus, heat shock proteins (HSPs) play a key role in the adaptation survival of the parasite inside the human host[9]. Heat shock proteins, which are a part of a large family of molecular chaperones, are well-known for their function in the refolding, maturation, and degradation of proteins[10]. These are divided into small heat shock proteins and major heat shock proteins[11,12], of which the major ones have a molecular mass of >43 kDa, and small heat shock proteins have molecular weights of <43 kDa[12]. Small heat shock proteins with molecular weights of 15 – 43 kDa are called heat shock protein β and are particularly known for their role in protecting cells from stress[13].

2. Materials and methods

Supplementary S1 contains a list of online web servers used for bioinformatic analyses used in this study.

2.1. Sequence retrieval

Sequences of selected heat shock proteins from *Pf*3D7 were retrieved from the PlasmoDB database. This database provides substantial *Plasmodium* spp. genome, proteome, and metabolome information. Genomic characteristics of the selected heat shock proteins were obtained from the National Centre of Biotechnological Information (NCBI) database by selecting the gene ID of the selected HSP to identify the protein's gene and chromosomal location.

2.2. Multiple sequence alignment

Protein sequences of Hsp 20, Hsp 40, Hsp 60, Hsp 70-1, and Hsp 90 from *Escherichia coli* and *Saccharomyces*

cerevisiae were retrieved from the NCBI. These sequences together with the PfHsps sequences were compiled to a txt file using Notepad++ (the HSP sequences were compiled separately according to their molecular weight). The sequences, together with the *P. falciparum* sequences, were aligned using the Bio-edit tool[14] using ClustalW and BLOSSUM62 matrix.

2.3. Homology modeling and structure validation

Phyre2[15], a protein structure prediction database, was used to generate 3D model structures using sequences of the *Pf*3D7 selected HSPs under intensive modeling mode. The modeled structures were visualized with PyMol. The structures were then validated using PROCHECK on the online tool PDBSum[16] found on the EBI database.

2.4. Protein preparation for docking and molecular dynamics (MD)

All the heat shock proteins (PfHsp20, PfHsp40, PfHsp60, PfHsp70-1, and PfHsp90) obtained from homology modeling were prepared with the aid of the protein preparation wizard provided in Schrodinger 2022-1[17].

2.5. Site mapping

Since the proteins were obtained through homology modeling, there were no active sites to work from. Instead of making use of a blind docking approach, we made use of the SiteMap[18,19], the tool provided in Schrodinger 2022-1. The tool allows for the identification of binding sites whose size, functionality, and extent of solvent exposure meet certain criteria. The OPLS4 force field was used for docking, at least 15 site points per reported site, a more limited definition of hydrophobicity, a fine grid, crop site maps at four from the nearest site point, and reporting up to five sites were all necessary for this study.

2.6. Molecular docking

All ligands were obtained directly from PubChem. Due to the size of the ligand library, we decided to make use of the QM Conformer and Tautomer Predictor[20] instead of using the conventional ligand preparation of Schrodinger[21,22]. This was done to ensure that we end up with quantum mechanical-based minimum energy conformers before docking to the active site of the proteins of interest[23]. The method generates the lowest energy tautomers or conformers for a set of structures with optional protonation or deprotonation. Due to the computational cost of this method, it is advised that this only be applied to small datasets[23].

2.7. MD

MD simulations were conducted with the aid of Desmond[24]. The free protein structures as well as those complexed to Put, Spd, and Spn were prepared using the TIP4P solvent model, 15 Å3 Orthorhombic boxes, OPLS4 force field, and each system were neutralized with an appropriate number of Na^+ or Cl^- counterions (Supplementary S2). A 0.15 M NaCl solution was created to mimic physiological conditions. All MD simulations were done with the NPT ensemble at a temperature of 300 K and pressure of 1.01325 bar. Due to wall time limitations on the high-performance computer being used for the simulations, we had to run the MD in steps of 50 ns for HSP20, HSP40, and HSP60, 30 ns for HSP70-1, and 25 ns for HSP90. On completion of the simulations, the various intervals were combined into a single 200 ns trajectory for analysis.

3. Results and discussion

3.1. Sequence retrieval and genomic analysis

Genomic analysis showed that HSP20 and HSP70-1 are located on the same chromosome (chromosome 8), while HSP40 is located on chromosome 13, HSP60 on chromosome 10, and HSP90 on chromosome 7 (Supplementary S3). The bioinformatics analysis of *Pf*3D7 heat shock proteins showed that these major HSPs have a few exons and introns in them, with HSP40 and HSP70 having 1 exon and no introns, HSP60 and HSP90 having 2 exons and 1 intron, and HSP20 having 3 exons and 1 intron.

3.2. Multiple sequence alignments of PfHsps and their homologs

All the heat shock proteins were aligned with *S. cerevisiae* and *E. coli* (Supplementary S4) in BioEdit. The similarity index between *P. falciparum* and *E. coli* was HSP20, HSP40, HSP60, HSP70, and HSP 90 at 20.63%, 19.34%, 67.41%, 58.30%, and 54.15%, respectively. While the similarity index between *P. falciparum* and *S. cerevisiae* HSP40, HSP60, HSP70, and HSP90 was higher at 32.90%, 71.92%, 79.32%, and, 75.70%, respectively, except for HSP20 which was 12.61%. This is due to *S. cerevisiae*'s small HSP (HSP20 family) being present as HSP26, a 26 kDa protein instead of 20 kDa.

3.3. Homology modeling and structure validation

All PDB structures (Figure 1) were generated from Phyre2. The projected structure of PfHSP20 comprises two sheets, four beta hairpins, seven strands, six helices, 15 beta turns, and six gamma turns, according to motif analysis. This demonstrated that the created structure was suitable for further investigation. The 3D structure of PfHSP40 reveals that the protein has five helices, nine helix-helix interactions, and two beta twists. The Ramachandran plot revealed that all of the residues were in core areas. As a result, the structure merits additional investigation. The 3D structure of HSP60 revealed five sheets, two beta-alpha-beta

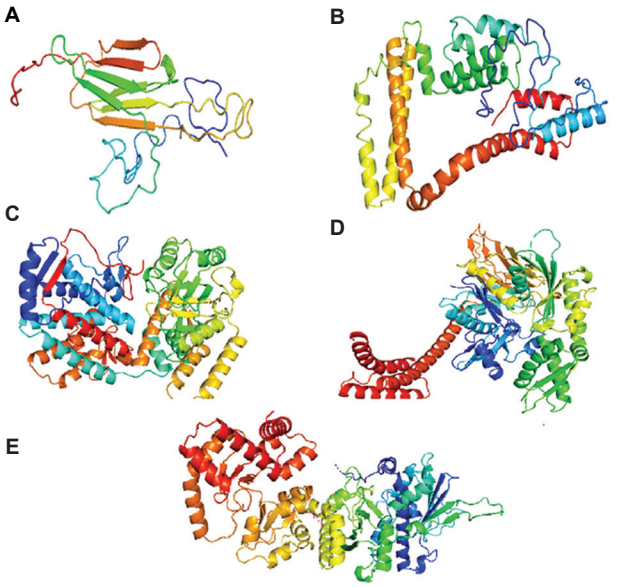

Figure 1. Three-dimensional structures of *Plasmodium falciparum* 3D7 (A) HSP20, (B) HSP40, (C) HSP60, (D) HSP70, and (E) HSP90 in cartoon format as visualized on PyMol.

units, three beta hairpins, one psi loop, two beta bulges, 17 strands, 27 helices, 36 helix-helix interactions, 25 beta turns, and five gamma turns. According to the Ramachandran plot data, this structure included 95.8% of the residues in the most desired areas, 3.9% of the residues in allowed regions, and 0.4% of the residues in the generously allowed regions. The motif description of PfHSP70's 3D structure is the same as that of PfHSP60. The plot of PfHSP70 Ramachandran indicated that 92.0% of the amino acid residues are in the core areas, 7.3% are in allowed regions, 0.5% are in generously allowed regions, and 0.2% are in banned regions. The generated PfHSP90 structure has one sheet, four beta hairpins, two beta bulges, nine strands, nine helices, 15 helix-helix interacts, 13 beta turns, and two gamma turns, with the Ramachandran plot indicating that 92.4% of the residues are in core regions and 7.6% are in allowed regions.

3.4. Docking sites identified in the heat shock proteins

The heat shock proteins' 3D models were modeled using Phyre2[15] and these were used to identify possible binding

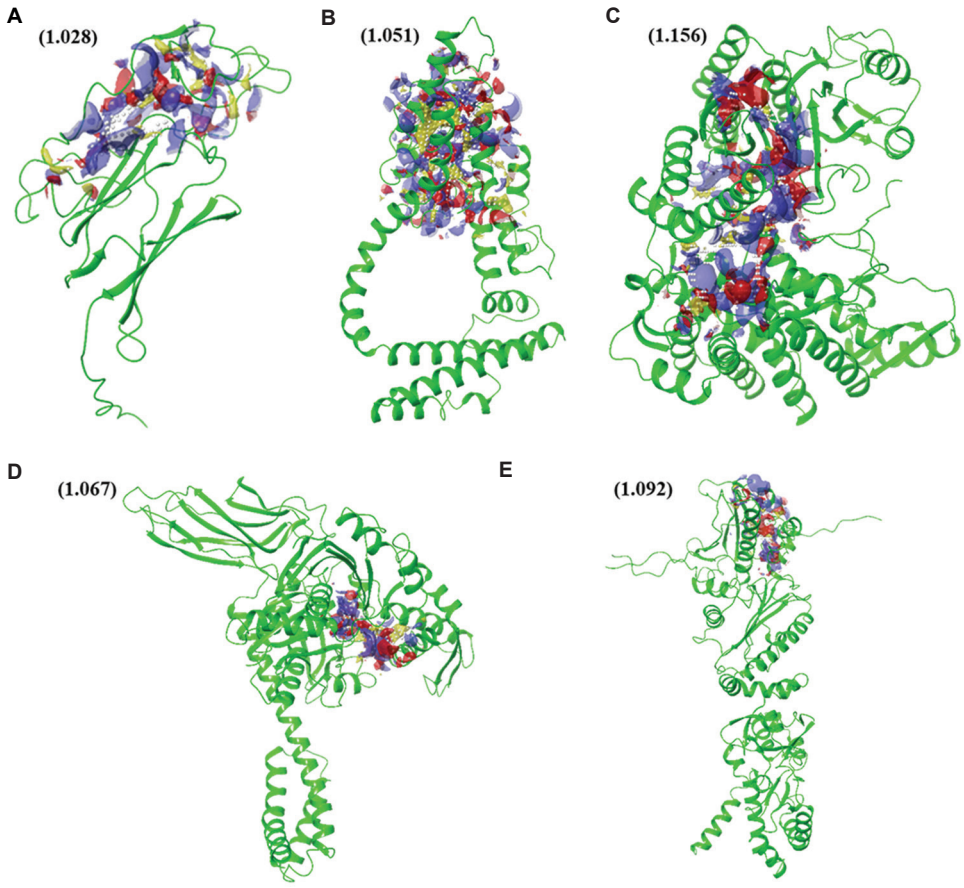

Figure 2. Active site identification of (A) HSP20, (B) HSP40, (C) HSP60, (D) HSP70, and (E) HSP90 identified through SiteMap. Site scores are given in brackets.

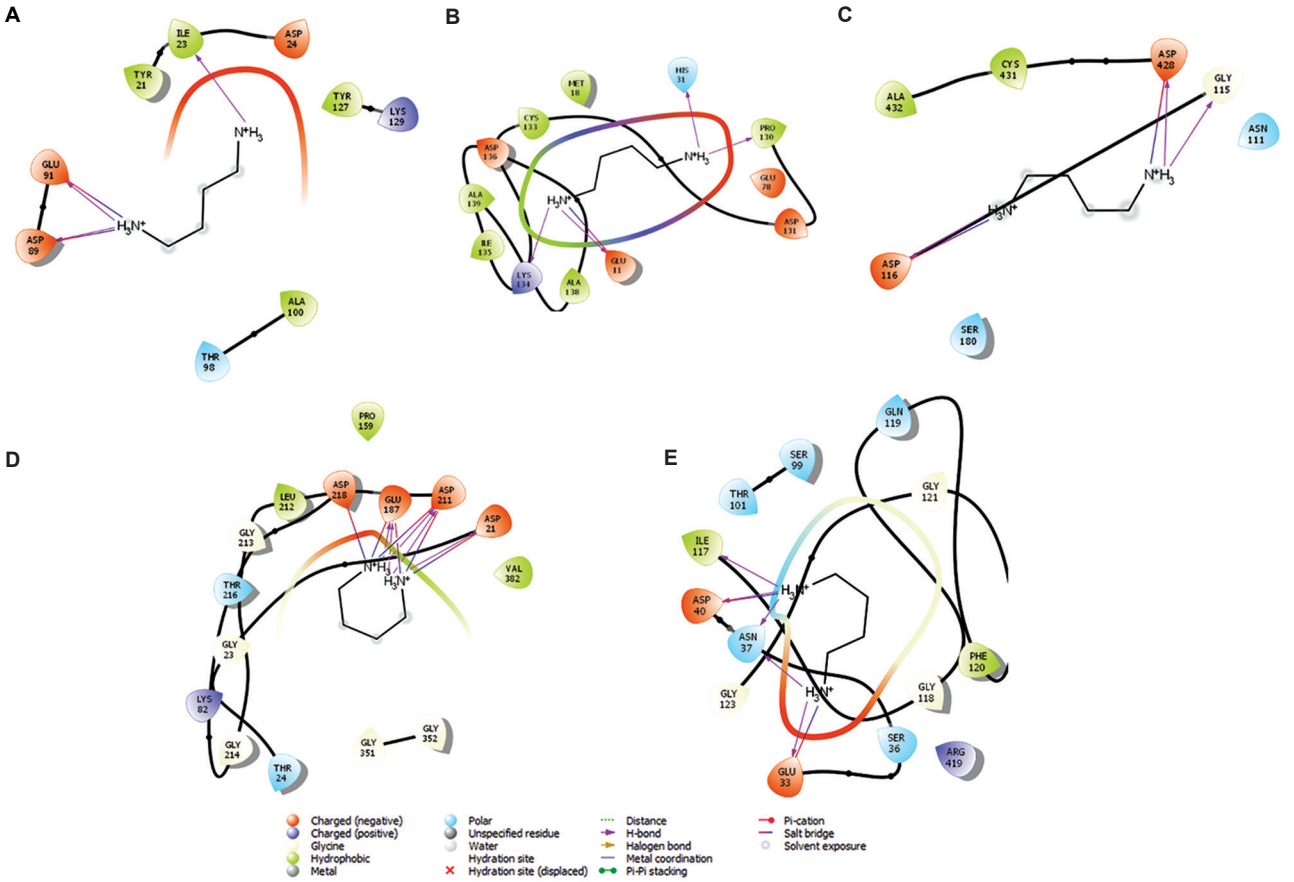

Figure 3. Ligand interaction diagram of (A) HSP20, (B) HSP40, (C) HSP60, (D) HSP70, and (E) HSP90 bound to Put.

Table 1. Docking scores of putrescine, spermidine, and spermine bound to the active site of heat shock proteins

Ligand name	CID	HSP20	HSP40	HSP60	HSP70	HSP90
Putrescine	3452892	−3.19	−5.41	−5.95	−6.63	−6.68
Spermidine	6992097	−4.54	−8.18	−7.34	−7.99	−6.19
Spermine	446718	−3.07	−5.86	−8.66	−4.41	−4.76

sites. Active sites were identified by making use of the Sitemap tool[18] provided within the Schrodinger software suite. For a site to be considered a good potential docking site the following needs to hold true, site score > 1, d score > 1, and a volume > 225. Based on the results obtained (Supplementary S5), those sites provided in Figure 2 were the ones chosen for docking as they obeyed the criterion specified. This approach was chosen as opposed to blind docking since it was computationally more appealing and has been shown to provide good estimates for active site identification[6,7].

3.5. Molecular docking

Those ligand conformations that provided the lowest docking scores after being bound to the active sites of the heat shock proteins are provided in Table 1.

In the case of Put, the docking scores appear to drop as the protein structure increases in size. This could be due to the binding pocket getting larger as the proteins get bigger and since Put is a small ligand, it can fit better within the active site. For Spd, the lowest docking score (−8.18 kcal/mol) is obtained when the ligand is bound to HSP40, while for Spn, the lowest docking score (−8.66 kcal/mol) is obtained for HSP60. Figures 3–5 provide the ligand interaction diagrams for the different ligands bound to the active sites of the heat shock proteins considered in this work.

A summary of all the hydrogen bond interactions and salt bridges formed between the ligand and amino acid residues contained within the active site of the proteins is provided in Table 2. For HSP20, the amino acid Asp89 has a hydrogen bond that takes place between all three ligands, while Glu91

has a hydrogen bond present for ligands Put and Spd. Asp24 shows a hydrogen bond between Spd and Spn. It is this combination of salt bridges and hydrogen bond interactions that adds to the protein-ligand complex stability.

3.6. MD

Before we investigated the results obtained for the various HSP complexes, we first needed to make sure that the environment chosen for our MD studies was appropriate. Figure 6 shows the root mean square deviation (RMSD) results obtained for 200 ns simulations of (A) HSP20, (B) HSP40, (C) HSP60, (D) HSP70, and (E) HSP90 when there were no ligands present within the active site of the proteins.

The RMSD is used for measuring the changes that take place in the protein while present in a solvated environment[25]. A protein's stability can be determined by the deviations produced during the MD simulation. Figure 6 does show that PfHsp20, PfHsp40, and PfHsp70 stabilize within the 200 ns, but PfHsp60 and PfHsp90 appeared to have some excess fluctuations towards the end of the 200 ns. Although this was the case, it was decided that we would make use of a maximum of 200 ns for the protein-ligand complex simulations due to the limited resources that we had access to at the high-performance computing center.

MD simulations of the Hsps with the polyamines showed that putrescine best binds to PfHsp60 and PfHsp70 (Figure 7) compared to the other Hsps. Put seems to remain strongly bound to the active site of PfHsp60 for around 125 ns before the ligand begins to drift away from the active site, reaching distances of up to 14 Å from the starting structure (Figure 7A). For ligands to be considered good inhibitors, they need to remain bound to the active site for

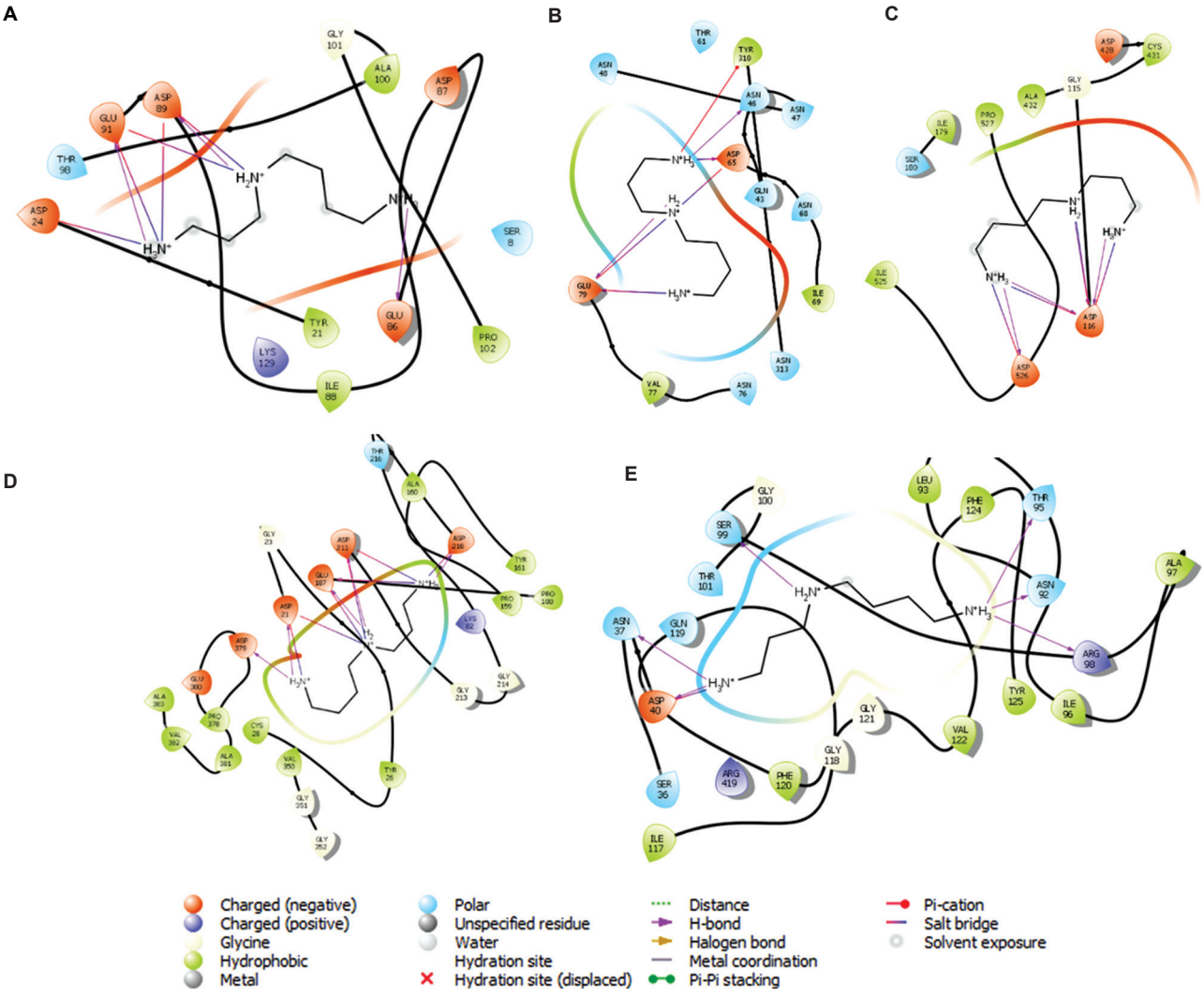

Figure 4. Ligand interaction diagram of (A) HSP20, (B) HSP40, (C) HSP60, (D) HSP70, and (E) HSP90 bound to Spd.

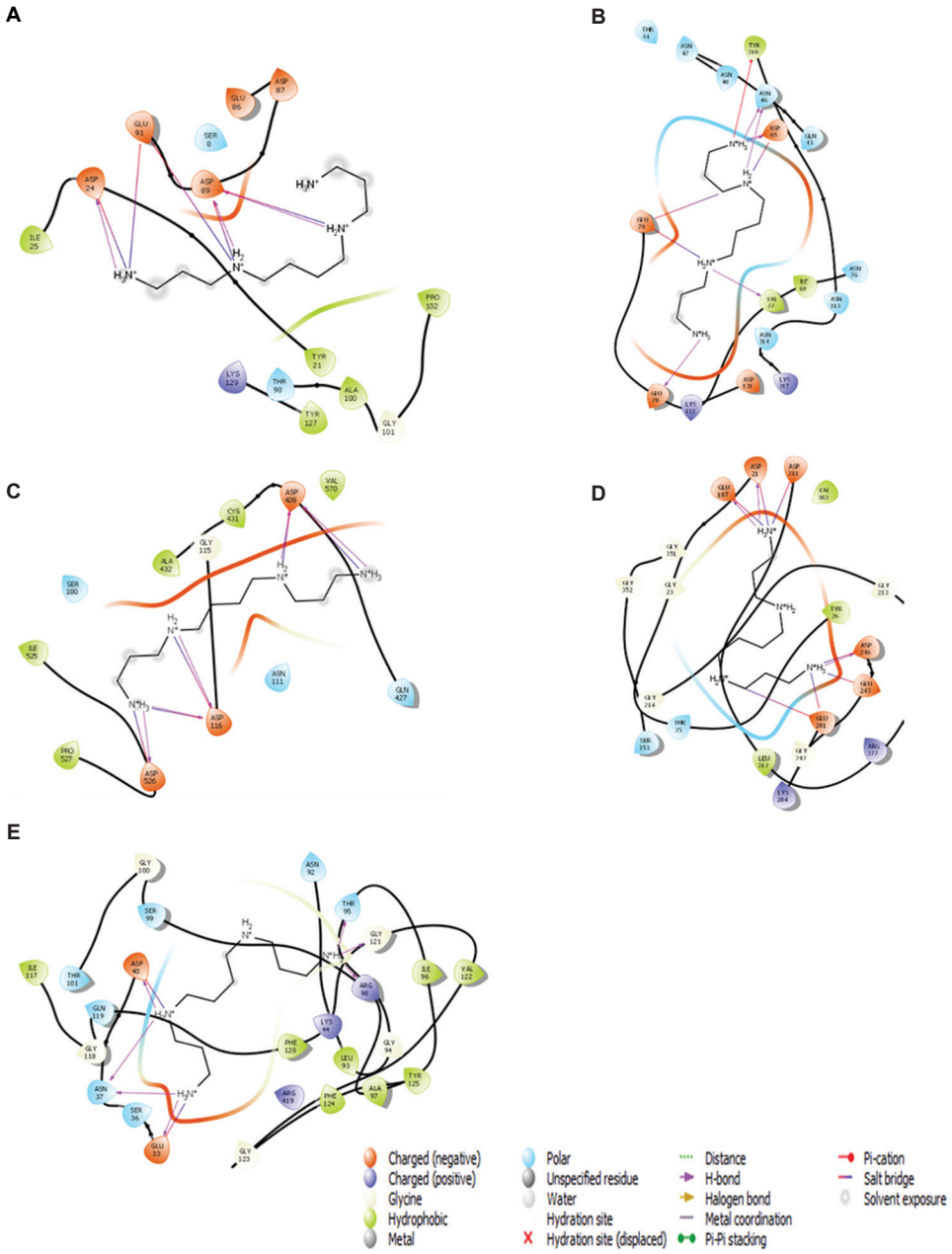

Figure 5. Ligand interaction diagram of (A) HSP20, (B) HSP40, (C) HSP60, (D) HSP70, and (E) HSP90 bound to Spn.

longer periods. From the RMSD provided in Figure 7A, we can see that a conformation change in the protein structure results in the ligand leaving the protein's active site. However, for PfHsp70 (Figure 7B), the ligand Put does have the potential to be a ligand that can bind to the protein for the entire 200 ns timeframe as we see the highest deviation that the ligand has from its starting structure is about 6.0 Å, which takes place around 100 – 120 ns. With that said 6.0 Å is not exactly a small deviation from the active site so this might be a weak binding ligand should it possess the ability to bind to the active site. As was the case for PfHsp60, changes in the conformation of PfHsp70 are what bring about the changes found in the ligand, when the protein RMSD goes up then so too does the ligand RMSD and vice versa.

Spd and Spn were only observed to stay bound to PfHsp70 for longer compared to the other Hsps tested. For PfHsp70-Spd (Figure 7C), the ligand does appear to be bound to the active site of the protein for the duration of the MD simulation with the largest difference for the ligand

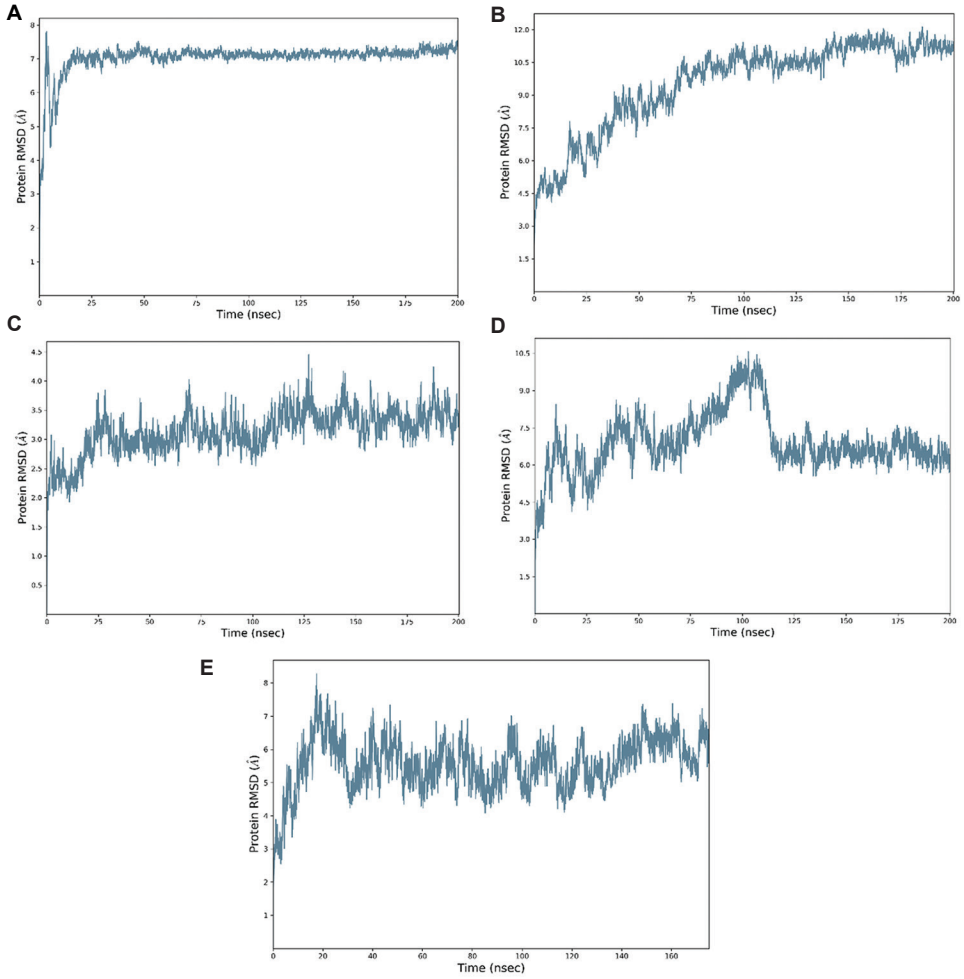

Figure 6. Root mean square deviation of alpha carbon backbone for free (A) PfHsp20sp, (B) PfHsp40, (C) PfHsp60, (D) PfHsp70, and (E) PfHsp90 during 200 ns molecular dynamics simulation.

Table 2. Amino acid residue interactions obtained from the ligand interaction diagrams

Ligand	HSP20		HSP40		HSP60		HSP70		HSP90	
	H-bond	S-bridge	H-bond	S-bridge	H-bond	S-bridge	H-bond	S-bridge	H-bond	S-bridge
Putrescine	Ile23 Asp89 Glu91	Asp89 Glu91	Glu11 His31 Pro130 Lys134	Glu11	Gly115 Asp116 Asp428	Asp116 Asp428	Asp21 Glu187 Asp211 Asp218	Asp21 Glu187 Asp211 Asp218	Glu33 Asn37 Asp40 Ile117	Glu33 Asp40
Spermidine	Asp24 Glu86 Asp89 Glu91	Asp24 Asp89 Glu91	Asn46 Asp65 Glu79	Asp65 Glu79	Asp116 Asp526	Asp116 Asp526	Asp21 Glu187 Asp211 Asp218 Asp379	Asp21 Glu187 Asp211 Asp218	Asn37 Asp40 Asn92 Thr95 Arg98 Ser99	Asp40
Spermine	Asp24 Asp89	Asp24 Asp89 Glu91	Asn46 Asp65 Val77 Glu78	Asp65 Glu79	Asp116 Asp428 Asp526	Asp116 Asp428 Asp526	Asp21 Glu187 Asp246	Asp21 Glu187 Asp211 Glu243 Asp246 Glu281	Glu33 Asn37 Asp40 Thr95 Arg98 Gly121	Glu33 Asp40

being 5.5 Å from its starting structure. When compared to the PfHsp70-Put complex (difference of 6 Å), it does seem to indicate that Spd is a better binder when compared to Put. The PfHsp70-Spn (Figure 7D) seems to show weak binding as the ligand fluctuations appear to reach up to 7.5 Å in this case.

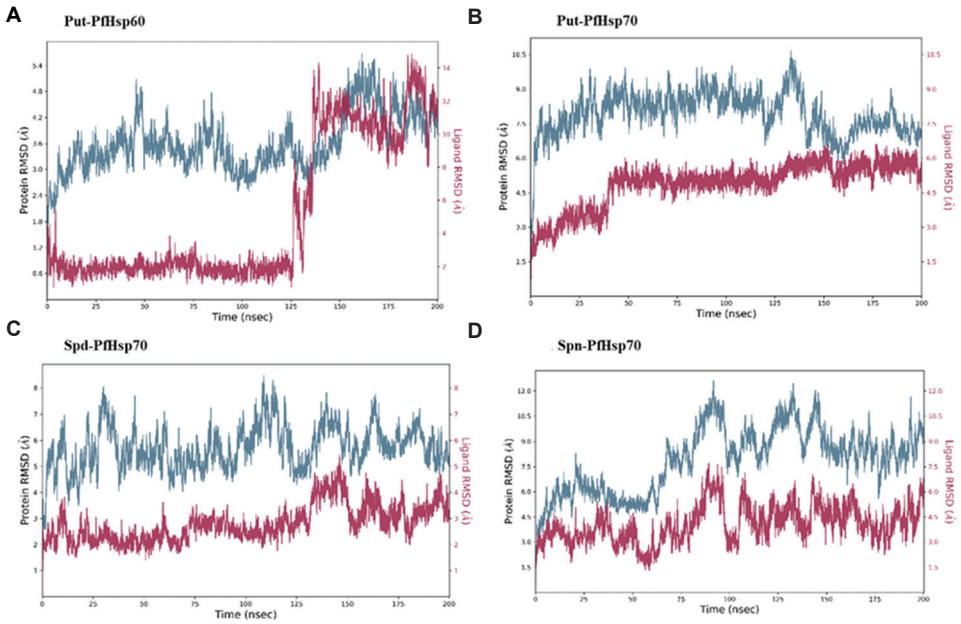

Figure 7. Root mean square deviation of the alpha carbon backbone and ligand fluctuations for (A) Put-PfHsp60, (B) Put-PfHsp70, (C) Spd-PfHSP70, and (D) Sp-PfHSP70 during 200 ns MD simulation.

4. Conclusions

Malaria is a major cause of death in many parts of the world, especially in Sub-Saharan Africa. The current treatment available in the market is not effective, due to the ever-changing parasite genome which then becomes resistant to the current drugs available in the market. Therefore, urgent alternative treatment for malaria is required[26,27]. This study focused on three important polyamines namely: Putrescine, spermidine, and spermine to establish the interaction with selected heat shock proteins. The interesting part we observed from this study was that all the focused polyamines were able to interact with selected heat shock proteins. However, the interesting part shown by the MD was that the bigger the molecular chaperones the longer they interact with some polyamines. This interaction that we observed between polyamines and heat shock proteins is a start toward the development of an alternative treatment for malaria. We will make follow-up studies based on the information; we got from this present study.

The emanation and spread of *Plasmodium* parasites that are resistant to antimalarial therapy is one of the main problems in the treatment of malaria. This is a result of the *Plasmodium* parasite's ongoing evolution and the creation of novel strategies for surviving drug toxicity. Studies of antimalarial drug development have been focused on polyamine biosynthesis by targeting precursors such as ornithine decarboxylase, adenosylmethionine decarboxylase, and spermidine synthase and protein-protein interactions between *Plasmodium falciparum* chaperones spotting out Hsp90, Hsp70, and Hsp40 as potential targets with little attention being paid to the interaction between polyamines and molecular chaperones. Therefore, to study these interactions, the binding sites of all 3D structures were identified using SiteMap, and docking was performed using the Schrödinger software with OPLS4 force field and XP.1.

Acknowledgments

The authors wish to acknowledge the University of Fort Hare, the National Research Foundation for student support, and the University of Cape Town for supporting Dr. S. Makumire. We would also like to acknowledge the Centre For High-Performance Computing, Rosebank, Cape Town for providing the computational resources used during this work.

Funding

This research was funded by the University of Fort Hare SEED grants (C415) and the SAMRC-Self-Initiated Research grants (PA19).

Conflict of interest

The authors declare no conflicts of interest. The funders had no role in the design of the study; in the collection, analyses, or interpretation of data; in the writing of the manuscript, or in the decision to publish the results.

Author contributions

Conceptualization: Xolani H. Makhoba
Investigation: Godlo Sesethu
Methodology: Maxam Nombalentle, Mthembu Yamkela, Mpumza Anelisa
Writing – original draft: Stanley Makumire, Krishna K. Govender, Xolani H. Makhoba
Writing – review and editing: Noxolo Mkwetshana

Ethics approval and consent to participate

Not applicable.

Consent for publication

Not applicable.

Availability of data

Not applicable.

References

1. WHO, 2020, World Malaria Report 2020: 20 Years of Global Progress and Challenges. Geneva: World Health Organization, p299.
2. Varo R, Chaccour C, Bassat Q, 2020, Update on malaria. *Med Clín* (*Barc*), 155: 395–402.
   https://doi.org/10.1016/j.medcli.2020.05.010
3. Tse EG, Korsik M, Todd MH, 2019, The past, present and future of anti-malarial medicines. *Malar J*, 18: 93.
   https://doi.org/10.1186/s12936-019-2724-z
4. Antony HA, Parija SC, 2016, Antimalarial drug resistance: An overview. *Trop Parasitol*, 6: 30–41.
   https://doi.org/10.4103/2229-5070.175081
5. Mbengue A, Bhattacharjee S, Pandharkar T, *et al*., 2015, A molecular mechanism of artemisinin resistance in *Plasmodium falciparum* malaria. *Nature*, 520: 683–687.
   https://doi.org/10.1038/nature14412
6. Belete TM, 2020, Recent progress in the development of new antimalarial drugs with novel targets. *Drug Des Devel Ther*, 14: 3875–3889.
   https://doi.org/10.2147/DDDT.S265602
7. Hart RJ, Ghaffar A, Abdalal S, *et al*., 2016, *Plasmodium* AdoMetDC/ODC bifunctional enzyme is essential for male sexual stage development and mosquito transmission. *Biol Open*, 5: 1022–1029.
   https://doi.org/10.1242/bio.016352
8. Müller IB, Gupta RD, Lüersen K, *et al*., 2008, Assessing the polyamine metabolism of *Plasmodium falciparum* as chemotherapeutic target. *Mol Biochem Parasitol*, 160: 1–7.
   https://doi.org/10.1016/j.molbiopara.2008.03.008
9. Pavithra SR, Kumar R, Tatu U, 2007, Systems analysis of chaperone networks in the malarial parasite *Plasmodium falciparum*. *PLoS Comput Biol*, 3: 1701–1715.
   https://doi.org/10.1371/journal.pcbi.0030168
10. Jee H, 2016, Size dependent classification of heat shock proteins: A mini-review. *J Exerc Rehabil*, 12: 255–259.
    https://doi.org/10.12965/jer.1632642.321
11. Miller DJ, Fort PE, 2018, Heat shock proteins regulatory role in neurodevelopment. *Front Neurosci*, 12: 821.
    https://doi.org/10.3389/fnins.2018.00821
12. Ganea E, 2001, Chaperone-like activity of alpha-crystallin and other small heat shock proteins. *Curr Protein Pept Sci*, 2: 205–225.
    https://doi.org/10.2174/1389203013381107
13. Wynn RM, Davie JR, Cox RP, *et al*., 1994, Molecular chaperones: Heat-shock proteins, foldases, and matchmakers. *J Lab Clin Med*, 124: 31–36.
14. Hall TA, 1999, BioEdit: A user-friendly biological sequence alignment editor and analysis program for Windows 95/98/NT. *Nucleic Acids Symp Ser*, 41: 95–98.
15. Kelley LA, Mezulis S, Yates CM, *et al*., 2015, The Phyre2 web portal for protein modeling, prediction and analysis. *Nat Protoc*, 10: 845–858.
    https://doi.org/10.1038/nprot.2015.053
16. Laskowski RA, Jabłońska J, Pravda L, *et al*., 2018, PDBsum: Structural summaries of PDB entries. *Protein Sci*, 27: 129–134.
    https://doi.org/10.1002/pro.3289
17. Maestro S, 2020, Schrödinger Release 2020-3: Maestro. New York, USA: Schrödinger, LLC.
18. Halgren T, 2007, New method for fast and accurate binding-site identification and analysis. *Chem Biol Drug Des*, 69: 146–148.
    https://doi.org/10.1111/j.1747-0285.2007.00483.x
19. Halgren TA, 2009, Identifying and characterizing binding sites and assessing druggability. *J Chem Inf Model*, 49: 377–389.
    https://doi.org/10.1021/ci800324m
20. Berthold MR, Cebron N, Dill F, *et al*., 2009, KNIME-the Konstanz information miner: Version 2.0 and beyond. AcM SIGKDD Explor Newslett, 11: 26–31.
    https://doi.org/10.1145/1656274.1656280
21. LigPrep S, 2019, Schrödinger Release 2019-4. New York, USA: Schrödinger LLC.
22. Wass MN, Kelley LA, Sternberg MJ, 2010, 3DLigandSite: Predicting ligand-binding sites using similar structures.

Nucleic Acids Res, 38: W469–W473.

https://doi.org/10.1093/nar/gkq406

23. Duhovny D, Nussinov R, Wolfson HJ, 2002, Efficient unbound docking of rigid molecules. In: Algorithms in Bioinformatics: Second International Workshop, WABI 2002 Rome, Italy, September 17–21, 2002 Proceedings. Springer Berlin Heidelberg, p185–200.
24. Bergdorf M, Robinson-Mosher A, Guo X, *et al*., 2021, Desmond/GPU Performance as of April 2021. DE Shaw Research, Technical Report DESRES/TR-2021-01.
25. Aier I, Varadwaj PK, Raj U, 2016, Structural insights into conformational stability of both wild-type and mutant EZH2 receptor. *Sci Rep*, 6: 34984.

https://doi.org/10.1038/srep34984

26. Makhoba XH, 2021, A double line of defense: Heat shock proteins and polyamines act as contributing factors to drug resistance of some *Plasmodium* parasites. In: *Plasmodium* Species and Drug Resistance. London: Intechopen.
27. Makhoba XH, Viegas C Jr., Mosa RA, *et al*., 2020, Potential impact of the multi-target drug approach in the treatment of some complex diseases. *Drug Des Dev Ther*, 14: 3235–3249.

https://doi.org/10.2147/DDDT.S257494

ACCSCIENCE PUBLISHING

INNOSC Theranostics and Pharmacological Sciences

ORIGINAL RESEARCH ARTICLE

Network pharmacology-based findings of the immunomodulatory activity of phytocompounds from *Withania somnifera* and *Aloe barbadensis*

Funmilayo I. D. Afolayan*, Deborah G. Joseph, and Ridwan A. Salaam

Department of Zoology, University of Ibadan, Nigeria

Abstract

Immunomodulation constitutes a crucial part of individual organisms' defense systems. Moreover, the utilization of plant-based natural products as herbal medicine for immunomodulation has garnered significant interest. Herein, we examined the immunomodulatory potentials of active phytocompounds extracted from *Withania somnifera* and *Aloe barbadensis* by employing ADMET screening, network pharmacology, and molecular docking techniques. This study follows the paradigm in drug discovery, which has shifted from a "one-target, one-drug" mode to a "network-target, multiple-component-therapeutics" mode. Phyto compounds sourced from *W. somnifera* and *A. barbadensis* were mined from online databases, including Dr. Duke's Phytochemical Ethnobotanical Database. After screening these active compounds, their potential targets were predicted through *in silico* ADMET property prediction models. Network pharmacology was utilized to establish a "compound-protein/gene-disease" network and reveal the regulatory mechanism of small molecules in a high-throughput manner through STRING, Cytohubba plugin in Cytoscape, and the g: Profiler software. A molecular docking simulation was performed to examine the binding affinity between the selected hub targets and bioactives. The findings showed that phytocompounds derived from the *W. somnifera* and *A. barbadensis* exhibit immunomodulatory effects by inhibiting specific protein targets, notably AKT1, HCK, JAK2, PDPK1, KIT, and IL2. Molecular docking analysis further revealed the potential of withanolide G, somniferine, and somniferanolide as promising immunomodulatory compounds against HCK, JAK2, and PDPK1 proteins, which are involved in multiple myeloma pathways, encompassing the PI3K-Akt signaling pathway, NOD-like receptor signaling pathway, and Toll-like receptor signaling pathway. In conclusion, these compounds are recommended for further *in vivo* and *in vitro* investigations to ascertain their potential as treatments for multiple myeloma.

Keywords: Immunomodulation; *Withania somnifera*; *Aloe barbadensis*; Phytocompounds; Multiple myeloma; Network pharmacology

***Corresponding author:**
Funmilayo I. D. Afolayan
(fidifede@gmail.com)

Citation: Afolayan FID, Joseph DG, Salaam RA, 2024, Network pharmacology-based findings of the immunomodulatory activity of phytocompounds from *Withania somnifera* and *Aloe barbadensis*. *INNOSC Theranostics and Pharmacological Sciences*, 7(1): 1076. https://doi.org/10.36922/itps.1076

Received: June 13, 2023

Accepted: August 16, 2023

Published Online: September 14, 2023

1. Introduction

The human body is protected by various non-specific defense mechanisms against infections and intruders, notably pathogens. On breaching the mucosal surface barrier,

these pathogens encounter two further lines of defense: The innate and acquired immune responses. This robust host defense is adequate to safeguard us against immune-related illnesses and pathogenic invaders, facilitated by the efficient interplay between innate and acquired immunity[1]. In addition, there are alternative avenues for modulating immune responses, including naturally occurring or synthesized compounds capable of modifying these pathways[2].

Natural compounds are a common foundation for the development of therapeutic treatments. In the last four decades, around a quarter of all approved medications (excluding biologicals) were derived from natural sources, and another quarter was found in the environment, often by exploiting the pharmacophore of these molecules[3]. Among these, plant-derived immunomodulators are a fascinating subject of study, offering a multitude of potential avenues[4]. For this study, our focus rests on *Withania somnifera* and *Aloe barbadensis* as the pivotal therapeutic plant candidates for *in silico* analysis.

W. somnifera (also known as Ashwagandha) is a biologically active plant that boasts an extensive spectrum of medicinal compounds, including steroidal lactones (withanolides), sitoindosides, and numerous other beneficial steroidal alkaloids, that have been used for ages to treat a variety of ailments[5]. On the other hand, *A. barbadensis* Miller is a perennial, xerophytic, succulent, and shrubby or arborescent plant in the Asphodelaceae (Liliaceae) family with a pea-green tint. It is primarily found in arid regions across Africa, Asia, Europe, and North America[6]. Both *W. somnifera* and *A. barbadensis* have found use as aphrodisiacs, analgesics, liver tonics, diuretics, hypocholesterolemic agents, anxiolytics, antidepressants, immunomodulatory substances, and anti-inflammatory agents[5,7].

Multiple myeloma, a hematopoietic malignancy, constitutes approximately 10% of all hematologic malignancies. Until the 2000s, limited success and advancements were observed, and achieving protracted survival was unlikely. This malignancy follows a multistep process, originating as a clonal plasma cell cancer[8]. The premalignant stage, termed monoclonal gammopathy of unknown significance, often serves as the initial indicator, heralding the onset of multiple myeloma. This is succeeded by asymptomatic smoldering multiple myeloma and eventually active multiple myeloma[9]. The immune system progressively weakens as the disease evolves. To enhance treatment outcomes, immunomodulatory drugs (IMiDs), proteasome inhibitors (PI), and monoclonal antibodies have been introduced, ushering in an era of improved therapeutic experiences, with immunomodulation exhibiting some level of anti-multiple myeloma efficacy[10].

Computational (*in silico*) approaches are commonly used in drug development. The notable advantage of employing *in silico* approaches lies in their ability to rapidly predict outcomes for a vast array of phytochemicals offering high-throughput predictions. In addition, they are able to predict therapeutically relevant molecules based on chemical structures even before their physical synthesis. As a result, *in silico* approaches find early application in the drug development process, particularly for compounds intended for synthesis. This proves especially important when there lacks an existing drug molecule with curative effects against a human disease. Incorporating computational approaches at the outset also helps reduce the risk of false positives, which could otherwise result in a high attrition rate during the later phases of drug development[11].

One of the key aspects of computational studies is network pharmacology. Through the integration of bioinformatics, cheminformatics, and network biology, network pharmacology has emerged as a dominating approach for elucidating the complicated pharmaceutical mechanism of action associated with the bioactive constituents found within diverse herbs and their pairings[12]. Network pharmacology operates as an efficient tool to construct a "compound-protein/gene-disease" network, shedding light on the regulatory principles orchestrated by small molecules in a high-throughput manner[13]. Moreover, network pharmacology delves into the impact of plant bioactive constituents on both the organism's interactome and the diseasome levels[14].

In this study, a pharmacology network was used to deduce the potential curative benefits and pharmacology activities of the active phytocompounds sourced from two herbal plants, *W. somnifera* and *A. barbadensis*. *In silico* docking was also utilized to analyze their binding affinities at the diseasome level, with a specific focus on multiple myeloma.

2. Materials and methods

The network pharmacology approach was implemented, adhering to a sequence of essential procedural stages. All information relating to bioactives, their targets, immune gene targets, immune system pathways (I-PW), protein-protein interactions (PPi), gene targets relevant to multiple myeloma, the interplay between bioactives and immune targets for multiple myeloma and I-PW-associated interacting proteins (IA-IP) was derived from different knowledge bases (databases). The focal health condition under investigation throughout this study was multiple myeloma.

2.1. Chemical composition of each herbal plant

An exhaustive literature search was conducted for each herbal remedy, aiming to capture all available information regarding their constituents. The compound composition of these plants was further extracted from Dr. Duke's Phytochemical Database (https://phytochem.nal.usda.gov/) and the Indian Medicinal Plants, Phytochemistry, and Therapeutics (IMPPAT) (https://cb.imsc.res.in/imppat/)[15]. Structure files of molecules, provided in mol format, were retrieved from PubChem[16] and ChEMBL[17], including their canonical SMILES.

2.2. Screening of potential active phytocompounds

The attributes of absorption, distribution, metabolism, and excretion (ADME) were recognized as pivotal indicators of herb or potential medication potency. To unveil the possible bioactive components within each of the two herbal plants, three ADME-related models were used, including the evaluation of oral bioavailability (OB) and drug-likeness (DL). The technique also includes the identification and inclusion of the main components present within the plants[17]. OB refers to the percentage of an orally administered dose of a medication that enters the systemic circulation unaltered. High OB is frequently indicative of bioactive compounds possessing drug-like properties suitable for medicinal applications[18]. DL is a qualitative concept employed in drug design to gauge the "drug-likeness" of a prospective product. This assessment aids in the optimization of pharmacokinetic and medicinal characteristics, including solubility and chemical stability. Typically, variables such as OB ≤30 – 33% and/or DL ≤0.1 are widely adopted criteria[19].

The ADMET profiles of all potential substances were estimated using SwissADME and AdmetSar 2.0. In addition, the DL score was estimated based on "Lipinski's Rule of Five" parameters (molecular weight, Log P, hydrogen bond donors, and hydrogen bond acceptors) using the Molinspiration online web server[20,21].

2.3. Targets of the bioactives

Target genes/proteins in humans that interact with active phytochemical substances from two herbal plants were investigated using the Similarity Ensemble Approach (SEA)[22], SwissTargetPrediction[23], and PharmMapper[24].

Data for each protein, including its standard protein name, gene ID and organism (set to *Homo sapiens*), were derived from UniProt[25] ("UniProt: a hub for protein information," 2014) using the UniProt ID provided in BindingDB.

2.4. Related targets in the immune system and the involved pathways

Related targets in the immune system were searched using the innate immune database[25]. Subsequently, the STRING database and the pathway database were utilized to determine the different pathways associated with the immune system. The I-PW were then evaluated and analyzed.

Moreover, the STRING database was used to identify the interacting partners of these bioactive targets searched in the KEGG pathway to find IA-IP.

2.5. Targets of multiple myeloma and control drugs

The multiple myeloma-associated human genes/proteins were obtained from two different databases: GeneCards[26] and DisGeNET[27]. The search query employed the specific term "multiple myeloma," with the search parameters confined to the species "*Homo sapiens*." The targets of control IMiDs (Lenalidomide and Thalidomide) were also retrieved from GeneCards and Disgenet, subsequently overlapping with the targets of the identified bioactives.

2.6. PPi

The overlap of related gene targets of the bioactives and the immune system was regarded as the bioactives' immune targets at the interactome level. Similarly, the overlap of related gene targets of the bioactives' immune targets and multiple myeloma was regarded as bioactive-multiple myeloma's immune gene targets at the diseasome level. These interactions were obtained using Venny 2.0[28]. Subsequently, the STRING database was employed to identify the possible inter-protein interactions[29]. This database compiles both established and predicted PPi. STRING uses five sources to uncover relationships within the database: genomic context predictions, high-throughput lab trials, co-expression, automated text mining, and existing database information. Several variables for STRING-based PPi identification can be used to ensure the reliability of the generated data. These variables include interactions derived exclusively from high-throughput laboratory experiments, a minimum required interaction score of 0.7 (a high confidence score according to STRING), and the highest score of interactors.

2.7. Network construction

A network is a diagrammatic representation that depicts the interactions between numerous components known as nodes. These nodes are interconnected by edges, which are lines that connect them. In this study, the nodes encompass the herbal plants under investigation, the bioactives within these herbal plants, the bioactives' targets, and the

I-PWs associated with these targets. Furthermore, the nodes include the connection between bioactive-multiple myeloma's immune targets.

The bioactive-immune target (compound-target [C-T]) (interactome level) and the bioactive-multiple myeloma's immune gene target (diseasome level) networks were constructed by linking the active compounds and their corresponding targets, and the active compounds, their immune targets and their corresponding multiple myeloma targets, respectively. In addition, the bioactive-multiple myeloma's immune targets-pathway (compound-target-pathway [C-T-P]) network was built by linking the bioactive-multiple myeloma's immune targets with relevant signaling pathways.

These networks were constructed and visualized using Cytoscape 3.2.1, an open-source Java-based software platform designed for visualizing complex networks and integrating them with diverse attribute data[30]. Furthermore, the Cytoscape network analyzer tool facilitated network analysis.

In these networks, nodes represent active phytochemical compounds derived from the herbal plant, targets, or signaling pathways, while edges signify the interactions between the nodes[31]. The degree of a node corresponds to the number of connections it maintains to other nodes within the network[32].

2.8. Functional enrichment analysis (gene ontology [GO]) at the interactome and diseasome levels

The functional enrichment analysis of the bioactives' immune targets (interactome level) and also the analysis of the bioactive-multiple myeloma's immune gene targets (diseasome level) was conducted using two tools: These tools are robust online server-based platforms specialized in functional STRING and g: Profiler profiling of gene or protein sets. To identify the immune pathways and other interacting pathways involving the bioactives, the KEGG database was employed. The GO process involves the identification of biological processes, molecular functions, and cellular compartments associated with these gene sets. It also provided estimations of the degree of enrichment of these gene sets in each of the three different categories[33]. This comprehensive analysis aimed to identify the plants' target-immune pathways, as well as their relevant interacting pathways on the interactome level and also on the diseasome level (which concerns multiple myeloma)[34].

2.9. Molecular docking simulation

The molecular docking simulation of the hub genes (core genes) and their corresponding bioactive components was performed using PyRx software[35], an application that allows for interactively visualizing and analyzing molecular structures and data. To begin, we downloaded the 3D structures of chemicals and proteins from Pubchem and the Protein Data Bank (PDB)[31], respectively. Subsequently, using the Discovery Studio[36] and the Dock Prep plugin (in the Chimera program), the structures of proteins and bioactives were prepared for the docking process. This encompassed replacing missing side chains, as well as adding hydrogens and charges, all integral to the preparation process. Furthermore, the molecular docking was carried out utilizing the PyRx software and the AutoDock Vina plugin[37]. Finally, the Discovery Studio and Ligplot+ were used to visually present 3D and docking models[38].

3. Results

3.1. Chemical composition of each herbal plant

After eliminating duplicates, a total of 67 compounds were identified in *W. somnifera*, and a total of 159 compounds were identified in *A. barbadensis*, resulting in a combined count of 226 compounds.

3.2. Screening of potential active compounds/ingredients

All 226 compounds underwent ADMET and drug-likeness screenings. Among these, 19 bioactives were sourced from *A. barbadensis*, and 18 bioactives were sourced from *W. somnifera*. These bioactives include the major constituents of each plant, even though some did not meet the inclusion criteria. Consequently, 36 compounds were selected as phytocompounds for further analysis (Table 1).

3.3. Targets of the bioactives

Active phytocompounds in *A. barbadensis* bioactives predicted a total of 590 targets, while *W. somnifera* bioactives indicated 684 targets. Using Swiss Target Prediction and Pharmmapper, a total of 820 targets emerged after all duplicates were removed.

3.4. Related targets in the immune system and the involved pathways

A total of 1378 immune genes were identified from the innate immune database. An overlap between these immune gene targets and the bioactives' targets produced a total of 169 bioactive immune targets.

3.5. Targets of multiple myeloma and control drugs

From GeneCards, 3,045 multiple myeloma gene targets were retrieved, and Disgenet contributed a further 1740, culminating in 1088 gene targets associated with multiple myeloma after eliminating duplicates.

Table 1. The values for the chemical descriptors used in the prediction of potential active compound

Compounds	Mol. form.	Mol. weight	nHBA	nHBD	OB	DL	Toxicity
Aloesin*	$C_{19}H_{22}O_9$	394.37	9	5	0.55	0.33	III
Aloesol*	$C_{13}H_{14}O_4$	234.25	4	2	0.55	0.26	III
Aloin*	$C_{21}H_{22}O_9$	418.39	3	9	0.55	0.52	III
Rhein*	$C_{15}H_8O_6$	284.22	6	3	0.55	0.46	II
Steroids*	$C_{22}H_{32}O_3$	344.49	3	0	0.55	1.23	III
Thiamin*	$C_{12}H_{17}N_4OS$	265.35	3	2	0.55	0.87	III
Xylose*	$C_5H_{10}O_5$	150.13	5	4	0.55	0.29	IV
Homonataloin*	$C_{22}H_{24}O_9$	432.42	9	6	0.55	0.35	III
Beta sitosterol*	$C_{29}H_{50}O$	414.71	1	1	0.55	0.78	I
Stigmasterol*	$C_{29}H_{48}O$	412.69	1	1	0.55	0.62	I
10-Hydroxyaloin*	$C_{21}H_{22}O_{10}$	434.39	10	8	0.55	0.86	IV
Casanthranol*	$C_{21}H_{22}O_{10}$	434.39	10	7	0.55	0.61	III
Kampferol*	$C_{15}H_{10}O_6$	286.24	6	4	0.55	0.5	II
7-hydroxyaloin*	$C_{21}H_{22}O_{10}$	434.39	10	8	0.55	0.36	IV
Folic acid*	$C_{19}H_{19}N_7O_6$	441.4	9	6	0.55	1.09	III
Epicatechin*	$C_{15}H_{14}O_6$	290.27	6	5	0.55	0.64	IV
(-)-Desoxyaloin*	$C_{21}H_{22}O_8$	402.39	8	6	0.55	0.47	
L pyroglutamic acid*	$C_5H_7NO_3$	129.11	3	2	0.55	0.3	III
Niacinamide*	$C_6H_6N_2O$	122.12	2	1	0.55	0.37	IV
24-methyldesmosterol**	$C_{28}H_{46}O$	398.66	1	1	0.55	0.76	II
27-deoxywithaferin A**	$C_{28}H_{38}O_5$	454.6	5	1	0.55	0.29	IV
2,3-didehydrosomnifericin**	$C_{28}H_{40}O_7$	488.61	7	4	0.55	0.52	III
Delta-7-alvenasterol**	$C_{29}H_{48}O$	412.69	1	1	0.55	0.25	III
Guggleserone**	$C_{21}H_{28}O_2$	312.45	2	0	0.55	0.72	III
Hydrocortisone**	$C_{21}H_{30}O_5$	362.46	5	3	0.55	1.67	III
Sominone**	$C_{28}H_{42}O_5$	458.63	5	3	0.55	0.39	III
Somniferanolide**	$C_{28}H_{36}O_6$	468.58	6	2	0.55	0.19	I
Somniwithanolide**	$C_{28}H_{38}O_6$	470.6	6	3	0.55	0.5	III
Withaferin A**	$C_{28}H_{38}O_6$	470.6	6	2	0.55	0.37	I
Withanolide G**	$C_{28}H_{38}O_5$	454.6	5	2	0.55	0.5	IV
Withanolide Q**	$C_{28}H_{38}O_6$	470.6	6	3	0.55	0.75	III
Quercetin**	$C_{15}H_{10}O_7$	302.24	7	5	0.55	0.52	II
Somniferine**	$C_{36}H_{36}N_2O_7$	608.68	9	2	0.55	1.09	III
Somnifericin**	$C_{28}H_{42}O_7$	490.63	7	4	0.55	0.54	III
Dihydrowithaferin A**	$C_{28}H_{40}O_6$	472.61	6	2	0.55	0.42	I
Chlorogenic acid**	$C_{16}H_{18}O_9$	354.31	9	6	0.55	0.79	III

Notes: *refers to phytocompounds in *Aloe barbadensis*, while **refers to phytocompounds in *Withania somnifera*. Toxicity class I to VI ranges from fatal if swallowed to non-toxic.

Abbreviations: Mol. Form: Molecular formula; Mol. weight: Molecular weight; nHBA: Number of hydrogen bond acceptors; nHBD: Number of hydrogen bond donors; OB: Oral bioavailability; DL: Drug likeness.

The sum of targets for the control IMiDs, Thalidomide (20 targets retrieved) and Lenalidomide (28 targets retrieved), totaled 48. This set of targets overlapped with the bioactives' immune targets, resulting in a total of 90 bioactive-multiple myeloma immune gene targets.

3.6. Network-based evaluation of the immunomodulatory mechanisms of active phytocompounds

To comprehend the "multi-components, multi-target, and multi-pathway" immunomodulatory mechanisms of *W. somnifera* and *A. barbadensis*, a compound-target network was constructed. This network linked active phytochemical compounds to their corresponding immune targets, which were subsequently analyzed. The compound-target network for these two herbal plants comprised 205 nodes and 1338 edges, encompassing 36 active compounds and 169 targets. Among the active phytochemical compounds, their categorization was based on degrees of connectivity. Notably, withanolide Q (degree = 70), 2,3-didehydrosomnifericin (degree = 69), steroids (degree = 65), hydrocortisone (degree = 63), 27-deoxywithaferin A (degree = 62), withaferin A (degree = 61), somniferine (degree = 59), withanolide G (degree = 58), somniferanolide (degree = 55), Ssominone (degree = 53), chlorogenic acid (degree = 47), somniwithanolide (degree = 47), rhein (degree = 43), gugglesterone (degree = 39), and somnifericin (degree = 39) displayed the highest number of connections with the immune-related targets. This pattern indicated their potential role as primary active compounds responsible for the immunomodulatory activity of *W. somnifera* and *A. barbadensis*. Furthermore, more than 70 targets demonstrated interactions with two or more active phytochemical compounds, demonstrating the multi-compound, multitarget pharmacological properties of these herbal plants.

The STRING database also identified the PPi, forming a network comprising 169 nodes and 1,553 edges, with a PPi enrichment *P*-value of <1.0e-16 (Figure 1). This value indicates that the interactions among these proteins exceed what would be expected in a randomly selected group of proteins with equivalent size and degree distribution from the genome. This enrichment signifies that these proteins are interconnected beyond chance, indicating a cohesive physiological relationship among them. On delving into the disease-gene association, several immune-associated diseases were identified: autoimmune lymphoproliferative syndrome, myeloid neoplasm, combined immunodeficiency, autoimmune disease of the musculoskeletal system, primary immunodeficiency disease, autoimmune disease, immune system disease, and hematopoietic system disease. A subset of these targets also displayed connections to various immune pathways (Table 2), thereby shedding light on the pathways through which the bioactives exert their immunomodulatory effects.

3.7. Network-based analysis of active phytocompounds' immunomodulatory potential in multiple myeloma

To delve into the network-based analysis of the systems-level immunomodulatory properties of the phytocompounds present within the herbal plants, a C-T network was constructed (Figure 2). This network comprised 99 nodes and 447 edges, achieved through associating active compounds with their corresponding multiple myeloma-gene targets. The nodes included 37 active compounds, 2 control drugs, and 60 bioactive-multiple myeloma immune gene targets. Targets not involved in KEGG immune pathways were excluded.

Within this network, 10 active phytochemical compounds, including withanolide Q (degree = 25), hydrocortisone (degree = 24), somniferine (degree = 22), 2,3-didehrdrosomnifericin (degree = 22), 27-deoxywithaferin A (degree = 21), steroids (degree = 20), withaferin A (degree = 19), withanolide G (degree = 17), somniferanolide (degree = 17), and lenalidomide (degree = 16), had the most linkages with multiple myeloma-related targets (Figure 2), thereby implying their pivotal roles as key phytocompounds responsible for the herbal plants' immunomodulatory efficacy against multiple myeloma. Furthermore, 40 targets displayed two or more interactions with the active phytocompounds (Figure 2), demonstrating herbal medicines' multi-compound, multi-target pharmacology.

In the context of the bioactive-multiple myeloma's immune (C-T) network, the hub node target genes were identified. Nodes possessing a degree larger than or equal to twice the network's average node degree were classified as hubs. Core nodes, in particular, have been demonstrated to play an essential role in a wide variety of biological processes[39]. Among the multiple myeloma-associated targets of the bioactives, several stand out as core gene targets with potential roles in the immunomodulatory potential of active phytocompounds in herbal plants (Figure 3). Specifically, these include alpha serine/threonine protein kinase 1 (AKT1) (degree = 29), HCK proto-oncogene (HCK) (degree = 27), 3-phosphoinositide-dependent protein kinase 1 (PDPK1) (degree = 26), Janus kinase 2 (JAK2) (degree = 26), proto-oncogene c-KIT (KIT) (degree = 24), matrix metallopeptidase 9 (MMP9) (degree = 23), growth factor receptor bound protein 2 (GRB2) (degree = 22), interleukin 2 (IL2) (degree = 21), Bruton tyrosine kinase (BTK) (degree = 19), and mouse double minute 2 homolog (MDM2) (degree = 19).

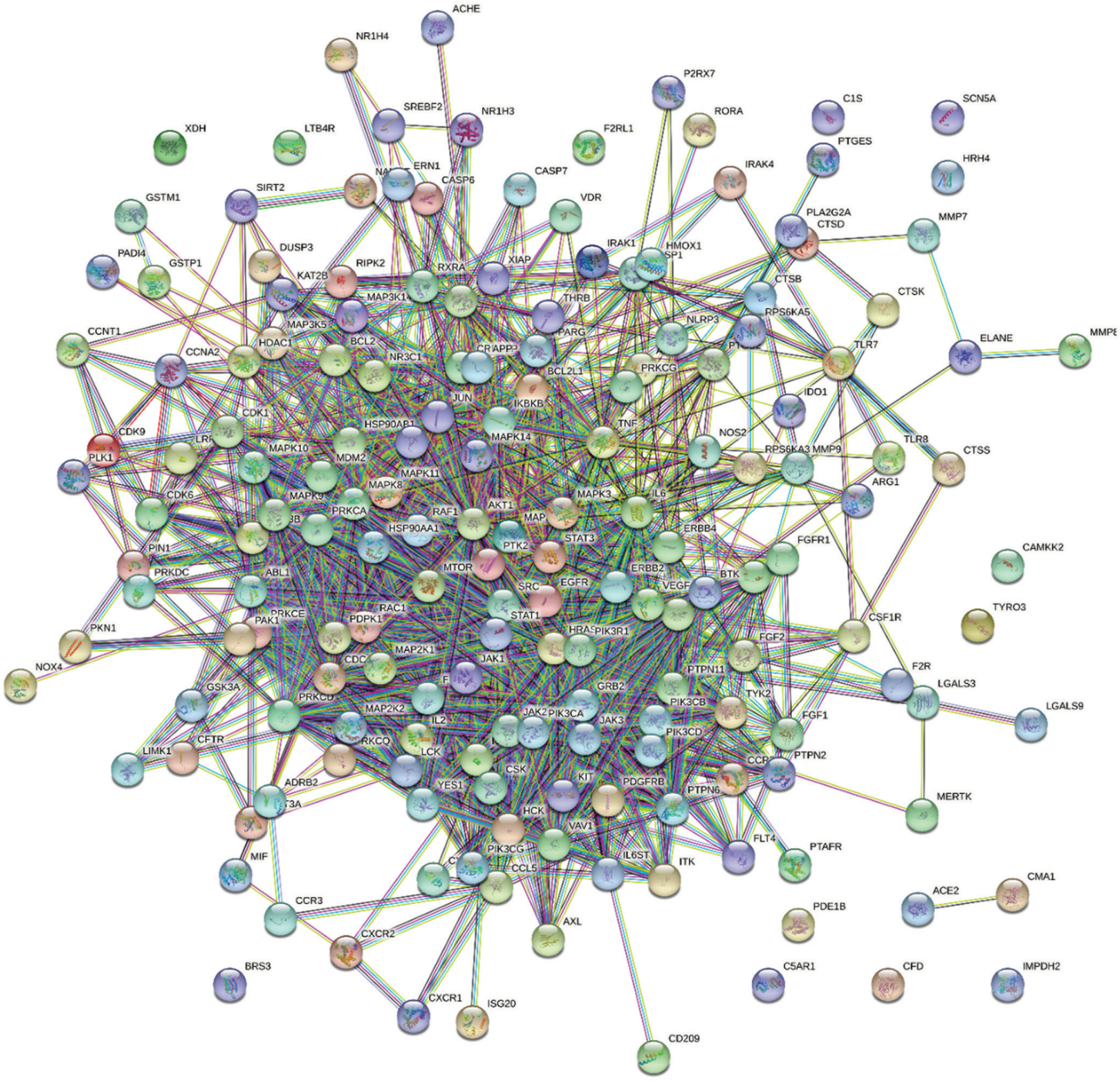

Figure 1. Diagrammatic representation of the protein-protein interaction (with a confidence score of 0.7 and above) between the different bioactives' immune targets. Round globes indicate each bioactive immune target; the lines show their interactions with one another; round globes without lines indicate a confidence interaction score lower than 0.

Furthermore, a PPi interaction was also carried out on the multiple myeloma-related targets of the bioactives, leading to the identification of hub targets. This network comprised 65 nodes and 554 edges, demonstrating a PPi enrichment *P*-value of <1.0e-16. Among these hub targets, key players emerged, including mitogen-activated protein kinase 3 (MAPK3), signal transducer and activator of transcription 3 (STAT3), alpha serine-threonine protein kinase 1 (AKT1), Harvey rat sarcoma virus (HRAS), heat-shock protein 90-alpha (HSP90AA1), growth factor receptor bound Protein 2 (GRB2), phosphatidylinositol 3-kinase regulatory subunit alpha (PIK3R1), interleukin 2 (IL2), and interleukin 6 (IL6).

3.8. Functional enrichment analysis of the active phytocompounds immune targets

GO enrichment analysis was used to investigate the functional roles of the immunomodulatory-associated

Table 2. Depicting all of the bioactives' immune gene targets as well as the immune pathways in which they are involved

KEGG ID	IMMUNE PATHWAY	GENE (NO)	GENE INVOLVED FROM THE LIST
hsa04622	RIG-I-like receptor signaling pathway	23	NFKBIA, NFKB1, MAPK14, TRAF2, RIPK1, IFNA1, CASP10, CXCL10, TRIM25, CASP8, ATG5, CHUK, IFNA2, IFNB1, MAPK8, RELA, CYLD, MAPK9, TNF, IKBKB, TRAF6, TRAF3, IKBKG
hsa04666	Fc gamma R-mediated phagocytosis	20	MAPK1, PIK3R2, RAF1, MAPK3, PIK3CA, FCGR2A, PIK3CB, ARPC5, MAP2K1, SPHK1, GAB2, FCGR3A, SYK, PIK3CD, INPP5D, PRKCA, PTPRC, PIK3R1, HCK, AKT1
hsa04670	Leukocyte transendothelial migration	18	PIK3R2, MAPK14, PIK3CA, ICAM1, PIK3CB, PTPN11, PTK2, CTNNB1, ACTB, MMP9, PIK3CD, CXCL12, ITGB1, PTK2B, ITGB2, CXCR4, PRKCA, PIK3R1
hsa04611	Platelet activation	16	MAPK1, PIK3R2, MAPK14, MAPK3, PIK3CA, FCGR2A, PIK3CB, ACTB, PIK3CG, SYK, PIK3CD, ITGB1, PIK3R1, AKT1, ITGB3, BTK
hsa04640	Hematopoietic cell lineage	14	CD22, EPOR, KITLG, IL4, IL1A, IL1B, CSF1R, KIT, CD14, CD1D, IL6, TNF, CD19, ITGB3
hsa04658	Th1 and Th2 cell differentiation	27	MAPK1, IL2RB, NFKBIA, NFKB1, IL2, IFNG, MAPK14, IL4, MAPK3, NOTCH1, STAT5B, IL13, FOS, STAT5A, JAK1, STAT1, CD247, CHUK, JUN, IL2RG, JAK2, MAPK8, RUNX3, RELA, MAPK9, IKBKB, IKBKG
hsa04664	Fc epsilon RI signaling pathway	27	MAPK1, PIK3R2, MAPK14, IL4, RAF1, KRAS, MAPK3, PIK3CA, PIK3CB, MAP2K1, IL13, PDPK1, GAB2, NRAS, SYK, PIK3CD, GRB2, MAPK8, MAP2K7, MAPK9, TNF, INPP5D, HRAS, PRKCA, PIK3R1, AKT1, BTK
hsa04650	Natural killer cell mediated cytotoxicity	33	MAPK1, PIK3R2, IFNG, KLRK1, TNFSF10, RAF1, KRAS, MAPK3, PIK3CA, ICAM1, IFNAR1, IFNA1, PIK3CB, MAP2K1, PTPN11, CD247, FCGR3A, NRAS, NCR2, SYK, PIK3CD, IFNA2, IFNB1, GRB2, PTK2B, ITGB2, PTPN6, TNF, HLAB, HRAS, PRKCA, MICA, PIK3R1
hsa04062	Chemokine signaling pathway	39	MAPK1, NFKBIA, PIK3R2, CCL2, NFKB1, CCR7, RAF1, KRAS, MAPK3, PIK3CA, STAT3, PIK3CB, CCR2, STAT5B, MAP2K1, CXCL10, CXCL11, CCR4, PTK2, GPR29, PIK3CG, STAT1, NRAS, CHUK, CXCR3, PIK3CD, JAK2, GRB2, CXCL12, PTK2B, RELA, CXCR4, HRAS, PIK3R1, IKBKB, HCK, AKT1, CCL5, IKBKG
hsa04662	B cell receptor signaling pathway	30	CD22, MAPK1, NFKBIA, PIK3R2, NFKB1, RAF1, KRAS, MAPK3, PIK3CA, PIK3CB, MAP2K1, FOS, MALT1, NRAS, CHUK, BCL10, JUN, SYK, PIK3CD, GRB2, RELA, PTPN6, INPP5D, HRAS, PIK3R1, IKBKB, CD19, AKT1, BTK, IKBKG
hsa04657	IL-17 signaling pathway	34	MAPK1, NFKBIA, CCL2, NFKB1, IFNG, MAPK14, IL4, TRAF2, MAPK3, IL1B, HSP90B1, IL13, CXCL10, FOS, MAPK7, HSP90AA1, IL17A, CASP8, PTGS2, S100A9, CHUK, JUN, MMP9, LCN2, MAPK8, RELA, IL6, MAPK9, TNF, IKBKB, TRAF6, TRAF3, TNFAIP3, IKBKG
hsa04659	Th17 cell differentiation	38	MAPK1, IL2RB, NFKBIA, TGFB1, NFKB1, IL2, IFNG, MAPK14, IL4, AHR, MAPK3, IL1B, IL21, STAT3, STAT5B, FOS, SMAD3, HSP90AA1, STAT5A, JAK1, IL17A, STAT1, MTOR, CD247, CHUK, JUN, IL2RG, IRF4, IL6ST, JAK2, MAPK8, RELA, IL6, MAPK9, IKBKB, HIF1A, IL22, IKBKG
hsa04620	Toll-like receptor signaling pathway	47	MAPK1, NFKBIA, PIK3R2, NFKB1, MAPK14, RIPK1, MAPK3, MAP3K8, IL1B, PIK3CA, CD80, IFNAR1, CTSK, IFNA1, PIK3CB, TLR3, MAP2K1, CD14, CXCL10, FOS, CXCL11, CD86, CASP8, STAT1, IRAK1, CHUK, JUN, CD40, TLR4, PIK3CD, IFNA2, IFNB1, SPP1, MAPK8, MAP2K7, RELA, IL6, MAPK9, TNF, MYD88, PIK3R1, IKBKB, TRAF6, AKT1, TRAF3, CCL5, IKBKG
hsa04660	T cell receptor signaling pathway	43	MAPK1, NFKBIA, PIK3R2, NFKB1, IL2, IFNG, MAPK14, IL4, RAF1, KRAS, MAPK3, MAP3K8, PIK3CA, PIK3CB, MAP2K1, CTLA4, FOS, MALT1, CD28, PDCD1, PDPK1, CD247, NRAS, CHUK, BCL10, JUN, PIK3CD, GRB2, MAPK8, MAP2K7, RELA, PTPN6, MAPK9, TNF, HRAS, PTPRC, IL10, NCK1, PIK3R1, IKBKB, AKT1, MAP3K14, IKBKG
hsa04625	C-type lectin receptor signaling pathway	42	BCL3, MAPK1, NFKBIA, PIK3R2, NFKB1, IL2, MAPK14, IRF1, RAF1, KRAS, MDM2, MAPK3, IL1B, PIK3CA, PIK3CB, MALT1, NLRP3, PTPN11, CASP8, STAT1, MAPKAPK2, PTGS2, NRAS, NFKB2, CHUK, BCL10, JUN, SYK, PIK3CD, MAPK8, RELA, IL6, CYLD, MAPK9, TNF, HRAS, IL10, PIK3R1, IKBKB, AKT1, MAP3K14, IKBKG
hsa04621	NOD-like receptor signaling pathway	46	MAPK1, NFKBIA, MEFV, NAMPT, CCL2, NFKB1, MAPK14, TRAF2, RIPK1, MAPK3, IL1B, BIRC3, YWHAE, IFNAR1, IFNA1, IL18, BCL2L1, P2RX7, HSP90AA1, NLRP3, TRPV2, JAK1, CASP8, STAT1, ATG5, CHUK, XIAP, JUN, TLR4, TXN, IFNA2, IFNB1, MAPK8, BCL2, RELA, IL6, MAPK9, TNF, MYD88, IKBKB, TRAF6, TRAF3, CCL5, BIRC2, TNFAIP3, IKBKG
hsa04623	Cytosolic DNA-sensing pathway	16	NFKBIA, NFKB1, RIPK1, IL1B, IFNA1, IL18, CXCL10, ADAR, CHUK, IFNA2, IFNB1, RELA, IL6, IKBKB, CCL5, IKKG
hsa04672	Intestinal immune network for IgA production	14	TGFB1, IL2, AICDA, IL4, CD80, IL15, CD28, CD86, CD40, CXCL12, IL6, CXCR4, IL6, MAP3K14

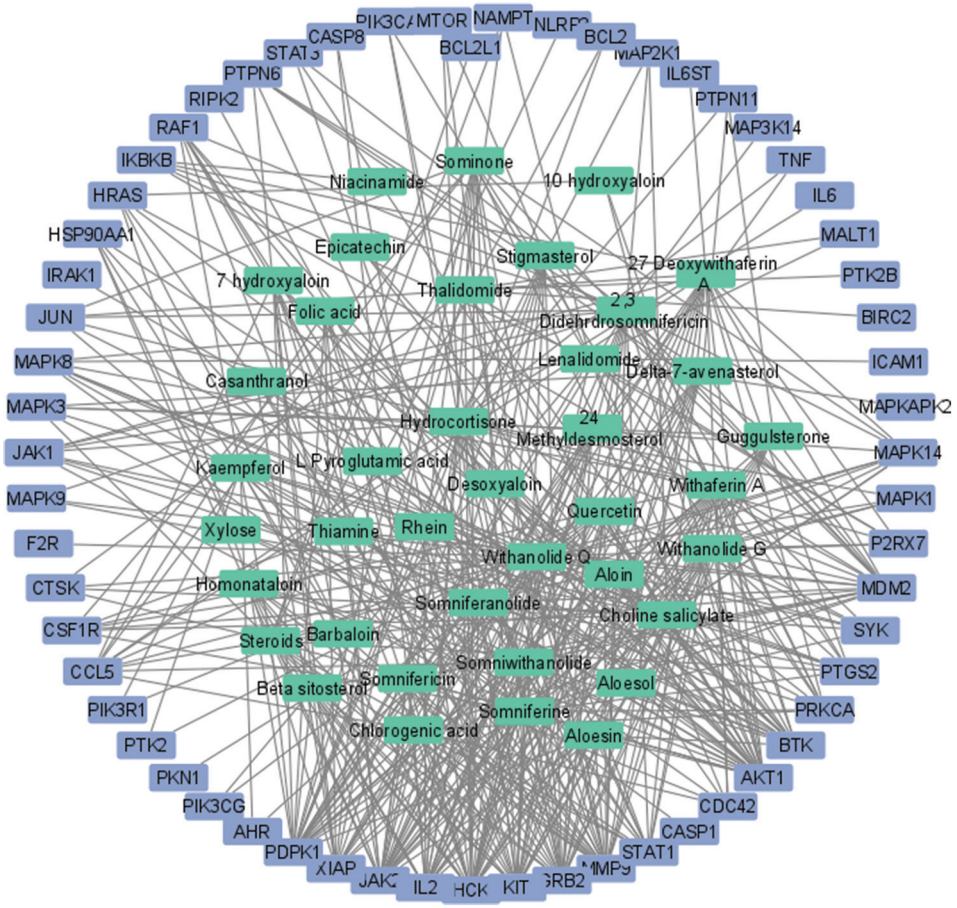

Figure 2. A diagrammatic representation of the Compound-Target Network of the bioactives and the multiple myeloma-associated gene targets. Turquoise boxes indicate the bioactives/compounds; cobalt blue boxes indicate the bioactive-multiple myeloma gene targets; black lines indicate the interactions between the two components.

targets within active phytocompounds in the context of multiple myeloma.

The targets in GO terms associated with the regulation of diverse biological processes (GO: BP) were significantly enriched. These processes include cellular response to chemical stimulus, response to organic substance, cell differentiation, cell proliferation, cell migration, immune response, regulation of programmed cell death, regulation of immune system process, and more.

Similar enrichments were evident with the targets in GO terms associated with molecular functions (GO: MF). These functions include protein kinase activity, phosphotransferase activity, alcohol group as acceptor, catalytic activity acting on a protein, enzyme binding and more.

The significant enrichment of the targets in GO terms associated with their cellular compartments (GO: CC) was also observed. The distribution spanned compartments such as the cytosol, cell periphery, cytoplasm, cytoplasmic vesicle, intracellular vesicle, and beyond.

The immune system is known to be closely controlled by the precise coordination of many important signaling pathways. Deviations in the regulation of immune-related pathways can result in a variety of immunological disorders. To delve further, KEGG pathway enrichment analysis was employed (Figure 4). This pathway-level analysis of the active phytocompounds immune-related targets revealed connections with at least 17 immune pathways and other relevant pathways (Figure 3). These encompass, among others, the PI3-AKT pathway, VEGFA pathway, JAK-STAT signaling pathway, and mTOR signaling pathway.

3.9. Hub gene targets and molecular docking simulation

The top 10 hub genes from the top 40 compound-target networks between the bioactives and the bioactive-multiple myeloma gene targets were identified using

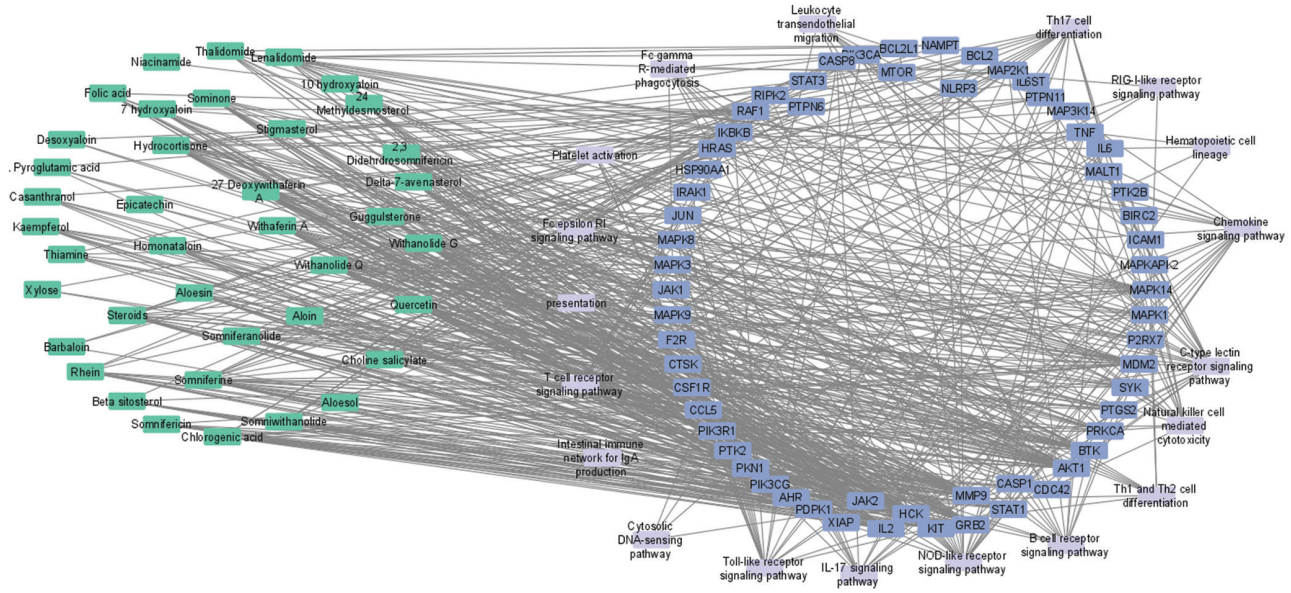

Figure 3. A diagrammatic representation of the Compound-Target-Immune Pathway Network between the bioactives and the bioactive-multiple myeloma immune-associated gene targets. Turquoise boxes indicate the bioactives; cobalt blue boxes indicate the bioactive-multiple myeloma immune-associated gene targets; lilac boxes indicate the immune pathways these gene targets are associated with; the lines represent their interaction.

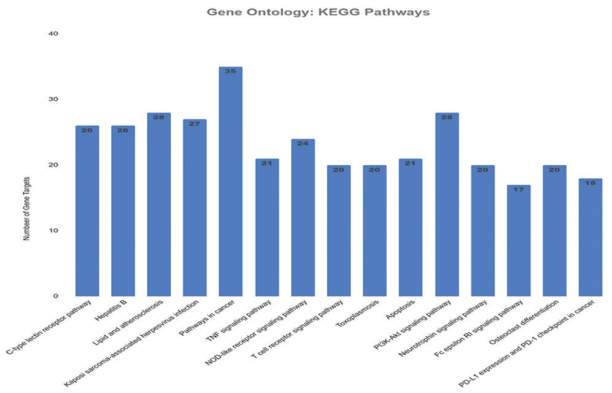

Figure 4. The number of active phytocompounds' gene targets involved in the top 15 signaling pathways, including immune and other important pathways.

Cytohubba. Subsequently, molecular docking simulations were performed using corresponding immunomodulatory bioactives selected from the top 21 bioactives. These bioactives encompassed AKT1, JAK2, HCK, PDPK1, MMP9, KIT, GRB2, IL2, MDM2, BTK, MAPK3, STAT3, HRAS, and HSP90AA1, which were included in the targets designated for docking. The selected bioactives included withanolide Q, hydrocortisone, somniferine, 2,3-didehrdrosomnifericin, 27-deoxywithaferin A, steroids, withaferin A, withanolide G, somniferanolide, somniwithanolide, sominone, quercetin, chlorogenic acid, rhein, homonataloin, 7-hydroxyaloin, delta-7-avenasterol, folic acid, somnifericin, gugglesterone, and stigmasterol. The interaction relationships between the aforementioned hub genes and their corresponding bioactives were analyzed. Simultaneously, lenalidomide and thalidomide were selected as the positive control drugs.

Docking scores were obtained after the binding of phytoconstituents to specific multiple myeloma targets. Lower docking scores indicated higher and stronger binding affinity of components to their respective target. Molecular docking is a technique for predicting energetically advantageous ligand binding conformations within a target protein's active region[40]. This binding was accompanied by the generation of hydrogen bonds, as well as hydrophobic interactions such as Pi-Pi and Pi-cation interactions. These interactions collectively indicated the stability of complexes generated subsequent to ligand binding with the target protein[40]. A total of 21 phytoconstituents of *W. somnifera* and *A. barbadensis* were screened against various targets of multiple myeloma.

The individual docking scores (binding affinity energy) of the selected phytoconstituents are presented in Table 3. Furthermore, detailed insights into the receptor-ligand interactions in both three-dimensional (3D) and two-dimensional (2D) are showcased in Figures 5-7. From these analyses, the top three complexes were selected based on the interactions between the ligand-protein, binding affinity and the ADMET profiles of the compounds. The 2D diagrams present the binding process, highlighting the formation of hydrogen bonds and hydrophobic

Table 3. Illustrating the Target Binding Affinity of the hub targets and some of the highly connected active phytocompounds from the network analysis

Phytochemical	AKT1	HCK	PDPK1	JAK2	KIT	MMP9	GRB2	IL2	BTK	MDM2	MAPK3	STAT3	HRAS
Withanolide Q	−12.4	−9.6	−10.5	−9.8	−8.7	−8.5	−8	−7.6	−9.8**	−8.4	−9.1	−8.3	−9.2
Hydrocortisone	−10	−8.5	−7.8	−8	−8.8	−8	−6.5	−6.3	−8.6	−7.3	−7.8	−7.9	−7.4
2,3−didehrdrosomnifericin	−12.1	−9.4	−9.5	−7.9	−9.2	−8.5	−8	−7	−9.1	−7.6	−9.2	−8.2	−8.8
Somniferine	−8.9	−10.1*	−8.2	−8.4	−9.4	−10*	−8.6*	−7.8	−8	−8.3	−9.3	−9.3	−9.5
Withaferin A	−12.3	−9.3	−9.9	−9.3	−9.5	−9	−8	−7.5	−8.9	−8.2	−8	−8	−9.9*
Withanolide G	12.5*	−9.7	10.7*	10.3	10	−9.1	−8.6*	−7.9*	−9.2	−8.7*	−8.3	−8.3	−8.8
27−deoxywithaferin A	−12.1	−10	−9.9	−10.4	−10.5*	−9.2	−8.4	−7.5	−9.7	−8.1	−9.1	−9.1	−8.9
Somniferanolide	−13.1**	−9.7	−9.6	−10.6*	−10.1		−8.2	−7	−9.2	−8.7	−9.3	−9.3*	−9.9*
Somniwithanolide	−11.3	−8.9	−9.3	−7.1	−8.2	−8.2	−7.2	−6.3	−8.4	−7.1	−8.5	−8.5	−9
Chlorogenic acid	−9.3	−8.3	−8.5	−9.2	−7.9	−7.4	−7	−5.8	−7.6	−7.4	−8.7	−7.8	−8.6
Delta7avenasterol	−11.7	−8.8	−9.6	−9.6	−8.9	−8.5	−7.4	6.5	−8.7	−7.4	−8.9	−7.3	−8.5
Quercetin	−9.8	−9.1	−9.1	−8.8	−9.5	−9.7	−6.7	−6.6	−8.6	−7.1	−8.6	−8.2	−8.3
Rhein	−10.5	9.1	−9.9	−9.3	−9.1	−8.5	−7.1	−6.5	−9.1	−7.4	−9.1	−9.1	−7.7
7−hydroxyaloin	−8.9	−9.3	−8.4	−7.8	−7.8	−8.4	−6.9	−6.2	−8.1	−6.7	−8.1	−8	−7.8
Guggulsterone	−11.3	−8.8	−9.7	−7.3	−9	−8.4	−7.3	−6.8	−9.2	−8.3	−8.2	−8.9	−7.6
Homonataloin	−8.5	−8.4	−7.5	−8.2	−8.6	−8.3	−7	−6.4	−7.7	−7	−7.6	−8.1	−7.2
Somnifericin	−11.2	−9.5	−9.6	−10	−9.1	−8.4	−7.5	−7	−9	−8.4	−8.1	−9	−8.7
Folic acid	−10	−8.9	−9.5	−9.2	8.5	−8.6	−7.3	−6.8	−9.3*	−7.9	−10.1*	−8.7	−9.4
Stigmasterol	−11.4	−9	−9.7	9.3	−9	−8.1	−7.6	−6.5	−8.8	−8	−8	−8	−8.6
Controls													
Lenalidomide	−9.3	−8.9	−7.4	−8.4	−7.7	−7.7	−6.6	−5.7	−7.8	−6.6	−8.1	−7.9	−7.6
Thalidomide	−9.9	−8.8	−7.7	−8.6	−8	−9	−6.9	−6.2	−8.1	−6.9	−8.4	−7.4	−7.8

Notes: *Values with the highest binding affinity with regards to network pharmacology and mostly as a whole except the two instances. **Values with the highest binding affinity regardless of network pharmacology.

interactions between the amino acids of the receptors and the best-docked phytoconstituents.

The binding affinity energy table (Table 3) revealed that withanolide G, somniferine, and somniferanolide consistently emerged as the best-docked phytoconstituents across the majority of the multiple myeloma targets. This is indicative that the phytochemicals have the potential immunomodulatory capabilities in the context of multiple myeloma. With further validation, these compounds could prove to be useful lead compounds.

4. Discussion

This study harnessed the power of network pharmacology to investigate the immunomodulatory potential of *W. somnifera* and *A. barbadensis*. In the trajectory of multiple myeloma, patients experience progressive immunological dysfunction. As a result, several therapy options have emerged, aiming to navigate the immunosuppressive milieu of tumor microenvironments and stimulate the host's immune system, thereby eliciting an anticancer response[41]. While the intricate interplay among varied immunological components is not entirely understood, some advancements have brought us closer to a holistic view of the immune system and its role in host defense[42]. Capitalizing on their potent pharmacological attributes and minimal side effects, herbal medicines have become increasingly popular as therapeutic agents against various diseases[43]. Employing a network pharmacology approach, we investigated the functional roles of the gene targets of the bioactives. This exploration unraveled their immunomodulatory roles and the systems-level pharmacological processes that underpin the immunomodulatory effects of *W. somnifera* and *A. barbadensis* against multiple myeloma. This approach has previously been used in predicting potential lead compounds and understanding the mechanism of actions of different herbal plants in treating human diseases[31].

This study identified a selection of key gene targets, including AKT1, HRAS, HSP90AA1, GRB2, PIK3R1, and IL2. On delving into the interactome relationship

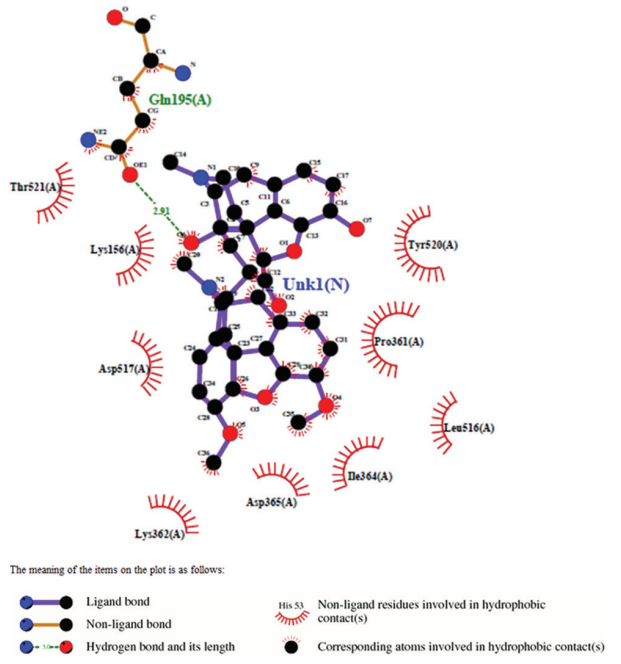

Figure 5. Ligplot+ analysis of the docked complex of the protein receptor HCK and somniferine. Protein residues involved include hydrophobic interactions represented as arcs and hydrogen bonding with dashed lines.

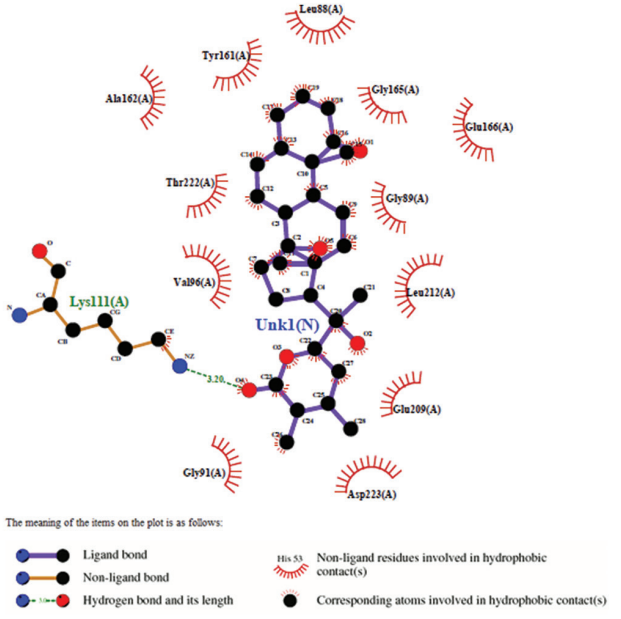

Figure 6. Ligplot+ analysis of the docked complex of the protein receptor PDPK1 and withanolide G. Protein residues involved include hydrophobic interactions represented as arcs and hydrogen bonding with dashed lines.

of the herbs' gene target, the majority of the gene targets exhibited interactions through the Toll-like receptor (TLR) signaling pathway. TLRs activate defense mechanisms that function autonomously from adaptive immunity. They

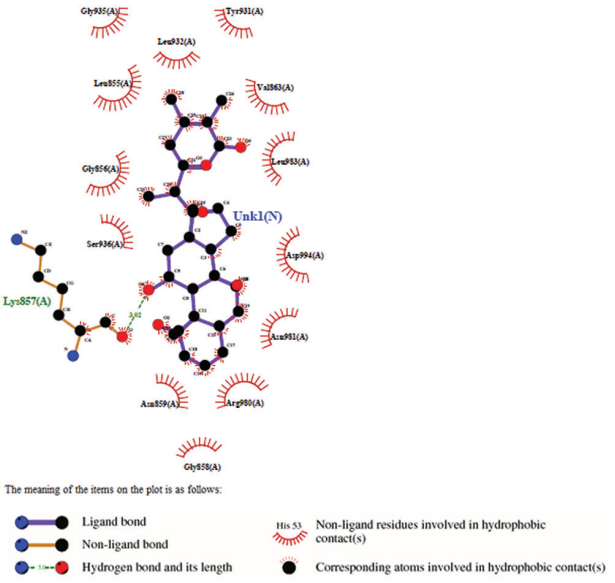

Figure 7. A ligplot+ analysis of the docked complex of the protein receptor JAK2 and somniferanolide. Protein residues involved include hydrophobic interactions represented as arcs and hydrogen bonding with dashed lines.

also play a significant part in the differentiation of naive T cells into effector T cells, a crucial step in adaptive immune responses. Transcription factors within the TLR signaling pathway (such as AP-1) regulate numerous genes, notably those encoding crucial proinflammatory cytokines like tumor necrosis factor-alpha (TNF-alpha), IL-1-beta, IL-6, IL-8, and IL-12. Certain TLRs also trigger interferon regulatory factors (IRFs) such as IRF3, IRF5, and IRF7, which subsequently bolster the production of type 1 (alpha and beta) interferons[44]. Another pathway through which most of the genes interact is the nucleotide-binding oligomerization domain (NOD) signaling pathway. Within this pathway, inflammasome-forming NOD-like receptors (NLRs) contribute to the conversion of procytokines into active IL-1 and IL-18, achieved by triggering caspase-1. TRAF is a group of cytoplasmic signaling adaptor proteins, responsible for packing, regulating and transducing IL1, TLRs, and IL17. These biological processes are vital for regulation of cell survival and immune cell function. These contribute significantly to regulating acute and chronic inflammation (Gissler *et al.*, 2022). Interleukins are involved in cell proliferation, migration, and also immune cell differentiation (Brocker *et al.*, 2010). Studies have shown that NF-κB are important in modulating the adaptive inflammatory response, such as enhanced expression of genes responsible for pro-inflammation. Contrarily, NOD-like receptors focus on regulating the host innate immune response by assembling mitogen-activated protein kinase (MAPK) and NF-κB (Franchi

et al., 2009). The release of inflammatory modulators is regulated by multiple signaling pathways, one of which is mitogen-activated protein kinase (MAPK) pathway. MAPK is responsible for multiple cellular processes, including cell survival, inflammation, stress response, and cell proliferation (Moens, Kostenko and Sveinbjørnsson, 2013).

Myeloid differentiation factor 88 (MyD88), TRIF, and other adaptor proteins bind to TLRs, inciting the activation of NF-κB and the consequent production of inflammatory cytokines[45]. This cascade triggers the expression of proinflammatory cytokines, chemokines, inducible enzymes such as cyclooxygenase (COX)-2 and inducible nitric oxide synthase (iNOS), growth factors, immune receptors, and adhesion molecules such as intercellular cell adhesion molecule 1 (ICAM-1) and vascular cell adhesion molecule 1 (VCAM-1) due to NF-κB activation[46]. The STAT protein family constitutes a potent force in immunoregulation. Several proteins, including JAK, GATA3 (a transcription factor that controls Th2 cytokine production), and RAR-related orphan receptor gamma (RORt-Th17 transcription factor), are involved in this process, as elucidated by O'Shea *et al.*[47]. Different STAT proteins also affect the levels of cytokines. Meanwhile, recent studies underscore the pivotal roles of STAT3 in tumor cell growth and proliferation, recommending it as a therapeutic target for inflammation-related diseases and tumor management[48].

The PI3K-Akt/mTOR pathway, which is targeted for anti-multiple myeloma treatment, has been identified as a hub. However, activating mutations in PI3K and AKT have not been detected in multiple myeloma patients[49]. At the same time, a small percentage of multiple myeloma patients experience a deficiency in the phosphatase and tensin homolog (PTEN)[50]. Despite this, the pathway plays a crucial role in the survival and proliferation of multiple myeloma cells. Elevated IL6 secretion by stromal cells, along with the elevated secretion of vascular endothelial growth factor (VEGF) and insulin-like growth factor (IGF) by multiple myeloma cells due to multiple myeloma interactions, contribute to the pathway's activation. These cytokines activate their corresponding binding sites on multiple myeloma cells, promoting tumorigenesis by upregulating signaling events such as the PI3K/AKT/mTOR, mitogen-activated protein kinase/extracellular signal-regulated kinase (MEK/ERK), and Janus kinase/signal transducer and activator of transcription (JAK/STAT) pathways. The complexity of the PI3K/AKT/mTOR pathway is amplified by the presence of multiple feedback loops and interactions with various other pathways. DEP domain-containing mTOR interacting protein (DEPTOR) has been identified as an effective inhibitor of both mTORC1 and mTORC2[51]. Increased expression of DEPTOR inhibited mTORC1, relieving the feedback inhibition of ribosomal protein S6 kinase. Consequently, this results in the activation of AKT and the survival of multiple myeloma cells.

Numerous pathways interact with the PI3K/AKT/mTOR pathway, in addition to the feedback loops within it. The PI3K/AKT/mTOR and RAS/RAF/MEK/ERK pathways exhibit the most intricate and well-documented interaction. Yu *et al.* further discovered that suppressing ERK using the MEK inhibitor U0126 enhances the binding of Grb2-associated binder-1 (Gab1) with PI3K, consequently activating the PI3K/AKT pathway[52]. A more recent study has demonstrated the successful treatment of metastatic and primary colorectal cancers by inhibiting the PI3K/mTOR pathways. This highlights the pathway's potential as a promising route for addressing these lethal cancers[53].

In addition to cell differentiation, proliferation, and survival, the MAPK pathway is an evolutionarily conserved cell regulatory signaling network. Inflammatory cytokines such as TNF-a, IL-6, and IGF1 activate this pathway, triggering subsequent kinase cascades, namely RAS, RAF, MEK, and MAPK, resulting in altered gene expression. The MAPK pathway harbors two main oncogenes, NRAS and KRAS, which are frequently aberrant in many malignancies. Notably, these genes are often affected in multiple myeloma, with a cumulative incidence of 20 – 35%[54]. RAS mutations are thought to be progressive events, as they are uncommon in the initial phases of multiple myeloma but become more common in later disease progression[55].

In terms of compounds, researchers have identified more than ten active phytochemical constituents. Withaferin A, for instance, has been shown to suppress TNF-induced NF-B activation in human myeloid leukemia KBM-5 cells[56]. In both *in vitro* and *in vivo* studies, sitosterol and kaempferol have also demonstrated hematological and immunomodulatory effects[57]. In a kidney cancer cell line, withaferin-A induced dose-dependent apoptotic cell death and PARP cleavage through the downregulation of the STAT-3 pathway[58].

GO enrichment analysis demonstrated that the targets of the active compounds in *W. somnifera* and *A. barbadensis* were involved in diverse immunomodulatory associated-molecular functions. Notably, the protein kinase activity is the most significantly enriched molecular function of the bioactive-multiple myeloma's immune gene target, which holds unique therapeutic potential in the treatment of multiple myeloma[59]. In the realm of multiple myeloma

medication development, the majority of anti-kinase research has centered on protein kinase targets, with a few significant exceptions. Manning *et al*. reported that the human genome encodes 518 distinct protein kinases, each facilitating the transfer of the gamma-phosphate group of ATP to the hydroxyl groups of proteins. These protein kinases are categorized into two types based on the phosphorylated amino acids. They are important components of biological signal transduction pathways that regulate cell proliferation, survival, and migration. While numerous tyrosine kinases (TKs) reside in the cytosolic domains of plasma membrane receptors, multi-capability serine/threonine kinases (S/TKs) can also be located in the plasma membrane; however, the majority is distributed throughout the cytosol and other cellular compartments. This observation aligns with the GO analysis of cellular compartments (CC), which highlights the cytosol as the most significantly enriched cellular compartment among the gene targets[60].

However, this study has a few limitations. First, it relies on the already identified chemical constituents from *W. somnifera* and *A. barbadensis*, potentially overlooking the immunomodulatory effect of unknown chemical constituents. In addition, although favorable binding affinities were observed between the hub targets and corresponding phytoconstituents during the molecular docking simulation, further studies are necessary to authenticate and validate these interactions.

5. Conclusion

The study's approach leverages network pharmacology and molecular docking techniques to uncover active phytocompounds and their potential mechanism of immunomodulation. Network pharmacology analysis revealed that HCK, PDPK1, and JAK2 are crucial immunomodulatory targets for multiple myeloma treatment. These effects are achieved through the inhibition of major signaling pathways that have been constitutively activated, aligning with previous research. Notably, the study highlights significant pathways, including the PI3K-Akt signaling pathway, NOD-like receptor signaling pathway, and TLR signaling pathways. The molecular docking analysis further supports these results, suggesting that with anolide G, Somniferine, and Somniferanolide from *W. somnifera* hold potential as IMiDs leads targeting PDPK1, HCK, and JAK2 hub proteins in multiple myeloma from the network pharmacology construction. These compounds exhibit promise in modulating key pathways in cancer, notably the PI3-AKT pathway, VEGFA pathway, JAK-STAT signaling pathway, and mTOR signaling pathway. Consequently, it is recommended that further *in vivo* and *in vitro* studies be conducted to assess the practical impacts of these lead compounds and their potential impact on immunomodulatory proteins against multiple myeloma.

Acknowledgments

None.

Funding

None.

Conflict of interest

The authors declare that they have no conflict of interest.

Author contributions

Conceptualization: Funmilayo I. D. Afolayan
Investigation: Deborah G. Joseph.
Writing – original draft: Joseph Deborah G.
Writing – review & editing: All authors

Ethics approval and consent to participate

Not applicable.

Consent for publication

Not applicable.

Availability of data

Supporting data can be obtained from the corresponding author following a formal request.

References

1. Yagi A, Yu BP, 2021, Immune modulation of *Aloe vera:* Acemannan and gut microbiota modulator. *J Gastroenterol Hepatol Res*, 4: 1707–1721.

2. Ayivi R, Ibrahim S, Colleran H, *et al*., 2021, COVID-19: Human immune response and the influence of food ingredients and active compounds. *Bioactive Compounds Health Dis*, 4: 100.

   https://doi.org/10.31989/bchd.v4i6.802

3. Newman DJ, Cragg GM, 2020, Natural products as sources of new drugs over the nearly four decades from 01/1981 to 09/2019. *J Nat Prod*, 83: 770–803.

   https://doi.org/10.1021/acs.jnatprod.9b01285

4. Tharakan A, Himanshu S, Irin RB, *et al*., 2021, Immunomodulatory effect of *Withania somnifera* (Ashwagandha) Extract--a randomized, double-blind, placebo controlled trial with an open label extension on healthy participants. *J Clin Med*, 10: 3644.

   https://doi.org/10.3390/jcm10163644

5. Afewerky HK, Ayodeji AE, Tiamiyu BB, *et al*., 2021, Critical

review of the *Withania somnifera* (L.) Dunal: Ethnobotany, pharmacological efficacy, and commercialization significance in Africa. *Bull Natl Res Cent*, 45: 176.

https://doi.org/10.1186/s42269-021-00635-6

6. Surjushe A, Vasani R, Saple DG, 2008, *Aloe vera*: A short review. *Indian J Dermatol*, 53: 163–166.

https://doi.org/10.4103/0019-5154.44785

7. Sánchez M, González-Burgos E, Iglesias I, *et al*., 2020, Pharmacological update properties of *Aloe vera* and its major active constituents. *Molecules*, 25: 1324.

https://doi.org/10.3390/molecules25061324

8. Rafei H, Haroun F, Tabbara IA, 2018, Novel immunotherapeutic agents for the treatment of multiple myeloma. *Am J Clin Oncol*, 42: 317–329.

https://doi.org/10.1097/COC.0000000000000506

9. Rajkumar SV, Landgren O, Mateos MV, 2015, Smoldering multiple myeloma. *Blood*, 125: 3069–3075.

https://doi.org/10.1182/blood-2014-09-568899

10. Guillerey C, Nakamura K, Vuckovic S, *et al*., 2016, Immune responses in multiple myeloma: Role of the natural immune surveillance and potential of immunotherapies. *Cell Mol Life Sci*, 73: 1569–1589.

https://doi.org/10.1007/s00018-016-2135-z

11. Leelananda SP, Lindert S, 2016, Computational methods in drug discovery. *Beilstein J Org Chem*, 12: 2694–2718.

https://doi.org/10.3762/bjoc.12.267

12. Huang C, 2014, Systems pharmacology in drug discovery and therapeutic insight for herbal medicines. *Brief Bioinform*, 15: 710–733.

https://doi.org/10.1093/bib/bbt035

13. Zhang R, Zhu X, Bai H, *et al*., 2019, Network pharmacology databases for traditional Chinese medicine: Review and assessment. *Front Pharmacol*, 10: 123.

https://doi.org/10.3389/fphar.2019.00123

14. Kibble M, Saarinen N, Tang J, *et al*., 2015, Network pharmacology applications to map the unexplored target space and therapeutic potential of natural products. *Nat Prod Rep*, 32: 1249–1266.

https://doi.org/10.1039/c5np00005j

15. Mohanraj K, Karthikeyan BS, Vivek-Ananth RP, *et al*., 2018, IMPPAT: A curated database of Indian medicinal plants, phytochemistry and therapeutics. *Sci Rep*, 8: 4329.

https://doi.org/10.1038/s41598-018-22631-z

16. Kim S, Chen J, Cheng T, *et al*., 2019, PubChem in 2021: New data content and improved web interfaces. *Nucleic Acids Res*, 49: D1388–D1395.

https://doi.org/10.1093/nar/gkaa971

17. Ru J, Li P, Wang J, *et al*., 2014, TCMSP: A database of systems pharmacology for drug discovery from herbal medicines. *J Cheminform*, 6: 13.

https://doi.org/10.1186/1758-2946-6-13

18. Aungst BJ, 2017, Optimizing oral bioavailability in drug discovery: An overview of design and testing strategies and formulation options. *J Pharm Sci*, 106: 921–929.

https://doi.org/10.1016/j.xphs.2016.12.002

19. Yue SJ, Xin LT, Fan YC, 2017, Herb pair Danggui-Honghua: Mechanisms underlying blood stasis syndrome by system pharmacology approach. *Sci Rep*, 7: 40318.

https://doi.org/10.1038/srep40318

20. Lipinski CA, Dominy BW, Feeney PJ, 2012, Experimental and computational approaches to estimate solubility and permeability in drug discovery and development settings. *Adv Drug Deliv Rev*, 64: 4–17.

https://doi.org/10.1016/j.addr.2012.09.019

21. Abdul-Hammed M, Adedotun IO, Falade VA, *et al*., 2021, Target-based drug discovery, ADMET profiling and bioactivity studies of antibiotics as potential inhibitors of SARS-CoV-2 main protease (M^{pro}). *Virusdisease*, 32: 642–656.

https://doi.org/10.1007/s13337-021-00717-z

22. Keiser MJ, Roth BL, Armbruster BN, *et al*., 2007, Relating protein pharmacology by ligand chemistry. *Nat Biotechnol*, 25: 197–206.

https://doi.org/10.1038/nbt1284

23. Daina A, Michielin O, Zoete V, 2019, SwissTargetPrediction: Updated data and new features for efficient prediction of protein targets of small molecules. *Nucleic Acids Res*, 47: W357–W364.

https://doi.org/10.1093/nar/gkz382

24. Wang X, Shen Y, Wang S, 2017, PharmMapper 2017 update: A web server for potential drug target identification with a comprehensive target pharmacophore database. *Nucleic Acids Res*, 45: W356–W360.

https://doi.org/10.1093/nar/gkx374

25. Gane PJ, Bateman A, Martin MJ, *et al*., 2014, UniProt: A hub for protein information. *Nucleic Acids Res*, 43: D204–D212.

https://doi.org/10.1093/nar/gku989.

26. Safran M, Dalah I, Alexander J, *et al*., 2018, GeneCards version 3: The human gene integrator. *Database* (*Oxford*), 2010: baq020.

https://doi.org/10.1093/database/baq020

27. Pinero J, Bravo A, Queralt-Rosinach N, *et al*., 2017, DisGeNET: A comprehensive platform integrating information on human disease-associated genes and variants. *Nucleic Acids Res*, 45: D833–D839.

https://doi.org/10.1093/nar/gkw943

28. Oliveros JC, 2007, VENNY. An Interactive Tool for Comparing Lists with Venn Diagrams. Available from: https://bioinfogp.cnb.csic.es/tools/venny/index.html [Last accessed on 2021 Jul 10].

29. Szklarczyk D, Franceschini A, Wyder S, *et al*., 2015, STRING v10: Protein-protein interaction networks, integrated over the tree of life. *Nucleic Acids Res*, 43: D447–D452.

https://doi.org/10.1093/nar/gku1003

30. Shannon P, Markiel A, Ozier O, *et al*., 2003, Cytoscape: A software environment for integrated models of biomolecular interaction networks. *Genome Res*, 13: 2498–2504.

https://doi.org/10.1101/gr.1239303

31. Afolayan FID, Tarkaa CT, 2023, Network pharmacology-based assessment of anti-inflammatory action of phytocompounds derived from *Nigella sativa* and *Moringa oleifera*. *Drug Discov*, 17: e13dd1016.

32. Barabasi AL, Oltvai ZN, 2004, Network biology: Understanding the cell's functional organization. *Nat Rev Genet*, 5: 101–113.

https://doi.org/10.1038/nrg1272

33. Reimand J, Kull M, Peterson H, *et al*., 2007, g: Profiler--a web-based toolset for functional profiling of gene lists from large-scale experiments. *Nucleic Acids Res*, 35: W193–W200.

https://doi.org/10.1093/nar/gkm226

34. Swamydas M, Murphy EV, Ignatz-Hoover JJ, *et al*., 2022, Deciphering mechanisms of immune escape to inform immunotherapeutic strategies in multiple myeloma. *J Hematol Oncol*, 15: 17.

https://doi.org/10.1186/s13045-022-01234-2

35. Dallakyan S, Olson AJ, 2015, Small-molecule library screening by docking with PyRx. *Methods Mol Biol*, 1263: 243–250.

https://doi.org/10.1007/978-1-4939-2269-7_19

36. BIOVIA, 2022, BIOVIA Workbook, Release 2020: BIOVIA Pipeline Pilot, Release 2022. San Diego: Dassault Systèmes.

37. Eberhardt J, Santos-Martins D, Tillack AF, *et al*., 2021, AutoDock vina 1.2.0: New docking methods, expanded force field, and python bindings. *J Chem Inform Model*, 61: 3891–3898.

https://doi.org/10.1021/acs.jcim.1c00203

38. Sahu N, Mishra S, Kesheri M, *et al*., 2022, Identification of Cyanobacteria-based natural inhibitors against SARS-CoV-2 druggable target ACE2 using molecular docking study, ADME and toxicity analysis. Indian J Clin Biochem, 38: 361–373.

https://doi.org/10.1007/s12291-022-01056-6

39. Cho DY, Kim YA, Przytycka TM, 2012, Chapter 5: Network biology approach to complex diseases. *PLoS Comput Biol*, 8: e1002820.

https://doi.org/10.1371/journal.pcbi.1002820

40. Gupta M, Sharma R, Kumar A, 2018, Docking techniques in pharmacology: How much promising? *Comput Biol Chem*, 76: 210–217.

https://doi.org/10.1016/j.compbiolchem.2018.06.005

41. Cohen OC, Shadmi E, Keinan-Boker L, *et al*., 2019, The association between patients' perceived continuity of care and beliefs about oral anticancer treatment. *Supportive Care Cancer*, 27: 3545–3553.

https://doi.org/10.1007/s00520-019-04668-6

42. Medzhitov R, 2007, Recognition of microorganisms and activation of the immune response. *Nature*, 449: 819–826.

https://doi.org/10.1038/nature06246

43. Ramakrishnan V, Kumar S, 2018, PI3K/AKT/mTOR pathway in multiple myeloma: From basic biology to clinical promise. *Leuk Lymphoma*, 59: 2524–2534.

https://doi.org/10.1080/10428194.2017.1421760

44. McDonald SJ, Sharkey JM, Sun M, *et al*., 2020, Beyond the brain: Peripheral interactions after traumatic brain injury. *J Neurotrauma*, 37: 770–781.

https://doi.org/10.1089/neu.2019.6885

45. Kawai T, Akira S, 2007, Signaling to NF-κB by Toll-like receptors. *Trends Mol Med*, 13: 460–469.

https://doi.org/10.1016/j.molmed.2007.09.002

46. Napetschnig J, Wu H, 2013, Molecular basis of NF-κB signaling. *Annu Rev Biophys*, 42: 443–468.

https://doi.org/10.1146/annurev-biophys-083012-130338

47. O'Shea JJ, Plenge R, 2012, JAK and STAT signaling molecules in immunoregulation and immune-mediated disease. *Immunity*, 36: 542–550.

https://doi.org/10.1016/j.immuni.2012.03.014

48. Hu YS, Han X, Liu XH, 2019, STAT3: A potential drug target for tumor and inflammation. *Curr Top Med Chem*, 19: 1305–1317.

https://doi.org/10.2174/1568026619666190620145052

49. Ismail SI, Mahmoud IS, Msallam MM, 2010, Hotspot mutations of PIK3CA and AKT1 genes are absent in multiple myeloma. *Leuk Res*, 34: 824–826.

https://doi.org/10.1016/j.leukres.2009.11.018

50. Chang H, Qi XY, Claudio J, 2006, Analysis of PTEN deletions and mutations in multiple myeloma. *Leuk Res*, 30: 262–265.

https://doi.org/10.1016/j.leukres.2005.07.008

51. Peterson TR, Laplante M, Thoreen CC, 2009, DEPTOR is an mTOR inhibitor frequently overexpressed in multiple myeloma cells and required for their survival. *Cell*, 137: 873–886.

https://doi.org/10.1016/j.cell.2009.03.046

52. Yu CF, Liu ZX, Cantley LG, 2002, ERK negatively regulates the epidermal growth factor-mediated interaction of Gab1 and the phosphatidylinositol 3-kinase. *J Biol Chem*, 277: 19382–19388.

https://doi.org/10.1074/jbc.M200732200

53. Narayanankutty A, 2019, PI3K/Akt/mTOR pathway as a therapeutic target for colorectal cancer: A review of preclinical and clinical evidence. *Curr Drug Targets*, 20: 1217–1226.

https://doi.org/10.2174/1389450120666190618123846

54. Chang WJ, Gonzalez-Paz N, Price-Troska T, 2008, Clinical and biological significance of RAS mutations in multiple myeloma. *Leukemia*, 22: 2280–2284.

https://doi.org/10.1038/leu.2008.142

55. Rasmussen T, Kuehl M, Lodahl M, *et al*., 2005, Possible roles for activating RAS mutations in the MGUS to MM transition and in the intramedullary to extramedullary transition in some plasma cell tumors. *Blood*, 105: 317–323. https://doi.org/10.1182/blood-2004-03-0833

56. White PT, Subramanian C, Motiwala HF, *et al*., 2016, Natural withanolides in the treatment of chronic diseases. *Adv Exp Med Biol*, 928: 329–373.

https://doi.org/10.1007/978-3-319-41334-1_14

57. Swarnalatha S, Puratchikody A, 2014, Cytokine mediated immunomodulatory properties of kaempferol-5-O-β-D-glucopyranoside from methanol extract of aerial parts of *Indigofera aspalathoides* Vahl ex DC. *Int J Res Pharm Sci*, 5: 73–78.

58. Choi MJ, Park EJ, Min KJ, *et al*., 2011, Endoplasmic reticulum stress mediates withaferin A-induced apoptosis in human renal carcinoma cells. *Toxicology In Vitro*, 25: 692–698.

https://doi.org/10.1016/j.tiv.2011.01.010

59. Abramson HN, 2016, Kinase inhibitors as potential agents in the treatment of multiple myeloma. *Oncotarget*,7: 81926–81968.

https://doi.org/10.18632/oncotarget.10745

60. Manning G, Whyte DB, Martinez R, *et al*., 2002, The protein kinase complement of the human genome. *Science*, 298: 1912–1934.

https://doi.org/10.1126/science.1075762

ACCSCIENCE PUBLISHING

INNOSC Theranostics and Pharmacological Sciences

ORIGINAL RESEARCH ARTICLE

Anti-ulcer activity of aqueous ethanol extract of *Rheum spiciforme* and its fractions in animal model

Hafiz Muhammad Irfan*, Maham Idrees, and Kainat Jabeen

Department of Pharmacology, University of Sargodha, 40100, Sargodha, Punjab, Pakistan

Abstract

Helicobacter pylori infection, pepsin, ischemia, hypoxia, smoking, alcohol intake, hydrochloric acid, and nonsteroidal anti-inflammatory drugs are the causal factors of ulceration. In third-world countries, approximately one in two individuals has signs of gastric ulceration. Extensive literature suggested that plant-derived drugs hold the potential in the treatment of peptic ulcer, and *Rheum spiciforme* (family: *Polygonaceae*) has been known in the folk medicine for possessing medicinal effect on ulceration. To explore further along this line, the current study was designed to investigate the effects of aqueous ethanol extract of *R. spiciforme* roots and its fractions on peptic ulcer and to identify bioactive compounds responsible for mitigating this pathological condition. Animal model of ethanol-induced gastric ulcer was utilized in this study. The animals were pre-treated with crude plant extract, given at doses 125, 250, and 500 mg/kg, and then orally administered with butanol, aqueous, and dichloromethane fractions at doses of 250 mg/kg for 7 days. Following the treatments, a significant decrease in ulcerative lesions, ulcer index, ulcer severity score, volume, free acidity, and total acidity of gastric juice as well as a marked increase of gastric pH in the groups treated with plant extract at doses of 250 and 500 mg/kg were noted. Moreover, butanol fraction has been shown to produce effects equipotent to that of the reference drug omeprazole. Liquid chromatography-mass spectrometry analyses show that the plant extract contains emodin, aloe-emodin, and quercetin. In conclusion, this study demonstrated that the aqueous ethanol extract of *R. spiciforme* and its butanol fraction exhibited gastro-protective effect.

Keywords: *Rheum spiciforme*; Protective role; Ulcer; Ethanol; Fractions

***Corresponding author:**
Hafiz Muhammad Irfan
(muhammad.irfan@uos.edu.pk)

Citation: Irfan HM, Idrees M, Jabeen K, 2024, Anti-ulcer activity of aqueous ethanol extract of *Rheum spiciforme* and its fractions in animal model. *INNOSC Theranostics and Pharmacological Sciences*, 7(1): 1343.
https://doi.org/10.36922/itps.1343

Received: July 20, 2023

Accepted: August 29, 2023

Published Online: October 13, 2023

1. Introduction

A peptic ulcer is a common pathological condition of the gastrointestinal tract with more a high prevalence in Asian countries[1]. It is defined as a lesion of mucosa that infiltrates into the muscularis mucosae layer of the stomach or duodenal bulb, leaving behind a cavity accompanied by acute and chronic inflammation[2]. Peptic ulcer develops when the equilibrium between the "offensive" and "defensive" factors that govern the integrity of the luminal surface of the epithelial cells is disrupted. The offensive factors include *Helicobacter pylori* infection, pepsin, bile acids, ischemia, smoking, hypoxia, alcohol intake, hydrochloric acid, and nonsteroidal anti-inflammatory drugs, while the mucus

layer, growth factors, bicarbonate, mucosal blood flow, and prostaglandins constitute the line of defense against the ulceration[3].

Peptic ulcer commonly develops along the gastrointestinal tract, especially the stomach and duodenum, where gastric acid and pepsin are secreted. Commonly observed symptoms of peptic ulcer include bloating, burning, pressure or feeling of fullness, occasional bloody or dark stools, pain in the chest, fatigue, vomiting, changes in appetite, indigestion, and weight loss[1]. Numerous drugs, including proton pump inhibitors and H2 receptor antagonists, are included in the treatment regimen of peptic ulcer[4]. Nevertheless, these drugs lead to the occurrence of adverse effects and relapses and interact with other drugs. As an effort to reduce adverse effects stemming from these drugs and prevent relapses, the relentless search for potent herbal medication is still relevant and crucial[5].

Rheum spiciforme, mostly found in the Himalayan region of Kashmir, belongs to family Polygonaceae[6], which comprises 60 species, among which seven species are found in the Indian subcontinent and the Himalayan region of Kashmir. It is a wild plant capable of surviving in harsh environments [7]. The petioles, stems, and leaves of *R. spiciforme* are traditionally included in the meals of a few Tibetan communities[8], while the roots are applied in the treatments of bone fractures, backache, joint pain, joint swelling, rheumatic pain, stomachache, intestinal infections, and dysentery[7]. In light of the potential medicinal values mentioned above, the current study aimed to investigate the anti-ulcer activity of *R. spiciforme*.

2. Materials and methods

2.1. Chemicals and drugs

The list of chemicals and drugs used in his study is as follows: diethyl ether (Riedel-de Haen), sodium hydroxide (Merck®, Germany), 10% formalin, Topfer Reagent, paraffin wax, phenolphthalein, hemotoxylin, eosin, 0.1 N sodium hydroxide, analytical-grade absolute ethanol (Merck®, Germany), n-butanol, dichloromethane (Riedel-de Haen), normal saline, distilled water, hydrochloric acid, Mayer's reagent, Wagner's reagent, sodium chloride, ethanol, and omeprazole (Sigma, Germany).

2.2. Animals

Healthy adult albino rats (6–8 weeks old) of either sex were obtained from the Animal House, College of Pharmacy, University of Sargodha, Sargodha. The rats weighed between 150 and 180 g. Standard rat pellet diet and tap water were given to the animals, which were kept on a standard light-dark cycle (12 h with light on and 12 h in the dark) at room temperature[9]. All animals were treated in accordance with the standard ethical guidelines set forth by the National Research Council[10].

2.3. Collection and authentication of medicinal plant

The identification of *R. spiciforme* based on the ethnobotanical literature[11]. The roots of *R. spiciforme* were acquired from a local market during the full bloom season of the plant, *i.e.*, in July. The identification and authentication of the plant was performed by assistant professor Dr. Shair Wali Khan from Karakoram International University, Gilgit-Baltistan. After cleaning, the dried roots of *R. spiciforme* were powdered using an electric blender.

2.4. Preparation of crude extract and its fractions

Aqueous ethanol extract of *R. spiciforme* was prepared through maceration. For the extraction purpose, the dry powder was immersed in aqueous ethanol (30:70; analytical grade, Merck®, Germany) for 48 h with regular shaking[12]. The mixture obtained was filtered after 3 days using a muslin cloth and grade 1 Whatman filter paper. The filtrate was then passed through a rotary evaporator and afterward, it was dried at room temperature.

Activity-guided fractionation of *R. spiciforme* was performed using three different organic solvents in increasing polarity so that the relative active fraction could be obtained[13]. Next, 100 g of the active fraction was mixed in 250 mL of distilled water to produce aqueous (48%) fraction. Separately, two solvents – dichloromethane and butanol – were added in increasing polarity, eventually generating concentrated dichloromethane (20%) and butanol (25%) fractions, respectively. After drying, these fractions were then applied in the anti-ulcer activity evaluation.

2.5. Evaluation of gastro-protective effect of crude extract on rats with ethanol-induced ulcer

Rats were divided into five groups and each group consisted of six animals (n = 6). Group I was the control group that received a vehicle once per day for 7 days and then was induced for ulcer development on day 7. Group II was the reference group given 20 mg/kg omeprazole (p.o). Groups III, IV, and V were given aqueous ethanol extract of *R. spiciforme* at doses of 125, 250, and 500 mg/kg body weight once per day for 7 days, respectively[14]. Gastric ulcer was induced by administering ethanol (5 mL/kg) to rats after 1-h pre-treatment with crude extract and omeprazole on day 7[15].

2.6. Evaluation of gastro-protective effect of plant extract fractions on rats with ethanol-induced ulcer

In this experiment, the animals were divided randomly into five groups, with each group containing six rats (n = 6).

Group I was the control group that was given a vehicle once per day for 7 days. Group II was the reference group administered with 20 mg/kg omeprazole once per day for 7 days. Groups III, IV, and V were treated with butanol, aqueous, and dichloromethane fractions of plant extract at 250 mg/kg once per day for7 days. Then, gastric ulcer was induced in adherence to protocols briefly mentioned in section 2.5[15].

2.7. Macroscopic evaluation of ulcer

2.7.1. Estimation of ulcer severity

Stomach of each rat was cut open with an incision on the greater curvature. After the gastric contents were removed, gastric lesion on the stomach was examined with the naked eyes. The length of the ulcer was measured using Vernier Calliper, and the ulcer severity was estimated by means of scoring[16].

2.7.2. Estimation of ulcer index

The ulcer index is defined as mean ulcer severity score for each animal. The ulcer index was calculated using the following formula[17]:

$$UI = UN+US+UP\times10-1 \quad (I)$$

where UI = ulcer index, UN = average number of ulcer per animal, US= average severity score, and UP = percentage of animal with ulcer

2.7.3. Percentage inhibition of ulcer

Percentage inhibition of ulcer is also known as percentage protection. Percentage inhibition of ulceration was calculated using the following formula[18]:

$$\text{Inhibition of ulceration} = \frac{(UI_{Ctrl} - UI_{Test})\times100}{UI_{Ctrl}} \quad (II)$$

where UI_{Ctrl} = Ulcer index of control group, and UI_{Test} = ulcer index of test group.

2.7.4. Evaluation of pH

Before pH measurement, 1 mL gastric juice was diluted with 1 mL of distilled water, and then, pH meter was used to measure the pH of the solution[19].

2.7.5. Determination of free and total acidity

One milliliter of gastric juice solution, diluted in a 1:1 ratio with distilled water, was poured into a conical flask. A few drops of a phenolphthalein indicator were added to the solution. Titration was performed with 0.01 N NaOH until a sustained pink coloration appeared. The volume of 0.01 N NaOH used was noted. Topfer reagent was used to determine the free acidity. Titration of gastric juice with 0.01 N NaOH was performed until a yellow coloration appeared. The volume of 0.01N NaOH used was noted. The total and free acidity was calculated using the following formula[17].

$$\text{Acidity} = \frac{V_{NaOH}\times N\times100 \text{ mEq/L}}{0.1} \quad (III)$$

where V_{NaOH} = volume of NaOH solution used, and N = normality.

2.7.6. Determination of gastric juice volume

Gastric juice was centrifuged at 500 rpm for 5 min, and then, the supernatant was separated and its volume was measured using a graduated cylinder[20].

2.8. Liquid chromatography-mass spectrometry (LC-MS) analysis of bioactive fractions

In the present study, active constituents in most active fractions (butanol fractions) were identified by means of LC-MS using methanol (100%) as the mobile phase. A thermo electron (LTQ-Orbitrap XL mass spectrometer) equipped with a nanoelectrospray ion source (Thermo Fisher Scientific, Bremen, Germany) was utilized in positive and negative ionization modes as per requirements.

The separated target compounds were detected in direct injection mode. The collision-induced dissociation (CID) was based on the parent ion fragmentation efficiency. The capillary temperature was set at 280°C and the sample flow at 8 μL/min[21].

2.9. Statistical analysis

Data were analyzed using GraphPad Prism, and descriptive statistics were used to describe the results. The results are expressed as mean ± standard error of mean. One-way analysis of variance (ANOVA) followed by Dunnett and Bonferroni's *post hoc* test was carried out. A P-value <0.05 was considered statistically significant.

3. Results

3.1. Gastro-protective effect of *R. spiciforme* on gastric mucosal injury in ethanol-induced ulcer rat model

The extract at a dose of 125 mg/kg resulted in a non-significant decrease (6.50 ± 0.95) in number of lesions in comparison with the control group (7.83 ± 0.47), whereas a remarkable reduction in the number of lesions in mucosa was observed when the 250 and 500 mg/kg doses were used (2.50 ± 0.4 and 1.66 ± 0.4, respectively). The 125, 250, and 500 mg/kg doses of the plant extract considerably reduced the ulcer severity score (22.67 ± 7.3, 7.16 ± 1.70, and 6.83 ± 1.77) compared to the control group (32.33 ± 2.81).

In addition, the ulcer index was decreased (12.88, 10.97, and 9.18) at doses of 125, 250, and 500 mg/kg; notably, the effect of the 500 mg/kg dose on ulcer index was more pronounced with respect to the other two doses. The gastroprotective effect of the crude plant extract was also measured in terms of percentage inhibition of ulcer; it was found that the extract at the dose of presented 125 mg/kg dose engendered a gastric damage inhibition of 8.13%, while higher doses at 250 mg/kg and 500 mg/kg inhibited the damage by 21.75% and 34.52% (Table 1).

3.2. Gastro-protective effect of crude plant extract on pH, volume, and acidity of gastric juice

R. spiciforme crude extract at 250 and 500 mg/kg doses markedly increased the pH of gastric juice ($P < 0.05$ and $P < 0.001$, respectively) in comparison with control group, while increase in pH was observed following treatment with 125 mg/kg of the extract was non-significant as compared to the control group (Figure 1). The 250 and 500 mg/kg doses of the crude extract reduced the volume of gastric juice significantly ($P < 0.01$), whereas the 125 mg/kg dose only mildly reduced the gastric juice volume (4.46 ± 0.264 mL) in comparison with the control group (4.61 ± 0.47 mL). The 250 and 500 mg/kg doses of aqueous ethanol extract significantly reduced the free acidity ($P < 0.05$ and $P < 0.001$, respectively) as compared to the control group, but the 125 mg/kg dose led to only non-significant decrease in the acidity of gastric juice. On the other hand, total acidity was significantly reduced by 250 and 500 mg/kg doses ($P < 0.05$ and $P < 0.001$, respectively), as shown in Figure 1.

3.3. Effect of *R. spiciforme* root extract's fractions on gastric mucosal injury in rats with ethanol-induced ulcer

The 250 mg/kg dose was used to prepare the butanol, aqueous, and dichloromethane fractions of plant extract. The butanol fraction caused a marked reduction in lesion formation (1.66 ± 0.42) in comparison to the control group (7.16 ± 0.30), as presented in Table 2. Both aqueous and dichloromethane fractions were found to mildly reduce number of lesions (5.50 ± 2.46 and 5.33 ± 0.88, respectively) in comparison with the control group. Butanol fraction of the extract also decreased the ulcer severity score markedly down to 5.66 ± 1.49, while aqueous and dichloromethane fractions reduced the ulcer severity score non-significantly (25.33 ± 7.49 and 23.83 ± 3.21, respectively) as compared with control group (31.50 ± 3.56). The 250 mg/kg dose of butanol fraction reduced the ulcer index to 9.063 ± 0.18, producing an effect resembling that of the reference drug (9.32 ± 0.31). Aqueous fraction significantly lowered the ulcer index (11.41 ± 0.9492) while dichloromethane fraction non-significantly reduced the ulcer index (12.88 ± 0.71) as compared with the control group.

3.4. Effect of fractions of *R. spiciforme* on gastric juice parameters in rats with ethanol-induced ulcer

Both butanol and aqueous fractions significantly elevated the pH of gastric juice ($P < 0.001$ and $P < 0.05$, respectively) as compared to ulcer control, dwarfing the minute, non-significant pH elevation achieved by dichloromethane fraction (Figure 2). Regarding other gastric juice parameters, butanol fraction was singled out for its significant lowering effects on these parameters ($P < 0.001$), namely the volume of gastric juice, free, and total acidity, in comparison with control group.

3.5. LC-MS results

Figure 3 shows the LC-MS chromatogram of butanol fraction of *R. spiciforme* extract detected at negative and positive modes. The peaks of emodin and aloe emodin were obtained at 3.42 retention time with molecular weight 270.00 g/moL. The compounds – emodin and aloe-emodin – were identified based on the molecular weight in the butanol fraction of plant extract, with the aid of a standard reference graph.

4. Discussion

The ulcer usually manifests as an open sore of the skin or the mucosal membrane, characterized by sloughing

Table 1. Gastro-protective effect of *R. spiciforme* crude extract on gastric mucosal injury in rats with ethanol-induced ulcer

Treatment (mg/kg)	Number of lesions	Severity score	Ulcer index	Percentage inhibition of ulcer (%)
Control	7.833 ±0.4773	32.33±2.813	14.02±0.2522	NA
Omeprazole	2.167±0.6009***	8.083±2.758***	9.356±0.3295***	33.26
RS-CE (125 mg/kg)	6.500±0.9574^{ns}	22.67±7.311^{ns}	12.88±0.7148^{ns}	8.13
RS-CE (250 mg/kg)	2.500±0.4282***	7.167±1.701***	10.97±0.1909***	21.75
RS-CE (500 mg/kg)	1.667±0.4216***	6.833±1.778***	9.180±0.2045***	34.52

Notes: Values are expressed as means±standard error of mean (n=6); ***P<0.001, ns: Non-significant versus control group, analyzed by one-way analysis of variance (with Dunnett's test).
Abbreviation: RS-CE: *Rheum spiciforme* crude extract.

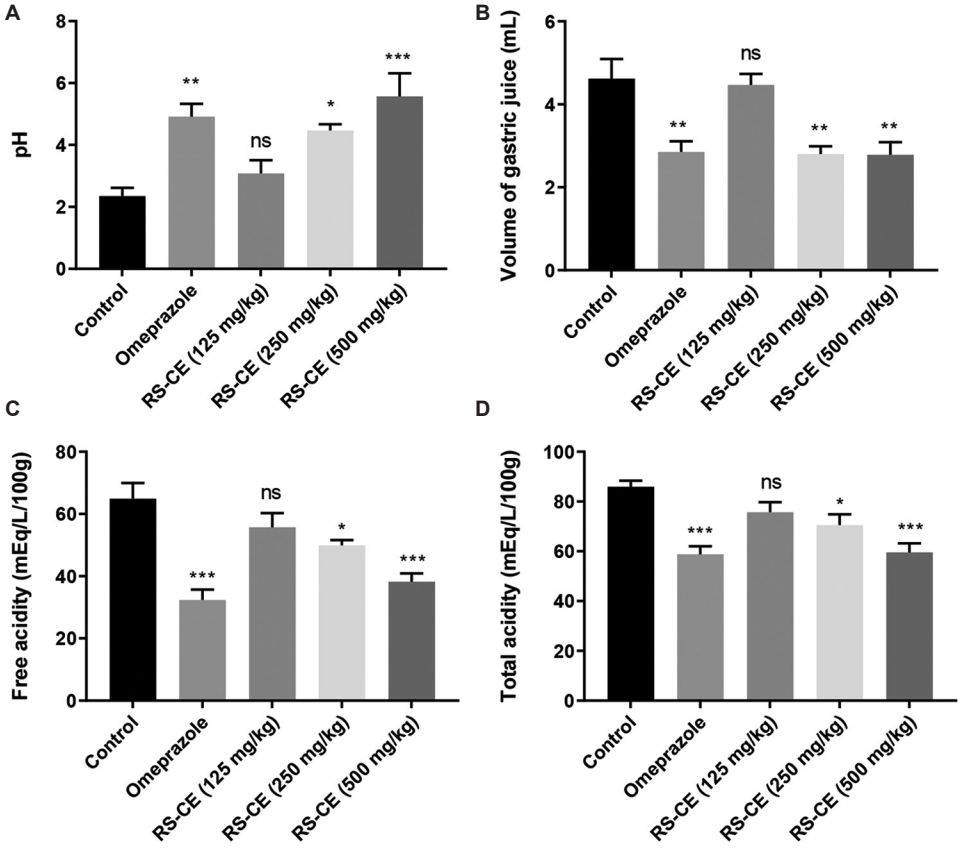

Figure 1. Effect of *Rheum spiciforme* crude root extract on gastric juice parameters: (A) pH, (B) volume of gastric juice, (C) free acidity, and (D) total acidity in rats with ethanol-induced ulcer. Values are expressed as means ± standard error of mean ($n = 6$); *$P < 0.05$, **$P < 0.01$, ***$P < 0.001$, ns: Non-significant versus control group, analyzed by one-way analysis of variance (with Dunnett's test).
Abbreviations: UC: Ulcer control; RS-CE: *R. spiciforme* crude extract.

Table 2. Effect of plant root extract fractions on gastric mucosal damage in rats with ethanol-induced ulcer

Treatments (mg/kg)	Number of lesions	Ulcer severity score	Ulcer index	Percentage inhibition of ulcer (%)
Control	7.167±0.3073	31.50±3.566	13.87±0.3836	NA
Omeprazole	2.167±0.6009*	7.750±2.620**	9.322±0.3132***	32.79
RS-BF	1.667±0.4216*	5.667±1.498***	9.063±0.1856***	34.66
RS-AF	5.500±2.460^{ns}	25.33±7.491^{ns}	11.41±0.9492*	17.74
RS-DCMF	6.500±0.9574^{ns}	22.67±7.311^{ns}	12.88±0.7148^{ns}	7.14

Notes: Values are expressed as means±standard error of mean (n=6); *P<0.05, **P<0.01, ***P<0.001, ns: Non-significant versus control group analyzed by one-way analysis of variance (with Dunnett's test). Abbreviations: RS-BF: *Rheum spiciforme* butanol fraction, RS-AF: *R. spiciforme* aqueous fraction, RS-DCMF: *R. spiciforme* dichloromethane fraction.

of inflamed dead tissue. The prevalence of peptic ulcer is disproportionately higher in developing countries where it is estimated that about 70% of their population suffers from peptic or gastric ulcers; in contrast, the highest prevalence rate ever recorded from the developed countries is 40%[3].

The present study evaluated the anti-ulcer potential of *R. spiciforme* root extract and its fractions in rats with ethanol-induced ulcer. Several parameters concerning ulcer, such as number of ulcerative lesions, ulcer severity score, percentage inhibition of ulcer, ulcer index, volume, pH, free, and total acidity of gastric juice, were approximated to characterize the gastro-protective effects of *R. spiciforme*. The pH of gastric juice normally ranges between 2.9 and 3.3 but could be reduced to 2.3 following ethanol intake, which triggers ulceration due to a significant decrease in pH. Due to the enhanced production of histamine, the release of gastric juice increases, thereby causing an increase in the hydrogen ions concentration (more acidic pH), which is

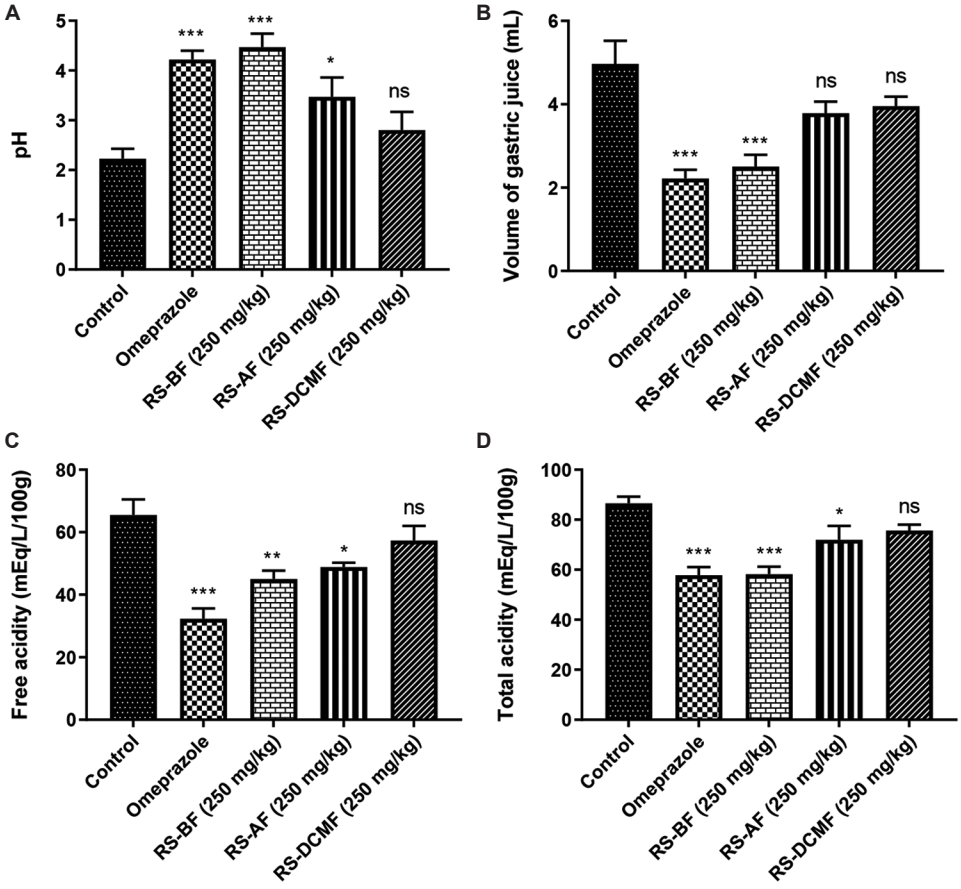

Figure 2. Effect of *Rheum spiciforme* root extract's fractions on gastric juice parameters: (A) pH, (B) volume of gastric juice, (C) free acidity, and (D) total acidity in rats with ethanol-induced ulcer. Values are expressed as means ± standard error of mean (n=6); *P<0.05, **P<0.01, ***P<0.001, ns: Non-significant versus control group analyzed by one-way analysis of variance (Dunnett's test).
Abbreviations: RS-BF: *R. spiciforme* butanol fraction, RS-AF: *R. spiciforme* aqueous fraction, RS-DCMF: *R. spiciforme* dichloromethane fraction.

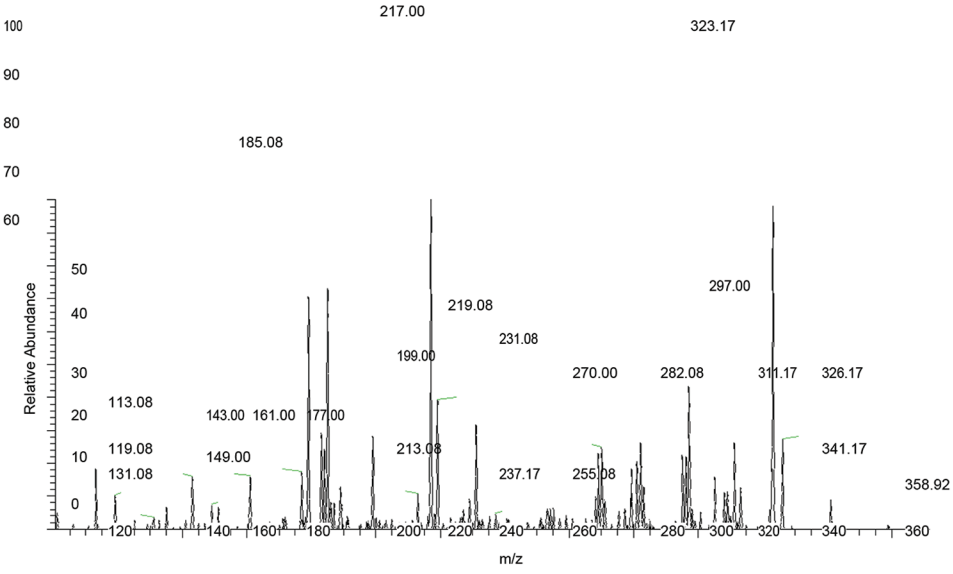

Figure 3. Liquid chromatography-mass spectrometry chromatogram at the retention time 3.42.

claimed to be an offensive factor triggering ulceration. Moreover, parameters such as the number of ulcerative lesions, ulcer severity scores, ulcer index, volume, and acidity of gastric juice were markedly increased[3]. The oral administration of aqueous ethanol extract of *R. spiciforme* at higher doses reduced the number of lesions, ulcer index, and severity score, which were otherwise aggravated by ethanol. Our results were congruent with other published work, in which Ranunculus millefoliatus ethanol extract at 250 mg/kg dose was demonstrated to exhibit anti-ulcer activity[22]. In the clinical setting, omeprazole is used as a standard anti-ulcerative medication. As a proton pump inhibitor, omeprazole prevents ulceration by inhibiting the H-K-ATPase in the stomach wall irreversibly, thereby blocking gastric acid release. This study revealed that the anti-ulcerative efficacy of *R. spiciforme* extract was comparable to that of omeprazole, suggesting that the mechanism underlying the *R. spiciforme*-mediated anti-ulceration might be similar to that of proton pump inhibitor.

As compared to control group, the extracts at 250 and 500 mg/kg doses markedly increased the pH and intuitively reduced the acidity (both free and total) of gastric juice. Likewise, the volume of gastric juice was also significantly decreased in groups of animals treated with the plant extract as compared to the control group (Figure 1). The effects produced by *R. spiciforme* mirrors the anti-secretory activity of *Aloe vera* demonstrated by Borra *et al.*[23].

In the present study, crude extract of *R. spiciforme* was further utilized for the preparation of different fractions (butanol, aqueous, and dichloromethane), which were investigated for their anti-ulcer activity in ethanol-induced ulcer model. Compared with the control group, the butanol fraction stands out to be the only specially prepared fraction capable of producing significant gastro-protective effects, evident by the significant reductions in the severity score and ulcer index ($P < 0.001$) (Table 2). These findings indicated that the butanol fraction was as effective as the reference drug, omeprazole (20 mg/kg), in the treatment of ulcer. The results of the present study, such as the increase in the pH as well as the decrease in the volume, free acidity, and total acidity of gastric juice, were consistent with the findings by Lee *et al.*[24] and Ahmed *et al.*[25]

The ethanol-induced ulcer model treated with aqueous fraction also exhibited fewer lesions and reduced severity score and ulcer index; however, these results were not statistically significant probably due to the presence of less bioactive constituents responsible for the anti-ulcer effect. This justification is inspired by the presence of less bioactive constituents present in the aqueous fraction of root bark of *Aralia elata*[24]. Similarly, the non-significant results observed with the dichloromethane fraction might be due to the absence of bioactive constituents responsible for anti-ulcer activity. A previous study has in fact shown that the *Markhamia tomentosa* leave extract in dichloromethane fraction has non-significant anti-ulcer activity[9].

The anti-ulcer effect of flavonoids, which are cytoprotective constituents, has been confirmed in previous studies[7]. The flavonoids provide defense to the gastric mucosa against damage by enhancing the prostaglandins level in the mucosal lining of the stomach[26]. The increased prostaglandin level in the mucosa of stomach and reduced histamine secretion from mast cells achieved through the blocking of histidine decarboxylase and the inhibition of *H. pylori* growth are the mechanisms behind the gastro-protective effect of flavonoids. In addition, flavonoids act as scavengers of free radicals, which play an important role in the formation of gastrointestinal tract lesions. Hence, coupled with a less toxic profile and properties, flavonoids have high medicinal value in the treatment of ulcers. Apart from that, flavonoids are therapeutically useful in the treatment of gastrointestinal diseases, especially those associated with *H. pylori* infection[27]. Thus, we postulate that the presence of flavonoids is accountable for the anti-ulcer potential of the crude extract of *R. spiciforme*. Furthermore, the LC-MS analysis of the butanol fraction, which is the most active fraction, of the crude extract revealed that the anthraquinones, flavonoids, alkaloids, and carbohydrates are the active constituents of the fraction. We also found that quercetin is the predominant type of flavonoid in the fraction. Quercetin activates the cyclooxygenase, which activates the production of local prostaglandin[28]. Earlier studies have demonstrated that emodin and aloe emodin possess anti-ulcer properties, and the flavonoids, particularly quercetin, possess antioxidant, anti-inflammatory, and anti-ulcer activities[21]. Hence, these active constituents present in the aqueous ethanol extract of *R. spiciforme* and its butanol fraction might play vital roles in suppressing the formation of ulcer.

5. Conclusions

Taken together, the aqueous ethanol extract of *R. spiciforme* possesses gastro-protective activity, on the basis of its capacity in suppressing ulcer formation in animal models and lowering gastric acid secretion. Furthermore, owing to the presence of emodin and aloe emodin, butanol fraction of the extract is more effective than other fractions in improving the ulcer-related parameters.

Acknowledgments

The authors would like to acknowledge the National Institute for Biotechnology and Genetic Engineering (NIBGE) for providing facility used for LC-MS analysis.

Funding

This work was funded by the College of Pharmacy, University of Sargodha regular research fund for postgraduate students.

Conflict of interest

The authors have no conflicts of interest.

Author contributions

Conceptualization: Hafiz Muhammad Irfan
Investigation: Hafiz Muhammad Irfan, Maham Idrees
Writing – original draft: Hafiz Muhammad Irfan
Writing – review & editing: Kainat Jabeen

Ethics approval and consent to participate

The experiments on animals were performed in accordance with the animal ethics guidelines (Approval No. AEA-PMY-22).

Consent for publication

Not applicable.

Availability of data

The raw data used in this work can be obtained from the corresponding author on reasonable request.

References

1. Sung JJ, Kuipers EJ, El-Serag HB, 2009, Systematic review: The global incidence and prevalence of peptic ulcer disease. *Aliment Pharmacol Ther*, 29: 938–946.
2. Najm WI, 2011, Peptic ulcer disease. *Prim Care*, 38: 383–394, vii.
3. Rao SP, Amrit I, Singh V, *et al*., 2015, Antiulcer activity of natural compounds: A review. *Res J Pharmacogn Phytochem*, 7: 124.
4. Yuan Y, Padol IT, Hunt RH, 2006, Peptic ulcer disease today. *Nat Clin Pract Gastroenterol Hepatol*, 3: 80–89.
5. Ayaz M, Junaid M, Ahmed J, *et al*., 2014, Phenolic contents, antioxidant and anticholinesterase potentials of crude extract, subsequent fractions and crude saponins from *Polygonum hydropiper* L. *BMC Complement Altern Med*, 14: 1–9.
6. Khan SW, Khatoon S, 2008, Ethnobotanical studies on some useful herbs of Haramosh and Bugrote valleys in Gilgit, northern areas of Pakistan. *Pak J Bot*, 40: 43.
7. Tabin S, Kaur K, Singh V, *et al*., 2016, Meiotic and ethnobotanical studies on rheum species from Kashmir Himalaya. *Cytologia*, 81: 295–300.
8. Boesi A, 2014, Traditional knowledge of wild food plants in a few Tibetan communities. *J Ethnobiol Ethnomed*, 10: 1–19.
9. Sofidiya MO, Agunbiade FO, Koorbanally NA, *et al*., 2014, Antiulcer activity of the ethanolic extract and ethyl acetate fraction of the leaves of *Markhamia tomentosa* in rats. *J Ethnopharmacol*, 157: 1–6.
10. National Research Council, 2010, Guide for the Care and Use of Laboratory Animals. Washington, DC: The National Academies Press.
11. Shah NC, 1982, Herbal folk medicines in northern India. *J Ethnopharmacol*, 6: 293–301.
12. Irfan HM, Asmawi MZ, Khan NA, *et al*., 2016, Effect of ethanolic extract of *Moringa oleifera* Lam. Leaves on body weight and hyperglycemia of diabetic rats. *Pak J Nut*, 15: 112–117.
13. Irfan HM, Asmawi MZ, Khan NA, *et al*., 2017, Anti-diabetic activity-guided screening of aqueous-ethanol *Moringa oleifera* extracts and fractions: Identification of marker compounds. *Trop J Pharm Res*, 16: 543–552.
14. Sahoo SK, Sahoo HB, Priyadarshini D, *et al*., 2016, Antiulcer activity of ethanolic extract of *Salvadora indica* (W.) leaves on albino rats. *J Clin Diagn Res*, 10: FF07.
15. Al-Sayed E, El-Naga RN, 2015, Protective role of ellagitannins from *Eucalyptus citriodora* against ethanol-induced gastric ulcer in rats: Impact on oxidative stress, inflammation and calcitonin-gene related peptide. *Phytomedicine*, 22: 5–15.
16. Abd El-Hady FK, El Awdan SA, Ibrahim AM, 2013, Anti-ulcerative potential of Egyptian propolis against oxidative gastric injury induced by indomethacin in rats. *Asian J Med Pharm Res*, 3: 35–42.
17. Reddy VP, Sudheshna G, Afsar S, *et al*., 2012, Evaluation of anti-ulcer activity of *Citrullus colocynthis* fruit against pylorus ligation induced ulcers in male wistar rats. *Int J Pharm Pharm Sci*, 4: 446–451.
18. Rasve VR, Paithankar VV, Shirsat MK, *et al*., 2017, Evaluation of antiulcer activity of *Aconitum heterophyllum* on experimental animal. *World J Pharm Pharm Sci*, 7: 819–839.
19. Dashputre N, Naikwade N, 2011, Evaluation of anti-ulcer activity of methanolic extract of *Abutilon indicum* Linn leaves in experimental rats. *Int J Pharm Sci Drug Res*, 3: 97–100.
20. Amr AR, Maysa ME, 2010, Anti-ulcer effect of cinnamon and chamomile aqueous extracts in rat models. *J Am Sci*, 6: 209–216.
21. Vijayalakshmi M, Kiruthika R, Bharathi K, *et al*., 2015, Phytochemical screening by LC-MS analysis and *in vitro* anti-inflammatory activity of *Marsilea quadrifolia* plant extract. *Int J Pharmtech Res*, 8: 148–157.
22. Abdoulrahman K, 2023, Anti-ulcer effect of *Ranunculus millefoliatus* on absolute alcohol-induced stomach

ulceration. *Saudi J Biol Sci*, 30: 103711.

23. Borra SK, Lagisetty RK, Mallela GR, 2011, Anti-ulcer effect of *Aloe vera* in non-steroidal anti-inflammatory drug induced peptic ulcers in rats. *Afr J Pharm Pharmacol*, 5: 1867–1871.
24. Lee EB, Kim OJ, Kang SS, *et al*., 2005, Araloside A, an antiulcer constituent from the root bark of *Aralia elata*. *Biol Pharm Bull*, 28: 523–526.
25. Ahmed O, Nedi T, Yimer EM, 2022, Evaluation of anti-gastric ulcer activity of aqueous and 80% methanol leaf extracts of *Urtica simensis* in rats. *Metabol Open*, 14: 100172.
26. Lemos M, De Barros MP, Sousa JP, *et al*., 2007, *Baccharis dracunculifolia*, the main botanical source of Brazilian green propolis, displays antiulcer activity. *J Pharm Pharmacol*, 59: 603–608.
27. Seitimova GA, Shokan AK, Tolstikova TG, *et al*., 2023, Antiulcer activity of anthraquinone-flavonoid complex of *Rumex tianschanicus* Losinsk. *Molecules*, 28: 2347.
28. Borrelli F, Izzo AA., 2000, The plant kingdom as a source of anti-ulcer remedies. *Phytother Res*, 14: 581–591.

ACCSCIENCE PUBLISHING

INNOSC Theranostics and Pharmacological Sciences

ORIGINAL RESEARCH ARTICLE

Drug repurposing approach for identifying Pfmrk inhibitors as potential antimalarial agents: An *in silico* analysis

Abhishek Sahu*, Tanuj Handa, and Debanjan Kundu

School of Biochemical Engineering, Indian Institute of Technology (Banaras Hindu University), Varanasi, Uttar Pradesh, India

Abstract

Malaria represents a major global health concern, primarily due to the emergence of resistance against most currently available antimalarial drugs. This pressing issue necessitates the discovery of novel antimalarial agents to combat the escalating resistance. A cyclin-dependent kinase (CDK)-like protein, Pfmrk, found in *Plasmodium falciparum*, plays a crucial role in regulating cell proliferation and exhibits a 36.28% sequence homology with its human counterpart hCDK7. Pfmrk forms a complex with plasmodial cyclin (Pfcyc-1) and stimulates kinase activity. Pfcyc-1 from *P. falciparum*, with the highest sequence homology to human cyclin (cyclin H), binds and activates Pfmrk in a cyclin-dependent manner. This discovery provides the first indication that cyclin subunits may regulate both human and plasmodial CDKs in a similar fashion. In this study, we conducted molecular docking and simulation analysis to investigate the interaction between Pfmrk and a selection of the FDA-approved drugs retrieved from the ZINC15 database. The top five drugs – Lurasidone, Vorapaxar, Donovex, Alvesco, and Orap – were screened based on their binding energies, with the best-docked scores ranging between −8 kcal/mol and −12 kcal/mol. Further, evaluation through molecular dynamics simulations for 100 nanoseconds revealed that Lurasidone exhibited the highest binding affinity (−105.90 ± 57.72 kJ/mol) followed by Donovex (−92.877 ± 17.872 kJ/mol). They exhibited stable interactions with the amino acid residues located in the active site of Pfmrk. The results of the *in silico* investigation indicate that Lurasidone and Donovex exhibit antimalarial potential and could serve as promising Pfmrk inhibitors. Further, development of new drugs based on these findings warrants subsequent *in vitro* studies.

Keywords: Pfmrk; *Plasmodium falciparum*; Molecular docking; Drug discovery; Molecular dynamics

***Corresponding author:**
Abhishek Sahu
(abhisheksahu.bce20@itbhu.ac.in)

Citation: Sahu A, Handa T, Kundu D, 2024, Drug repurposing approach for identifying Pfmrk inhibitors as potential antimalarial agents: An *in silico* analysis. *INNOSC Theranostics and Pharmacological Sciences*, 7(1): 1313. https://doi.org/10.36922/itps.1313

Received: June 15, 2023

Accepted: September 6, 2023

Published Online: November 2, 2023

1. Introduction

The term "Malaria" originates from the Italian word "mal-aria," signifying its association with the noxious air prevalent in regions characterized by stagnant, swampy environments. Malaria is primarily transmitted through the bites of female *Anopheles* mosquitoes carrying the infectious *Plasmodium* species, which belong to the eukaryotic unicellular organisms, classified under the Apicomplexa phylum[1]. Several *Plasmodium* species can infect humans, including *Plasmodium falciparum*, *Plasmodium vivax*,

Plasmodium ovale, and *Plasmodium malariae*. Among these, *P. falciparum* is associated with the most severe and potentially fatal cases of malaria. According to the World Health Organization (WHO), a staggering 300 – 500 million malaria cases are reported annually, with the majority of these cases occurring in Africa. High prevalence is also observed in regions such as India, Sri Lanka, Thailand, Indonesia, Vietnam, China, and Cambodia. In addition, malaria claims the lives of more than 2 million individuals each year[2].

The parasite's complex life cycle involves plasmodial cyclin-dependent kinases (CDKs) and cyclin proteins for its persistence in both vertebrate and invertebrate hosts[3]. These proteins play essential roles in the parasite's survival, both extracellularly and intracellularly. Plasmodial CDKs, such as Pfmrk, belong to the Apicomplex, a specific protein kinase subfamily analogous to CDKs. Pfmrk, akin to CDK7, functions as an upstream kinase, facilitating the activation of multiple CDKs during a cell cycle[4]. It is also known as a CDK-activating kinase due to this role. Pfmrk activates Cdkl, Cdk2, Cdk3, Cdk4, and Cdk6 by activating the C-terminal domain (CTD) of RNA polymerase II through its kinase activity, as shown in Figure 1. Pfmrk exhibits dual functionality in the regulation of gene expression and control of the cell cycle, rendering Pfmrk a promising candidate for drug targeting. Plasmodial cyclins, such as Pfcyc-1 from *P. falciparum*, share the highest sequence homology with human cyclin (cyclin H) and are involved in the activation of Pfmrk in a cyclin-dependent manner. Multiple studies have confirmed that the C-terminal domain of RNA polymerase II serves as an endogenous substrate of Pfmrk[5]. While it has been demonstrated that plasmodial CDKs can be inhibited by mammalian CDK inhibitors[6], the existence of CDK inhibitory proteins in *Plasmodium* remains undiscovered. Therefore, Pfmrk holds promise as a drug target in antimalarial drug screening.

In the present study, we have leveraged this foundational knowledge to determine the potential of selected drugs to interact with and potentially inhibit the Pfmrk protein. The extensive molecular docking and simulation study identified two promising candidate drugs. These drugs warrant further investigation in *in vitro* studies, with the aim of their potential addition to drug panels for malaria treatment in the future.

2. Materials and methods

2.1. Sequence homology between Pfmrk and hCDK7

Sequence homology between Pfmrk and hCDK7 was assessed through multiple sequence alignment, employing the Clustal Omega (1.2.4) tool (https://www.ebi.ac.uk/Tools/msa/clustalo/). The Fast Amino Acid Sequence Search Tool (FASTA) sequence of Pfmrk (ID: P90584) and hCDK7 (ID: P50613) was retrieved from the UniProt database (https://www.ebi.ac.uk/Tools/msa/clustalo/). Subsequently, the Clustal Omega tool was used to estimate the sequence identity between Pfmrk and hCDK7, as shown in Figure S1.

2.2. Protein preparation

In the absence of the experimental structure of the target protein Pfmrk, the FASTA sequence of the target enzyme

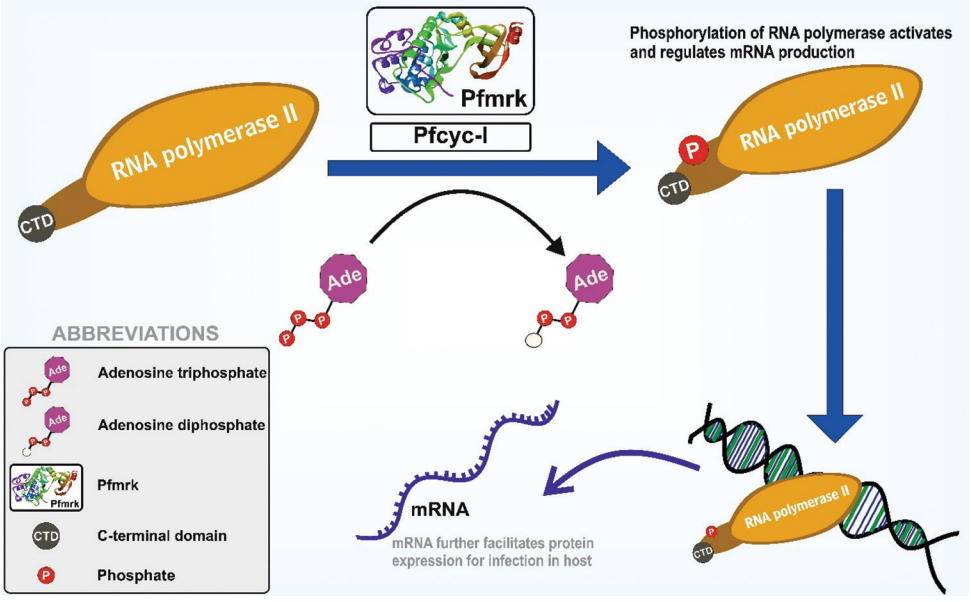

Figure 1. Graphical representation of gene expression induced by Pfmrk through C-terminal domain activation of RNA polymerase II. Pfcyc-1 further activates Pfmrk in a cyclin-dependent manner, with the C-terminal domain of RNA polymerase II serving as a substrate.

Pfmrk (ID: P90584) was retrieved from the UniProt database. To construct the protein model, the Galaxy TBM server[7] was employed, as shown in Figure 2. The model underwent validation using the SAVES v6.0 server PROtein structure CHECKing (PROCHECK)[8] for Ramachandran plot analysis. The model featuring the highest percentage of residues in the most favored region was selected (Figure S2A). In addition, the model's quality was validated using the PROSa webserver (Figure S2B). Subsequently, the modeled protein underwent energy minimization through SWISS Protein Data Bank (PDB) viewer software[9].

2.3. Active site identification and selection for molecular docking

The catalytically active site of Pfmrk comprises specific residues, including L16, M75, M91, I93, and F143, which collectively form a hydrophobic pocket for ATP binding[5]. In hCDK7, the ATP binding site and these five residues differ from those in Pfmrk, featuring distinct amino acids, including D16, I75, F91, F93, and L143 (Waters *et al.*, 2000). To facilitate molecular docking, a grid box was prepared based on these five residues located within the active site of Pfmrk. Detailed information about the amino acids present in the protein's docking site, along with their coordinates, are presented in Table 1.

2.4. Ligand preparation

A total of 1576 compounds available for purchase in the U.S. Food and Drug Administration-approved category were sourced from the ZINC 15 database, provided in MOL2 format (https://zinc.docking.org/substances/subsets/fda+for-sale/). In accordance with Lipinski's rule, these 1576 compounds were screened, and the removal of duplicates, empty structures (salts), isotopes, and inorganic compounds was carried out using the FAF drugs4 server[11]. This process yielded a final database containing 1467 compounds. All compounds from ZINC15 were already in a ready-to-dock conformation. These compounds, provided in MOL2 format, were imported to PyRx software for energy minimization and subsequently converted to the PDB format with charges and atom types (PDBQT) for docking[12].

2.5. Molecular docking and compound screening

Molecular docking was conducted using MGLTools v.1.5.6 Autodock and Raccoon virtual screening tools[13]. The grid was centered on the active site of Pfmrk that contains amino acid residues, and the grid box was constructed with the following coordinate dimensions: center_ x = 266.09, center_y = 319.852, center_z = 310.061, size_x = 60, size_y = 54, size_z = 54. The principal docking protocol incorporated AUTODOCK4 in conjunction with the Lamarckian Genetic Algorithm[13,14]. The compound selection was based on two criteria: the lowest binding free energy (kcal/mol) and the presence of the combination with the highest number of clusters for each compound.

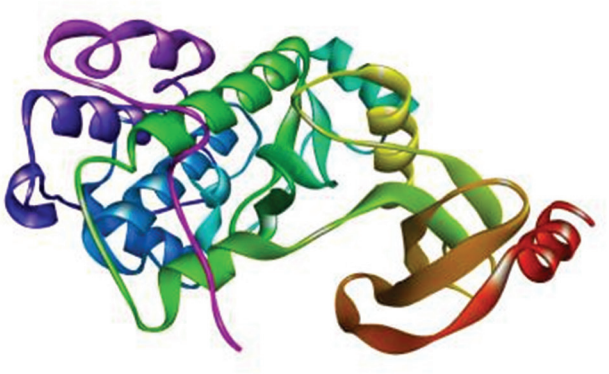

Figure 2. Modeled structure of Pfmrk obtained through Galaxy TBM Web server.

Table 1. Detailed information about the docking proteins, docking sites, and their corresponding coordinates and references

Pfmrk protein sites	Coordinates (X, Y, Z)	Reference
Docking site: Phe15, Lys23, Met91, ILe93, Tyr96, Ser138, Ala140, and Phe143	X_266.09, Y_319.852, Z_ 310.061	[5]
ATP binding site: Leu16, Met75, Met91, Ile93, and Phe143	X_266.09, Y_319.852, Z_310.061	[10]

2.6. Molecular dynamic simulation research

Molecular dynamic simulations were conducted to validate the docking results for Pfmrk and the protein-ligand complexes. Using GROningen MAchine for Chemical Simulations (GROMACS) v 2018.8, the top five drugs were subjected to simulation as a positive control. The PRODRG server version 2.5[15,16] was employed to produce boundary and topographic files for the ligands using the GROMOS force field. The GROMOS 54a7 force field was deployed to prepare both the Pfmrk and ligand complexes. To ensure an appropriate solvation environment, SPC/E water molecules were added to our system, enclosing it within a cubic frame with a dimension of 1.2 nm[17].

During the ionization step, the system was neutralized by adding the appropriate number of Na^+ and Cl^- ions. Energy minimization for all systems was performed with an acceptance of 1000 kJ/mol, and a maximum number of steps was set at 50,000. The particle mesh Ewald (PME) method was deployed to establish a cutoff value of

1.2 nm for both long-range and short-range interactions. In addition, the equilibration procedure for number of particles, volume, and temperature (NVT) and number of particles, pressure, and temperature (NPT) was performed for 1 ns. During this equilibration, the particle number, volume, and temperature were held constant during the post-energy minimization. NVT equilibration was performed using the Berendsen thermostat[15,18] operating with a coupling constant of 0.002 fs at a temperature of 300 K. To identify long-range interactions, the PME method[19] was employed with a cutoff value of 1.2 nm and a Fourier spacing of 0.16 nm. For NPT equilibration, various parameters, including particle count, pressure, and temperature, were fixed. Successful NPT equilibration required the use of the Berendsen isotropic pressure, a time constant of 2 fs, a pressure bar of 1, and isothermal compaction of 4.5×10^{-5} bar. Following the completion of both equilibration steps, simulations for each system were executed for 100 ns with a time step (dt) of 2 fs and a leap-frog integrator[15]. Finally, the simulation results of all the systems were analyzed using standard commands within the GROMACS platform. The LINear Constraint Solver (LINCS) algorithm was used to restrain all bond lengths[14,20].

2.7. Molecular mechanics Poisson-Boltzmann surface area analysis

The molecular mechanics Poisson-Boltzmann surface area (MM-PBSA) method was performed using the gmx_MMPBSA tool and the pbsa.mdp script to evaluate the free binding energy of the top five drugs binding to Pfmrk, along with their respective binding modes. In an effort to optimize computational efficiency, the free energy evaluation was carried out for the final 40 ns of the simulation run. Dielectric constants for both solute and solvent were set at 2 and 80, respectively[14,21,22].

2.8. Visual analysis

The Discovery Studio Visualizer software was used to generate a two-dimensional diagram representing potential interactions within the protein-ligand complex, which serves as a valuable resource for further study (Dassault Systemes BIOVIA 2020). Potential hydrophobic interactions were analyzed using Protein-ligand Interaction Profiler[14].

3. Results

3.1. Docking results

As mentioned earlier, the active site of Pfmrk includes non-conserved amino acids, namely, Phe15, Leu16, Lys23, Met75, Met91, ILe93, Tyr96, Ser138, Ala140, and Phe143. The maximum number of amino acids was enclosed within the grid box. The top five drugs – Lurasidone, Vorapaxar, Donovex, Alvesco, and Orap – exhibited the lowest binding energy and demonstrated the maximum possible interaction with the amino acids situated within the enzyme's active site (Figure 3).

Among these top five drugs, Lurasidone was found to exhibit the lowest binding energy of −12.03 kcal/mol with an inhibitor constant (Ki) of 1.52 nM. Lurasidone forms a non-covalent interaction (alkyl and pi-alkyl) with two critical residues, Ala140 and Phe143, located within the enzyme's Protein Active Site (PAS). Vorapaxar exhibited a binding energy of −10.06 kcal/mol with a Ki of 39.14 nM. Its interaction with the enzyme involves a non-covalent interaction (pi-alkyl) with the essential residue Ile93. Besides these two drugs, Donovex, Alvesco, and Orap exhibited higher binding energy with higher Ki value. These drugs show non-covalent interactions (alkyl and pi-alkyl) with Phe143 and Ala140 key residues within the PAS of the enzyme. Furthermore, a significant non-covalent interaction was observed between Pfmrk and the drug in the ATP-binding region and around our ligand-binding site. A comprehensive overview of these interactions, binding free energy, and Ki, as determined through molecular docking, are shown in Table 2.

3.2. Molecular simulation

The Pfmrk and its associated ligand complexes were simulated for 100 ns, during which five different types of analysis were performed to validate the docking results. To assess the overall stability of the systems, the root-mean-square deviation (RMSD) curve was obtained for both Pfmrk and the holoprotein clusters using the gmx_rms tool. Throughout the simulation, the gmx_gyrate tool was used to calculate the radius of gyration (Rg) of the system. In addition, the root-mean-square fluctuation (RMSF) for the total protein and complex was assessed using the gmx_rmsf tool. To gain insights into the stability of the Pfmrk and complex, the mean number of hydrogen bonds between them was calculated using the gmx_hbond tool. An atomic distance cutoff of 0.35 nm was set between the donors and acceptors.

3.3. RMSD, Rg, and RMSF

The comparison of the RMSD curves between Pfmrk and the other five complexes indicates a close resemblance between the Vorapaxar curve and that of Pfmrk. All five drug complexes exhibited minimal fluctuations, with the curve of all the drugs converging within the range of 0.3 to 0.5 nm. Alvesco and Donovex demonstrated exceptional stability throughout the entire simulation run of 100 ns. The Orap complex exhibited sudden fluctuations up to 40 ns, after which the RMSD remained stable (Figure 4A). In

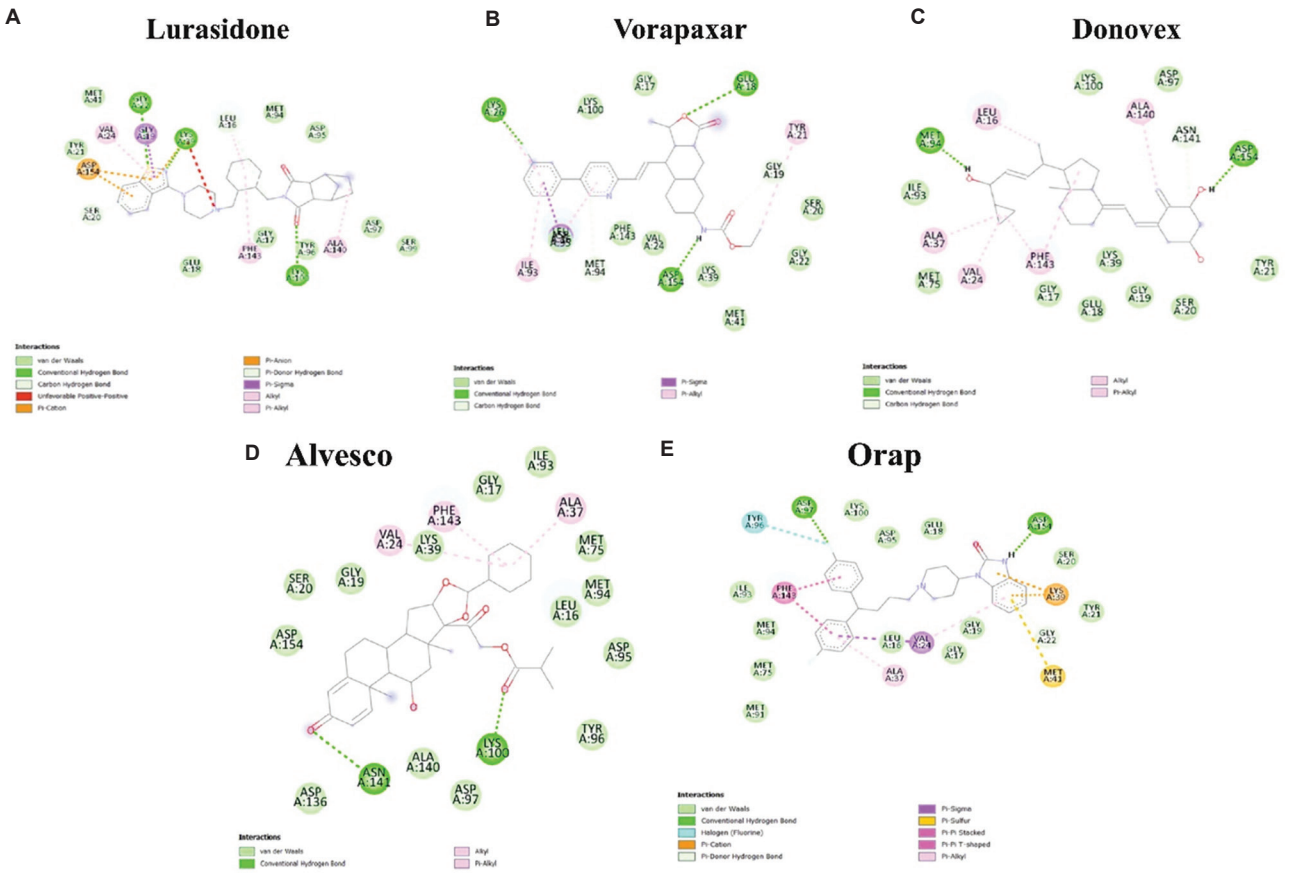

Figure 3. 2D Interaction of Pfmrk with (A) Lurasidone, (B) Vorapaxar, (C) Donovex, (D) Alvesco, and (E) Orap, as visualized in Biovia Discovery studio visualizer.

Table 2. Details of various drugs, their binding energy, Ki values, and interactions with active site residues

FDA-approved drug	Free binding energy (kcal/mol)	Inhibition constant (K_i)	Hydrogen bond interactions	Non-covalent bond interactions
Lurasidone	−12.03	1.52 nM	Lys 39, Lys 100, Gly 22	Leu 16, Val 24, Phe 143 pi-alkyl, Ala 140, Asp 154 (2), lys39 pi-anion, Gly 19 pi-sigma
Vorapaxar	−10.06	39.14 nM	Lys 26, Glu 18, Asp 15,	Ile 93 Pi-alkyl, Tyr 21, Gly 19 C-H bond, Met 94, Leu 16 pi-sigma
Donovex	−8.69	429.05 nM	Met 94 (2), Asp154	Leu 16, Ala 140, Phe 143 (2), Va l24, Ala 37
Alvesco	−8.68	435.75 nM	Asn 141, Lys 100	Val 24 (2), Ala 37, Ala 140, Phe 143
Orap	−8.46	633.3 nM	Asp 154, Asp 97	Lys39 (2), Phe143 (2) Pi-Pi stacked, Ala37 pi alkyl, Met41 Pi cation, Val24, Lys39

terms of Rg, all five complexes displayed a higher degree of compactness compared to Pfmrk. Among them, Donovex, Vorapaxar, and Alvesco exhibited the highest degree of compactness, with the highest deviation of 2.12 nm. Orap and Lurasidone displayed Rg curves resembling that of Pfmrk, which converge at around 2.22 nm (Figure 4B).

According to the docking results, Alvesco and Donovex form a non-covalent interaction with the Ala140, Phe143, and Leu16 residues within the active site of Pfmrk. This interaction results in a reduction of the RMSF curve within the range of residues 15 – 143. Meanwhile, Lurasidone exhibits a superior RMSF curve trajectory within the entire amino acid stretch of 15 – 143 (Figure 5).

3.4. Solvent-accessible surface area (SASA) and hydrogen bonding

The SASA results for all protein-ligand complexes exhibited lower values than Pfmrk, indicating a strong

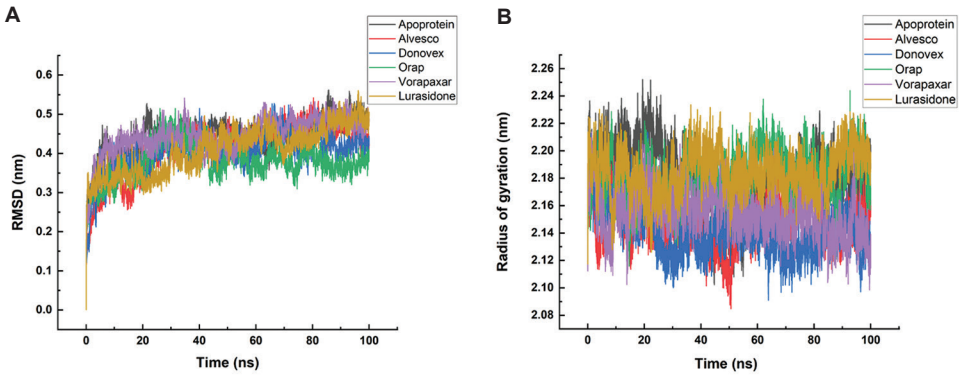

Figure 4. Analysis of the RMSD and Rg results obtained from a molecular dynamics simulation. (A) A comparison of the RMSD trajectories for 100 ns of all protein-ligand complexes and Pfmrks. (B) A comparison of the Rg values for each protein-ligand complex and the Pfmrk over a 100 ns period.

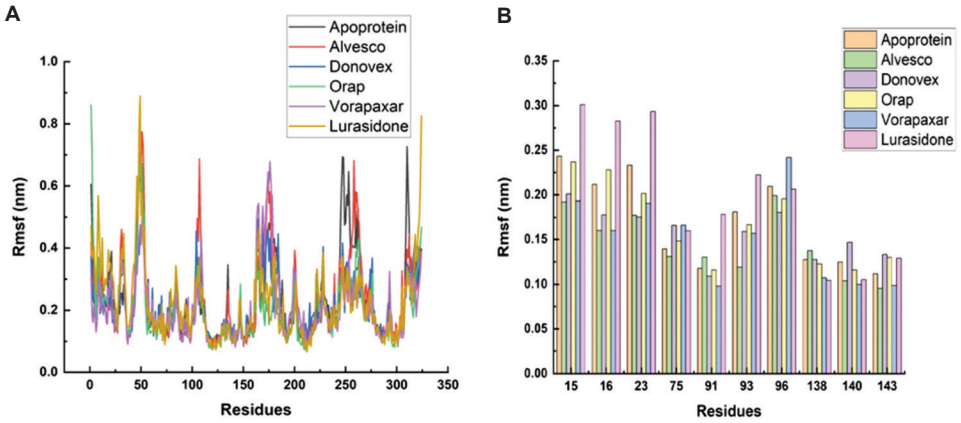

Figure 5. Analysis of the root-mean-square fluctuation (RMSF) results obtained from a molecular dynamics simulation. (A) A comparison of all six drug complexes and the Pfmrk RMSF values for a 100 ns course. (B) A comparison of the RMSF values for the active site residues of each of the six drug complexes and the Pfmrk for a 100 ns course.

binding affinity between the ligands and Pfmrk, consequently increasing the compactness of Pfmrk. These SASA results are presented in Table S1. Simultaneously, the Pfmrk was found to be more folded in the presence of ligands. The Pfmrk complexed with Donovex displayed the lowest SASA value, which contributed to the increased compactness of Pfmrk. The hydrogen bond (H-bond) analysis of all protein-ligand complexes is represented in Table S2. H-bond analysis conducted using MD simulation reveals that Alvesco forms three hydrogen bonds with Lys100, Ser138, and Ala140 and forms an average of one hydrogen bond with the amino acid residues within the active site of Pfmrk.

In contrast, the docking result for Alvesco also reveals the formation of one H-bond (Lys100) under static conditions, as evidenced in our docking results. Donovex forms a more extensive network of hydrogen bonds with amino acids (Met 94, Asp154, Ile 93, Ser138, Ala140, and Phe143). In addition, it forms an average of one H-bond with the residues within the active site of our Pfmrk. Furthermore, the docking result for Donovex forms a two-H-bond (Met 94 and Asp 154). In the case of Lurasidone, it forms hydrogen bonds with specific amino acids (Gly22, Lys39, and Lys100). Furthermore, it forms an average one H-bond with the residues within the active site of our Pfmrk, whereas the docking results for Lurasidone also indicate the formation of a three-H-bond with Gly22, Lys39, and Lys100. Our results indicate that the hydrogen bonds observed during the docking phase often exhibit instability over the course of an extended simulation period. The presence of stable hydrogen bonds is necessary for maintaining stable protein-ligand interactions.

Orap forms two hydrogen bonds with specific amino acids (Lys23 and Asp154) and forms an average of two H-bonds with residues within the active site of our Pfmrk. Conversely, the docking result for Orap indicates the formation of a one-H-bond with Asp154. In comparison, Vorapaxar forms one H-bond with amino acids (Glu18,

Lys26, Tyr96, and Lys100) within the residues of our binding site. This is in contrast to our docking result, which indicated the formation of two H-bonds with Lys 26 and Glu18.

3.5. Secondary structure analysis

The comparative analysis of Dictionary of Protein Secondary Structure (DSSP) secondary structures for both Pfmrk and the ligands was calculated using molecular dynamics simulation and is summarized in Table S3. The secondary structure analysis of Pfmrk reveals similar content in terms of β-sheet, β-bridge, bend, turn, α-helix, 5-helix, and 3-helix when compared to the ligands. In addition, Alvesco and Donovex exhibit a broader range of secondary structures, encompassing coil, β-sheet, β-bridge, and bend. This observation suggests that these ligands have maximum non-covalent interactions with Pfmrk. Orap demonstrates a more significant turn content, signifying its contribution to enhancing protein compactness relative to the other ligands.

3.6. MM-PBSA free energy analysis

The total free binding energy for Donovex was determined to be −92.87 ± 17.87 kJ/mol, while Lurasidone exhibited a slightly higher value of −105.9 ± 57.72 kJ/mol. These energy values were notably higher than those of the other ligands, as indicated in Table 3. Donovex and Lurasidone emerged as the primary contributors to van der Waals forces, underscoring the significance of hydrophobic interactions in our protein-ligand interactions. In addition, these two ligands were observed to exert a notable influence on promoting a more folded state of Pfmrk. Their strong binding affinity was evident through their ability to bind to the protein's active site and other binding regions with relatively higher binding affinity, as reflected in their considerably low binding energy values.

4. Discussion

Malaria remains one of the most dreaded public health concerns, exerting a significant global impact. One of the world's most affected regions by malaria includes certain regions of Africa, where both children and pregnant women are primarily affected. The spread of this deadly disease is influenced by local hygiene and overall environmental conditions. Organizations like the WHO and other leading research institutions continuously strive to improve living conditions and bolster our ability to combat this disease[23-25]. There are two most important strategies for controlling this condition: vector control, which is highly dependent on our living environment, and the development of medicine or vaccines. Although the first vaccine developed for malaria, RTS, S, shows promise, its impact on transmission remains limited, which, in turn, does not significantly affect endemicity[26,27]. The most pressing challenge in managing cases of malaria is the increasing resistance to the current panel of drugs. Drug resistance and cross-resistance among drug combinations are prompting the scientific community to explore alternatives beyond the current array of medications. The review by Pandey *et al*. provides an updated account[23]. As a result, there is an urgent need to identify alternatives, particularly in the most affected regions, including several third-world countries. Therefore, a drug repurposing strategy could be an effective means to screen drugs and expedite the drug development process.

This *in silico* study aims to identify the potential FDA-approved drugs that could target the Pfmrk protein kinase. Through the utilization of molecular docking and subsequent molecular dynamics simulations, we focused on gaining insight into the binding interactions between these screened drugs and Pfmrk's ATP binding site. Our approach particularly focused on the unique characteristics of the active site, marked by the presence of critical residues such as Leu16, Met75, Met91, Ile93, and Phe143. Our findings highlighted the critical role of H-bonds, hydrophobic interactions, and other non-covalent interactions in establishing robust ligand-protein binding.

Given Pfmrk's dual function in both *P. falciparum* cellular replication and its overall life cycle, targeting ATP binding has emerged as a potential strategy to inhibit its kinase activity. Through rigorous analysis, we identified

Table 3. Comprehensive comparative analysis of energetic components in protein-drug complexes formed post-simulation

Ligands	van der Waal energy (kJ/mol)	Electrostatic energy (kJ/mol)	Energy of solvation (kJ/mol)	SASA energy (kJ/mol)	Binding energy (kJ/mol)
Alvesco	−121.789±69.283	−1.518±7.973	65.713±46.072	−13.350±7.725	−70.944±54.776
Donovex	−126.353±20.061	−2.796±2.679	51.327±15.995	−15.054±2.503	−92.877±17.872
Lurasidone	−127.589±64.217	−7.726±7.060	40.816±23.777	−11.408±5.727	−105.907±57.728
Orap	−103.655±100.467	−3.910±6.977	42.897±56.765	−9.701±9.853	−74.369±75.259
Vorapaxar	−5.003±28.557	−0.642±4.782	16.218±40.884	−0.269±4.157	10.304±41.271

Abbreviation: SASA: Solvent-accessible surface area.

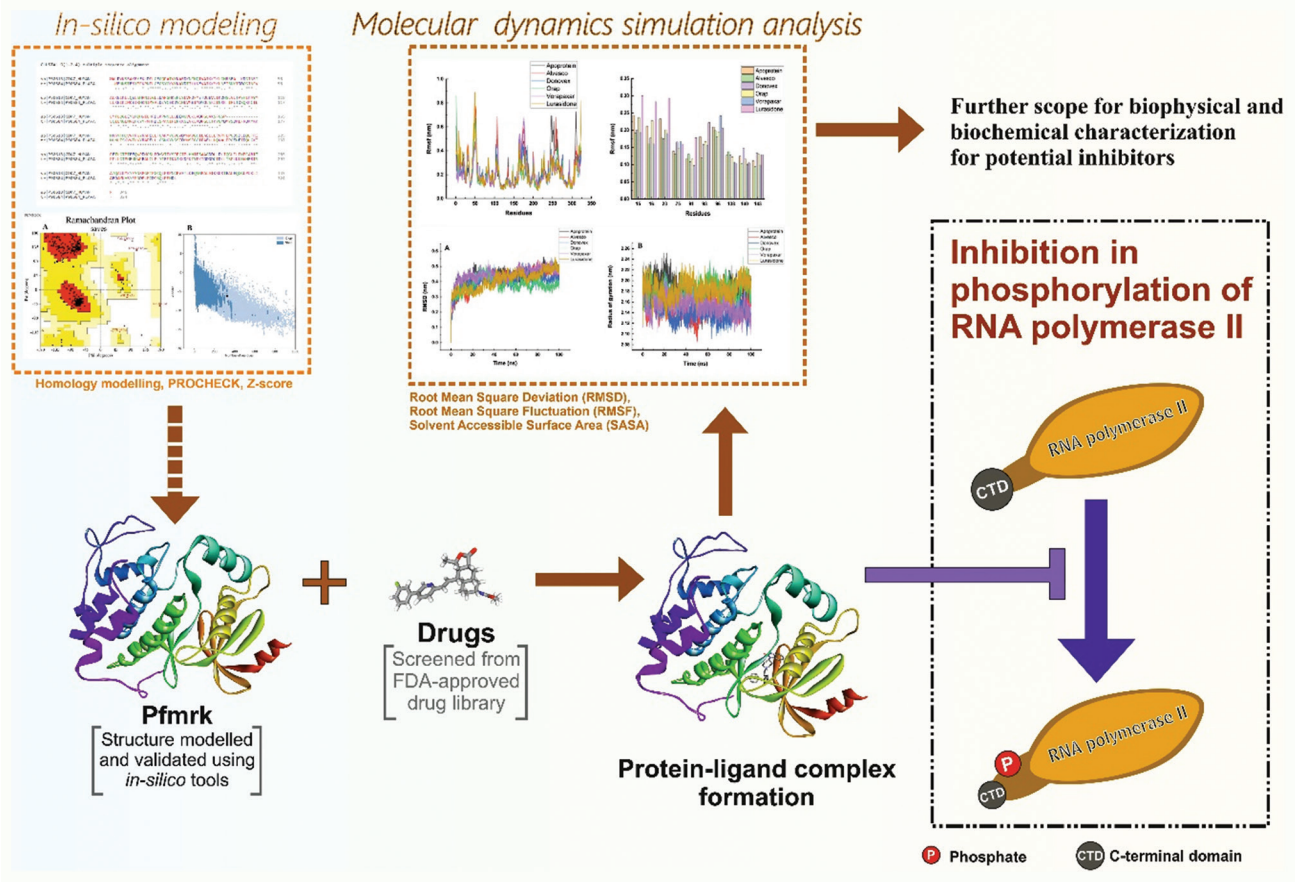

Figure 6. An overview of the entire process involved in this study.

five FDA-approved drugs – Lurasidone, Vorapaxar, Donovex, Alvesco, and Orap – as potential inhibitors due to their strong binding affinities and favorable energy profiles. Furthermore, the original use and year of approval of the FDA-approved drugs is summarized in Table S4. Remarkably, Donovex and Lurasidone yielded the most promising results, characterized by non-covalent interactions with critical residues such as Leu16, Ala140, Phe143, Ile93, and Phe143.

Molecular dynamics simulations provided additional validation for our molecular docking results. These simulations confirmed that Donovex and Lurasidone exhibited strong binding to the ATP binding site, as indicated by our analysis of RMSD, RMSF, Rg, SASA, H-bonding, and MM-PBSA study. These interactions, particularly key residues Ile93 and Phe143, highlighted their potential to inhibit ATP binding, subsequently affecting Pfmrk kinase activity and, ultimately, the transcription machinery.

Significantly, our research addressed the pressing need for new antimalarial targets in light of the growing resistance of *P. falciparum* parasites to existing drugs. Pfmrk has emerged as a promising target, exhibiting a sequence homology of 36.28% with hCDK7. The significant differences between these proteins further highlighted the potential for drug development without harming the host.

5. Conclusion

In this study, we conducted an investigation to explore the potential repurposing of FDA-approved drugs against the Pfmrk protein, a modeled target. Our study identified Alvesco, Donovex, Lurasidone, Orap, and Vorapaxar as potential candidates among FDA-approved drugs, demonstrating strong binding affinities with Pfmrk. Molecular docking and simulation studies further revealed that Donovex and Lurasidone exhibit potential as inhibitors of the modeled Pfmrk protein, acting by binding to its ATP-binding site. The results suggest that Donovex and Lurasidone have the potential to function as kinase inhibitors, making them valuable candidates for further investigation in the context of Pfmrk inhibition. An overview of the entire process involved in this study is illustrated in Figure 6.

In conclusion, our work underlines the significance of targeting Pfmrk as a potential antimalarial strategy. These findings lay a promising foundation for further experimental validation and the development of novel antimalarial drugs.

Acknowledgments

The infrastructure support, the resources and guidance provided by IIT BHU and PARAM Shivay Facility under the National Supercomputing Mission, Government of India at the Indian Institute of Technology BHU, Varanasi are gratefully acknowledged.

Funding

The research supported by research fellowship granted by the Indian Institute of Technology (BHU).

Conflict of interest

The authors declare no conflicts of interest.

Author contributions

Conceptualization: Abhishek Sahu
Formal analysis: Abhishek Sahu, Debanjan Kundu
Investigation: Abhishek Sahu, Tanuj Handa
Methodology: All authors
Writing – original draft: Abhishek Sahu, Debanjan Kundu
Writing – review & editing: All authors

Ethics approval and consent to participate

Not applicable.

Consent for publication

Not applicable.

Availability of data

Data can be requested from corresponding author following formal request.

References

1. Tuteja R, 2007, Malaria- an overview. *FEBS J*, 274: 4670–4679.
2. Breman JG, 2001, The ears of the hippopotamus: manifestations, determinants, and estimates of the malaria burden. *Am J Trop Med Hyg*, 64: 1–11.
   https://doi.org/10.4269/ajtmh.2001.64.1
3. Doerig C, Billker O, Haystead T, *et al*., 2008, Protein kinases of malaria parasites: An update. *Trends Parasitol*, 24: 570–577.
   https://doi.org/10.1016/j.pt.2008.08.007
4. Fisher RP, 2005, Secrets of a double agent: CDK7 in cell-cycle control and transcription. *J Cell Sci*, 118: 5171–5180.
   https://doi.org/10.1242/jcs.02718
5. Keenan SM, Geyer JA, Welsh WJ, *et al*., 2005, Rational inhibitor design and iterative screening in the identification of selective plasmodial cyclin-dependent kinase inhibitors. *Comb Chem High Throughput Screen*, 8: 27–38.
   https://doi.org/10.2174/1386207053328183
6. Li Z, Le RK, Geyer JA, *et al*., 2001, Influence of human p16INK4 and p21CIP1 on the *in vitro* activity of recombinant *Plasmodium falciparum* cyclin-dependent protein kinases. *Biochem Biophys Res Commun*, 288: 1207–1211.
   https://doi.org/10.1006/bbrc.2001.5920
7. Ko J, Park H, Heo L, *et al*., 2012, Galaxy WEB server for protein structure prediction and refinement. *Nucleic Acids Res*, 40: W294–W297.
   https://doi.org/10.1093/nar/gks493
8. Laskowski RA, MacArthur MW, Moss DS, *et al*., 1993, PROCHECK: A program to check the stereochemical quality of protein structures. *J Appl Crystallogr*, 26: 283–291.
   https://doi.org/10.1107/s0021889892009944
9. Guex N, Peitsch MC, 1997, SWISS-MODEL and the Swiss-PdbViewer: An environment for comparative protein modeling. *Electrophoresis*, 18: 2714–2723.
   https://doi.org/10.1002/elps.1150181505
10. Waters PJ, Parniak MA, Akerman BR, *et al*., 2000, Characterization of phenylketonuria missense substitutions, distant from the phenylalanine hydroxylase active site, illustrates a paradigm for mechanism and potential modulation of phenotype. *Mol Genet Metab*, 69: 101–110.
    https://doi.org/10.1006/mgme.2000.2965
11. Lagorce D, Sperandio O, Galons H, *et al*., 2008, FAF-Drugs2: Free ADME/tox filtering tool for drug discovery and chemical biology projects. *BMC Bioinform*, 9: 396.
    https://doi.org/10.1186/1471-2105-9-396
12. Dallakyan S, Olson AJ, 2015, Small molecule library screening by docking with PyRx. *Methods Mol Biol*, 1263: 243–250.
    https://doi.org/10.1007/978-1-4939-2269-7_19
13. Morris GM, Huey R, Lindstrom W, *et al*., 2009, AutoDock4 and AutoDockTools4: Automated docking with selective receptor flexibility. *J Comput Chem*, 30: 2785–2791.
    https://doi.org/10.1002/jcc.21256
14. Kundu D, Dubey VK, 2021, Potential alternatives to current cholinesterase inhibitors: An *in-silico* drug repurposing approach. *Drug Dev Ind Pharm*, 47: 919–930.
    https://doi.org/10.1080/03639045.2021.1952216
15. Borkotoky S, Banerjee M, 2021, A computational

prediction of SARS-CoV-2 structural protein inhibitors from *Azadirachta indica* (Neem). *J Biomol Struct Dyn*, 39: 4111–4121.

https://doi.org/10.1080/07391102.2020.1774419

16. Van Aalten DM, Bywater R, Findlay JB, *et al*., 1996, PRODRG, a program for generating molecular topologies and unique molecular descriptors from coordinates of small molecules. *J Comput Aided Mol Des*, 10: 255–262.

https://doi.org/10.1007/BF00355047

17. Abraham MJ, Murtola T, Schulz R, *et al*., 2015, GROMACS: High-performance molecular simulations through multi-level parallelism from laptops to supercomputers. *SoftwareX*, 1–2: 19–25.

18. Bussi G, Donadio D, Parrinello M, 2007, Canonical sampling through velocity rescaling. *J Chem Phys*, 126: 014101.

https://doi.org/10.1063/1.2408420

19. Kawata M, Nagashima U, 2001, Particle mesh Ewald method for three-dimensional systems with two-dimensional periodicity. *Chem Phys Lett*, 340: 165–172.

20. Hess B, Bekker H, Berendsen HJ, *et al*., 1997, LINCS: A linear constraint solver for molecular simulations. *J Comput Chem*, 18: 1463–1472.

21. Genheden S, Ryde U, 2015, The MM/PBSA and MM/GBSA methods to estimate ligand-binding affinities. *Expert Opin Drug Discov*, 10: 449–461.

https://doi.org/10.1517/17460441.2015.1032936

22. Musyoka TM, Kanzi AM, Lobb KA, *et al*., 2016, Structure-based docking and molecular dynamic studies of plasmodial cysteine proteases against a South African natural compound and its analogs. *Sci Rep*, 6: 23690.

23. Pandey SK, Anand U, Siddiqui WA, *et al*., 2023, Drug development strategies for malaria: With the hope for new antimalarial drug discovery-an update. *Adv Med*, 14: 5060665.

https://doi.org/10.1155/2023/5060665

24. Kelsey A, Stillinger D, Pham TB, *et al*., 2020, Global governing bodies: A pathway for gene drive governance for vector mosquito control. *Am J Trop Med Hyg*, 103: 976–985.

https://doi.org/10.4269/ajtmh.19-0941

25. Nasir SMI, Amarasekara S, Wickremasinghe R, *et al*., 2020, Prevention of reestablishment of malaria: historical perspective and future prospects. *Malar J*, 19: 452.

https://doi.org/10.1186/s12936-020-03527-8

26. Wilson AL, Courtenay O, Kelly-Hope LA, *et al*., 2020, The importance of vector control for the control and elimination of vector-borne diseases. *PLoS Negl Trop Dis*, 14: e0007831.

https://doi.org/10.1371/journal.pntd.0007831

27. Nsanzabana C, 2019, Resistance to artemisinin combination therapies (ACTs): Do not forget the partner drug. *Trop Med Infect Dis*, 4: 26.

https://doi.org/10.3390/tropicalmed4010026

Our Journals

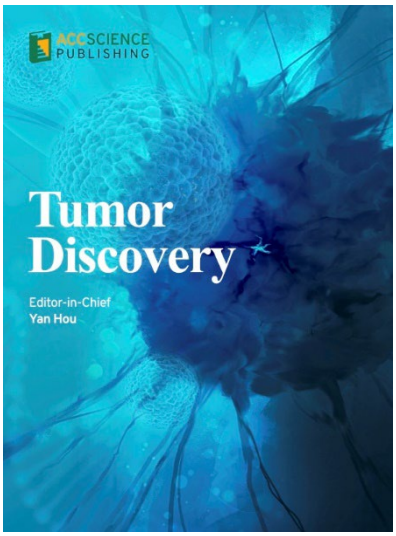

Tumor Discovery is a peer-reviewed and open-access journal that aims to present new cancer research with strong emphasis on fundamental and translational studies. *Tumor Discovery* covers topics, including but not limited to the following:

- Etiology and pathogenesis of cancer
- Mechanisms and molecular pathways underlying cancer initiation and progression
- Tumor metastasis
- Tumor evolution and heterogeneity
- Tumor microenvironment and tumor-host interactions
- Cancer genetics and genomics
- Cancer characterization using omics approaches
- Discovery and validation of cancer biomarker
- Discovery of new therapeutic targets
- New approaches of diagnostic and treatment modalities
- Statistical methods in cancer research

Global Translational Medicine is a quarterly journal that focuses on medicine, biological sciences, and biomaterials engineering. The goal of *Global Translational Medicine* is to provide a platform to researchers for showcasing their latest research works in translational medicine so as to advance the field towards the betterment of human health. Despite the advancement of omics and new technologies, the process of transforming these technologies and scientific research results into effective therapies and putting them into clinical use still has a long way to go. *Global Translational Medicine* provides a platform to fill the gaps in preclinical and inter-disciplinary research, to promote clinical translation of scientific research results, and to contribute to the conception of new and improved preventive measures as well as diagnostic and therapeutic techniques of diseases.

Global Translational Medicine covers the following themes: cardiovascular disease, metabolism/diabetes/obesity, neuroscience/neurology, cancer, biomaterials and their applications in medicine, proteomics/metabolomics, pharmacogenomics, biomarkers, bioinformatics and data mining, animal and clinical research, and medical methods arising from interdisciplinary crossover.

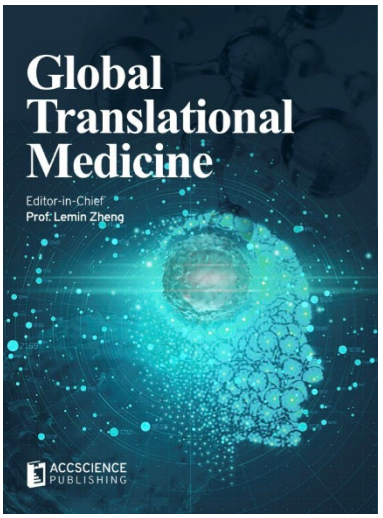

Start a new journal

Write to us via email if you are interested to start a new journal with AccScience Publishing. Please attach your CV, professional profile page and a brief pitch proposal in your email. We shall inform you of our decision whether we are interested to collaborate in starting a new journal.

Contact: info@accscience.com

https://accscience.com/journal/ITPS

Contact
www.accscience.com
8 Burn Road, #15-03 Trivex, Singapore 369977
Email: editorial@accscience.com
Phone: +65 8182 1586